SEMI-ANALYTIC METHODS FOR AVERAGING AND RECTIFICATION OF COMPLEX DYNAMICAL SYSTEMS

A Dissertation

by

ROSHAN THOMAS EAPEN

Submitted to the Graduate and Professional School of
Texas A&M University
in partial fulfillment of the requirements for the degree of

DOCTOR OF PHILOSOPHY

Chair of Committee:	Manoranjan Majji
Co-Chair of Committee:	Kyle T. Alfriend
Committee Members:	John L. Junkins
	Robert A. Gustafson
Head of Department:	Srinivas Rao Vadali

August 2021

Major Subject: Aerospace Engineering

ABSTRACT

Dynamical Systems Theory (DST) serves as a means to understand and describe the changes that occur over time in physical systems. It involves a detailed analysis of a model based on the particular laws governing its change. These laws are in turn derived from suitable theory: Newtonian mechanics, Lagrangian and Hamiltonian mechanics, fluid dynamics, etc. All these models can be conceptually unified in the mathematical notion of a dynamical system.

Broadly, there are two approaches to study dynamical systems: a numerical approach and an analytic approach. A numerical approach involves the propagation of the dynamical equations of motion, usually a set of ordinary or partial differential equations that govern the evolution of each state of the dynamical system. Analytic approaches, in contrast, results in a closed-form solution of the dynamical system that maps the states at a particular time to those at another time. With increasing complexity of physical systems, numerical computations become increasingly expensive, and analytical solutions seldom exist. DST then provides us with tools to analyze such complex behaviors by emphasizing geometric interpretations over purely numeric solutions. Leveraging internal symmetries and examining trajectory bundles in the phase volume help us decipher qualitative dynamical behavior. To emphasize the importance of such methods, two particular dynamical systems are treated in this dissertation. The attitude motion of a rigid body in Keplerian orbit is a dynamical system where the nature of motions has a strong parametric dependence. The restricted three-body problem is another dynamical system that exhibits a wide range of complex motions. Both these systems are studied, and new techniques, metrics, and insights are obtained through the use of DST and analytical averaging techniques.

We show that the use of Classical Rodrigues Parameters for the attitude motion of the rigid body subject to gravity-gradient torques enables us to characterize the equilibria associated with the rotational motion about its mass center. A parametric study of the stability of equilibria shows that large oscillations are induced due to the energy exchange between the pitch and roll-yaw motions, specifically near the 2:1 resonant commensurability regions. A visualization tool is devel-

oped to study these pitch oscillations and gain insight into the rigid body motion near the internal resonance conditions. A measure of coupling between the pitching and roll-yaw motions is developed to quantify the energy exchange utilizing information from the state transition matrix. Poincaré surface of sections, bifurcation diagrams and phase-plane plots are used to examine the attitude motion of a rigid body under various conditions. Further, an analytic treatment of the rigid body dynamics in the Serret-Andoyer variables is carried out for a fast-rotating rigid body assumption. The case for a slow-rotating rigid body is also examined, and the validity of the dynamical model is tested by developing a theory for Lunar free librations.

It becomes evident that both numerical and analytic methods rely heavily on the manner in which they are described: i.e., the coordinate system used. Consequently, a judicious choice of the coordinate system dramatically simplifies the problem at hand. Through the use of Hamilton-Jacobi theory and recent advances in approximation theory, this work presents a systematic procedure to mathematically obtain the best choice of coordinates that simplify the evolution of a dynamical system through rectification. Pursuit of such techniques has culminated in the development of a novel semi-analytic method to treat general dynamical systems. Several examples demonstrate the efficacy of the proposed method in obtaining a functional form of the solution of the dynamical system. Applications to the main problem in artificial satellite theory, treatment of non-conservative dynamical systems and the two-point boundary value problem are investigated. Agreement with classical solutions establish closure with analytical methods and provides strong evidence in support of the methodology developed.

DEDICATION

The scientist does not study nature because it is useful; he studies it because he delights in it, and he delights in it because it is beautiful.

Henri Poincaré

This dissertation is dedicated to my late grandfather, Thomas Eapen

Thank you for your endless love, support, sacrifices, prayers, and encouragement

ACKNOWLEDGMENTS

First and foremost, I would like to thank the Lord Almighty for all the blessings he has showered onto me and enabled me to write this last note in my research work. Throughout my graduate education at Purdue, as in the rest of my life, I have been blessed with making the acquaintance of some extraordinary people who have supported and steered me towards my goal. Words are not enough to express how grateful I am to those people and I would like to make an attempt at thanking them for being a part of this incredible journey.

I am greatly indebted to my advisors, Dr. Manoranjan Majji and Dr. Terry Alfriend. It has been nothing short of an honor and privilege to have them guide me through my research. They have indeed taught me how good research is done. I appreciate their contribution of time, and ideas to help make my Ph.D. research productive and stimulating.

Because of the research environment sustained by them, I have crossed paths with many people who have had a direct or indirect influence on my research. I have been very fortunate to have made the acquaintance of first rate astrodynamicists during my journey: Dr. John Junkins, Dr. Kathleen Howell, Dr. Puneet Singla, and others. I thank them for the time they invested in guiding me through my research and providing me with inputs on improving its content. Specifically, Prof. John Junkins is acknowledged for suggesting the osculating surface that led to the development of Binet-Poincaré sections of this work, Prof. Kathleen Howell for the work on multi-body dynamics in the planar circular restricted three-body problem, Dr. Puneet Singla for the guidance in the development of the semi-analytic method. I would also like to acknowledge my committee members, Dr. Junkins and Dr. Robert Gustafson for taking the time to review my dissertation and suggesting improvements.

I would be remiss if I didn't thank the Hagler Institute of Advanced Studies for the Heep graduate fellowship to support me during my time here. I would like to thank the National Science Foundation and the Air Force Office of Scientific Research for the financial support through the award numbers: NSF CMMI-1634590, FA9550-15-1-0313, and FA9550-17-1-0088. I would also

thank Texas A&M university for supporting me through teaching and research assistantships, and the Aerospace Graduate Student Excellence Fellowship award. I acknowledge DOD STTR Phase 2 - *Reconstruction and Pose Estimation of Space Objects*, with Vision Systems Inc. (VSI) as the prime organization which produced a rendering pipeline that partially supported my graduate study. VSI and AFRL are acknowledged for their support. Our collaborators, Drs. Joe Mundy and Daniel Crispell are gratefully acknowledged for the opportunity to work together. Drs. Carolina Restrepo (NASA-GSFC), Jerry Tessendorf (Clemson), Sarah Stevens (JPL), Anup Katake (JPL),Alejandro M San Martin (JPL), Nicolas Trawney (JPL), Eli D. Skulsky (JPL), Tejas Kulkarni (JPL), and Mr. Ronney Lovelace (NASA-JSC) are acknowledged for their encouragement, guidance and support in the development of the rendering pipeline for the DOD STTR Phase 2 project.

I would like to immensely thank my girlfriend, Christin. I cannot put into words how understanding and supportive you are of me and my goals. Thank you for being there for me, for helping me, and proof-reading this work!! I am forever grateful for your love and for everything you do, and I will always be there for you.

I am immensely grateful to all of the friends I made throughout my academic journey: Smritinanden Paul, Kaushik Prabhu, Nagavenkat Adurthi, Karthikeya Sharma, Tyler Doogan, Raman Goyal, Sandeep, Rupali, Utkarsh, Roshan Kumar, Vivek Muralidharan, and many others. I am also greatful to my church group: Titus and Crystal Bagby, Aigula, Mpume, Hannah, Adam, Bob and Hira, Devika, and others. Thank you for your warm embrace and for keeping me anchored while at Texas A&M. Your encouragement, prayers, and love have been with me and have shaped me into the person I am today.

Most of all, I would like to thank my parents, for providing me with more than just my genetic material, for being a light in the dark, for encouraging me and motivating me throughout my life. And, most important of all, my sister, Sherin. Thank you for being the tether to back home. Without you I would be lost. Thank you!

CONTRIBUTORS AND FUNDING SOURCES

Contributors

This work was supported by a dissertation committee consisting of Professor Manoranjan Majji, Terry Alfriend, and John Junkins of the Department of Aerospace Engineering and Professor Robert Gustafson of the Department of Mathematics. Also, Dr. Kathleen Howell of Purdue university assisted in the research portion completed as a part of the Hagler Fellowship, and Dr. Puneet Singla of Pennsylvania State University assisted in the research on semi-analytic methods. VSI and AFRL are acknowledged for their support. Our collaborators, Drs. Joe Mundy and Daniel Crispell are gratefully acknowledged for the opportunity to work together on the DOD STTR Phase 2 project.

All work for the dissertation was completed independently by the student.

Funding Sources

Graduate study was supported by the Heep Graduate fellowship by the Hagler institute of advanced study. The work is also partially supported by the National Science Foundation under Award No. NSF CMMI-1634590. It is also partially supported by the U.S. Air Force Office of Scientific Research (FA9550-15-1-0313 and FA9550-17-1-0088). DOD STTR Phase 2 - Reconstruction and Pose Estimation of Space Objects, with Vision Systems Inc. (VSI) as the prime organization produced a rendering pipeline that partially supported my graduate study. The final semester of study was supported by Jack E. and Frances Brown Chair II account and the 2021 Summer Aerospace Graduate Excellence Fellowship Award.

NOMENCLATURE

DST	Dynamical Systems Theory
PCR3BP	Planar Circular Restricted Three-Body Problem
CRP	Classical Rodrigues Parameters
DCM	Direction Cosine Matrix
DOF	Degree of Freedom
PSS	Poincaré Surface of Sections
TPBVP	Two Point Boundary Value Problem
LEO	Low Earth Orbit
MEO	Medium Earth Orbit
GEO	Geostationary Earth Orbit
EPO	Earth Parking Orbit
VLBI	Very Long Baseline Interferometry
RAAN	Right Ascension of Ascending Node
AOP	Argument of Perigee
VPM	Method of Variation of Parameters

TABLE OF CONTENTS

Page

LIST OF FIGURES

FIGURE Page

LIST OF TABLES

TABLE Page

1. INTRODUCTION

Challenges in dynamical systems have fascinated physical scientists, mathematicians, and engineers for thousands of years. Notable among such endeavors are those of celestial mechanics, especially the study of the motions of the bodies in the solar system. Attempts to understand and model their observed motions incorporated Kepler's laws (for orbital motion), Cassini's laws (for attitude motion), and led to the development of Newtonian mechanics. This marks the beginning of the study of dynamical problems using differential equations, and the birth of dynamical astronomy [16]. The distinguished elegance and simplicity of such equations have engaged the minds of the greatest mechanicians and mathematicians of the eighteenth and nineteenth century, particularly due to its inherent difficulty, and continues to do so even today. Problems in astrodynamics have set the stage for impressive implementations and breakthroughs in the study of dynamical systems to apply the principles of mechanics to the determination of the motion of objects in space. Spacecraft trajectories (launch through re-entry), orbits of astronomical bodies, including planets, asteroids and comets, attitude motion and control of spacecrafts, rotational dynamics of celestial bodies, all lie within the realm of astrodynamics.

In a broader sense, Dynamical Systems Theory (DST) attempts to understand and describe the changes that occur over time in physical systems. It involves a detailed analysis of a model based on specific laws governing its change, and are derived from strict physical and mathematical framework. All of these models can be conceptually unified in the mathematical notion of a dynamical system, which consists of two main components: the *phase-space* and the *dynamics*. The phase-space is a collection of all possible states of the dynamical system in question. Each state represents a snapshot of the dynamical system at a particular instant in time. The dynamics is a deterministic rule for how a state evolves. In various settings, intricate behavior is observed, even though the equations themselves are not involved. Thus, a simple algebraic form of the equation does not imply that the dynamical behavior is simple.

Broadly speaking, there are two approaches to study dynamical systems: a numerical approach

and an analytical approach. A numerical approach entails the propagation of the dynamical equations of motion, usually a set of ordinary or partial differential equations that govern the evolution of each state of the dynamical system. The numerical approach works in a way that maps the states at a particular initial time (also called epoch) to another instant in time (in the future) that is close to the epoch. This process is then continued to obtain the time history of all states between the epoch and the final time. Analytical approaches, conversely, lead to a closed-form solution of the dynamical system that maps the states at an epoch to those at a final time. While a complete analytical theory exists for linear ordinary differential equations, nonlinear systems are largely inaccessible, apart from successful applications of perturbations methods to weakly nonlinear problems. Several notable exceptions exist to this lack of analytical solutions: the famous two-body problem of orbital motions and the planar pitch attitude motion of rigid bodies in orbit.

Analysis has remained the preferred tool for studying dynamical systems. Even prior to the arrival of the space-age, perturbation methods were widely used in celestial mechanics applications for determining the motion of heavenly bodies. Poincaré 's work in the late-nineteenth century showed that perturbation methods might not yield correct results. He then married analysis and geometry in his development of a qualitative approach to the study of dynamical systems [17]. The Modern methods of qualitative analysis of dynamical systems emerges in the work of Poincaré [18, 19, 20], Birkhoff [21], Lyapunov, Andronov, and Arnold[22, 23]. In the last half century, there has been an explosion of research utilizing the qualitative tools laid out by these giants (Poincaré , Birkhoff, Andronov, Arnold, Smale [24, 25, 21, 22], and others) to understand the behavior of dynamical systems through geometric and topological properties of solutions of differential equations and iterated maps. These methods help develop a qualitative understanding of the properties of the dynamical system, thereby facilitating advances in their analytical formulation.

The focus of this work is to employ various tools of DST to understand the underlying physics at work for dynamical systems of significance to space applications. A major portion of this dissertation is dedicated to justifying, developing, and evaluating analytical and semi-analytical methods for notable astrodynamics problems. One of the key astrodynamics problems considered in this

dissertation is the attitude motion of a rigid body under the influence of gravity-gradient torques. This problem and its variations serve as a bench-test for the proposed developments in DST. In addition, semi-analytical methods are also developed to treat the main problem in artificial satellite theory and its variants. This work is organized into three parts. The first part is dedicated to the study of various qualitative tools of DST and its application to the treatment of the attitude motion of a rigid body in the presence of gravity-gradient torques. The intuitive information obtained from these methods is utilized in the second part of this work to analytically study the attitude motion of a rigid body. The third part of this work integrates the two approaches discussed previously to develop semi-analytical architectures for the treatment of a general dynamical system. In the subsequent sections, each of the three challenges is discussed in detail, providing a literature survey of existing methodologies, preliminaries for the formulation of the problem, and novel developments in each of the research topics. This document is organized as follows:

- Chapter 2: Qualitative treatment of dynamical systems

  The two dynamical systems studied in this investigation are the attitude motion of a rigid body in Keplerian orbit and the planar circular restricted three-body problem. The derivation of the equations of motion for the attitude problem is presented and several features of this dynamical model are highlighted, including equilibrium points and their associated stability, integrals of motion, parametric bifurcations, regular and chaotic solutions, and long term evolution. Extension to a higher fidelity dynamical model is also presented. Following this, the Earth-Moon-satellite restricted three-body problem is discussed. The scope of this chapter is to present the reader with qualitative analysis tools to study the dynamical behavior of the aforementioned dynamical systems. To this end, visualization tools, topological transformations, and quantitative metrics are developed to characterize various nonlinear phenomena such as energy exchange in resonance regions, parametric bifurcations, and invariant manifold behaviors. The methodologies developed are applied to problems in space applications, particularly to studying long-term evolution of the attitude motion of orbiting satellites and identifying transport opportunities in cislunar space. The qualitative nature of

the results are primarily dependent on the choice of coordinates used to describe the dynamical system and is limited in the qualitative information one can obtain because of this choice. Another limitation is the extensive computational requirement for simulating a large set of initial conditions to accurately capture the qualitative behavior.

- Chapter 3: Analytic treatment of dynamical systems

  The attitude motion of a rigid body is studied exclusively from an analytical point of view in this chapter. Some of the limitations outlined in the previous chapter are addressed by resorting to the Hamiltonian formulation for the attitude motion and leveraging the internal symmetries of the problem. The attitude motion is treated from two perspectives: a fast-rotating rigid body, with applications to long-term behavior of artificial satellites and debris, and a slow-rotating rigid body, with applications to natural rotational motion of planetary bodies. The scope of this chapter is to present the reader with the formulation of the dynamical model and to present techniques for partial and complete reduction of the dynamical system through symplectic transformations, and Hamilton-Jacobi theory. One of the limitations of analytical methods is that a complete reduction is possible only for integrable dynamical systems. The complexity in the dynamical systems considered in this investigation renders them non-integrable. One must resort to combining the analytic methodologies with qualitative insights from the previous chapter to describing different dynamical behaviors.

- Chapter 4: Semi-analytic treatment of dynamical systems

  The full dynamical model of the attitude motion of a rigid body is non-integrable and no closed-form solutions exist, except under extensively simplifying assumptions. The limitations described in the outline of the previous chapter are addressed by marrying the analytical insights from Hamilton-Jacobi theory and recent numerical advancements in approximation theory. The scope of this chapter is to develop a systematic procedure to treat complex dynamical systems such as the ones described in this investigation. As opposed to choosing the coordinate system for qualitative studies and analytic reductions, the technique developed

seeks to find a judicious set of coordinates that simplify the motion of the dynamical system through the process of rectification. This method can be applied to treat both Hamiltonian and non-Hamiltonian dynamical systems by discretizing the phase-volume and establishing local integrability within this domain. Application to optimal control and two-point boundary value problems are also presented.

- Chapter 5: Concluding remarks

  A summary of the results presented in preceding chapters is provided along with recommendations for future work.

2. QUALITATIVE TREATMENT OF DYNAMICAL SYSTEMS

Dynamics is an interdisciplinary subject today. Originally a branch of physics, it began with Newton in the 1600s with the discovery of laws of motion and universal gravitation, and the explanation of Kepler's laws of planetary motion. Specifically, Newton solved the problem of two bodies, i.e. the problem of calculating the motion of planets around the sun with the inverse square law of gravitational attraction. Subsequent generations of mathematicians, physicists, and engineers have striven to extend Newton's analytical methods to the three-body problem (e.g., sun, Earth and moon). Finally, it was realized that the problem of three bodies was impossible to solve in the sense of explicit formulas for the movement of three bodies [26, 27].

The breakthrough came with the work of Poincaré in the late 1800s. He introduced a new point of view, one that emphasized qualitative, rather than quantitative questions. He developed a powerful geometric approach to analyzing such questions, and the approach has flowered into the modern subject of Dynamical Systems Theory, with applications reaching far beyond celestial mechanics [26, 28]. To motivate discussions for the remainder of this dissertation, certain terminologies and definitions are introduced.

2.1 A mathematical description of dynamics

To introduce the logical structure of dynamics, certain terminologies are introduced and distinctions are made. There are broadly two types of dynamical systems: *differential equations* and *iterated maps* (also known as difference equations). Differential equations describe the evolution of systems in a continuous time, whereas iterated maps arise in problems where time is discrete. Differential equations are widely used throughout this dissertation to describe the dynamical system. Therefore, focusing attention on them, the main distinction is between ordinary and partial differential equations.

Ordinary differential equations contain ordinary derivatives, i.e., there is only one independent variable (usually, time). Partial differential equations, in contrast, impose relations between various

partial derivatives of a multivariate function. A very general framework for ordinary differential equations is provided by the system of equations as follows:

$$\begin{aligned} \dot{x}_1 &= f_1(x_1, \cdots, x_n) \\ &\vdots \\ \dot{x}_n &= f_n(x_1, \cdots, x_n) \end{aligned} \tag{2.1}$$

Here, the over-dots denote differentiation with respect to time, t, i.e., $\dot{x}_i = dx_i/dt$. The solution to the system of equations can be obtained numerically by specifying initial and/or boundary conditions for the states. For example, the simple harmonic oscillator given by the differential equation: $\ddot{x} = -kx$. This system can be written in the form of Eq. (2.1) by defining $x_1 = x$ and $x_2 = \dot{x}$.

$$\begin{aligned} \dot{x}_1 &= x_2 \\ \dot{x}_2 &= -kx_1 \end{aligned}$$

The above description is called the *state-space* representation, and the variables x_1 and x_2 are the states of the system. The initial conditions for this system are given as: $x_1(t_0) = x_{1_0}$, and $x_2(t_0) = x_{2_0}$. The system is *linear*, because all the x_i on the right-hand side appear to first power only. Further, the principle of superposition applies to linear systems wherein by superimposing two different initial conditions, the resulting motion is the algebraic sum of the individual motions [22]. Contrastingly, nonlinear systems have nonlinear terms on the right-hand side, e.g., trigonometric terms, exponential terms, logarithmic terms, polynomials of degree two or higher, etc. For example, consider the swinging of a pendulum governed by the equation, $\ddot{x} + \frac{g}{L}\sin x = 0$. Here, x is the angle of the pendulum from vertical, g is the acceleration due to gravity, and L is the length of the pendulum. The motion of the pendulum can be described in state-space form as a set of nonlinear ordinary differential equations, with the state space variables being $x_1 = x$ and $x_2 = \dot{x}$

[26, 28].

$$\dot{x}_1 = x_2 \tag{2.2}$$

$$\dot{x}_2 = -\frac{g}{L}\sin x_1 \tag{2.3}$$

with initial conditions as described before. The non-linearity makes the pendulum equation difficult to solve analytically. The equation can be solved in terms of elliptic functions, however, elliptic functions can be generally difficult to evaluate. The motion of the simple pendulum, harmonic oscillator, etc. are quite simple to explain qualitatively. At low energy, it swings back and forth, and at high energy, it whirls over the top and wraps around in circular motion. These motions are called *librations* and *circulations*, respectively. Using geometric methods, there are ways to extract this information from the differential equations of the dynamical system. The first part of this dissertation is focused on developing and utilizing such qualitative methods to treat dynamical systems. To ascertain this, divide Eq. (2.1) by Eq. (2.2) and attempt to solve it.

$$\frac{dx_1}{dx_2} = \frac{x_2}{-\frac{g}{L}\sin x_1} \tag{2.4}$$

$$-\frac{g}{L}\sin x_1 \, dx_1 = x_2 \, dx_2 \tag{2.5}$$

$$\frac{x_2^2}{2} - \frac{g}{L}\cos x_1 = C \tag{2.6}$$

where, C is a constant of integration. For different values of C, one can plot this implicit equation in Eq. (2.6) to obtain a graphical view of the motion of the simple pendulum. This is shown in Fig. 2.1.

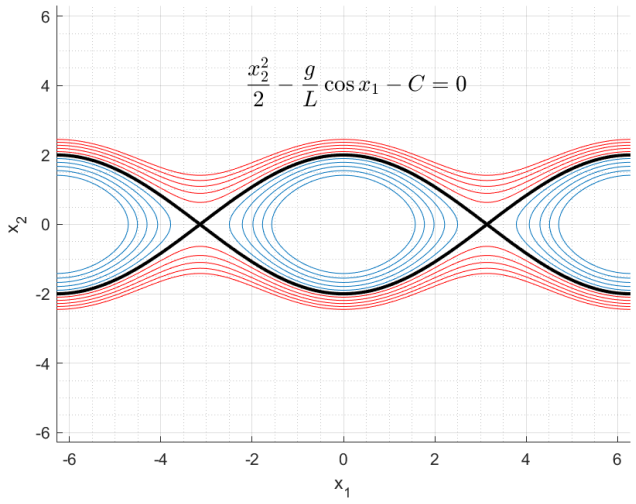

Figure 2.1: Phase portrait of the simple pendulum. The curves in red show circulatory motion while those in blue are librations. The black curve denotes the separatrix.

Figure 2.1 illustrates the behavior of the pendulum. The low energy libration and high energy circulations are shown in blue and red, respectively. The curve that divides the two types of motion (shown in black) is called the *separatrix*, and it has some important properties. These curves (in red and black) are called *trajectories*, and the space of $x_1 - x_2$ is called the *phase-space* for the system. The phase-space for the general system in Eq. (2.1) is the space with coordinates $x_1, \cdots, x_n$. Because this space is $n-$dimensional, the system is referred to as an $n-$*dimensional system*, and n represents the dimension of the phase-space. For autonomous systems, i.e., systems with no explicit time dependence, n is usually even.

Equation (2.1) is not general enough, since it does not include explicit time dependence. The dynamical systems with explicit time dependence are called *nonautonomous* dynamical systems. For example, consider the forced harmonic oscillator given the governing equations: $\ddot{x} + kx = F\cos t$. The equations of motion in state space form can now be written following previous methods discussed, or one can introduce an additional variable $x_3 = t$. Then, $\dot{x}_3 = 1$. Thus, the system

of equations take the form

$$\begin{aligned} \dot{x}_1 &= x_2 \\ \dot{x}_2 &= -kx_1 + F\cos x_3 \\ \dot{x}_3 &= 1 \end{aligned} \tag{2.7}$$

This is an example of a $(n+1)$ dimensional system [26]. The terminologies and definitions outlined in this section are carried forward throughout the dissertation. To motivate the discussion of the different tools in DST that enable qualitative and geometric analysis, two particular dynamical systems are studied as a test problem: (a) the attitude motion of a rigid body in Keplerian orbit; (b) the Planar Circular Restricted Three-body Problem (PCR3BP). The preliminaries for attitude dynamics are presented in the next section.

2.2 Attitude motion preliminaries

The attitude (or orientation) of a rigid body is described using attitude parameters that completely describe the orientation of the rigid body relative to some frame of reference. Thr attitude parameterizations are non-unique and various sets of parameterizations have been used in this analysis. Each set has its strengths and weaknesses. The following four sets of truths about attitude coordinates are generally accepted [29, 30, 31]

1. A minimum of three coordinates is required to describe the relative angular displacement between two reference frames F_1 and F_2.

2. Any minimal set of three attitude coordinates will contain at least one geometrical orientation where the coordinates are singular, namely at least two coordinates are undefined or not unique.

3. At or near such a geometric singularity, the corresponding kinematic differential equations are also singular.

4. The geometric singularities and associated numerical difficulties can be avoided altogether

through a regularization. Redundant sets of four or more coordinates exist, which are universally determined and contain no geometric singularities.

In this dissertation, two primary sets of attitude parameters are used to describe the attitude motion of a rigid body in Keplerian orbit: the Euler angles, and the Classical Rodrigues Parameters. Their description and kinematic relations are now given.

2.2.1 The Euler angles

Euler angles are the most commonly used attitude parameters, particularly because of their ease in relating to physical representation of the orientation of a rigid body. They describe the orientation of a reference frame $\mathcal{B}\{\hat{b}_1, \hat{b}_2, \hat{b}_3\}$ to the frame $\mathcal{N}\{\hat{n}_1, \hat{n}_2, \hat{n}_3\}$ through three successive rotations about sequentially displaced body-fixed axes ($\hat{\mathbf{b}}$). The direction cosine matrix (DCM) can be parameterized in terms of Euler angles, utilizing successive rotations about each of the body axes through three single-axis rotation matrices that are a function of a single parameter.

$$
\begin{aligned}
M_1(\theta) &= \begin{bmatrix} 1 & 0 & 0 \\ 0 & \cos\theta & \sin\theta \\ 0 & -\sin\theta & \cos\theta \end{bmatrix} \\
M_2(\theta) &= \begin{bmatrix} \cos\theta & 0 & -\sin\theta \\ 0 & 1 & 0 \\ \sin\theta & 0 & \cos\theta \end{bmatrix} \\
M_3(\theta) &= \begin{bmatrix} \cos\theta & \sin\theta & 0 \\ -\sin\theta & \cos\theta & 0 \\ 0 & 0 & 1 \end{bmatrix}
\end{aligned}
\tag{2.8}
$$

Utilizing these expressions and noting that a general orientation has three degrees of freedom,

the orientation can be described using three angles. One example is the following.

$$[C_{1-2-3}(\alpha, \beta, \gamma)] = [C_3(\gamma)][C_2(\beta)][C_1(\alpha)] \tag{2.9}$$

In using such a description of the orientation, the second angle in the sequence is restricted to be different from the first and third. Consequently, there are twelve Euler angle orientation sets: six symmetric and six asymmetric.

$$\text{symmetric} : (1-2-1), \quad (1-3-1), (2-1-2), \quad (2-3-2), (3-1-3), \quad (3-2-3)$$

$$\text{asymmetric} : (1-2-3), \quad (1-3-2), (2-1-3), \quad (2-3-1), (3-1-2), \quad (3-2-1)$$

The Euler angles of any sequence are global in that they are defined everywhere. However, certain orientations give non-unique parameter values. For the symmetric orientations, the middle angles of zero or $\pm\pi$ result in only the sum of first and third angles as unique, while the individual angles are non-unique. A similar situation occurs for asymmetric sets when the second angle equals $\pm\pi/2$. For this reason, the asymmetric sets are useful in describing small departures from a nominal orientation to avoid singularities. While the Euler angles provide a physical interpretation of the orientation, the resulting equations are transcendental. The following section describes another set of attitude parameters, the Classical Rodrigues Parameters (CRPs), that result in purely algebraic expressions. The CRP parameterization is utilized throughout this chapter.

2.2.2 The classical Rodrigues parameters

The CRPs are a three component vector **q** also called the Gibbs vector. The CRPs can be obtained conveniently using Euler's principal rotation theorem, which states: *A rigid body or co-ordinate reference frame can be brought from an arbitrary initial orientation to an arbitrary final orientation by a single rigid rotation through a principal angle ϕ about the principal axis $\hat{e}$; the principal axis being a judicious axis fixed in both the initial and final orientation.* [29, 32] To further elucidate this, a skew-symmetric matrix is defined using the components of a vector. For a

given vector $\mathbf{z} = [z_1, z_2, z_3]^T$, the skew-symmetric matrix is defined as $\tilde{z}$ where the entries of the matrix are composed of the elements of the vector $\mathbf{z}$: $z_1 = \tilde{z}_{32} = -\tilde{z}_{23}$, $z_2 = \tilde{z}_{13} = -\tilde{z}_{31}$, and $z_1 = \tilde{z}_{21} = -\tilde{z}_{12}$. [29]

The direction cosine matrix as a function of the Euler principal axis and angle is then given as[33, 29]:

$$[C(\hat{e}, \phi)] = [1] - \sin\phi[\tilde{\hat{e}}] + (1 - \cos\phi)[\tilde{\hat{e}}][\tilde{\hat{e}}] \tag{2.10}$$

where $[1] = I_{3\times3}$ is the identity matrix of dimension, three. Using this as a starting point, one can define many different three-parameter sets for describing the rigid body attitude by considering $\mathbf{q} = f(\phi)\hat{e}$. Choosing $f(\phi) = \tan(\phi/2)$ gives the CRPs, $\mathbf{q}$. The attitude matrix for the CRPs is given as:

$$[C] = [1] - \frac{2}{1 + \mathbf{q}^T\mathbf{q}}\tilde{\mathbf{q}} + \frac{2}{1 + \mathbf{q}^T\mathbf{q}}\tilde{\mathbf{q}}\tilde{\mathbf{q}} \tag{2.11}$$

These parameters can also be obtained using the Cayley transform as [29, 32]:

$$[C] = ([1] + \tilde{\mathbf{q}})^{-1}([1] - \tilde{\mathbf{q}}) = ([1] - \tilde{\mathbf{q}})([1] + \tilde{\mathbf{q}})^{-1} \tag{2.12}$$

The inverse Cayley transform gives the direction cosine matrix from the CRPs as:

$$\tilde{\mathbf{q}} = ([1] + [C])^{-1}([1] - [C]) = ([1] - [C])([1] + [C])^{-1} \tag{2.13}$$

Using these relations for the CRPs, the following sections develop the kinematic and dynamic equations for attitude motion.

2.2.3 Attitude kinematics

Suppose the direction cosine matrix, $[C]$, relates the parameterization of a vector in frames $\mathcal{A}$, and $\mathcal{B}$: $\mathbf{u}_\mathcal{B} = [C]\mathbf{u}_\mathcal{A}$. To study the rotational kinematics, differentiating the relation $[C][C]^T = [1]$, we obtain the following.

$$[0] = \frac{d}{dt}([C])[C]^T + [C]\frac{d}{dt}([C]^T) = \frac{d}{dt}([C])[C]^T + (\frac{d}{dt}([C])[C]^T)^T \tag{2.14}$$

with $\frac{d[C]}{dt}$ indicating the time derivative of the individual elements of $[C]$. The last expression generates a skew-symmetric matrix between $\mathcal{A}$ and $\mathcal{B}$.

$$[\Lambda] = -\frac{d}{dt}([C])[C]^T \tag{2.15}$$

Rearranging the above equation results in a matrix differential equation that governs the evolution of $[C]$.

$$\frac{d}{dt}[C] = -[\Lambda][C] \tag{2.16}$$

The elements of $[\Lambda]$ can be written as follows.

$$\Lambda_{ij} = -\frac{d}{dt}([C_{i1}, C_{i2}, C_{i3}])[C_{j1}, C_{j2}, C_{j3}]^T \tag{2.17}$$

Now, since $[C]$ can be written as a function of any of the attitude parameters: $[C] = [C(u_1, u)2, \cdots]$ (such as in Eq. (2.9), Eq. (2.12)), Eq. (2.17) can be written as follows.

$$\Lambda_{ij} = -\Big[\frac{\partial C_{ik}}{\partial u_1} C_{jk}, \frac{\partial C_{ik}}{\partial u_2} C_{jk}, \cdots\Big][\dot{u}_1, \dot{u}_2, \cdots]^T \tag{2.18}$$

Now, noting that Λ is the skew-symmetric matrix of angular velocities, one can arrive at the following expression.

$$[\omega_1, \omega_2, \omega_3]^T = [B][\dot{u}_1, \dot{u}_2, \cdots]^T \tag{2.19}$$

The matrix $[B]$ has dimensions $3 \times n_p$, where n_p is the number of attitude parameters, and it relates the elements of the angular velocity in the body frame to the time-derivative of the attitude parameters. The inverse relationship is fairly straightforward for a three-parameter set such as CRPs or Euler angles.

$$[\dot{u}_1, \dot{u}_2, \cdots]^T = [A][\omega_1, \omega_2, \omega_3]^T \tag{2.20}$$

with $[A] = [B]^{-1}$.

Particularly for the CRPs the $[A]$ and $[B]$ matrices are given as follows.

$$[B] = \frac{2}{1+\mathbf{q}^T\mathbf{q}}([1]-\tilde{q}) \qquad\qquad [A] = \frac{1+\mathbf{q}^T\mathbf{q}}{4}([1]+[C]^T) \tag{2.21}$$

The kinematic relations expressed in this section aids in describing the orientation of a rigid body with respect to a frame of reference. In order to determine the motion of such a rigid body, the dynamic relations are introduced in the following section.

2.3 Attitude dynamics of a rigid body

A rigid body can be considered a continuum of differential mass elements, dm. Newton's equations of motion can be applied to the differential mass element as:

$$\mathrm{d}\mathbf{f} = \frac{d^2}{dt^2}(\mathbf{r})\mathrm{d}m = \ddot{\mathbf{r}}\mathrm{d}m \tag{2.22}$$

where, $\mathbf{r}$ is the inertial position vector of dm and depends on coordinates and time, $\mathbf{r} = \mathbf{r}(x,t)$. This vector may be written as a combination of two vectors $\mathbf{r}(x,t) = \mathbf{r}_c(t) + \boldsymbol{\rho}(x,t)$, where $\mathbf{r}_c$ is the inertial position of the center of mass, and $\boldsymbol{\rho}$ is the position of dm relative to the mass center. The vector d$\mathbf{f}$ represents the sum of impressed forces acting on dm i.e. the sum of externally applied forces and internally applied forces: $\mathrm{d}\mathbf{f} = \mathrm{d}\mathbf{f}_{ex} + \mathrm{d}\mathbf{f}_{in}$. Now, Euler noted that "a rigid body does not spontaneously assume any motion in virtue of any internal forces there may be within it, and these internal forces do not contribute to any of its motion as a whole" [34] implying that $\int \mathrm{d}\mathbf{f}_{in} = 0$. Therefore, integrating over the complete continuum gives the translational equations of motion of a rigid body [35]:

$$\frac{d^2}{dt^2}\int \mathbf{r}\mathrm{d}m = \int \frac{d^2\mathbf{r}}{dt^2}\mathrm{d}m = \int \ddot{\mathbf{r}}\mathrm{d}m = \int \mathrm{d}\mathbf{f} = \mathbf{f} \tag{2.23}$$

thus,

$$\mathbf{f} = \frac{d^2}{dt^2}\int \mathbf{r}\mathrm{d}m = m\ddot{\mathbf{r}}_c \tag{2.24}$$

Like translational motion by Newton, Euler's principle for rotational motion of a finite contin-

uum is the statement: $\mathbf{l}_o = \dot{\mathbf{h}}_o$, where o is a fixed point, and $\mathbf{h}_o = \int \mathbf{r} \times \dot{\mathbf{r}} \mathrm{d}m$. Here, $\mathbf{l}_o$ is a vector of external moments. Considering the fixed point as the center of mass (i.e. $[\star]_o = [\star]_c$) and using the transport theorem, Euler's equations are expressed as:

$$\dot{\mathbf{h}}_c = \frac{^{\mathcal{B}}d}{dt}(\mathbf{h}_c) + \boldsymbol{\omega} \times \mathbf{h}_c = \mathbf{l}_c \tag{2.25}$$

where h_c is the angular momentum about the center of mass. This can be defined as

$$\mathbf{h}_c = \int_{\mathcal{B}} \mathbf{r} \times (\boldsymbol{\omega} \times \mathbf{r}) \mathrm{d}m = \Big(\int_{\mathcal{B}} -[\tilde{r}][\tilde{r}] \mathrm{d}m \Big) \boldsymbol{\omega} \tag{2.26}$$

Carrying out the triple cross-product and identifying that

$$\Big(\int_{\mathcal{B}} -[\tilde{r}][\tilde{r}] \Big) \mathrm{d}m = {}^{\mathcal{B}}[I_c]$$

where $[I_c]$ is the inertia matrix defined about the center of mass. Since $\boldsymbol{\omega}$ does not vary inside the continuum, it can be taken outside the integral. The angular momentum vector of a rigid body about its center of mass can then be written as:

$$\mathbf{h}_c = [I_c]\boldsymbol{\omega} \tag{2.27}$$

Equation (2.25) can then be written as:

$$\frac{^{\mathcal{B}}d}{dt}\mathbf{h}_c = \frac{^{\mathcal{B}}d}{dt} I_c \boldsymbol{\omega} + I_c \frac{^{\mathcal{B}}d}{dt}\boldsymbol{\omega} = I\dot{\boldsymbol{\omega}} \tag{2.28}$$

Noting that the derivative of angular velocity is the same as seen in $\mathcal{B}$ and the $\mathcal{N}$ frame,

$$\dot{\boldsymbol{\omega}} = \frac{^{\mathcal{N}}d}{dt}\boldsymbol{\omega} = \frac{^{\mathcal{B}}d}{dt}\boldsymbol{\omega} + \boldsymbol{\omega} \times \boldsymbol{\omega} = \frac{^{\mathcal{B}}d}{dt}\boldsymbol{\omega} \tag{2.29}$$

Therefore, we get the famous Euler's rotational equations of motions as:

$$I_c\dot{\boldsymbol{\omega}} = -\tilde{\omega} I_c \boldsymbol{\omega} + \mathbf{l}_c \tag{2.30}$$

By choosing a body-fixed coordinate system aligned to the principal body axes, the inertia matrix $I_c = \text{diag}[I_1, I_2, I_3]$ will be diagonal. The equations of motion reduce to the following form:

$$\begin{aligned} I_1\dot{\omega_1} + (I_3 - I_2)\omega_2\omega_3 &= l_1 \\ I_2\dot{\omega_2} + (I_1 - I_3)\omega_1\omega_3 &= l_2 \\ I_3\dot{\omega_3} + (I_2 - I_1)\omega_1\omega_2 &= l_3 \end{aligned} \tag{2.31}$$

With Euler's equations of motion given above, the motion of a rigid body under the influence of gravity-gradient torque can be obtained. To do so, the next section outlines the derivation of gravity-gradient torque.

2.3.1 Gravity-gradient torque formulation

Consider the motion of a rigid body in a central force field of a particle P' with mass m'. This is illustrated in Fig 2.2.

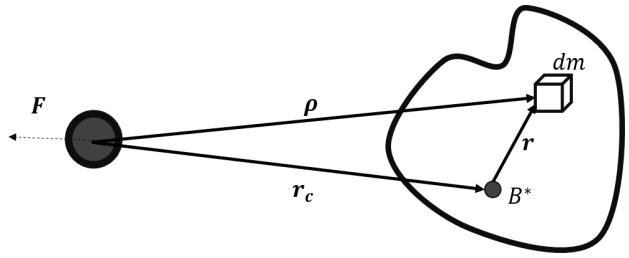

Figure 2.2: Gravity-gradient torque set-up. dm is a differential mass element, B^* is the center of mass, and the central body is located at r_c from the rigid body.

In Fig. 2.2, **r** denotes the vector locating the differential mass element dm from the center of mass, B^*. $\mathbf{r}_c$ is the position vector of the center of mass B^* from the central body P', and

$\mathbf{r}_c + \mathbf{r} = \rho$. $\mathrm{d}m = \nu d\tau$ is the differential mass element given in terms of the density ν and the differential volume element, $d\tau$. The gravitational force acting on the differential mass element can be expressed using Newton's universal law of gravitation as:

$$\mathbf{F} = -Gm' \int \boldsymbol{\rho}(\boldsymbol{\rho} \cdot \boldsymbol{\rho})^{-3/2} \nu d\tau \tag{2.32}$$

$$= -Gm' \int (\mathbf{r}_c + \mathbf{r}) \Big[(\mathbf{r}_c + \mathbf{r}) \cdot (\mathbf{r}_c + \mathbf{r}) \Big]^{-3/2} \nu d\tau \tag{2.33}$$

$$= -Gm' \int \mathbf{r}_c [\frac{\mathbf{r}_c}{r_c} + \frac{\mathbf{r}}{r_c}] \frac{1}{r_c^3} \Big[\frac{r_c^2}{r_c^2} + \frac{2\mathbf{r}_c \cdot \mathbf{r}}{r_c^2} + \frac{r^2}{r_c^2} \Big]^{-3/2} \nu d\tau \qquad (\text{for } |\mathbf{r}| << |\mathbf{r}_c|) \tag{2.34}$$

For simplicity, denote $\frac{\mathbf{r}_c}{r_c} = \hat{\mathbf{a}}_1$ and $\frac{\mathbf{r}}{r_c} = \mathbf{a}$. Thus, the external gravity force is rewritten as:

$$\mathbf{F} = -\frac{Gm'}{r_c^2} \int (\hat{\mathbf{a}}_1 + \mathbf{a})(1 + 2\hat{\mathbf{a}}_1 \cdot \mathbf{a} + \mathbf{a} \cdot \mathbf{a})^{-3/2} \nu d\tau \tag{2.35}$$

Now, using the expansion

$$(1+x)^m = 1 + mx + \frac{m(m-1)}{2!}x^2 + \frac{m(m-1)(m-2)}{3!}x^3 + \cdots$$

and keeping terms up to second order,

$$\mathbf{F} = \frac{-Gm'}{r_c^2} \int (\hat{\mathbf{a}}_1 + \mathbf{a}) \Big[1 - \frac{3}{2}(2\hat{\mathbf{a}}_1 \cdot \mathbf{a} + q^2) + q^2 + \frac{15}{8}((4\hat{\mathbf{a}}_1 \cdot \mathbf{a})^2 + 4\hat{\mathbf{a}}_1 \cdot \mathbf{a} q^2 + q^4) + \cdots] \nu d\tau \tag{2.36}$$

$$= \frac{-Gm'}{r_c^2} \int \hat{\mathbf{a}}_1 [1 - \frac{3}{2}(2\hat{\mathbf{a}}_1 \cdot \mathbf{a} + q^2) + \frac{15}{2}(\hat{\mathbf{a}}_1 \cdot \mathbf{a}\mathbf{a})] + \mathbf{a}[1 - 3\hat{\mathbf{a}}_1 \cdot \mathbf{a}] \nu d\tau \tag{2.37}$$

The following observations are made:

1. $\int \mathbf{a} \nu d\tau = 0$ because $\int \frac{\mathbf{r}}{r_c} \nu d\tau = 0$ since $\mathbf{r}$ is measured from the center of mass
2. $\int \hat{\mathbf{a}}_1 \cdot \mathbf{a} \nu d\tau = 0$ for reasons same as above.
3. $\int \hat{\mathbf{a}}_1 \nu d\tau = \hat{\mathbf{a}}_1 \int dm = M \hat{\mathbf{a}}_1$

The external gravity force takes the following form after some mathematical simplifications:

$$\mathbf{F} = -\frac{Gm'}{r_c^2}M\hat{\mathbf{a}}_1 + \frac{3}{2}\frac{Gm'}{r_c^2}\Big[\hat{\mathbf{a}}_1\int(\frac{r}{r_c})^2\mathrm{d}m - 5\hat{\mathbf{a}}_1(\hat{\mathbf{a}}_1\cdot\frac{\mathbf{r}}{r_c})\mathrm{d}m + 2\int(\frac{\mathbf{r}}{r_c})\hat{\mathbf{a}}_1\cdot\frac{\mathbf{r}}{r_c}\mathrm{d}m\Big] \tag{2.38}$$

Expanding and simplifying, we obtain the expression for the gravity force acting on the differential mass element.

$$\mathbf{F} = -\frac{GMm'}{r_c^2}\hat{\mathbf{a}}_1 + \frac{3}{2}\frac{Gm'}{r_c^4}\Big[\hat{\mathbf{a}}_1\int r^2\mathrm{d}m - 5\hat{\mathbf{a}}_1\hat{\mathbf{a}}_1\int\mathbf{r}\mathbf{r}\mathrm{d}m\cdot\hat{\mathbf{a}}_1 + 2\int\mathbf{r}\mathbf{r}\mathrm{d}m\cdot\hat{\mathbf{a}}_1\Big] \tag{2.39}$$

Noting that all of the three integrals given above are related to the inertia tensor of the body about its center of mass, $I_{\mathcal{B}}$. Specifically,

$$\text{trace}(I_{\mathcal{B}}) = 2\int r^2\nu d\tau \tag{2.40}$$

$$\int\mathbf{r}\mathbf{r}\nu d\tau = \frac{[1]\text{trace}(I_{\mathcal{B}})}{2} - I_{\mathcal{B}} \tag{2.41}$$

Substituting these in the expression for gravity force, the following is obtained.

$$\mathbf{F} = -\frac{Gm'M}{r_c^2}[\hat{\mathbf{a}}_1 + \sum_{i=2}^{\infty}\mathbf{f}^{(i)}] \tag{2.42}$$

$$\text{with } \mathbf{f}^{(2)} = \frac{1}{mr_c^2}\Big[\frac{3}{2}[\text{tr}(I_{\mathcal{B}}) - 5\hat{\mathbf{a}}_1\cdot I_{\mathcal{B}}\cdot\hat{\mathbf{a}}_1]\Big]\hat{\mathbf{a}}_1 + 3I_{\mathcal{B}}\cdot\hat{\mathbf{a}}_1 \tag{2.43}$$

Note that $\hat{\mathbf{a}}_1$ is the unit vector along the radial direction in the orbit frame and $I_{\mathcal{B}}$ is the inertial tensor in the body frame. The gravity gradient torque is then simply obtained as $\mathbf{l}_c = -\mathbf{r}_c \times \mathbf{F}$ which can be expanded and simplified as

$$\mathbf{l}_c = \frac{3Gm'}{r_c^3}\hat{\mathbf{a}}_1 \times I_{\mathcal{B}}\cdot\hat{\mathbf{a}}_1 \tag{2.44}$$

Expressing the body frame and the orbit frame through a direction cosine matrix is the attitude parameters (like Euler angles or CRPs), the final expression for the gravity-gradient torque is

obtained as follows.

$$\mathbf{l}_c = \frac{3Gm'}{r_c^3}\Big[C_{13}C_{12}(I_3 - I_2)\hat{\mathbf{b}}_1 + C_{11}C_{13}(I_1 - I_3)\hat{\mathbf{b}}_2 + C_{11}C_{12}(I_2 - I_1)\hat{\mathbf{b}}_3\Big] \tag{2.45}$$

Thus, the rigid body equations of motion under the influence of gravity-gradient torques can be written in their complete form as:

$$\begin{aligned} I_1\dot{\omega}_1 + (I_3 - I_2)\omega_2\omega_3 &= 3\Omega^2(I_3 - I_2)C_{12}C_{13} \\ I_2\dot{\omega}_2 + (I_1 - I_3)\omega_1\omega_3 &= 3\Omega^2(I_1 - I_3)C_{11}C_{13} \\ I_3\dot{\omega}_3 + (I_2 - I_1)\omega_2\omega_1 &= 3\Omega^2(I_2 - I_1)C_{12}C_{11} \end{aligned} \tag{2.46}$$

with $\Omega = \sqrt{Gm'/r_c^3}$. At this stage, three sets of inertia parameters are defined as follows:

$$K_1 = \frac{I_2 - I_3}{I_1} \qquad K_2 = \frac{I_3 - I_1}{I_2} \qquad K_3 = \frac{I_1 - I_2}{I_3}$$

The equations of motion are then rewritten in terms of the inertia parameters as:

$$\begin{aligned} \dot{\omega}_1 - K_1\omega_2\omega_3 &= -3\Omega^2 K_1 C_{12}C_{13} \\ \dot{\omega}_2 - K_2\omega_1\omega_3 &= -3\Omega^2 K_2 C_{11}C_{13} \\ \dot{\omega}_3 - K_3\omega_2\omega_1 &= -3\Omega^2 K_3 C_{12}C_{11} \end{aligned} \tag{2.47}$$

From a numerical analysis perspective, the dynamic equations are simulated along with the kinematic relations to obtain the time history of the evolution of the attitude parameters. Before diving into the characterization of motion, the inertia parameters are explained in detail.

2.3.2 Transformations between inertia parameters and the inertia tensor

Recall that the inertia parameters had the following relationship to the inertia tensor:

$$\begin{aligned} K_1 &= \frac{I_2 - I_3}{I_1} \\ K_2 &= \frac{I_3 - I_1}{I_2} \\ K_3 &= \frac{I_1 - I_2}{I_3} \end{aligned} \tag{2.48}$$

The three inertia parameters are not mutually independent. The following relation exists between K_3 and K_1, K_2:

$$K_3 = -\frac{K_1 + K_2}{1 + K_2 K_2} \tag{2.49}$$

Due to this relation, extracting the true inertia tensor elements from the inertia parameters is impossible, because the inertia parameters map to infinite combination of the inertia tensor elements. With respect to an arbitrary scaling parameter, in the values of I_1, I_2 and I_3, the following relations are obtained and tabulated in Tab. 2.1. The scaling parameters are α, β, and γ applied to I_1, I_2, and I_3, respectively.

Table 2.1: Transformations between inertia parameters and inertia tensor elements

I_1	α	$\beta\frac{1-K_2}{1+K_1}$	$\gamma\frac{1-K_2}{1+K_1K_2}$
I_2	$\alpha\frac{K_1+1}{1-K_2}$	β	$\gamma\frac{1+K_1}{1+K_1K_2}$
I_3	$\alpha\frac{1+K_1K_2}{1-K_2}$	$\beta\frac{1+K-1K_2}{1+K_1}$	γ

The mass distribution of the rigid body can therefore be described using only two inertia parameters: K_1 and K_2. For parametric studies of the motion of the rigid body, the space of $K_1 - K_2$ shall be used to qualitatively ascertain the nature of attitude motion. A complete description of the attitude motion required the combination of the attitude kinematics and the attitude dynamics equations. From previous sections, it is known that the dynamic and kinematic counterparts can be

combined to obtain the governing equations of motion for a rigid body. In the following section, the governing equation of a rigid body in Keplerian motion is derived and subjected to qualitative analysis.

2.4 Rigid body in Keplerian motion

The attitude dynamics of a rigid body in Keplerian motion is an important problem in astrodynamics [2, 36, 37, 38, 39, 40, 41, 42, 43, 44]. There are a great many practical situations such as communications, remote sensing, environmental monitoring, weather forecasting, etc., where it is required to maintain the satellite in a preferred orientation with respect to the Earth. Understanding the realm of possible orientations and the nature of deviations from them as a function of the satellites' mass distribution and orbital parameters is of utmost importance to achieve these goals. The main component of attitude motion pertaining to these goals is the analysis of the pitch DOF: i.e., the attitude motion of the rigid body about the nominal body-fixed axis aligned with the orbit normal, and its perturbations resulting from the inverse-square gravitational force.

There is extensive literature on the study of attitude motion [36, 45, 38, 44, 46, 40, 42, 47, 43, 48]. DeBra and Delp [36] carried out early parametric studies of the stability of attitude motion of a rigid body in the presence of gravitational torque. They studied the attitude dynamics of a rigid body in a circular orbit and discovered the regions of stable and unstable attitude motions about the origin in the inertia parameter space. Two regions in the parameter space were identified in this work: a Lagrange region, which is shown to be statically stable under linear analysis, and the DeBra-Delp [36] region, which is found to be linearly stable due to the gyroscopic terms. Euler angles were used to parameterize the attitude of the rigid body orbiting around the primary in a circular orbit. Kane [2] further extended this analysis to show that the stability of the equilibrium point does not depend on the inertia parameters alone but also on the amplitude of pitch oscillation. Both analyses rely on linearizing the attitude motions with the assumptions of small angular deviations from the equilibrium positions. Furthermore, small-angle approximations were made to obtain strong starting solutions to the coupled transcendental equations governing the equilibria.

The study of the stability of the equilibria of the attitude motions of a rigid body and its libra-

tions about them can be broadly classified into two techniques: *Numerical and Analytical*. Numerical techniques were employed to investigate the stability of the equilibrium point corresponding to the planar pitch degree of freedom [45, 38, 42, 47, 49]. These investigations revealed natural properties of the pitch dynamics about the origin as a function of the design parameters. Kane's [2] original observation that the pitch motion can be decoupled from the roll–yaw motion forms a basis for these studies. The existence of periodic motions and prediction of the onset of chaos were investigated for such motions [45, 38, 50, 42, 47]. Numerical approaches such as Poincaré surfaces were used by Karasopoulos and Richardson [38] and Tong and Rimrott [43] to identify regions of periodic, quasi-periodic and chaotic motions in the phase-space associated with the pitch degree-of-freedom. Lyapunov exponents [38] were used to numerically quantify the rate of divergence of neighboring trajectories as a measure of chaos. The quantitative measures thus obtained formed a basis to indicate chaotic behavior exhibited in the attitude dynamics of a rigid body in Keplerian motion. Floquet theory [2], chaos diagrams, and the Melnikov method [48] have also been used to study the planar pitch motion of a rigid body.

Literature documents extensive analytical studies on the spinning motion of rigid bodies in a Keplerian orbit [51, 44, 46, 52, 41, 40, 53]. These have led to the discovery of resonant commensurabilities in the natural frequency of motion of the rigid bodies [53, 41] and explained the physics behind some attitude phenomenon observed during numerical simulations which a linear analysis fails to accomplish. While these analytical studies are insightful in describing certain qualitative behavior of the motion, they fail to provide a complete understanding of the problem with the full nonlinear dynamics furnished by numerical techniques. Thus, there exists a gap between the analytical and numerical contributions to appreciate the physics of attitude motion of orbiting rigid bodies. This chapter develops analytical and semi-analytical approaches to bridge this gap, quantify the nature of attitude motion of an orbiting rigid body and reconcile the two approaches. Such techniques will be particularly useful in the study of long-term dynamics of uncontrolled space objects such as orbital debris where the attitude motion influence on the orbital dynamics is significant [54, 55, 56]. Also, the results and methodologies developed in the paper by Eapen et

al. [1, 57] can be applied to studying spacecraft mass distributions and its sensitivities to attitude motion for future space missions.

The present research focuses on the gravity-gradient perturbations that affect the rotational dynamics of a rigid body. Potential sources of external disturbance that cause undesirable pitching oscillations for certain values of the inertia parameter space are identified. In the first part of the chapter, the governing equations of motion are developed using the Classical Rodrigues Parameters (CRPs) to represent the orientation of the rigid body with respect to the orbital frame of reference. The assumption of an inverse-squared central force environment is shown to result in a one-way coupling between the pitch and roll–yaw attitude motions thereby allowing for the study of pitching motion exclusively. Parametric investigation in the eccentricity-inertia space is used to identify regions of libratory and circulatory behavior in the pitch oscillations for a rigid body in an eccentric orbit. The limiting case of zero eccentricity has some interesting dynamical properties. The conservative nature of the gravity-gradient torques permits certain simplifications allowing its treatment in an analytical fashion. An integral of motion is obtained in algebraic form resulting in a reduced dimension analysis of the pitch dynamics. An analytical limit for the separatrix is obtained as a function of the inertia parameter delineating the boundary between libratory and circulatory behaviors. To motivate the discussion for the attitude motion of a rigid body in a Keplerian orbit, the geometrical set-up of the problem is discussed.

2.4.1 The geometry of the problem

Three reference frames are used to describe the orientation of the rigid body with respect to the central body. They are illustrated in Fig. 2.30. The Inertial reference frame ($N\{\mathbf{n}_1, \mathbf{n}_2, \mathbf{n}_3\}$) has its origin at the center of the Earth with the $\hat{\mathbf{n}}_1$ axis along the vernal equinox, $\hat{\mathbf{n}}_3$ axis towards the north pole and the $\hat{\mathbf{n}}_2$ axis completing the dextral orthonormal set. The Orbital reference frame ($A\{\mathbf{a}_1, \mathbf{a}_2, \mathbf{a}_3\}$) has its origin at the center of mass of the rigid body with the $\hat{\mathbf{a}}_1$ axis directed towards the radial direction, $\hat{\mathbf{a}}_3$ axis along the orbit normal and $\hat{\mathbf{a}}_2$ completing the set. This coordinate frame is obtained by a 3-1-3 rotation through the angles: Ω (right ascension of the ascending node), i (inclination) and u, (argument of latitude $(\omega + f)$). The Body frame ($B\{\mathbf{b}_1, \mathbf{b}_2, \mathbf{b}_3\}$) has its origin

at the center of mass of the rigid body with its axes directed along the directions of the principal moments of inertia.

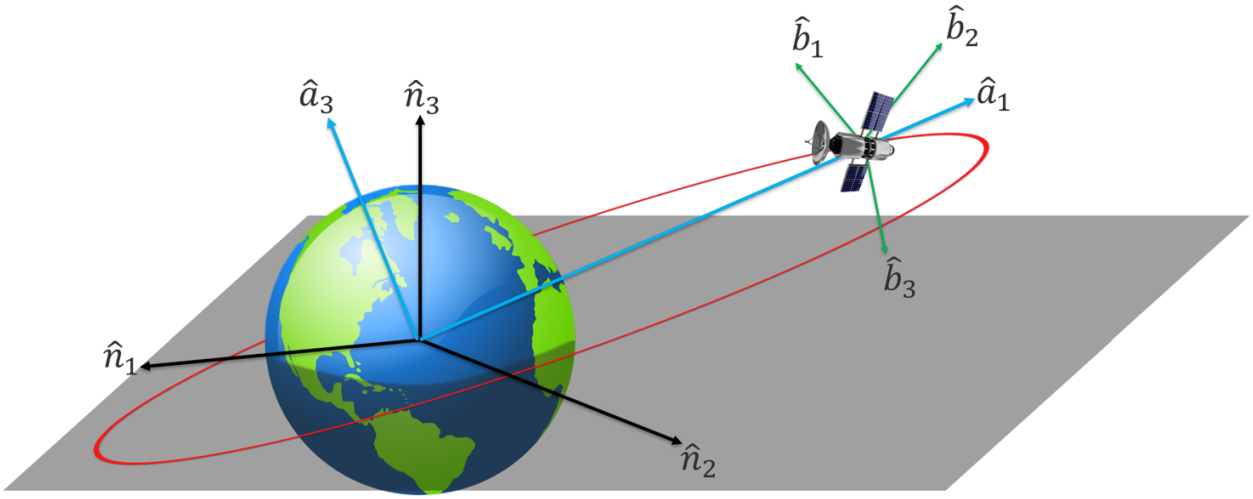

Figure 2.3: Rigid body set-up: The rigid body is orbiting a primary in a Keplerian orbit with $\hat{\mathbf{n}}_i$ representing the inertial coordinate frame, $\hat{\mathbf{a}}_i$ the orbit frame and $\hat{\mathbf{b}}_i$ the body-fixed coordinate frame.

The general case of Keplerian motion with the semimajor axis (a) and eccentricity (e) is studied. The kinematics of attitude motion is described with the aid of Classical Rodrigues Parameters (CRP): $\mathbf{q} = [q_1, q_2, q_3]^T$. The CRPs are related to the principal axis (e_i) of rotation of the rigid body and the principal angle (ϕ) and through the relation $q_i = e_i \tan\frac{\phi}{2}$ [29]. Therefore, the singularity condition in the CRPs occurs when the principal angle is 180 deg. The kinematic relations are then given by [32, 29]

$$\dot{\mathbf{q}} = \mathcal{A}\boldsymbol{\omega}_{B/A} \qquad \text{where, } \mathcal{A} = \frac{1}{2}(I_{3\times3} + [\tilde{q}] + \mathbf{q}\mathbf{q}^T) \text{ and } [\tilde{q}] = \begin{bmatrix} 0 & -q_3 & q_2 \\ q_3 & 0 & -q_1 \\ -q_2 & q_1 & 0 \end{bmatrix} \tag{2.50}$$

$$\boldsymbol{\omega}_{B/A} = \mathcal{B}\dot{\mathbf{q}} \qquad \text{where, } \mathcal{B} = \frac{2}{1+\mathbf{q}^T\mathbf{q}}(I_{3\times 3} - [\tilde{q}]) \tag{2.51}$$

The direction cosine matrix is given by [32, 29]:

$$[C] = [I_{3\times 3}] - \frac{2}{1+\mathbf{q}^T\mathbf{q}}[\tilde{q}] + \frac{2}{1+\mathbf{q}^T\mathbf{q}}[\tilde{q}][\tilde{q}] \tag{2.52}$$

The CRPs are a favorable set of parameters to use because they are a symmetric stereographic set which exhibit uniqueness [58]. Furthermore, the use of CRPs enables us to obtain purely algebraic expressions for the governing equations of motion as opposed to transcendental expressions when using Euler angles. The domain of linearization is also quite large as compared to the Euler angle parametrization [58]. The conversion from CRPs to the direction cosine matrix is also easily performed using the Cayley transform identity [32, 29].

$$C(q) = ([I_{3\times 3}] - [\tilde{q}])([I_{3\times 3}] + [\tilde{q}])^{-1}$$

It is noted that the direction cosine matrix transforms the vectors in the body frame to the orbital frame. Thus, the angular velocity of the rigid body relative to the orbital frame is $\boldsymbol{\omega}_{B/A} = \mathcal{B}\dot{\mathbf{q}}$. The angular velocity of the orbital frame relative to the inertial is given by $\boldsymbol{\omega}_{A/N} = \frac{df}{dt}\hat{a}_3$, where f is the true anomaly. To obtain a more physical representation, let us consider three Euler angles $(\theta_1, \theta_2, \theta_3)$ to be the yaw, roll and pitch angles, respectively. The pitch motion is defined as the motion in the orbital plane, i.e., about the orbit normal. The yaw and roll motions are described as about the first and second axes, respectively.

In setting up the problem, the transformation from the orbital frame to the body frame is done by performing a 1-2-3 Euler angle sequence rotation by angles θ_1, θ_2, and θ_3, respectively. Utilizing the DCM described using the CRP attitude parameters, the governing equations of motion are obtained in the following subsection.

2.4.2 Governing equations of motion

The attitude dynamics of a rigid body subjected to gravity-gradients is a well-studied problem [37, 45, 38, 42, 53, 48, 43]. The expression for gravity-gradient torque is given as follows [59, 29, 32, 60]:

$$\mathbf{M} = \frac{3\mu}{r^3}(\hat{\mathbf{a}}_1 \times I_B \cdot \hat{\mathbf{a}}_1) \tag{2.53}$$

Here, μ is the gravitational parameter, r is the distance from the center of the earth to the center of mass of the rigid body ($r = p/(1 + e\cos f)$), p is the semi-parameter ($p = a(1 - e^2)$), e is the eccentricity of the orbit, I_B is the inertia tensor expressed in the body frame about the center of mass of the rigid body and $\hat{\mathbf{a}}_1$ is the unit vector along the radial direction.

Differentiating Eq. (2.98) and substituting into Euler's equations of motion, we obtain the differential equation governing the attitude motion of the rigid body in a Keplerian orbit. We have

$$\boldsymbol{\omega}_{B/A} = \mathcal{B}\dot{\mathbf{q}} \tag{2.54}$$

$$\boldsymbol{\omega}_{A/N} = \frac{df}{dt}\hat{a}_3 = \frac{h}{r^2}\hat{a}_3 \tag{2.55}$$

$$\dot{\boldsymbol{\omega}_{A/N}} = \frac{d}{dt}\Big(\frac{h}{r^2}\hat{a}_3\Big) = \frac{-2h^2}{r^4}\frac{e\sin f}{1 + e\cos f}\hat{a}_3 \tag{2.56}$$

$$\dot{\boldsymbol{\omega}_{B/N}} = K\mathbf{M} \tag{2.57}$$

$$\boldsymbol{\omega}_{B/N} = \boldsymbol{\omega}_{B/A} + \boldsymbol{\omega}_{A/N} \tag{2.58}$$

$$\dot{\boldsymbol{\omega}_{B/A}} = \mathcal{B}\ddot{\mathbf{q}} + \dot{\mathcal{B}}\dot{\mathbf{q}} \tag{2.59}$$

$$\begin{aligned}
\ddot{\mathbf{q}} &= \mathcal{B}^{-}1(\dot{\boldsymbol{\omega}_{B/A}} - \dot{\mathcal{B}}\dot{\mathbf{q}}) \\
&= \mathcal{A}(\dot{\boldsymbol{\omega}_{B/A}} - \dot{\mathcal{B}}\dot{\mathbf{q}}) \\
&= \mathcal{A}(\dot{\boldsymbol{\omega}_{B/N}} - \dot{\boldsymbol{\omega}_{A/N}} - \boldsymbol{\omega}_{A/N} \times \boldsymbol{\omega}_{B/A}) \\
&= \mathcal{A}\Big(K\mathbf{M} + 2\frac{h^2}{r^4}\frac{e\sin f}{1 + e\cos f}\hat{a}_3 - \frac{h}{r^2}\hat{a}_3 \times \mathcal{B}\dot{\mathbf{q}}\Big)
\end{aligned} \tag{2.60}$$

The following regularization is considered to change the independent variable to the true anomaly [50, 61]:

$$\frac{d()}{dt} = \frac{h}{r^2}\frac{d()}{df} \tag{2.61}$$

$$\frac{dr}{dt} = \frac{hp}{r^2}\frac{e\sin f}{(1+e\cos f)^2} \tag{2.62}$$

$$\frac{d^2()}{dt^2} = \frac{h^2}{r^4}\frac{d^2()}{df^2} - \frac{2h}{r^3}\frac{hpe\sin f}{r^2(1+e\cos f)^2}\frac{d()}{df} \tag{2.63}$$

where h is the specific orbital angular momentum and is given by the relation: $h = \sqrt{\mu p}$ and f is the true anomaly. The equations governing the attitude motion of the rigid body is then obtained using true anomaly as the independent variable.

$$\mathbf{q}'' = \mathcal{A}\Big(K\mathbf{M} + \frac{2e\sin f}{1+e\cos f}(\hat{a}_3 + \mathbf{q}') - \mathcal{B}'\mathbf{q}' - \hat{a}_3 \times \mathcal{B}\mathbf{q}'\Big) \tag{2.64}$$

where $()' = \frac{d()}{df}$, $\mathcal{A}$ is given in Eq. (2.50), $K = \text{diag}[K_1, K_2, K_3]$ is a diagonal matrix with inertia parameters such that $K_1 = \frac{I_3 - I_2}{I_1}$, $K_2 = \frac{I_1 - I_3}{I_2}$, $K_3 = \frac{I_2 - I_1}{I_3}$, $\mathbf{M}$ is the expression for $\dot{\boldsymbol{\omega}}_{B/N}$ obtained from Euler's equations of rotational motion and the expression for $\mathcal{B}'$ is obtained by differentiating Eq. (2.98). They are delineated in Eq. (2.65) below:

$$M_1 = -\frac{2\,(q_1 + \mathrm{q}_2' + q_2\,q_3 + q_1\,\mathrm{q}_3' - q_3\,\mathrm{q}_1')\,(-{q_1}^2 - 2\,\mathrm{q}_2'\,q_1 - {q_2}^2 + 2\,\mathrm{q}_1'\,q_2 + {q_3}^2 + 2\,\mathrm{q}_3' + 1)}{({q_1}^2 + {q_2}^2 + {q_3}^2 + 1)^2} - \frac{3\,(2\,q_2 + 2\,q_1\,q_3)\,(2\,q_3 - 2\,q_1\,q_2)}{(e\,\cos(f) + 1)\,({q_1}^2 + {q_2}^2 + {q_3}^2 + 1)^2} \tag{2.65a}$$

$$M_2 = \frac{3\,(2\,q_2 + 2\,q_1\,q_3)\,({q_1}^2 - {q_2}^2 - {q_3}^2 + 1)}{(e\,\cos(f) + 1)\,({q_1}^2 + {q_2}^2 + {q_3}^2 + 1)^2} - \frac{2\,(\mathrm{q}_1' - q_2 + q_1\,q_3 - q_2\,\mathrm{q}_3' + q_3\,\mathrm{q}_2')\,(-{q_1}^2 - 2\,\mathrm{q}_2'\,q_1 - {q_2}^2 + 2\,\mathrm{q}_1'\,q_2 + {q_3}^2 + 2\,\mathrm{q}_3' + 1)}{({q_1}^2 + {q_2}^2 + {q_3}^2 + 1)^2} \tag{2.65b}$$

$$
\begin{aligned}
M_3 = &-\frac{4\,(q_1 + \mathrm{q}_2' + q_2\,q_3 + q_1\,\mathrm{q}_3' - q_3\,\mathrm{q}_1')\,(\mathrm{q}_1' - q_2 + q_1\,q_3 - q_2\,\mathrm{q}_3' + q_3\,\mathrm{q}_2')}{\left({q_1}^2 + {q_2}^2 + {q_3}^2 + 1\right)^2} \\
&- \frac{3\,(2\,q_3 - 2\,q_1\,q_2)\,\left({q_1}^2 - {q_2}^2 - {q_3}^2 + 1\right)}{(e\,\cos(f) + 1)\,\left({q_1}^2 + {q_2}^2 + {q_3}^2 + 1\right)^2}
\end{aligned}
\tag{2.65c}
$$

Since the gravity-gradient torque is conservative, we can develop the expression for the conserved total energy. The total energy of the rigid body can be computed by summing up the kinetic and potential energies associated with both translational and rotational motion of the body. For an object in Keplerian orbit, the translational energy is given by

$$E_t = K_t + V_t \tag{2.66}$$

$$= \frac{1}{2}|\mathbf{v}|^2 - \frac{\mu}{r} = \frac{1}{2}\Big(\frac{2\mu}{r} - \frac{\mu}{a}\Big) - \frac{\mu}{r} = -\frac{\mu}{2a} \tag{2.67}$$

The rotational kinetic energy of the rigid body is given by:

$$T_r = \frac{1}{2}\boldsymbol{\omega}_{B/N}^T I_B \boldsymbol{\omega}_{B/N} \tag{2.68}$$

where $\boldsymbol{\omega}_{B/N} = \boldsymbol{\omega}_{B/A} + \boldsymbol{\omega}_{A/N}$ The rotational potential energy of the rigid body is given by:

$$V_r = \frac{\mu}{2r^3}(3\hat{\mathbf{a}}_1^T I_B \hat{\mathbf{a}}_1 - \text{trace}(I_B)) \tag{2.69}$$

Landau & Lifshitz [62] provide the expression that relates the energies in an inertial reference frame and a non-inertial reference frame as:

$$E = E_{\text{inertial}} + \Delta E = E_{\text{inertial}} - \mathbf{L} \cdot \boldsymbol{\omega}_{A/N} \tag{2.70}$$

$$E = E_t + E_r - \frac{h}{r^2}\hat{a}_3^T I_B \boldsymbol{\omega}_{B/N} = \text{constant} \tag{2.71}$$

where $E_r = T_r + V_r$. Here, E_t is the energy associated with the two-body motion, E_r is that associated with the rotational motion and $\mathbf{L}$ is the specific angular momentum of the rigid body. The two-body energy is much larger than its rotational counterpart. This measure of energy (E) is used for parametric investigations into the nature of attitude motion.

Qualitative analysis of the attitude motion of a rigid body is hierarchically developed in the following subsections. These investigations are classified into the following four categories:

1. Pitch attitude dynamics of a rigid body in circular orbit.
2. Pitch attitude dynamics of a rigid body in eccentric orbit
3. Full 3-DOF roll-pitch-yaw dynamics in circular orbit
4. Full 3-DOF roll-pitch-yaw dynamics in eccentric orbit

Kane's [2] observation that the pitch motion decouples from the roll-yaw motion is the premise for the development of the first two categories mentioned above. This one-way decoupling enables us to obtain multiple geometric insight into the planar pitch motion of a rigid body. Examining this pitch motion is detrimental to maintain a desirable pointing accuracy of satellites in many applications such as communications, remote sensing, environmental monitoring, weather forecasting, etc.

2.4.3 Planar pitch dynamics of a rigid body in circular orbit

The case of a rigid body in a circular orbit (eccentricity $e = 0$) is examined. The rigid body is assumed to be of arbitrary shape and is defined using the inertia parameters K_1, K_2 and K_3. The equilibrium points for this system are identified, and the stability of oscillations about it is studied.

To obtain the equations of motion for the circular orbit case, we set the eccentricity ($e = 0$) in Eq. (2.64). For a circular orbit, we note $\frac{df}{dt} =$ constant, i.e., the independent variable (true anomaly, f) can be switched to time (t) without loss of information. Thus, Eq. (2.64) becomes

$$\ddot{\mathbf{q}} = \frac{1}{2}(I_{3\times 3} + \tilde{q} + \mathbf{q}\mathbf{q}^T)K_3\mathbf{G} + \frac{2\mathbf{q}^T\dot{\mathbf{q}}}{1 + \mathbf{q}^T\mathbf{q}}\dot{\mathbf{q}} \tag{2.72}$$

Eq. (2.82) gives us the complete nonlinear dynamics of a rigid body under the influence of gravity-gradient torques. The following section describes in detail the circumstances under which the pitch motion decouples from the roll and yaw motions.

2.4.3.1 The one way decoupling of pitch and roll-yaw motion

The expressions for $\ddot{q}_1$ and $\ddot{q}_2$ are identically zero when we set the initial conditions: $[q_1, q_2, \dot{q}_1, \dot{q}_2]$ = $[0, 0, 0, 0]$. This implies that the pitch dynamics can be studied with investigation of the roll-yaw motions for the initial condition $[q_1, q_2, q_3, \dot{q}_1, \dot{q}_2, \dot{q}_3] = [0, 0, q_{3_0}0, 0, \dot{q}_{3_0}]$. It is to be noted here that we are not in any way implying that the pitch motion does not affect roll and yaw motion and neither that the roll-yaw motion affects the pitch motion. This special circumstance due to the initial condition selection allows us to investigate pitch motion exclusively. Throughout this work, the one-way decoupling phenomenon mentioned is exactly that due to initial condition selection. One must not forget that due to energy conservation, there is coupling between the roll-pitch-yaw motions. Roll and yaw are linearly coupled and decoupled from pitch. But they are always nonlinearly coupled.

Based on this discussion, the governing equation for the pitch dynamics admits a one-way coupling between the pitch and roll-yaw motion. The pitch equation of motion can them be given by:

$$\ddot{q}_3 = \frac{3\Omega^2 K_3 q_3(q_3^2 - 1) + 2q_3\dot{q}_3^2}{1 + q_3^2} \tag{2.73}$$

where $\Omega = \sqrt{\frac{\mu}{r^3}}$ and K_3 is the asphericity parameter and is given by $K_3 = \frac{I_2 - I_1}{I_3}$. The first integral

is then obtained as:

$$F^2 = \frac{\dot{q}_3^2 + 3\Omega^2 K_3 q_3^2}{(1+q_3^2)^2} = \text{constant} \tag{2.74}$$

From a dynamical systems point of view, this constant of motion gives global information about the solutions of the system. Fixing this constant allows us to obtain a co-dimension one sub-manifold of the phase-space. Thus, we can rewrite the equation of motion by reducing one degree of freedom as in Eq. (2.75). Then, an initial condition with this integral constant will stay on that integral manifold for all time.

$$\dot{q}_3^2 = F^2(1-q_3^2) - 3\Omega^2 K_3 q_3^2 \tag{2.75}$$

Redefining the constant of integration in a different way helps gain some insight into the one-dimensional system in Eq. (2.75). The constant of motion is written in terms of a new variable (λ) and is defined as follows:

$$F^2 = 3K_3\Omega^2\lambda^2 \tag{2.76}$$

Equation (2.75) can then be written as:

$$\dot{q}_3^2 = F^2\Big((1-q_3^2)^2 - \frac{1}{\lambda^2}q_3^2\Big) \tag{2.77}$$

The study of the variable λ gives insight into the pitching motion of a gravity-gradient satellite in circular orbit. From analysis of the eigenvalues of the system, the pitching motion is libratory for values of $\lambda > \frac{1}{2}$ and tumbling for $\lambda < \frac{1}{2}$. Motion along a separatrix would occur in the limit as $\lambda \to \frac{1}{2}$, but this type of motion would require an infinite period and is physically impossible. The constant of motion for the separatrix curve is then given as a pure function of the inertia parameter: $F = \sqrt{\frac{3K\Omega}{4}}$

Eq. (2.74) is a constant of pitching motion with a phase portrait representing a simple pendulum. For a given value of the constant and one phase-space variable, the other can be com-

puted analytically. Thus, the complete phase portrait can be obtained given the initial conditions for the motion. Due to energy conservation, the extremities of the phase-space trajectory ($[q_{3_{\max}}, q_{3_{\min}}]$,$[\dot{q}_{3_{\max}}, \dot{q}_{3_{\max}}]$) can be computed as well. It is worthwhile to note that the first integral is not a transcendental function, as one would obtain if one were to use Euler angles to write the governing equations. This expression was obtained by Modi and Brereton [42] in transcendental form. The separatrix curves for different values of the inertia parameter are as shown in Fig. 2.4

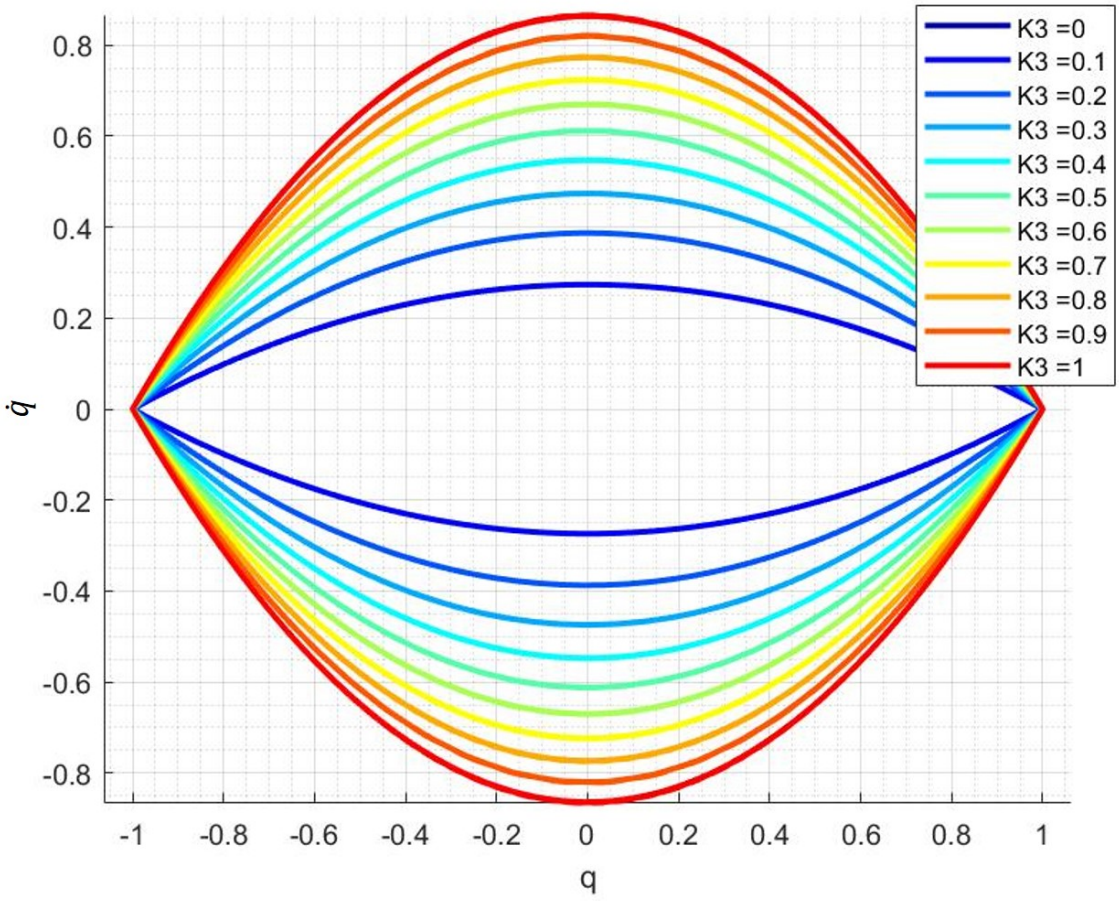

Figure 2.4: Phase-plane plot of separatrix curves for inertia parameters: $K_3 = [0, 1]$

Now, while the equations of pitching motion are expressed in CRP attitude parameters, the conversion to Euler angles is straightforward. Recalling that the CRPs are obtained by $\mathbf{q} = \tan(\phi/2)\hat{e}$,

the Euler angle and angle rate associated with the pitch motion is given as

$$\theta = 2\tan^{-1} q_3 \tag{2.78}$$

$$\dot{\theta} = \frac{2\dot{q}_3}{1+q_3^2} \tag{2.79}$$

which reduces the pitch equation of motion in terms of the Euler angles as:

$$\ddot{\theta} + \frac{3}{2}K_3 \sin 2\theta = 0 \tag{2.80}$$

which is the differential equation for the simple pendulum as expected. In the following section, the analysis of pitch attitude dynamics is examined in the general case of arbitrary eccentric orbit.

2.4.4 Pitch attitude dynamics of a rigid body in eccentric orbit

The case of a rigid body in an eccentric orbit (eccentricity $e = (0, 1]$) is examined. The rigid body is assumed to be of arbitrary shape and is defined using the inertia parameters K_1, K_2 and K_3. The orbit-attitude plane geometry can be described with reference to Fig. 2.5.

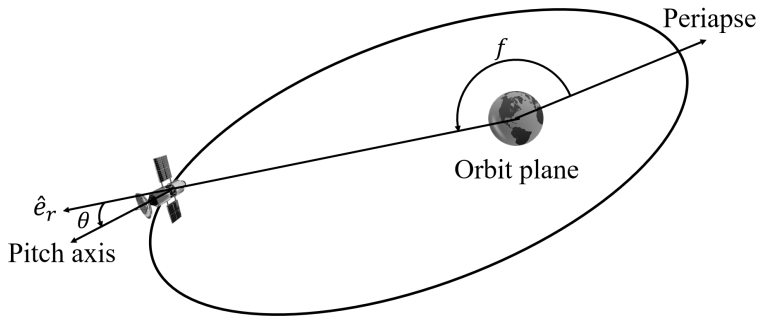

Figure 2.5: Orbit-Attitude geometry. The pitch motion is defined as the motion in the orbital plane, i.e., about the orbit normal.

In Fig. 2.5, the $\hat{e}_r$ is the radial direction, θ is the pitching angle, and f is the true-anomaly. Utilizing the regularization considered in Equations (2.61-2.63), the equations of motion are expanded

using true-anomaly as the independent variable in Eq. (2.64). Eq. (2.64) gives the complete non-linear dynamics of a rigid body under the influence of gravity-gradient torques. The expressions for q_1'' and q_2'' are identically zero when we set the initial conditions: $[q_1, q_2, q_1', q_2'] = [0, 0, 0, 0]$. The governing equation for the pitch dynamics admits a one-way coupling between the pitch and roll-yaw motion. The pitch equation of motion is then obtained in the same way as in the circular orbit case, and is as follows.

$$q_3'' = \frac{1}{1+q_3^2}\Big(2q_3{q_3'}^2 + \frac{e\sin f}{1+e\cos f}(1+q_3') - \frac{1}{1+e\cos f}3K_3q_3(1-q_3^2)\Big) \tag{2.81}$$

Eq. 2.81 allows for study of pitch motion exclusively. Recall here that $K_3 = \frac{I_2-I_1}{I_3}$ is the inertia parameter, e is the eccentricity of the orbit, and f is the true anomaly of the rigid body in the orbit. While the motions in roll-yaw result in a change in pitch motion, the pitch dynamics do not excite roll-yaw modes. There exists a one-way coupling between the pitch and roll-yaw motion resulting from the zero initial conditions in the state-space components associated with roll and yaw. Eq. 2.81 is a second-order ordinary differential equation with periodic coefficients and external forcing through the eccentricity variable. The behavior of the rigid body can be classified as librations or circulations. Librations occur physically when the true motion about the pitch axis is bounded in the neighborhood of the pitch equilibrium. Circulation, however, results when the pitch angle cycles through all possible values: [0,2π], i.e. a windup in the pitch angle. These types of motions can be visualized from the well-known topology of the phase portrait of the pendulum [63]. The distinction is made using the separatrix trajectory: motions lying inside the separatrix curve exhibit librations, while trajectories lying in the exterior exhibit circulation. The CRPs are particularly useful in investigating these motions, since the transition from libratory motions to circulation occurs at the singularity condition.

These regions of circulation and librations are a function of the parameters of the dynamical system, i.e., the eccentricity and the inertia parameter. To obtain regions of libratory and circulatory motion, the eccentricity-inertia ($e - K_3$) parameter space is studied. It is observed that there are

certain regions in the $e - K_3$ space where arbitrarily small initial conditions will result in bounded oscillatory behavior of the pitch motion, while others result in a circulatory motion of the rigid body. This is investigated for initial conditions of the order of $1e - 2$ and for 200 revs of the rigid body around the earth. A parametric diagram identifying regions of libration and circulation is provided in Fig. 2.6

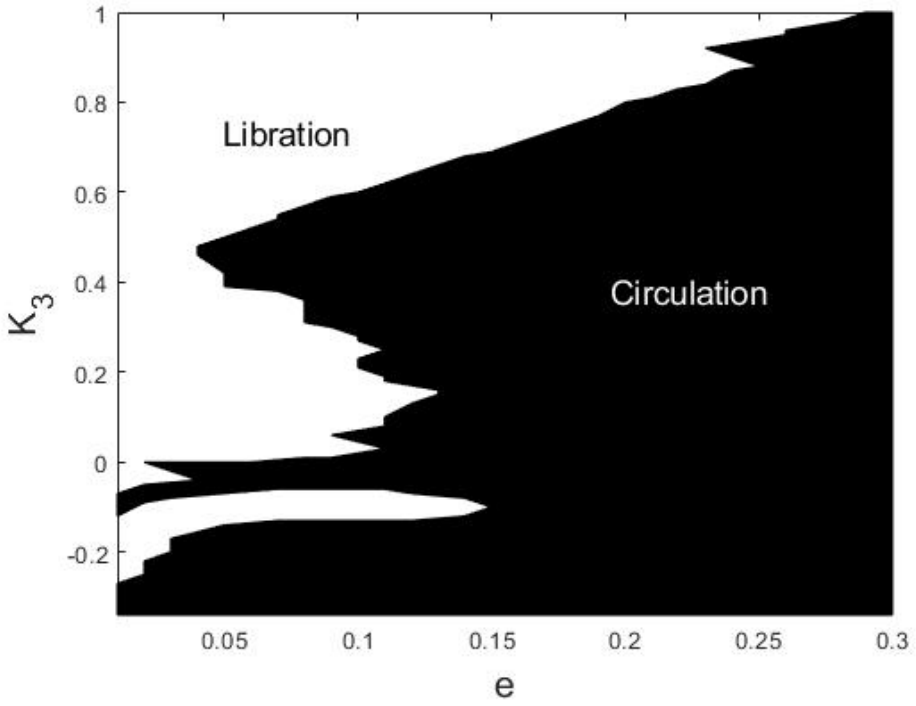

Figure 2.6: $K_3 - e$ parameter space: Regions in white have bounded motions while those in black result in an unbounded circulatory motion. Initial conditions are $[q_3, \dot{q}_3] = [0, 0]$. ©2020 Springer: *Celest Mech Dyn Astr*. Reprinted, with permission, from [1]

Figure 2.6 shows the regions of bounded motions for a small initial condition in [q_3,$\dot{q}_3$]. It is observed that the planar pitch motion for a rigid body in circular orbit is always stable when $K_3 > 0$. At higher eccentricities, we also obtain regions of bounded behavior when $K_3 < 0$. These regions are deemed unstable by linear analysis for a circular orbit. Zlatoustov [47] also obtained a similar result by investigating stability by the method of periodic coefficients. However, he obtained

regions beyond $e = 0.3$ to also be stable, which we did not obtain in the full numerical analysis of the equations of planar pitch motion. While numerical simulations and parametric analysis provide information about the boundedness of solutions, they may fail to identify certain internal symmetries of the existence of periodic, quasi-periodic and chaotic motions. DST provides us with certain geometric analysis tools that provide insight into the different dynamical phenomena in the pitch attitude motion of a rigid body. Particularly, we shall utilize two such techniques: the Poincaré surface of sections and the parametric bifurcation diagram.

2.4.4.1 Poincaré Surface of Sections (PSS)

The Poincaré map is defined in the state space. It serves as a map that transforms a continuous time flow into a discrete map of a dynamical system governed by a set of ordinary differential equations into. The Poincaré map is the intersection of a trajectory, which moves periodically, quasi-periodically, or chaotically, in an n-dimensional phase-space, with a surface transversal to the phase-space whose dimension is $n - 1$. The transversal condition implies that the normal of the hypersurface is not orthogonal to the tangent of the trajectory at the intersection point. More precisely, one considers a trajectory with initial conditions on the hyperplane and records the point at which this trajectory returns to the hyperplane. The PSS refers to the hyperplane, and the Poincaré map refers to the map of points in the hyperplane induced by the intersections.

A stroboscopic map contrasts the Poincaré map, which is that the hyper plane is defined in terms of the independent variable of the governing ordinary differential equations, i.e. time (t) or the true-anomaly (f). For periodically forced dynamical systems, including the pitch motion of a rigid body in Keplerian motion, the stroboscopic map often reveals hidden structures in the topology of the motion. The pitch dynamics are studied using a stroboscopic map of $(f \text{mod} 2\pi)$ in the phase plane $q - q'$. Both regular and chaotic motions are observed in the Poincaré maps. Periodic motion is characterized as fixed points on the map, quasi-periodic motions exhibit closed structures, and chaotic motions appear as non-ordered scattering points, which would completely fill an area of the PSS as the number of points, $N \to \infty$. Figure 2.7 presents 16 Poincaré maps for

eccentricities $e = 0.01, 0.05, 0.075, 0.15$ and the inertia parameter values $K_3 = [0.2, 0.5, 0.7, 0.9]$.

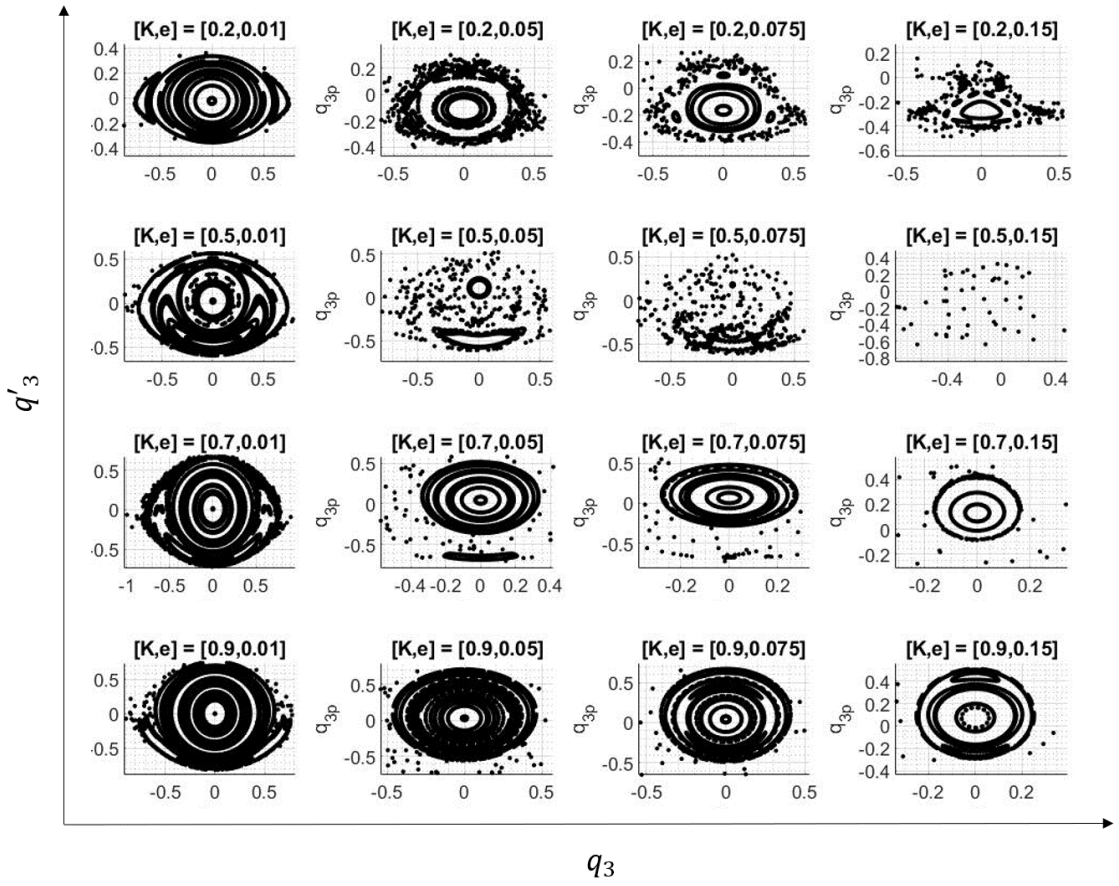

Figure 2.7: PSS for inertia and eccentricity parameter

In accordance with nonlinear dynamics theory, the general trend of the sequence of Poincaré maps is that with an increase in eccentricity, the area of the phase-space with regular motion shrinks, while chaotic motion expands [38]. Furthermore, from KAM theory [64, 65], the quasi-periodic motions are perceived to exist around periodic motions. Therefore, at the center of each closed curve, there exists a periodic orbit. The advantage of Poincaré maps is that the type of motion can be determined for an entire region of initial conditions in the phase-space. Figure 2.7 is obtained by propagating multiple initial conditions in the $q_3 - q_3'$ phase-space for 250 revolutions

of the rigid body about the central body. For example, one may deduce from the Poincaré map of $[K, e] = [0.5, 0.01]$ that a periodic orbit is obtained with an initial condition of $[q_{3_0}, q'_{3_0}] = [0, 0.019891]$. Similarly, another periodic orbit exists at $[q_{3_0}, q'_{3_0}] = [0, -0.474312]$. A disadvantage of Poincaré sections is that meticulous and lengthy sequences must be constructed to accurately estimate the parameter values at which a transition to chaos occurs for a particular initial state. While the initial condition response gives significant insight into the nature of motion, the effects of parameter variations on the motion of the rigid body (or any dynamical system in general) can be studied using bifurcation diagrams.

2.4.4.2 Bifurcation diagrams

Bifurcation diagrams are obtained using the same procedure as that of the Poincaré maps i.e. a system state is periodically sampled. However, rather than viewing the results in the phase-plane, the occurrence of states are recorded as a function of a parameter. Figure 2.9 illustrates the pitch angle bifurcation as a function of varying eccentricity for a fixed inertia parameter value of $K_3 = 1$. While the equations of motion are propagated using the CRP attitude parameterization, for physical intuition, the pitch Euler angle is plotted. The initial condition for the simulation is always taken to be $[q_3, q'_3] = [0, 0]$ to ensure that the behavior of motions is only due to the eccentricity forcing. Multiple period bifurcations can be observed in the bifurcation diagrams. Noting that the stroboscopic map records the states ($[\theta, \theta']$) at the perigee as a function of the eccentricity, a one period solution results in the pitch axis returning back to the same configuration after one orbit. Similarly, a three period solution results in the pitch axis returning back to the same configuration after three orbital periods. A schematic of n-period solutions and bifurcation points is shown below.

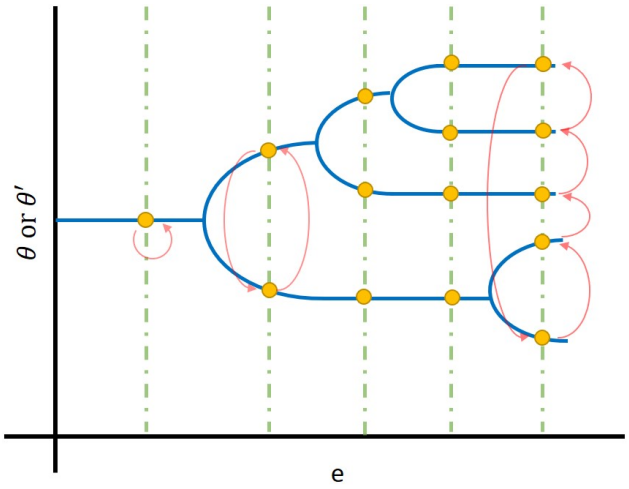

Figure 2.8: Schematic of $n-$period solutions and bifurcation points based on the eccentricity parameter

In Fig. 2.9, regions of regular and chaotic motions can be identified. A quick inference from the figure is that the onset of chaos occurs at eccentricities near 0.3. A particularly interesting structure is observed in the bifurcation diagram shown around eccentricity 0.25.

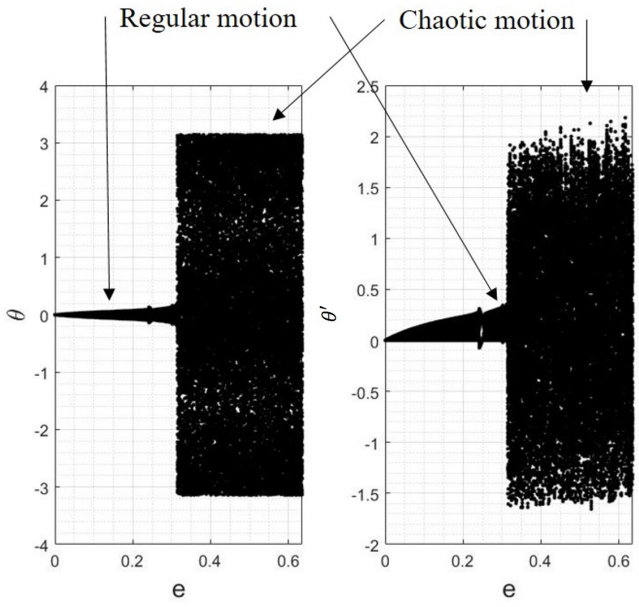

Figure 2.9: Pitch angle bifurcation diagram for $K_3 = 1$. Initial conditions are $[q_3, \dot{q}_3] = [0, 0]$.

Investigation of the bifurcation diagrams reveal certain interesting dynamical structure. Magnification of this region of the parameter space (Fig. 2.10) reveals these quasi-periodic motions. Period three solution of θ and period two solution of θ' exist here.

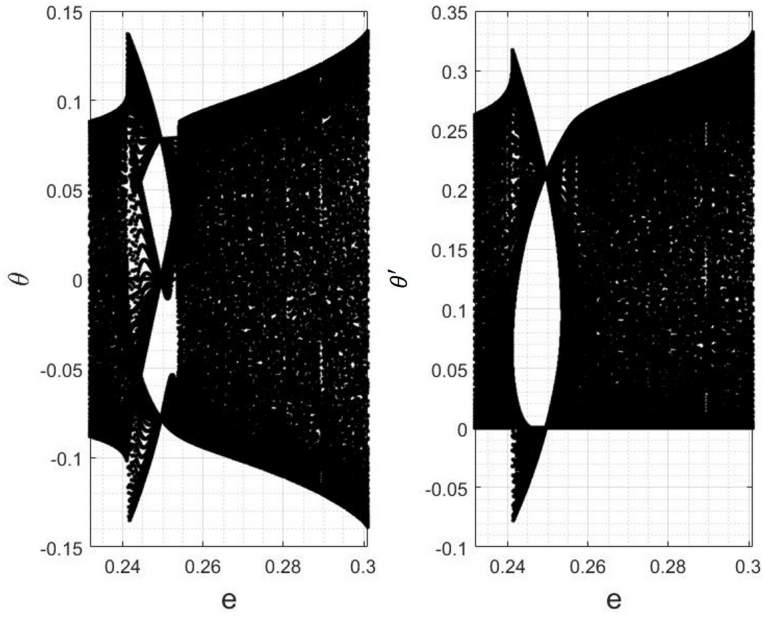

Figure 2.10: Pitch angle bifurcation diagram for $K_3 = 1$. Zoomed in on e = [0.22,0.301]

For smaller eccentricities, the motions are regular, i.e., periodic (at $e = 0$) and quasi-periodic ($e > 0$). This is illustrated in Fig. 2.11

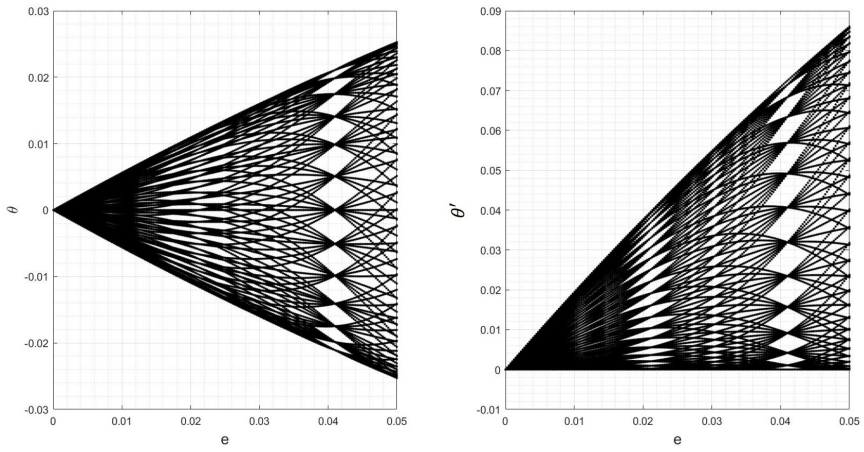

Figure 2.11: Pitch angle bifurcation diagram for $K_3 = 1$. Zoomed in on e = [0,0.05]

Furthermore, a magnification of the regions near eccentricity 0.3, (Fig. 2.12) reveals a complex mixture of regular and chaotic motions. Period five solutions of θ and period four solutions of θ' exist at $e = 0.313$, chaos occurs near $e = 0.312$ and quasi-periodic motions dominate at eccentricities between these values.

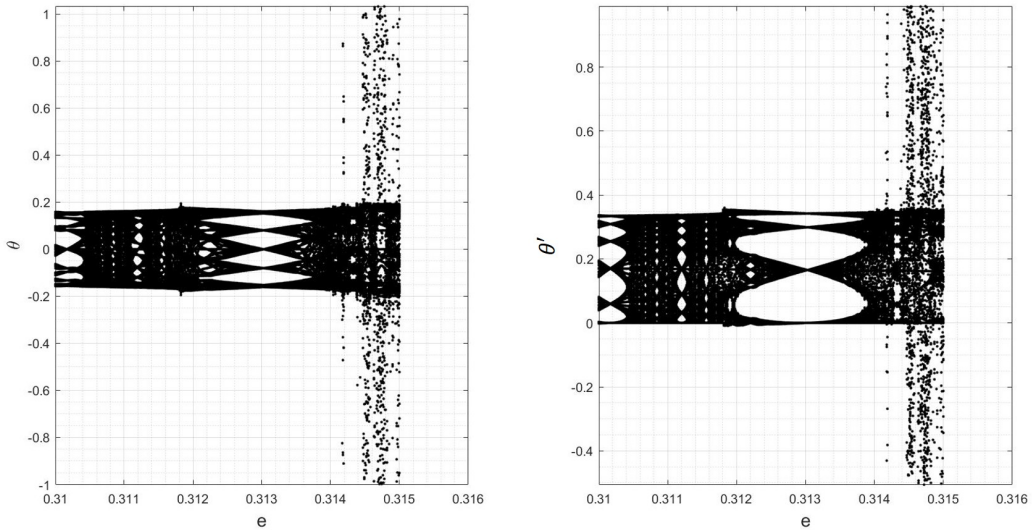

Figure 2.12: Pitch angle bifurcation diagram for $K_3 = 1$. Zoomed in on e = [0.31,0.316]

Figures 2.13 and 2.14 illustrate the bifurcation near $e = 0.312$. Areas of chaotic motion, quasi-

periodic motion, and even periodic motion appear and then disappear as eccentricity increases, apparently until a global onset of chaos is reached, somewhere about $e = 0.3145$. Period five and period three solutions are obtained at $e = 0.303$, as observed in Fig. 2.13. Note the rapid change in the nature of motions from Fig. 2.13 to Fig. 2.14. This structure is repeated again and again in further magnifications of the area near the onset of global chaos.

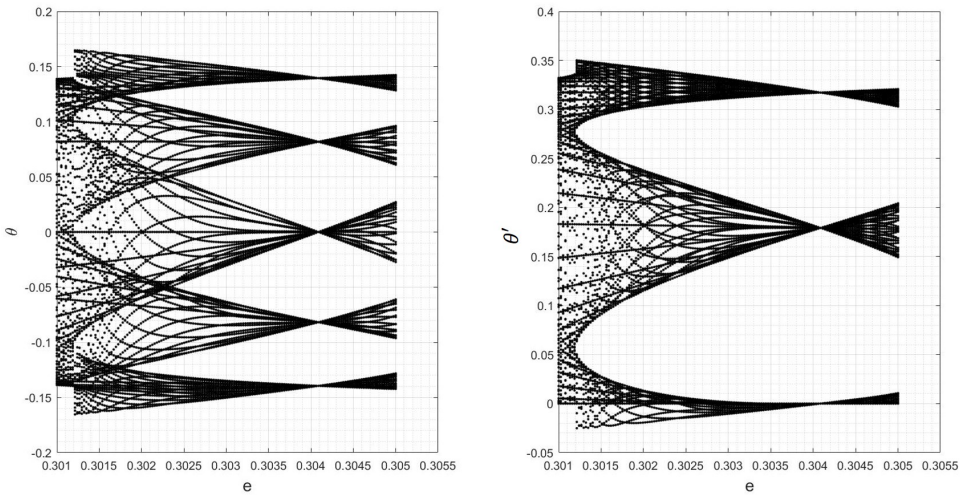

Figure 2.13: Pitch angle bifurcation diagram for $K_3 = 1$. Zoomed in on e = [0.301,0.3055]

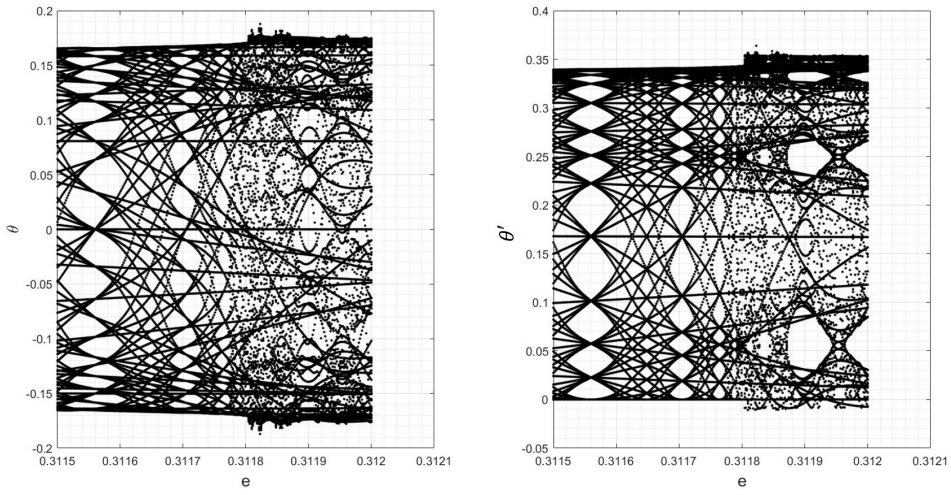

Figure 2.14: Pitch angle bifurcation diagram for $K_3 = 1$. Zoomed in on e = [0.3115,0.3121]

The bifurcation of the pitch angle and angle rate is complex even for the regular motions which are far from chaos revealing a fine, interwoven structure of smooth threads which form odd corners near $e = 0.304$. Note that the above analysis has been done for the inertia parameter value of $K_3 = 1$ i.e. a satellite representing a dumbbell shape. Both Poincaré maps and bifurcation diagrams may be constructed for a variety of realistic values of the rigid body inertia parameter, eccentricity and the initial states which serves in a useful capacity as an engineering tool in satellite or orbit design. For instance, the Poincaré sections identifies the existence of periodic orbits. From the Poincaré sections, one can discern that the initial condition in θ' to obtain a periodic orbit drifts with eccentricity. This drift is captured in Fig. 2.15 below.

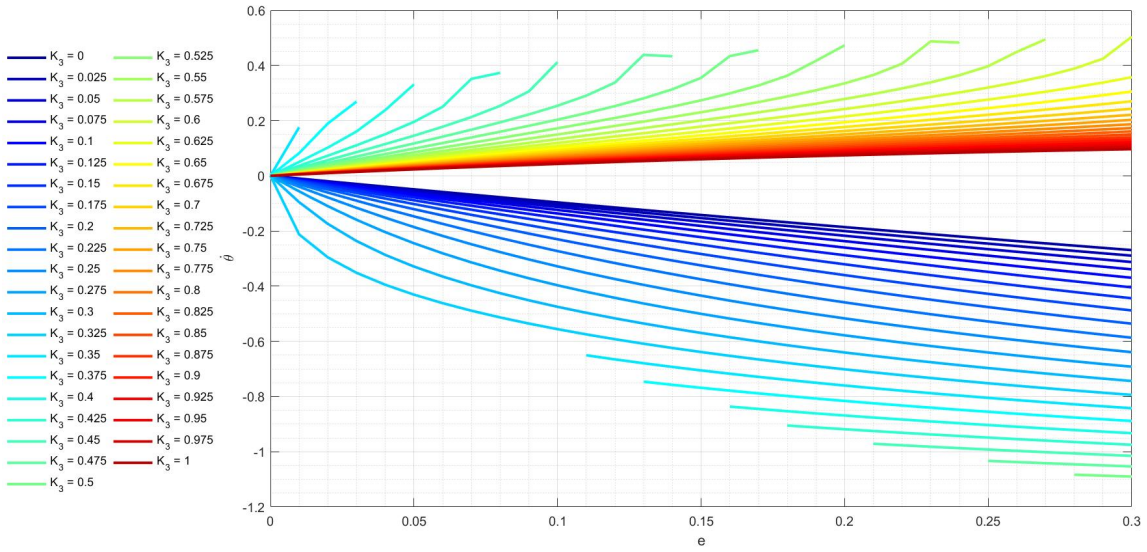

Figure 2.15: θ' initial condition drift for periodic solutions of the attitude motion. $\theta = 0$.

Such plots may be used to study the effect of varying system parameters (e and K_3) on the motion of a gravity-gradient satellite. We note here however, that discerning global behavior from local trends can be difficult, and additional methodologies must be pursued. In the following section, the effects of the roll and yaw motions and its influence on the pitch dynamics are examined, with an emphasis on circular as well as elliptical orbits.

2.4.5 Full 3-DOF roll-pitch-yaw dynamics in circular orbit

The case of a rigid body in a circular orbit (eccentricity $e = 0$) is considered next. The rigid body is assumed to be of arbitrary shape and is defined by the inertia parameters $K_1 = \frac{I_3 - I_2}{I_1}$, $K_2 = \frac{I_1 - I_3}{I_2}$ and $K_3 = \frac{I_2 - I_1}{I_3}$. The equilibrium points for this system are identified and the stability of oscillations about it is studied.

To obtain the equations of motion for the circular orbit case, we set the eccentricity ($e = 0$) in Eq. (2.64). For a circular orbit, we note that $\frac{df}{dt} =$ constant, i.e., the independent variable (true anomaly, f) can be switched to time (t) without loss of information.

Thus, Eq. (2.64) becomes

$$\ddot{\mathbf{q}} = \frac{1}{2}(I_{3\times 3} + \tilde{q} + \mathbf{q}\mathbf{q}^T)K_3\mathbf{G} + \frac{2\mathbf{q}^T\dot{\mathbf{q}}}{1+\mathbf{q}^T\mathbf{q}}\dot{\mathbf{q}} \tag{2.82}$$

Eq. (2.82) gives us the complete nonlinear dynamics of a rigid body under the influence of gravity-gradient torques. It is therefore of interest to examine the stability of different types of motion exhibited by the rigid body.

2.4.5.1 Stability of oscillations

Kane[2] shows that the stability of equilibria is evaluated with respect to the parameters of the dynamical system, i.e. inertia parameters and the amplitude of pitch oscillations. Defining the angle ϕ as the angle between the body $\hat{\mathbf{b}}_3$ and the orbit normal $\hat{\mathbf{a}}_3$, the oscillations were deemed unstable when the value of $\frac{\phi}{\phi_0}$ exceeded a predefined upper limit. That is, a small roll-yaw motion was seen to grow when excited by existing pitch motion until it reached a maximum amplitude whose value could not be made arbitrarily small by decreasing the initial conditions of the roll-yaw motion. An initial estimate of this *unstable* nature was made using Floquet theory [66] and linear models of the roll and yaw motions. Fig. 2.16 illustrates regions of stable and unstable motion in the inertia parameter space based on the definition of Kane[2]. This figure has been obtained using initial conditions exhibiting a maximum pitching amplitude of $5\ \mathrm{deg}$ for the entire inertia parameter space.

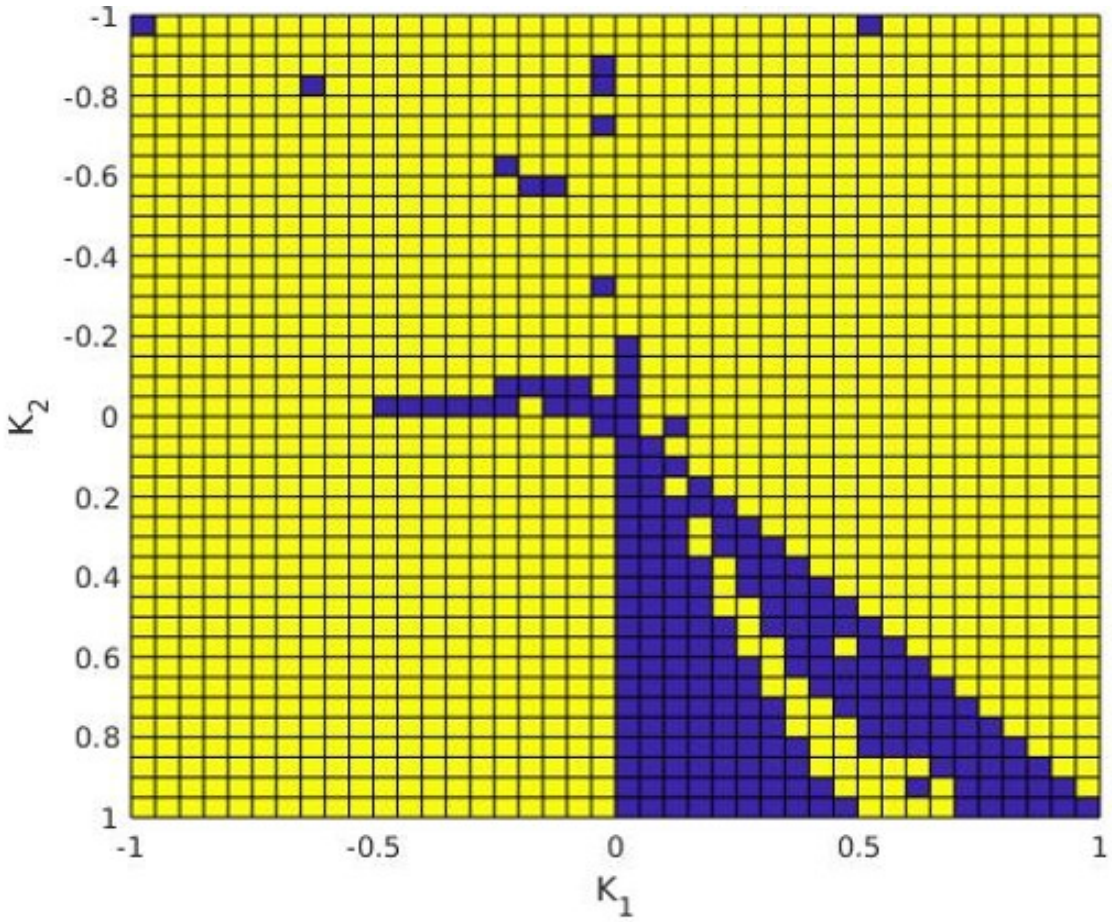

Figure 2.16: $K_1 - K_2$ parameter space: The figure is obtained for a $5\,\mathrm{deg}$ maximum amplitude of pitching motion. Regions in blue exhibit stable nature of oscillations and those in yellow exhibit unstable nature as defined by Kane[2] ©2020 Springer: *Celest Mech Dyn Astr*. Reprinted, with permission, from [1]

In this section, an alternate method based on energy transfer between the pitch and the roll-yaw motions is developed to study the stability of oscillations. Utilizing information from the constant total energy and the one-way coupling between the pitch and roll-yaw motions, the following procedure (Fig. 2.17) is employed to quantify the energy exchange between the pitch and roll-yaw motions.

Linear analysis [36] shows that the Lagrange region is statically stable. Furthermore, it can be shown that the Hamiltonian in the Lagrange region is positive definite and hence can be used as a Lyapunov function to study stability (see Malkin[67] for example). Implementing the procedure

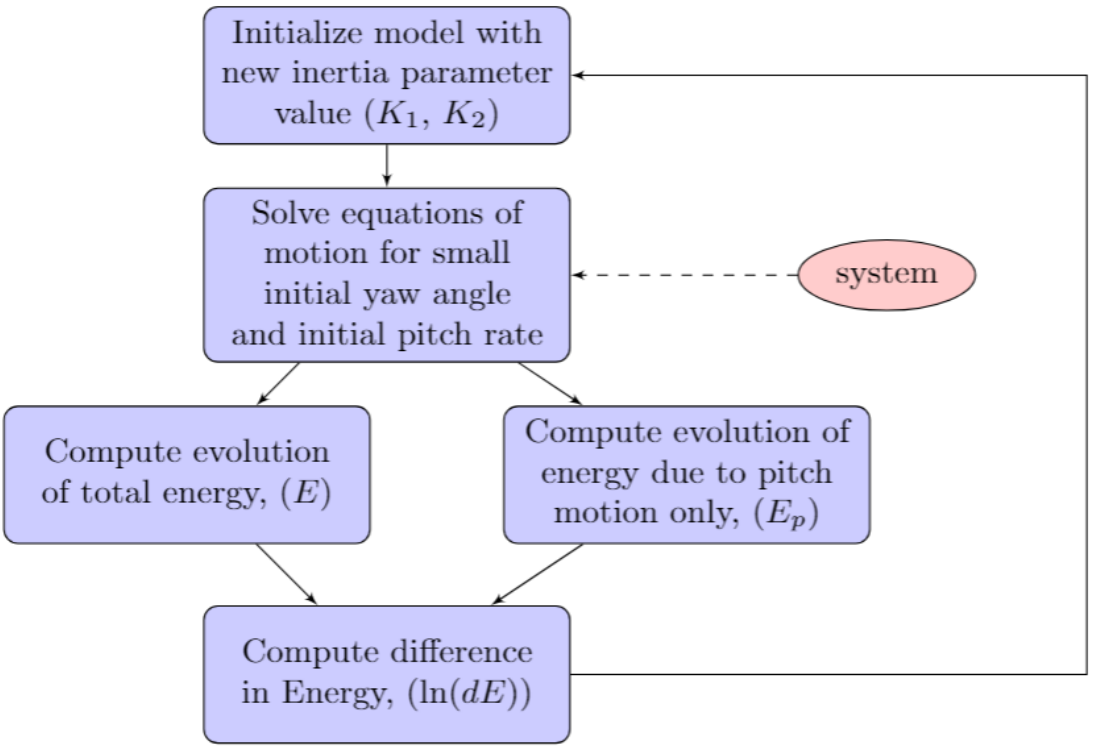

Figure 2.17: Procedure for the method of energy exchange employed to qualitatively assess the inertia parameter space ©2020 Springer: *Celest Mech Dyn Astr*. Reprinted, with permission, from [1].

above we obtain regions of energy transfer in the $K_1 - K_2$ inertia parameter space thus demonstrating that the apparent instability observed by Kane[2] is merely an energy transfer between the pitch and roll-yaw systems. In the DeBra-Delp region too, linear analysis shows the stability of the origin. However, the Hamiltonian is indefinite here and any energy dissipation will lead to instability[53].

The reason we can show energy transfer is because of the knowledge that the pitching motion is decoupled from the roll and yaw motion. However, the converse is not true. For certain values of the parameter space, the small roll-yaw motions are seen to grow when excited by an existing pitch motion, thus indicative of energy exchange. Let us consider a particular region of the inertia space: $K_1 = 0.5$ and $-0.82 \leq K_2 \leq -0.91$. Solving our system of nonlinear equations we obtain the following illustration of energy exchange (Fig. 2.18). It is observed here that this energy transfer does not occur at isolated points in the parameter space, but, the energy pumping increases and then decreases over a range of values (note the energy magnitudes on the y-axis scale).

Selecting isolated points in the Lagrange region, we can observe the same phenomenon Kane [2] observed regarding the pitch and roll-yaw angles: Roll-yaw oscillations increase in amplitude over time when excited by a small pitch motion. Figs. 2.19a, 2.19b and 2.19c demonstrate clearly how the roll-yaw angle is excited by the pitching motion for the given values of inertia. The dip in pitch amplitude accompanying the increase in roll-yaw motion is an indication of energy transfer. However, Kane [2] was unable to notice this phenomenon because of the application of Floquet theory [66] to the linearized periodic dynamical model. The unstable solutions from Floquet theory then suggests an exponential growth. A similar conclusion cannot be drawn for the DeBra-Delp region where linear stability is achieved through gyroscopic terms.

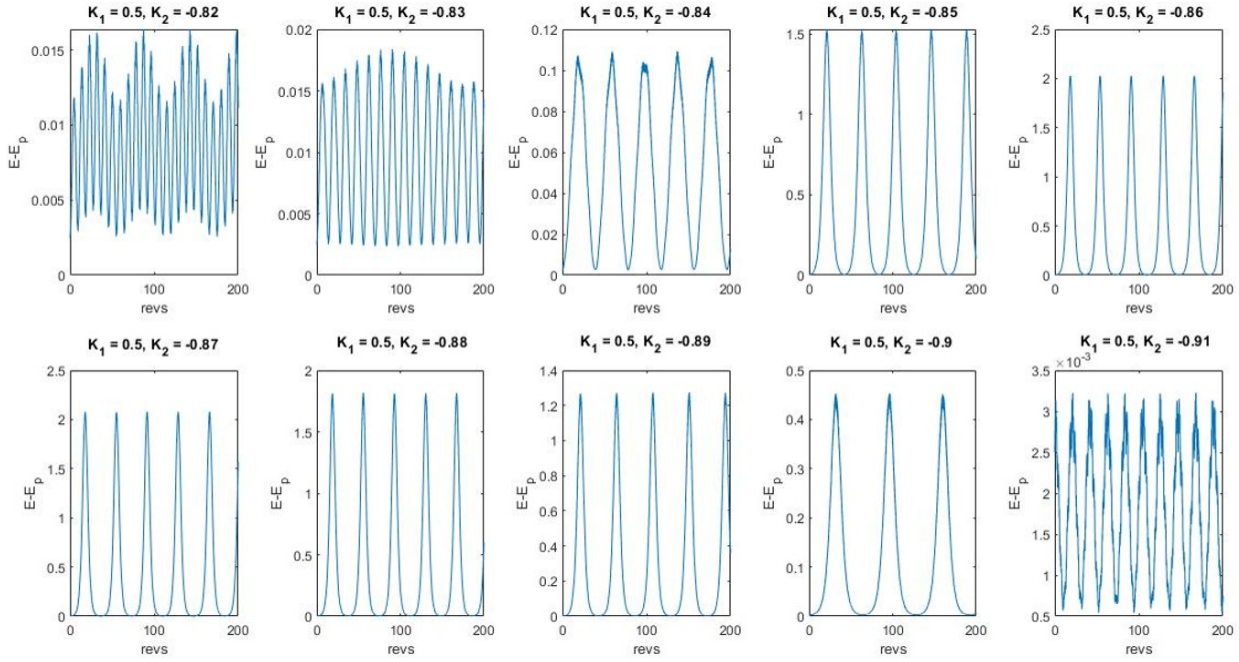

Figure 2.18: Energy pumping: The difference in total energy and that due to pitch is plotted for 200 revs for the inertia parameters $[K_1,K_2]$=[0.5,-0.87–0.91]. The magnitude of energy difference is shown to increase and decrease implying a continuous phenomenon rather than discrete points of stable and unstable oscillations. ©2020 Springer: *Celest Mech Dyn Astr*. Reprinted, with permission, from [1].

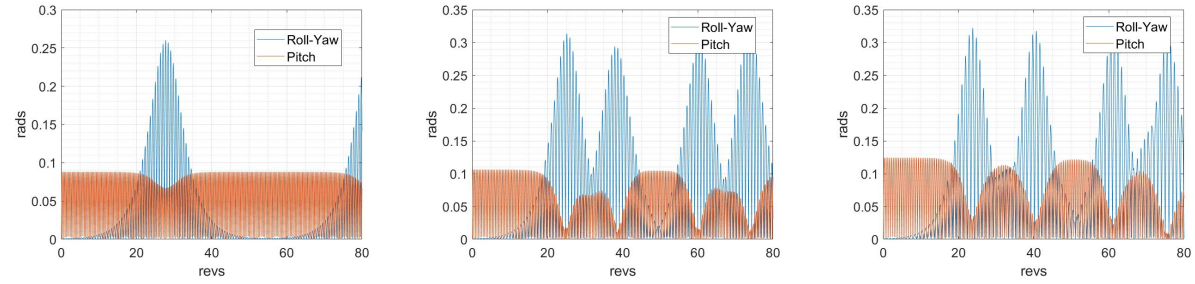

(a) $K_{1,2} = [0.5, -0.9]$ (b) $K_{1,2} = [0.4, -0.75]$ (c) $K_{1,2} = [0.3, -0.6]$

Figure 2.19: Magnitude of oscillations: The roll-yaw oscillations (blue) increase in amplitude over time accompanied by a corresponding dip in pitch oscillation (red) amplitude suggestive of energy exchange between the pitch and roll-yaw oscillations©2020 Springer: *Celest Mech Dyn Astr*. Reprinted, with permission, from [1].

The stable attitude motion coupled with large energy exchanges observed in Fig. 2.19 is indicative of resonance. One would expect this phenomenon to occur when the natural frequencies of pitch and roll-yaw are commensurable. Using linear analysis, the natural frequencies are obtained as a function of the inertia space variables.

$$\omega_{1,2} = \frac{\Omega}{\sqrt{2}}\Big[1 - K_1K_2 \mp \sqrt{16K_1K_2 + (3K_2 + K_1K_2 - 1)^2} - 3K_2\Big]^{\frac{1}{2}} \tag{2.83}$$

$$\omega_3 = \Omega\sqrt{3(K_1 + K_2)/(1 + K_1K_2)} \tag{2.84}$$

The linear analyses are valid for small oscillations about the equilibrium and the differential equations are linear with constant coefficients. Unstable solutions resulting from the linear system of equations then suggest an exponential growth, however, actual motion resulting from nonlinear equations are bounded. This information is lost in the linearization. Performing the energy-based stability analysis for the entire $K_1 - K_2$ space within the Lagrange and DeBra-Delp region, we see the prominent regions where these energy exchanges occur coincide with the curves of 2:1 ($\omega_3 = 2\omega_1$) resonance and 1:1 ($\omega_3 = \omega_1$) resonance. A slight change in energy transfer is also observed along the internal resonance condition of $\omega_3 = \omega_2 - \omega_1$. As suspected, we observe that the dominant energy exchange happens in the 2:1 resonant commensurability. This energy exchange is given by

$$dE = \frac{1}{T}\int_0^T (E - E_p)\mathrm{dt} \tag{2.85}$$

where, E is the total energy and E_p is the energy associated with the pitch motion.

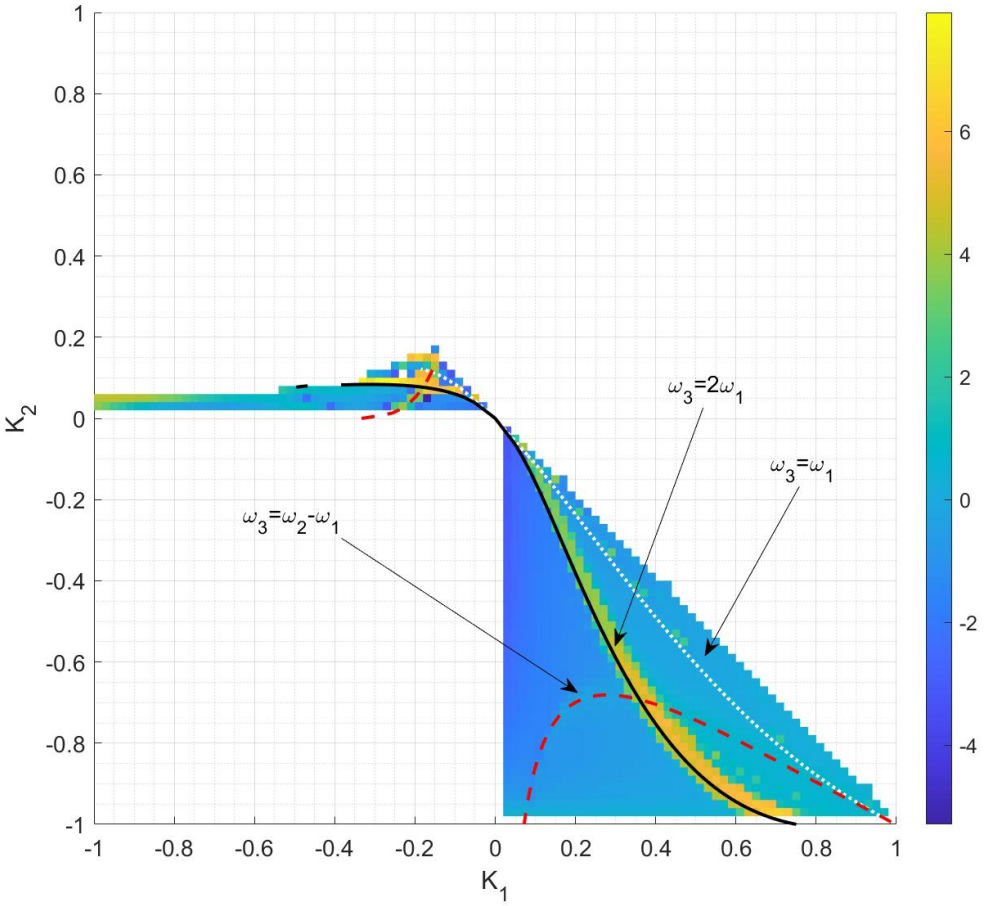

Figure 2.20: $K_1 - K_2$ parameter space: Shows regions of energy exchange in the Lagrange and Debra-Delp regions of the inertia parameter space. Three curves corresponding to the internal resonances $\omega_3 = 2\omega_1$, $\omega_3 = \omega_1$ and $\omega_3 = \omega_2 - \omega_1$ are identified as reasons for the energy exchange. The colors denote the value of $\log dE$ from Eq. 2.85 ©2020 Springer: *Celest Mech Dyn Astr*. Reprinted, with permission, from [1].

On comparing Fig. 2.16 with Fig. 2.20, it is observed that the regions of instability pointed out by Kane [2] actually correspond to regions where the energy exchange between pitch and roll-yaw motion is predominant. We note that energy transfer is more dominant where there is frequency commensurability between the natural frequencies of pitch and roll-yaw. We also observe that the magnitude of energy exchanges are not as dominant near the $\omega_3 = \omega_2 - \omega_1$ resonant curve or the 1:1 resonant curve.

2.4.5.2 *Maximum pitch angle sensitivity*

The effect of the maximum pitch amplitude on the amount of energy exchange, particularly in the neighborhood of the $\omega_3 = 2\omega_1$ commensurability curve is investigated in more detail. It is observed that an increase in the maximum pitch amplitude is accompanied with an increase in the magnitude of energy exchanged. This implies that the region exhibiting undesirable oscillations in the pitch and roll-yaw motions cover a larger part of the $K_1 - K_2$ parameter space. This effect of the influence of the maximum pitch amplitude is illustrated in Fig. 2.21

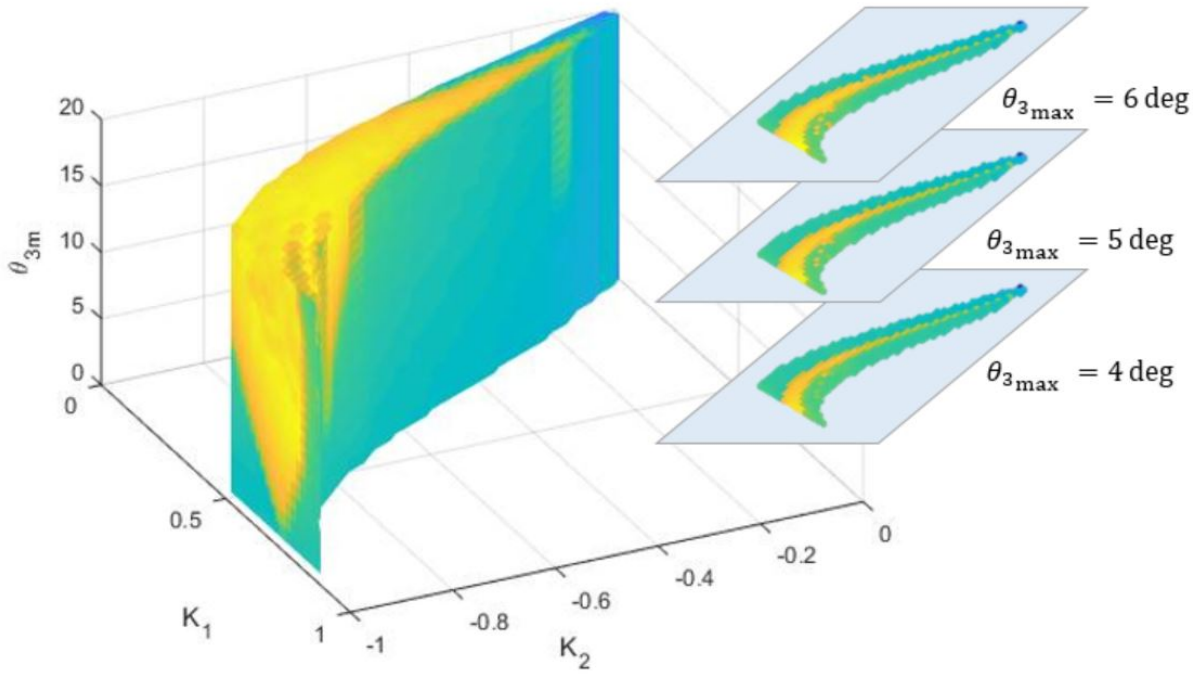

Figure 2.21: Effect of maximum pitch amplitude: The resonance region near the $\omega_3 = 2\omega_1$ commensurability is investigated as a function of the maximum pitch angle. Sections $\theta_{3_{max}} = 4\,\text{deg}, 5\,\text{deg}, 6\,\text{deg}$ are shown to indicate that high energy exchange regions can span a larger part of the inertia parameter space depending on the maximum amplitude of pitching oscillations. Color information is the same as that in Fig. 2.20 ©2020 Springer: *Celest Mech Dyn Astr*. Reprinted, with permission, from [1].

It is noted here that the stability analysis and the equations of motion were derived keeping the expression for the gravity torque truncated to second order. This is done practically because the

size of the rigid body under consideration is much smaller than the primary body. Fig. 2.21 demonstrates that regions of high energy exchange and therefore larger amplitude of pitching oscillations can span a large region of the inertia parameter space depending on the maximum amplitude of pitching motion. This is an important criterion in the design of space vehicles to avoid undesirable oscillations in pitch and roll-yaw motions. Furthermore, the parametric investigations into the attitude motions are useful in understanding its influence on long-term orbit propagation. Since no main-axis attitude motion can be assumed for non-controlled space objects such as spent rocket bodies [68, 54], the shape and inertia knowledge becomes useful in using the analyses presented here to assess the long term orbital evolution.

2.4.5.3 Energy-based approach for attitude motion visualization

The previous section shows how energy transfer between pitch and roll-yaw motions provides insights into the nature of the oscillations. In classical mechanics, when we consider the problem of the rapid motion of a non-symmetric rigid body about its center of mass, we normally use the Euler-Poinsot motion as a generating motion with zero external torques. The motions are considered rapid if the moment of external forces about a fixed point is small compared with the value of the kinetic energy of rotation [69]. Now, while the analytic solution for the general free motion of a rigid body is rather involved, polhodes serve as a geometrical way of qualitatively analyzing the motion due to Poinsot.

Poinsot's geometric interpretation of the torque-free motion of a rigid body uses a tri-axial ellipsoid of rotational kinematic energy intersecting with a sphere of magnitude of angular momentum. In this setup, the locus of angular velocity vector traces a space curve called the polhode. When the angular momentum vector is expressed in the inertial frame, this is known as the herpolhode. The point of contact then determines the space-fixed and body-fixed system [31]. To facilitate the Poinsot construction, consider the two constants of motion, the kinetic energy (T) and the magnitude of the angular momentum ($|\mathbf{L}|$). Each of these define an ellipsoid in $\boldsymbol{\omega}$ space (the energy and momentum ellipsoid, respectively). The motion of $\boldsymbol{\omega}$ is constrained to lie on the intersection of the two ellipsoids given as follows:

$$\frac{I_1}{2T}\omega_1^2 + \frac{I_2}{2T}\omega_2^2 + \frac{I_3}{2T}\omega_3^2 = 1 \tag{2.86}$$

$$I_1\omega_1^2 + I_2\omega_2^2 + I_3\omega_3^2 = \mathbf{L}^2 \tag{2.87}$$

In this section, we attempt to extend this qualitative reasoning to the case of a rigid body in orbit acted upon by gravity-gradient torques. Without loss of generality, we can write the total energy of this system as:

$$E = T + V \tag{2.88}$$

$$= \frac{1}{2}(I_1\omega_1^2 + I_2\omega_2^2 + I_3\omega_3^2) + V \tag{2.89}$$

Therefore, we can obtain a reduced energy, E_0 as:

$$E_0 = E - V = \frac{1}{2}I_1\omega_1^2 + \frac{1}{2}I_2\omega_2^2 + \frac{1}{2}I_3\omega_3^2 \tag{2.90}$$

Comparing with Eq. (2.86)

$$\frac{I_1}{2E_0}\omega_1^2 + \frac{I_2}{2E_0}\omega_2^2 + \frac{I_3}{2E_0}\omega_3^2 = 1 \tag{2.91}$$

Note that the reduced energy, E_0, is not a constant as E. However, inspired by the method of Poincaré sections, instantaneous intersections of the angular velocity $\boldsymbol{\omega}$ with the reference ellipsoid can be obtained. This reference ellipsoid is chosen based on the initial conditions of the nonlinear differential equations governing the motion of the rigid body in orbit. Equation 2.91 can be modified to obtain an ellipsoid which is a surface of constant energy in the momentum coordinates (a

space where the coordinates are the projections of the angular momentum along the body's principle moments of inertia) called the Binet ellipsoid [70, 27]. We define this osculating polhode as a ***Binet-Poincaré surface of section***.

The interpretations of the visualizations are similar to that of the torque-free polhode: for example, pure spin motions are stationary points. However, unlike Binet's construction, the osculating polhode curves need not be closed as they indicate how the angular momentum, **L**, enters and exits a reference Binet ellipsoid. The magnitude of departure from a pure spin condition is an indicator of the amplitude of oscillations about that axis. This makes it easy to verify the nature of oscillations with varying initial conditions. Multiple insights can be obtained from the osculating polhode such as changes in the behavior of the angular momentum vector as a function of the inertia parameters and the quasi-periodic motions of the angular momentum vector at the resonance conditions. The remainder of this section will demonstrate the above-mentioned characteristics of motion in detail.

2.4.5.4 Osculating polhode construction: The Binet-Poincaré section

To motivate the discussion on the construction of the Binet-Poincaré' Section, we rewrite Eq. 2.91 as:

$$\frac{L_1^2}{2E_0 I_1}\omega_1^2 + \frac{L_2^2}{2E_0 I_2} + \frac{L_3^2}{2E_0 I_3} = 1 \tag{2.92}$$

where L_1, L_2 and L_3 are the components of the angular momentum, **L**. Eq. 2.92 defines the Binet ellipsoid on which the osculating polhode curves are plotted. First, it is verified in Fig. 2.22 that the equilibrium points, i.e. points of pure spin about the major, minor and intermediate moments of inertia exists for a near-symmetrical rigid body. This figure is obtained for inertia parameter values: $[K_1, K_2] = [0.01, 0.01]$. From the inertia parameters given, this is an asymmetric rigid body and so the pure spin only occurs at the Equilibrium points i.e. spin about the axes of inertia.

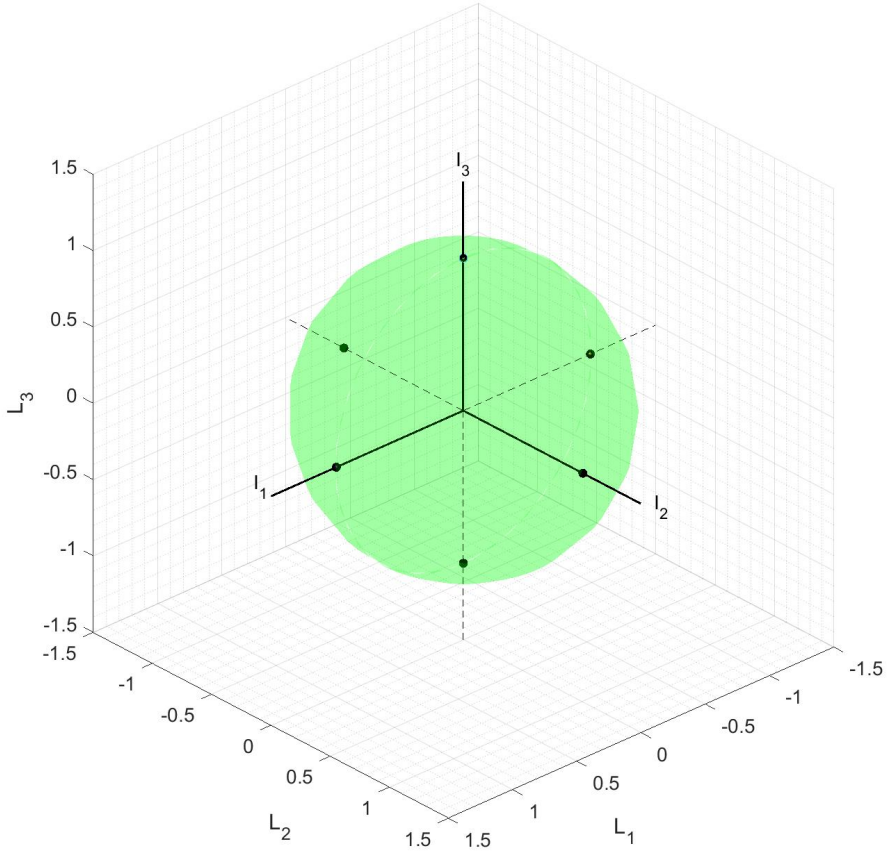

Figure 2.22: Equilibrium Points: The osculating polhode for a near-symmetrical rigid body ($[K_1, K_2] = [0.01, 0.01]$) with initial conditions resulting in pure spin about the three principal axes of inertia suggestive of equilibrium points like in the torque-free case ©2020 Springer: *Celest Mech Dyn Astr.* Reprinted, with permission, from [1].

In the previous sections, the decoupling of the roll-yaw motion from the pitch motion was demonstrated. To visualize this, we begin with a zero initial condition in roll-yaw and their rates. For an axisymmetric body, the osculating polhodes are similar in structure to the torque-free case as the motion departs from pure spin motion. This is illustrated in Fig. 2.23. This figure is obtained for inertia parameter values: $[K_1, K_2] = [0.98, 0.98]$ i.e. $I_1 = I_2 > I_3$.

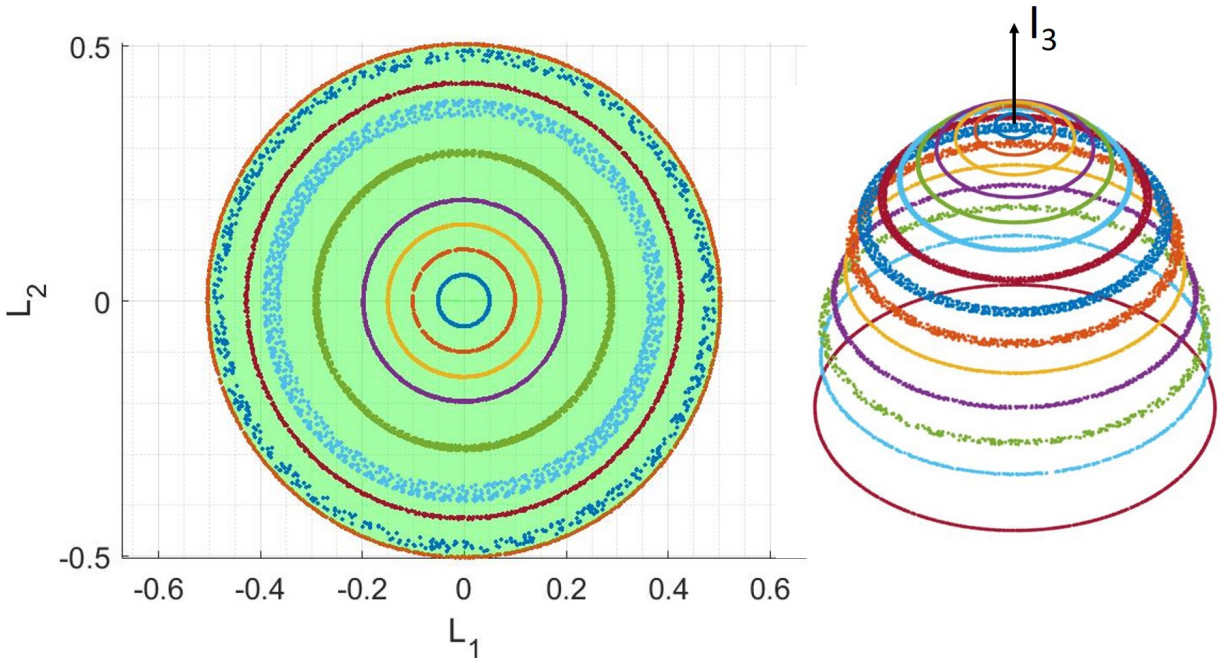

Figure 2.23: Osculating polhodes for the axisymmetric rigid body ($I_1 = I_2 > I_3$): The rigid body ($[K_1, K_2] = [0.98, 0.98]$) shows similar behavior as the polhodes for the torque-free case ©2020 Springer: *Celest Mech Dyn Astr*. Reprinted, with permission, from [1].

We note here that the concentric circular structures in Fig. 2.23 are a measure of the amplitude of oscillations about the spin axis (in this case, I_3). Fig. 2.24 depicts how the full angular momentum vector behaves. This figure is obtained using the initial conditions from Fig. 2.23. It enters and exits the energy ellipsoid multiple times portraying the short-period oscillations about the pitch axis.

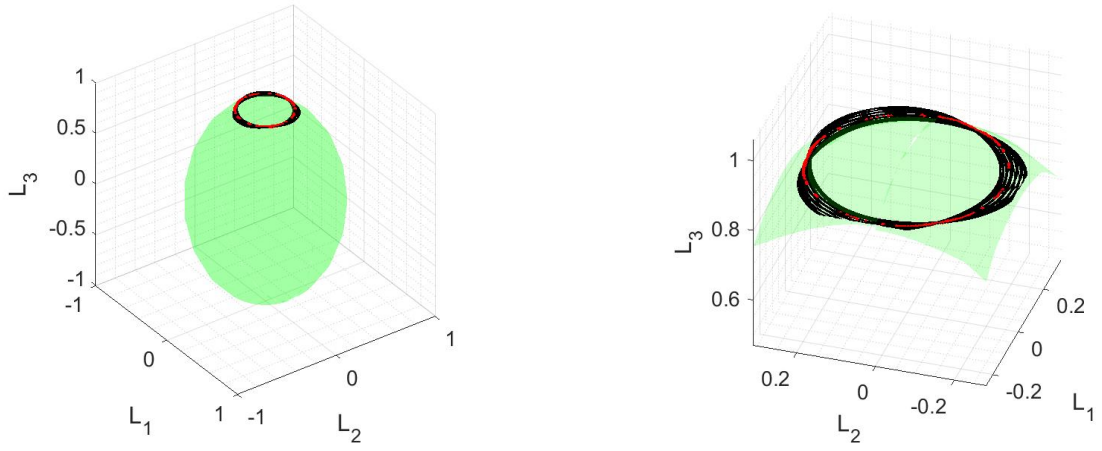

(a) Angular Momentum Vector

(b) (a) Zoomed in

Figure 2.24: Angular momentum trajectory: Fig. 2.24a shows how the angular momentum vector intersects the energy ellipsoid. The red points are the intersection points which is the osculating polhode. Fig. 2.24b shows a zoomed-in portion of Fig. 2.24a for better visualization ©2020 Springer: *Celest Mech Dyn Astr*. Reprinted, with permission, from [1].

A visualization tool is thus developed to qualitatively analyse the nature of oscillations. This can be utilized to gain valuable insight into the behavior of the angular momentum vector, particularly at the resonance conditions discussed in the previous sections.

2.4.5.5 Energy transfer and angular momentum behaviour for the inertia parameter space

Having developed a visualization tool for the energy and momentum ellipsoid, the qualitative analysis of rigid body motion is extended to the remainder of the inertia parameter space. The observation in the previous sections that *'small roll-yaw motion is seen to grow when excited by existing pitch motion until it reaches a maximum amplitude whose value could not be made arbitrarily small by decreasing the initial conditions of the roll-yaw motion.'* is validated. Fig. 2.25 shows the osculating polhode obtained for the inertia parameter pair: [K_1,K_2] = [0.5, -0.9]. This is a pair lying close to the 2:1 commensurability curve and is indicative of energy exchange between the pitch and roll-yaw motions. three sets of initial conditions in roll-yaw are analysed: $\theta_1 = 0.001, 0.01, 0.1$ and $\dot{\theta}_3 = 0.13$.

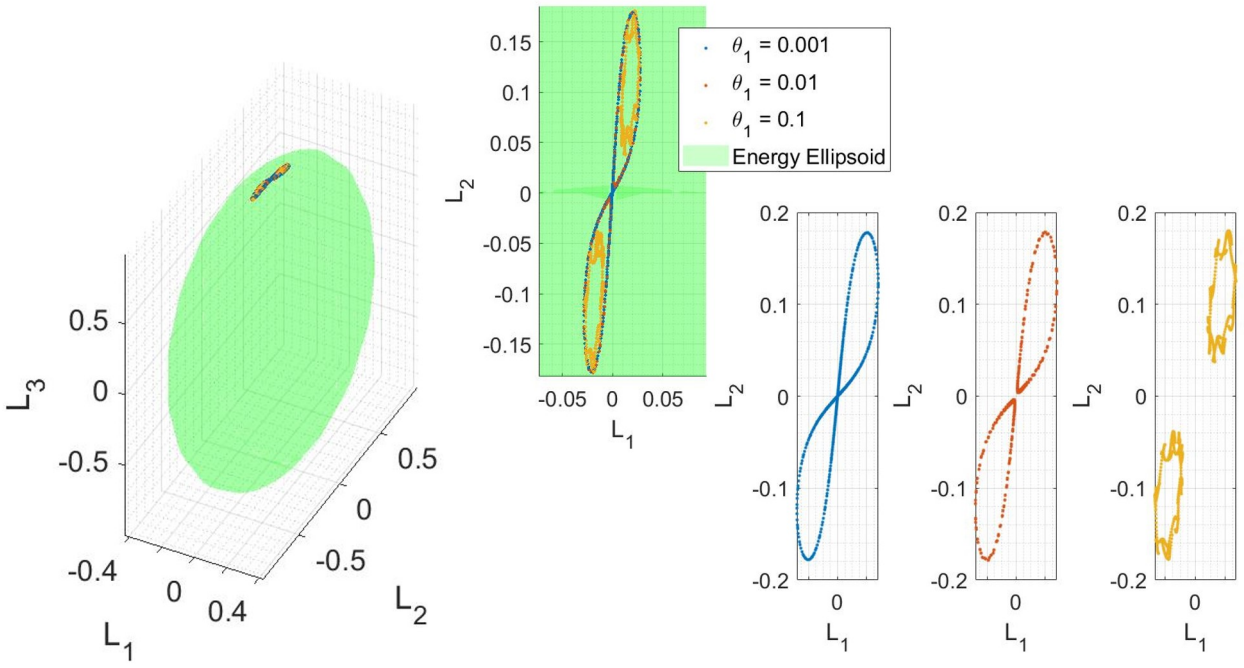

Figure 2.25: Initial condition response: The osculating polhodes are plotted for different initial conditions in $\theta_1 = 0.1$(yellow) ,0.01(red), 0.001(blue) to demonstrate that the amplitude of oscillations remains bounded with arbitrary change in initial conditions ©2020 Springer: *Celest Mech Dyn Astr*. Reprinted, with permission, from [1].

It is observed here that the maximum amplitude of pitch oscillation (i.e. the upper and lower bound on the L_1 and L_2 directions remain the same even when the roll-yaw initial condition is arbitrarily small. Closed islands on the osculating polhode are indicative of the bounded nature of the angular momentum vector. The separation between the islands is dependent on the magnitude of the initial conditions.

It is noted here that the osculating polhode plotted in Fig. 2.25 only records the instances that the angular momentum vector exits the Binet ellipsoid. The reason for doing so is to assess the motion of the angular momentum vector across a large region of the inertia parameter space. To understand this further, let us consider a set of inertia parameter pairs and view the Binet-Poincaré Section on the $L_1 - L_2$ plane. This is illustrated in Fig. 2.26.

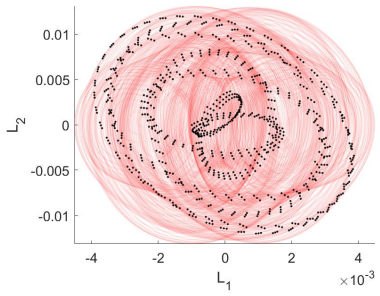

(a) $[K_1, K_2]$ = [0.5,-0.75]

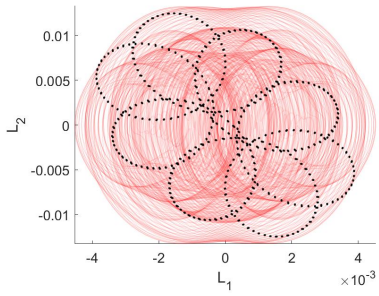

(b) $[K_1, K_2]$ = [0.5,-0.76]

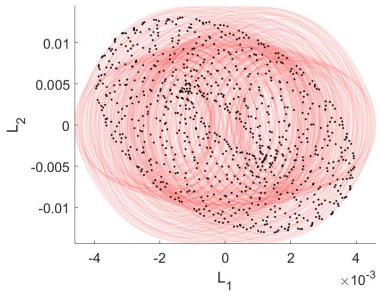

(c) $[K_1, K_2]$ = [0.5,-0.77]

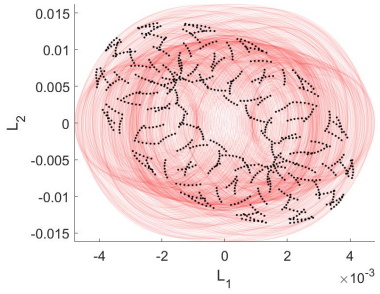

(d) $[K_1, K_2]$ = [0.5,-0.78]

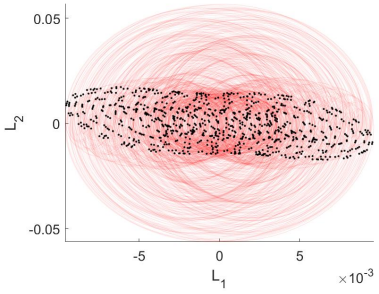

(e) $[K_1, K_2]$ = [0.5,-0.79]

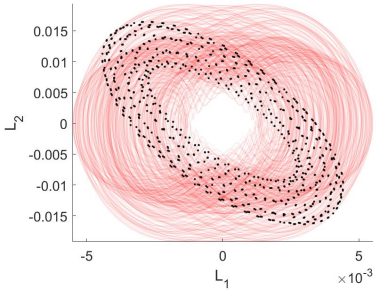

(f) $[K_1, K_2]$ = [0.5,-0.80]

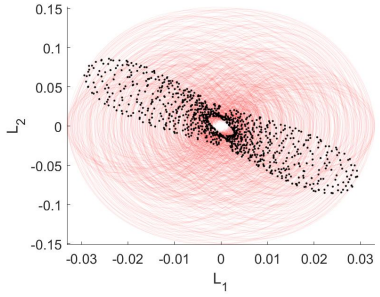

(g) $[K_1, K_2]$ = [0.5,-0.81]

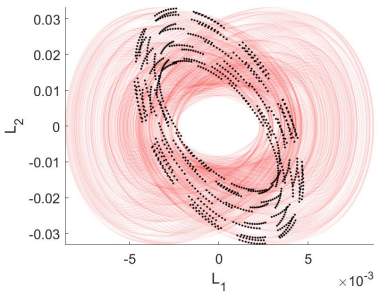

(h) $[K_1, K_2]$ = [0.5,-0.82]

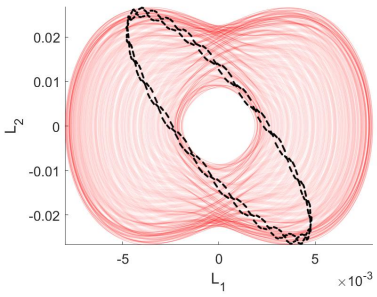

(i) $[K_1, K_2]$ = [0.5,-0.83]

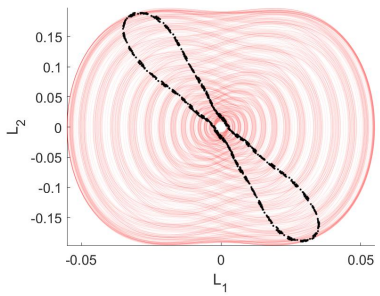

(j) $[K_1, K_2]$ = [0.5,-0.84]

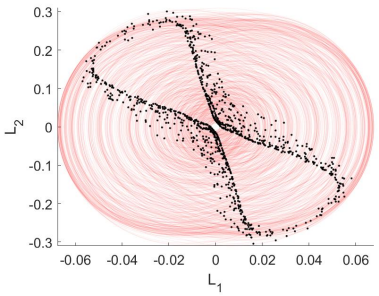

(k) $[K_1, K_2]$ = [0.5,-0.85]

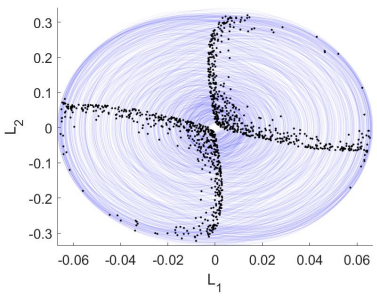

(l) $[K_1, K_2]$ = [0.5,-0.86]

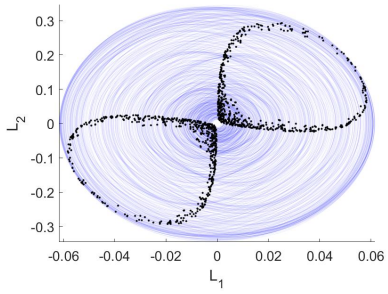

(m) $[K_1, K_2]$ = [0.5,-0.87]

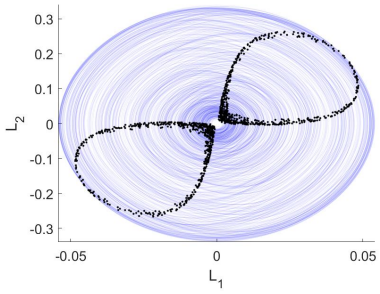

(n) $[K_1, K_2]$ = [0.5,-0.88]

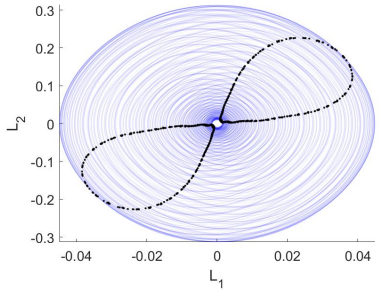

(o) $[K_1, K_2]$ = [0.5,-0.89]

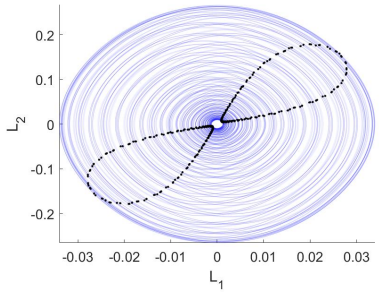

(p) $[K_1, K_2]$ = [0.5,-0.90]

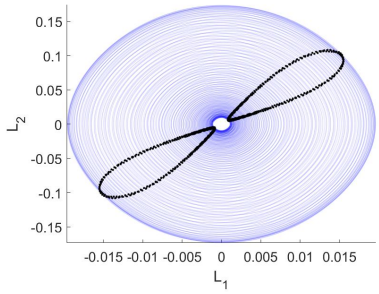

(q) $[K_1, K_2]$ = [0.5,-0.91]

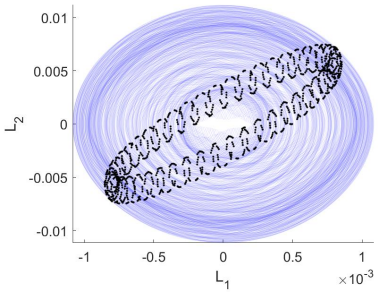

(r) $[K_1, K_2]$ = [0.5,-0.92]

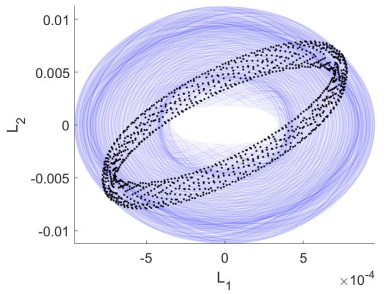

(s) $[K_1, K_2]$ = [0.5,-0.93]

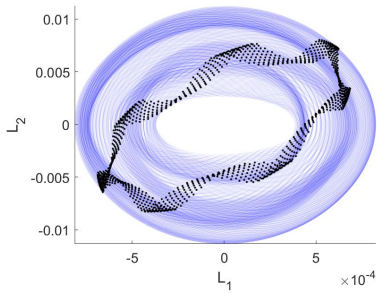

(t) $[K_1, K_2]$ = [0.5,-0.94]

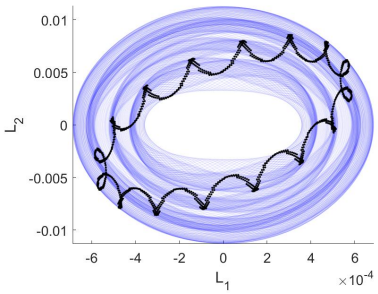

(u) $[K_1, K_2]$ = [0.5,-0.95]

Figure 2.26: Binet-Poincaré' Sections: Projections of the osculating polhode onto the $L_1 - L_2$ axes. Figs. 2.26a to 2.26k are associated with the inertia parameters above the $\omega_3 = 2\omega_1$ resonance curve and Figs. 2.26l to 2.26u are below. Figs. 2.26j to 2.26q correspond to the inertial parameters lying close to the resonant curve and thus exhibiting high magnitude of energy exchange ©2020 Springer: *Celest Mech Dyn Astr*. Reprinted, with permission, from [1].

There are many interesting observations in Fig. 2.26. As shown, the figure is split into two sets of figures (red and blue). Figs. 2.26a to 2.26k are associated with the inertia parameters above the $\omega_3 = 2\omega_1$ resonance curve and Figs. 2.26l to 2.26u are below. Figs. 2.26j to 2.26q correspond to the inertial parameters lying close to the resonant curve and thus exhibits a high magnitude of energy exchange. The following observations are made from the Fig. 2.26.

1. The two-lobe island structures in the osculating polhode arise because the inertia parameter pairs are close to the 2:1 commensurability curve.

2. The structures in the beginning of the red region (Figs. 2.26a to 2.26d) arise because the inertia parameter pairs are close to the $\omega_3 = \omega_2 - \omega_1$ internal resonance curve. This indicates that the motions are quasi-periodic in the internal resonance regions. However, these motions do not cause the pitch oscillation amplitude to increase as in the case of the 2:1 commensurability (Figs. 2.26j to 2.26q).

3. The inertia pairs that are not near any commensurability curve result in a single island structure (Figs. 2.26f, 2.26h, 2.26i, 2.26r, 2.26s, 2.26t, 2.26u). This can also be observed in the axisymmetric case explained earlier since axisymmetric rigid bodies do not lie near internal resonant regions.

4. As mentioned previously, the osculating polhode is obtained by recording the instances the angular momentum vector exits the energy ellipsoid. Given this knowledge, it is seen that there is a monotonic change in the phase of the angular momentum vector upon crossing the commensurability curve. The regions (quadrants in the $L_1 - L_2$ space) where the angular momentum exited the energy ellipsoid are now regions where it enters. This behavior is consistent over all the inertia parameter pairs.

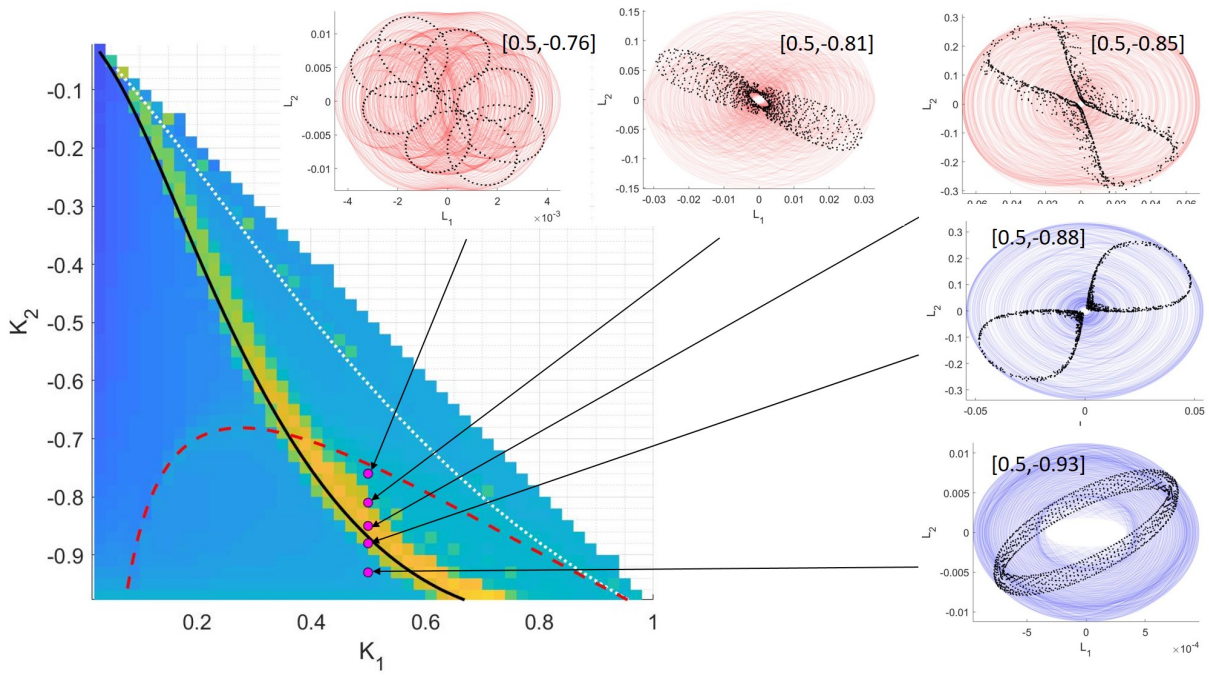

Figure 2.27: Binet-Poincaré Sections across the 2:1 resonant curve: The osculating polhodes demonstrate the monotonically changing phase of the angular momentum vector orientation. Distinct changes are seen in the regions above and below the resonant curve ($[K_2]$ = [-0.85,-0.88] -also characterized by large amplitude of oscillations) The sections close to regions of internal resonance of $\omega_3 = \omega_2 - \omega_1$ are also shown ©2020 Springer: *Celest Mech Dyn Astr*. Reprinted, with permission, from [1].

Fig. 2.27 illustrates the phenomenon explained above. It can be easily visualized that even though the complete motion of the angular momentum is similar for the red and blue regions near commensurability, the Binet-Poincaré' sections help gain insight into the direction of motion of the angular momentum. This is a very interesting behavior in that the direction of motion of the angular momentum shifts based on the inertia parameter pair and on crossing the 2:1 commensurability curve. The quadrants of entry and exit are interchanged in the $L_1 - L_2$ coordinate space.

Thus, the Binet-Poincaré' sections provide valuable insight into the coupled nature of the pitch and roll-yaw motions for a rigid body in Keplerian orbit. In the next section, a quantitative measure for this coupling is developed utilizing the information from the state transition matrix.

2.4.5.6 A quantitative measure of pitch and roll-yaw coupling using the state transition matrix

The state transition matrix (STM), by definition, is the sensitivity of the current state with respect to its initial state. By its construction, the dependencies of the pitch motion on the roll-yaw motion and vice versa are obtained. This is a very useful tool in quantifying the coupling between different degrees of freedom in the problem. For a general n-degree of freedom problem, there are $2n$ variables: $[q_i, \dot{q}_i], \quad i = 1, \cdots, n$. The STM can be formulated to measure the sensitivities of a particular set of degree of freedom as follows:

$$\Phi(t, t_0) = \begin{bmatrix} \Phi_{11} & \Phi_{12} \\ \Phi_{21} & \Phi_{22} \end{bmatrix} \tag{2.93}$$

where

$$\Phi_{11} = \frac{\partial(q_j, \dot{q}_j)}{\partial(q_{j0}, \dot{q}_{j0})}$$

$$\Phi_{12} = \frac{\partial(q_j, \dot{q}_j)}{\partial(q_{k0}, \dot{q}_{k0})}$$

$$\Phi_{21} = \frac{\partial(q_k, \dot{q}_k)}{\partial(q_{i0}, \dot{q}_{i0})}$$

$$\Phi_{22} = \frac{\partial(q_k, \dot{q}_k)}{\partial(q_{k0}, \dot{q}_{k0})}$$

where, $j \in n$ are the degrees of freedom of interest and $k \in (n - j)$ are the others. The STM also satisfies the differential equation

$$\dot{\Phi} = F\Phi \tag{2.94}$$

where $F = \dfrac{\partial f(\mathbf{q})}{\partial \mathbf{q}}$ is the Jacobian with $\dot{\mathbf{q}} = f(\mathbf{q})$ the state space equations

$$\Phi_{t_0,t_0} = I_{n\times n}$$

and the following relations:

$$\Phi^{-1}(t,t_0) = \Phi(t_0,t), \qquad \Phi^T J \Phi = J\Big(\begin{bmatrix} \mathbf{0}_n & I_n \\ -I_n & \mathbf{0}_n \end{bmatrix} \Big) \tag{2.95}$$

For the problem of rigid body attitude motion, the sensitivities of the pitch degree of freedom are investigated as a function of roll-yaw degrees of freedom. Here, $j = [3]$ and $k = [1,2]$. For the analysis presented in this section, the largest singular value (induced 2-norm) of the cross-correlation STM (Φ_{12}) is used as a measure of coupling between the pitch and roll-yaw motions normalized by the auto-correlation part (Φ_{22}). Because the measure is made non-dimensional by normalization, any other measure could also be used such as the 2-norm, trace or determinant of the sub-STMs.

$$\Sigma = \frac{||\Phi_{12}||_2}{||\Phi_{22}||_2} \tag{2.96}$$

Σ is a quantifiable measure of the coupling and therefore the energy exchange among the pitch and roll-yaw oscillations. For the initial condition based response, Fig. 2.28 demonstrates that the maximum amplitude of pitch oscillation is captured by Σ. For the near-resonant inertia pair, [0.5,-0.9], The maximum amplitude of pitching oscillations do not increase with the increase in initial amplitude. For each of the simulations, $\dot{\theta}_3 = 0.13$. We also obtain the decoupling between the pitch and roll-yaw oscillations when θ_1 = 0.

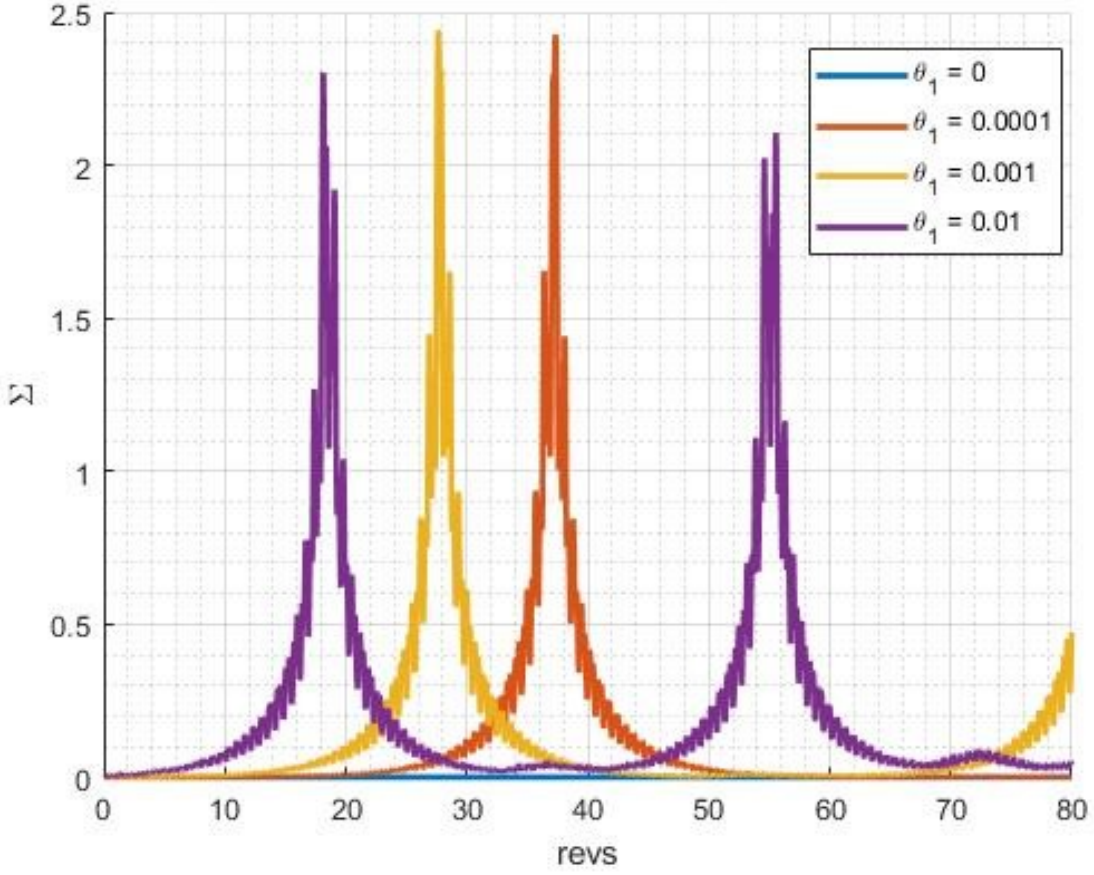

Figure 2.28: Σ coupling factor for an initial condition response in $[K_1, K_2]$ = [0.5,-0.9]: Shows that the amplitude of oscillations do not change with arbitrary changes in the initial conditions. Also, the decoupling of pitch and roll-yaw is demonstrated when $\theta_1 = 0$ (imperceptible flat line) ©2020 Springer: *Celest Mech Dyn Astr*. Reprinted, with permission, from [1].

Using this quantifiable measure facilitates the inertia parameter space analysis just as before. By doing so, the expected increase in the coupling strengths of pitch and roll-yaw motions are obtained near to the 2:1 resonant commensurability curve. This is illustrated in Fig. 2.29

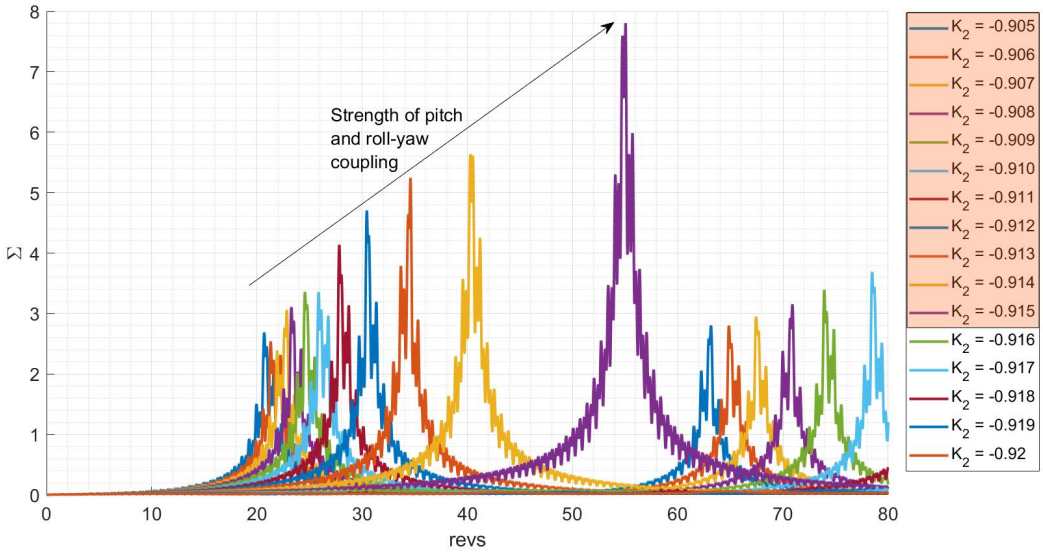

Figure 2.29: Σ coupling factor for resonant region inertia parameters: Shows the amplitude of oscillations increase as the inertia parameter set is closer to the 2:1 resonant commensurability curve ©2020 Springer: *Celest Mech Dyn Astr*. Reprinted, with permission, from [1].

This new measure gives a numerical value for the coupling between the state variables for any dynamical system. Its utility has been demonstrated by evaluating it for the problem of the rigid body in Keplerian orbit. As can be expected, the advantages of having an autonomous dynamical system go away when the effects of eccentricity is introduced. In the following section, the 3-DOF roll-yaw-pitch motion of a rigid body in Keplerian motion is considered. To facilitate the discussion for analytical treatment of dynamical systems, the equations of attitude motion for the rigid body are reintroduced using Serret-Andoyer variables. Numerical simulations and tools of dynamical systems theory are used to infer the nature of motion of the rigid body.

2.4.6 Full 3-DOF roll-pitch-yaw dynamics in eccentric orbit

The Euler-Poinsot problem is one of the classical problems of mechanics and describes the torque-free motion of a rigid body. The solution of any classical problem has broadly two steps: First: *Kinematics*, used to describe the orientation of the rigid body in relation to a spatial inertial frame. Second: *Dynamics*, represented by differential equations for the angular rates and the angular velocity rates. Both descriptions are discussed in the introduction of this chapter. The

analysis of these descriptions eventually led to taking advantage of the internal symmetries to reduce the Euler-Poinsot problem to a one degree of freedom problem, and using a perturbation method to obtain a solution [71]. The Hamiltonian form is effective in performing this reduction, as perturbed Hamiltonian systems can be solved analytically to any order through many methods, like the one used by Deprit [3]. Deprit & Elipe [71] has offered the full reduction of the Euler-Poinsot problem. To perform this reduction, one must resort to solving the Hamilton-Jacobi equation to obtain a generating function responsible for the canonical transformation from the action-angle variables to the Serret-Andoyer variables. These constants became the attitude-dynamics analogs of the Delaunay variables in the theory of orbits. Now, while Serret [72] had come up with a full reduction of the problem, Andoyer [73] suggested a partial reduction. Much later, the study by Andoyer was amended by Deprit, and it was shown canonicity can be proven by using differential forms, without explicitly finding a generating function [74].

The case of the torque-free rigid body can be extended to the study of the motion of a rigid body under the influence of gravity-gradient torques. In this section, we shall examine this extension as applied to the motion of a rigid body in an eccentric orbit by revisiting the formulation of the rigid body motion in the variables, as described by Serret and Andoyer. We begin with a transformation from the inertial frame to the body frame, using an intermediate coordinate system associated with the invariable frame. The invariable plane forms the invariable frame defined in the Euler-Poinsot problem with the normal to the plane in the direction of the rotational angular momentum.

2.4.6.1 Problem reformulation

Consider the motion of a rigid body about its mass center. The body frame, **B**, is a Cartesian dextral orthogonal frame defined by the unit vectors $\hat{b} = [b_1, b_2, b_3]^T$. The attitude of **B** is studied with respect to an inertial frame **I** defined by the unit vectors $\hat{s} = [s_1, s_2, s_3]^T$. We will start with a transformation from the inertial to the body frame, using an intermediate coordinate system associated with the invariable plane. Our attention is focused on the case where the rigid body is in a central inverse squared force field, and the only torques acting on it are due to the force field. In formulating the problem statement, we make the following assumptions: a) The rigid body is in

Keplerian motion, b) the rigid body is a triaxial ellipsoid with A, B and C as the principal moments of inertia, and c) the attitude motion does not affect the orbital motion.

Before we introduce the invariable plane to describe the orientation, we can represent it using the classical Eulerian description of a three-angle body-fixed rotation sequence. The orientation of this frame is given by a $3-1-3$ rotation through the angles as : $R = R(\psi, b_3)R(\theta, i_1)R(\phi, s_3)$ as illustrated in figure 2.30.

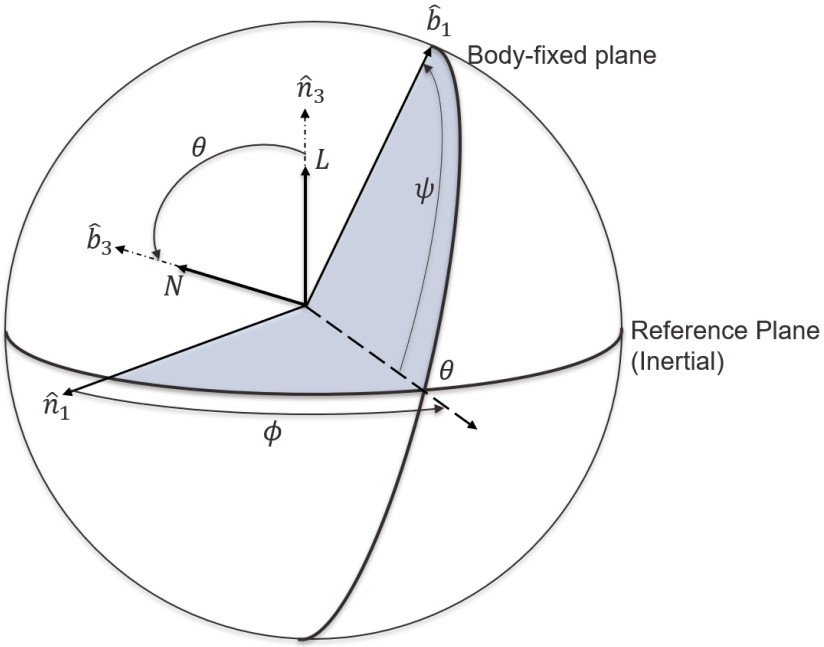

Figure 2.30: $3-1-3$ Eulerian description for attitude representation. $\hat{\mathbf{n}}$ is the inertial frame, $\hat{\mathbf{b}}$ is the body frame.

To write the kinematic equations, recall that the angular velocity can be expressed in the body frame as:

$$\boldsymbol{\omega} = \begin{bmatrix} 0 \\ 0 \\ \dot{\psi} \end{bmatrix} + R^T(\psi, \hat{b}_3) \begin{bmatrix} \dot{\theta} \\ 0 \\ 0 \end{bmatrix} + R^T(\psi, \hat{b}_3) R^T(\theta, \hat{i}_1) \begin{bmatrix} 0 \\ 0 \\ \dot{\phi} \end{bmatrix} \tag{2.97}$$

The Lagrangian for the torque-free case is then written as:

$$\mathcal{L}(\phi, \theta, \psi, \dot{\phi}, \dot{\theta}, \dot{\psi}) = T - V = \frac{1}{2}\boldsymbol{\omega}^T I \boldsymbol{\omega} \tag{2.98}$$

where I is the inertia tensor whose elements (A,B and C) are the principal moments of inertia along the diagonals. This is obtained by assuming that the body axes coincide with the principal axes of inertia. Using the expression from equation 2.98 for the Lagrangian, we obtain that the new generalized coordinates are the $3-1-3$ Euler angles. The conjugate momenta can then be written using the familiar expressions:

$$p_\Phi = \frac{\partial \mathcal{L}}{\partial \dot{\phi}}, \qquad p_\Theta = \frac{\partial \mathcal{L}}{\partial \dot{\theta}}, \qquad p_\Psi = \frac{\partial \mathcal{L}}{\partial \dot{\psi}} \tag{2.99}$$

We then obtain the Hamiltonian for the torque-free motion in terms of these action-angle variables through the Legendre transformation: $\mathcal{H} = \mathbf{p}^T\dot{\mathbf{q}} - \mathcal{L}$, where, $\mathbf{q}$ is the generalized coordinates, $[\phi, \theta, \psi]$, and, $\mathbf{p}$ is its conjugate momenta, $[p_\Phi, p_\Theta, p_\Psi]$.

$$\begin{aligned}\mathcal{H}(\mathbf{q}, \mathbf{p}) =& \frac{1}{2}\Big(\frac{s_\psi^2}{A} + \frac{c_\psi^2}{B}\Big)\Big(\frac{p_\Phi - p_\Psi c_\theta}{s_\theta}\Big)^2 + \frac{p_\Psi^2}{2C} + \frac{1}{2}\Big(\frac{c_\psi^2}{A} + \frac{s_\psi^2}{B}\Big)p_\Theta^2 \\ &+ \Big(\frac{1}{A} - \frac{1}{B}\Big)\Big(\frac{p_\Phi - p_\Psi c_\theta}{s_\theta}\Big)p_\Theta s_\psi c_\psi\end{aligned} \tag{2.100}$$

We note here that throughout the text, $s_\star = \sin(\star)$ and $c_\star = \cos(\star)$. Hamilton's equations of motion are then written as:

$$\frac{d}{dt}\begin{bmatrix}\mathbf{q} \\ \mathbf{p}\end{bmatrix} = \mathbf{J}\nabla_{[\mathbf{q},\mathbf{p}]}\mathcal{H} \tag{2.101}$$

where $\mathbf{J}$ is the symplectic matrix $\begin{bmatrix} 0 & I_{3\times3} \\ -I_{3\times3} & 0 \end{bmatrix}$. In the above Hamiltonian, we can observe that the coordinate ϕ is cyclic (since it does not appear in the Hamiltonian formulation) which renders its conjugate momentum Φ an integral of motion because of the relation that $\frac{dp_\Phi}{dt} = -\frac{\partial \mathcal{H}}{\partial \phi} = 0$. Physically, p_Φ is the inertial third component of the rotational angular momentum vector. These

variables, $[\phi, \theta, \psi, p_\Phi, p_\Theta, p_\Psi]$, are called the action-angle variables. Andoyer's [73] partial reduction and Deprit's [3] geometrical approach further reduce this two-dimensional Hamiltonian to a one-dimensional Hamiltonian through the construction of the invariable plane.

2.4.6.2 The Serret-Andoyer description

To understand the true essence of Andoyer's and Deprit's approach, consider the orientation of the body frame with respect to an inertial frame written in terms of a coordinate frame aligned with the invariable plane. Recall the invariable plane is a plane whose normal is in the direction of the rotational angular momentum vector. This is illustrated in figure 2.31. The body frame is obtained through a $3-1-3-1-3$ rotation with respect to the inertial frame, as

$$\hat{\mathbf{b}} = R_3(\nu)R_1(J)R_3(\mu)R_1(K)R_3(\lambda)\,\hat{\mathbf{s}}$$

where K denotes how the invariable plane is inclined with respect to the inertial frame, and J denotes how the invariable plane is inclined with respect to the inertial frame. We can observe from Fig. 2.31 that K is the angle between the rotational angular momentum vector M and its inertial third component, L. Similarly, J is the angle between the rotational angular momentum vector M and its body-fixed third component, N.

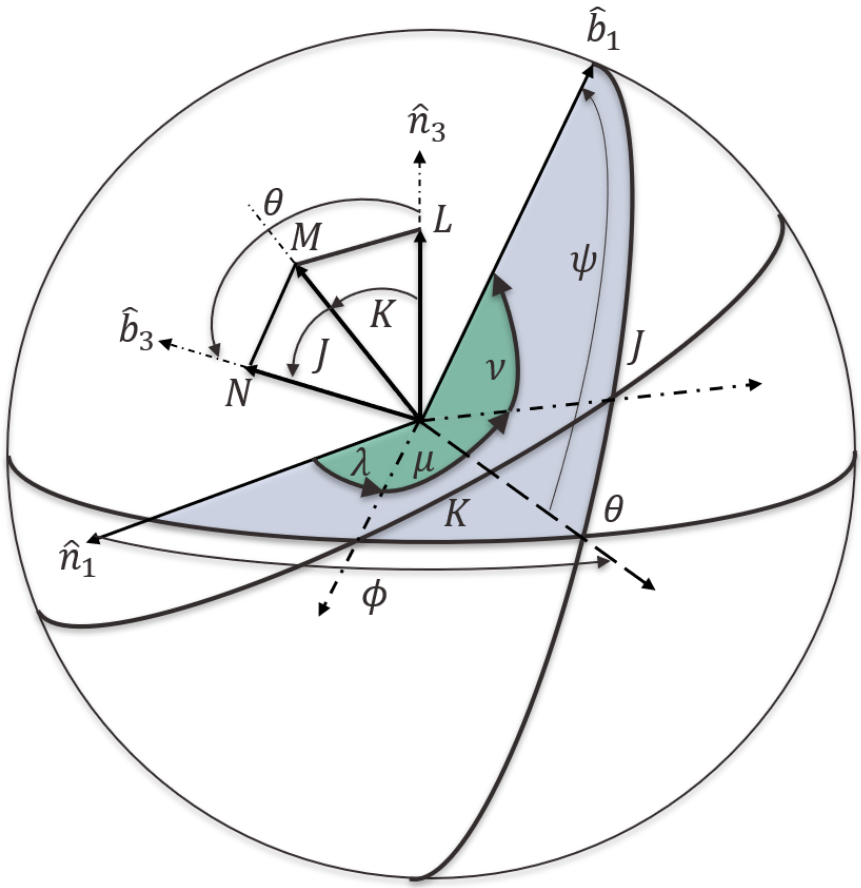

Figure 2.31: Body frame representation using the invariable frame [3, 4]. $[\lambda, \mu, \nu]$ are the coordinates and their corresponding momenta are $[L, M, N]$.

Deprit [3] observed that when the Hamiltonian lacks specific time dependence, a sufficient condition for the transformation to be canonical is:

$$p_\Phi d\phi + p_\Theta d\theta + p_\Psi d\psi = N d\nu + M d\mu + L d\lambda \tag{2.102}$$

Here, the momenta conjugate to the newly transformed coordinates (λ, ν, μ) are (L,N,M), respectively. Then, the transition from the Euler coordinates (ϕ, θ, ψ) to the coordinates (λ, μ, ν) becomes a canonical transformation if we choose the momenta (L, M, N) conjugate to (λ, μ, ν) as $L = p_\Phi, M = |G|, N = p_\Psi$, correspondingly, given that G is the rotational angular momentum.

From geometry, we can relate the angles K and J to the conjugate momenta as follows:

$$\cos K = \frac{L}{M} \qquad\qquad \cos J = \frac{N}{M}$$

The relationship between the Euler angles and the Serret-Andoyer variables can be obtained by equating the rotation matrices and extracting one from the other. We note here that the Euler angles are a function of both the coordinates and momenta of the Serret-Andoyer variables through the inclusion of the inclinations K and J.

$$R(\psi, b_3)R(\theta, i_1)R(\phi, s_3) = R_3(\nu)R_1(J)R_3(\mu)R_1(K)R_3(\lambda) \tag{2.103}$$

Given these relations, the torque-free Hamiltonian can be rewritten in terms of the Serret-Andoyer variables from equation 2.100 as:

$$\mathcal{H} = \frac{1}{2}\Big(\frac{s_\nu^2}{A} + \frac{c_\nu^2}{B}\Big)(M^2 - N^2) + \frac{N^2}{2C} \tag{2.104}$$

The Hamiltonian does not depend on μ and λ explicitly. Therefore, the corresponding generalized momenta, M and L are constants. Then Eq. (2.104) is simplified into the Hamiltonian of a two-dimensional system with a single independent co-ordinate ν. Hamilton's canonical equations with variables N and ν can be derived as

$$\dot{\nu} = \frac{\partial \mathcal{H}}{\partial N} = N\Big(\frac{1}{C} - \frac{\sin^2\nu}{A} - \frac{\sin^2\nu}{B}\Big) \tag{2.105}$$

$$\dot{N} = -\frac{\partial \mathcal{H}}{\partial \nu} = \frac{1}{2}(M^2 - N^2)\Big(\frac{1}{B} - \frac{1}{A}\Big)\sin 2\nu \tag{2.106}$$

where $\dot{\nu}$ is the spin velocity of the rigid body about $\hat{b}_3$. Dividing each side of Eq. (2.105) with Eq. (2.106) to eliminate the independent variable, t, a first order autonomous system is obtained as:

$$\frac{dN}{d\nu} = \frac{C(A-B)(M^2-N^2)\sin 2\nu}{N[AB - C(A\cos^2\nu + B\sin^2\nu)]} \tag{2.107}$$

Equation (2.107) determines a set of trajectories in the phase plane (ν, N). From Eq. (2.107) above, one can notice that there is a singularity at $N = 0$, i.e. the angle $J = \frac{\pi}{2}$. Therefore, the two pairs of values of $\nu = [0, \pi]$ and $\nu = [\frac{\pi}{2}, \frac{3\pi}{2}]$ correspond to rotations of the rigid body about the $\hat{b}_2$ and $\hat{b}_3$ axes, respectively. Let these singularities be denoted as:

$$\begin{aligned} S_1 &: \nu = 0 \text{ or } \pi, \text{ and } L = 0 \\ S_2 &: \nu = \frac{\pi}{2} \text{ or } \frac{3\pi}{2}, \text{ and } L = 0 \end{aligned} \tag{2.108}$$

then, the nature of the singularity can be obtained through simple linear analysis. Using Eqs. (2.105 and 2.106), the eigenvalues of the linearized dynamical system can be obtained to be:

$$e_1 = \pm\frac{G\sqrt{(A-B)(B-C)}}{B\sqrt{AC}} \qquad \text{for } S_1 \tag{2.109}$$

$$e_2 = \pm\frac{G\sqrt{(B-A)(A-C)}}{A\sqrt{BC}} \qquad \text{for } S_2 \tag{2.110}$$

Therefore, without loss of generality, assuming $A > B > C$ or $A < B < C$, one can obtain S_1 is a saddle point and S_2 is a center. Thus, a rotation about maximal or minimal moment of inertia is stable, and rotation about the intermediate moment of inertia is unstable. This result is corroborated from the previous section result on the torque-free Poinsot construction. The Serret-Andoyer variables are employed to simplify the Hamiltonian formulation of a rigid body in an elliptic orbit in the following section.

2.4.6.3 Rigid body in an elliptic orbit

The assumption of Keplerian motion allows the rigid body's orbit to lie on the $x - y$ plane of the inertial frame without loss of dynamical information. Aligning s_1 with the direction of perigee, s_2 with the semi-latus rectum direction and s_3 along the orbital angular momentum, the orbital reference frame is related to the body frame through the direction cosine matrix employing the

following rotations:

$$\hat{\mathbf{b}} = R_3(\nu)R_1(J)R_3(\mu)R_1(K)R_3(\lambda - f)\hat{\mathbf{o}} \tag{2.111}$$

where f is the true anomaly. McCullagh's approximation [59] gives the gravity-gradient potential. This gives the second order external potential of a body with principal moments of inertia, A, B and C.

$$\mathcal{V}_{ggt} = -\frac{k^2}{r}\Big(1 + \frac{tr(I) - 3\hat{r}^T I\hat{r}}{2r^2}\Big) \tag{2.112}$$

here k^2 is the gravitational parameter, and $r = \frac{p}{1+e\cos f}$ is the magnitude of the position vector of the rigid body from the center of mass of the central body. $\hat{r}$ is the unit vector in the direction of r and is given by:

$$\hat{\mathbf{r}} = R_3(\nu)R_1(J)R_3(\mu)R_1(K)R_3(\lambda)\begin{bmatrix}\cos f\\ \sin f\\ 0\end{bmatrix} = \begin{bmatrix}r_1\\ r_2\\ r_3\end{bmatrix} \tag{2.113}$$

Expanding out $tr(I) - 3\hat{r}^T I\hat{r}$, and using the relation that $r_1^2 + r_2^2 + r_3^2 = 1$, we get

$$tr(I) - 3\hat{r}^T I\hat{r} = (C - B)(1 - 3r_3^2) - (B - A)(1 - 3r_1^2) \tag{2.114}$$

The potential now becomes:

$$\mathcal{V}_{ggt} = -\frac{k^2}{r}\Big(1 + \frac{(C - B)(1 - 3r_3^2) - (B - A)(1 - 3r_1^2)}{2r^2}\Big) \tag{2.115}$$

The complete Hamiltonian can then be written ignoring the orbital energies, since they are always constant due to the assumption that the attitude motion does not affect the orbit. This Hamiltonian is the sum of the torque-free Hamiltonian from equation 2.104 and the gravity-gradient potential.

$$\mathcal{H} = \frac{1}{2}\Big(\frac{s_\nu^2}{A} + \frac{c_\nu^2}{B}\Big)(M^2 - N^2) + \frac{N^2}{2C} - \frac{k^2}{2r^3}\Big((C - B)(1 - 3r_3^2) - (B - A)(1 - 3r_1^2)\Big) \tag{2.116}$$

To bring this expression to a form that can enable the use of perturbation theory, Eq. (2.116) is modified as follows. First, we rearrange the Hamiltonian of the torque-free case as follows.

$$\mathcal{H}_0 = \Big(\frac{\sin^2\nu}{A} + \frac{\cos^2\nu}{B}\Big)\Big(\frac{M^2 - N^2}{2}\Big) + \frac{N^2}{2C} \tag{2.117}$$

$$= \frac{M^2}{2C}\Big[1 + \Big(\frac{\sin^2\nu}{A/C} + \frac{\cos^2\nu}{B/C} - 1\Big)\sin^2 J\Big] \tag{2.118}$$

The gravity-gradient potential is rewritten as:

$$\mathcal{V}_{ggt} = -\frac{k^2}{r}\Big(\frac{(C-B)(1-3r_3^2) - (B-A)(1-3r_1^2)}{2r^2}\Big) \tag{2.119}$$

$$= [C][-\frac{n^2}{2}]\frac{(1+e\cos f)^3}{(1-e^2)^3}\Big[(1-\frac{B}{C})(1-3r_3^2) - (\frac{B}{C} - \frac{A}{C})(1-3r_1^2)\Big)\Big] \tag{2.120}$$

$$= -\frac{M^2}{2C}\Big(\frac{n}{M/C}\Big)^2\frac{(1+e\cos f)^3}{(1-e^2)^3}\Big[(1-\frac{B}{C})(1-3r_3^2) - (\frac{B}{C} - \frac{A}{C})(1-3r_1^2)\Big)\Big] \tag{2.121}$$

where n is the constant orbital mean motion, and the eccentricity (e) and true anomaly (f) enter through the expansion of the radius vector $r = \frac{a(1-e^2)}{1+e\cos f}$. Utilizing expressions for r_1 and r_2 from Eq. (2.113) , we can expand the above expression. Further, we note from the torque free Hamiltonian that for an axisymmetric body ($A = B$), ν is cyclic. Therefore, we can split the total Hamiltonian into an axisymmetric part (independent of ν) and a symmetric part (containing ν).

$$\mathcal{V}_{ggt} = -\frac{M^2}{2C}\Big(\frac{n}{M/C}\Big)^2\frac{(1+e\cos f)^3}{(1-e^2)^3}\frac{1}{16}\Big(\Big(2 - \frac{B}{C} - \frac{A}{C}\Big)\mathcal{V}_{axi} + \frac{3}{2}\Big(\frac{B}{C} - \frac{A}{C}\Big)\mathcal{V}_{asy}\Big) \tag{2.122}$$

where $\mathcal{V}_{axi}$ corresponds to the axisymmetric part, and $\mathcal{V}_{asy}$ corresponds to the asymmetric part. Their expressions are given as follows:

$$\mathcal{V}_{axi} = \begin{pmatrix} 12\,\cos(J)\,\sin(J)\,\sin(K)\,(\cos(K)-1) \\ 12\,\cos(J)\,\sin(J)\,\sin(K)\,(\cos(K)+1) \\ 6\sin(J)^2\sin(K)^2 \\ -6\sin(K)^2\,\left(3\sin(J)^2-2\right) \\ -3\,(\cos(K)-1)^2\,\left(\cos(J)^2-1\right) \\ -3\,(\cos(K)+1)^2\,\left(\cos(J)^2-1\right) \\ -24\,\cos(J)\,\cos(K)\,\sin(J)\,\sin(K) \\ 2\,\left(3\sin(J)^2-2\right)\,\left(3\sin(K)^2-2\right) \end{pmatrix}^T \begin{pmatrix} \cos(\mu-2\,\phi) \\ \cos(\mu+2\,\phi) \\ \cos(2\,\mu) \\ \cos(2\,\phi) \\ \cos(2\,\mu-2\,\phi) \\ \cos(2\,\mu+2\,\phi) \\ \cos(\mu) \\ 1 \end{pmatrix} \tag{2.123}$$

$$\mathcal{V}_{asy} = \begin{pmatrix} -4\,\sin(J)\,\sin(K)\,(\cos(J)-1)\,(\cos(K)-1) \\ (\cos(J)-1)^2\,(\cos(K)-1)^2 \\ (\cos(J)-1)^2\,(\cos(K)+1)^2 \\ (\cos(J)+1)^2\,(\cos(K)-1)^2 \\ (\cos(J)+1)^2\,(\cos(K)+1)^2 \\ -4\sin(J)^2\,\left(3\sin(K)^2-2\right) \\ -2\,(\cos(J)-1)^2\,\left(\cos(K)^2-1\right) \\ -2\,(\cos(J)+1)^2\,\left(\cos(K)^2-1\right) \\ 6\sin(J)^2\sin(K)^2 \\ 6\sin(J)^2\sin(K)^2 \\ -4\,\sin(J)\,\sin(K)\,(\cos(J)-1)\,(\cos(K)+1) \\ -4\,\sin(J)\,\sin(K)\,(\cos(J)+1)\,(\cos(K)-1) \\ -4\,\sin(J)\,\sin(K)\,(\cos(J)+1)\,(\cos(K)+1) \\ 8\,\cos(K)\,\sin(J)\,\sin(K)\,(\cos(J)-1) \\ 8\,\cos(K)\,\sin(J)\,\sin(K)\,(\cos(J)+1) \end{pmatrix}^T \begin{pmatrix} \cos(2\,\nu-\mu+2\,\phi) \\ \cos(2\,\nu-2\,\mu+2\,\phi) \\ \cos(2\,\mu-2\,\nu+2\,\phi) \\ \cos(2\,\mu+2\,\nu-2\,\phi) \\ \cos(2\,\mu+2\,\nu+2\,\phi) \\ \cos(2\,\nu) \\ \cos(2\,\mu-2\,\nu) \\ \cos(2\,\mu+2\,\nu) \\ \cos(2\,\nu-2\,\phi) \\ \cos(2\,\nu+2\,\phi) \\ \cos(\mu-2\,\nu+2\,\phi) \\ \cos(\mu+2\,\nu-2\,\phi) \\ \cos(\mu+2\,\nu+2\,\phi) \\ \cos(\mu-2\,\nu) \\ \cos(\mu+2\,\nu) \end{pmatrix} \tag{2.124}$$

with $\phi = \lambda - f$, $\cos J = \frac{N}{M}$ and $\cos K = \frac{L}{M}$ are pure functions of the conjugate momenta. Notice a secular term in Eq. (2.123) . This secular drift in the momenta goes to zero at specific values of

J and K:

$$J = \pm \cos^{-1} \sqrt{\frac{1}{3}} \qquad K = \pm \cos^{-1} \sqrt{\frac{1}{3}} \tag{2.125}$$

We note here that for a fast-rotating rigid body, the orbital frequency is usually orders of magnitude smaller than the tumbling frequency. Thus, $(\frac{n}{M/C})^2$ is a small quantity, and the problem of a fast-rotating rigid body can be studied using perturbation methods with the Hamiltonian of the form $\mathcal{H} = \mathcal{H}_0 + \epsilon \mathcal{H}_1$.

2.4.6.4 Simplification to a tumbling rigid body

A tumbling rigid body exhibits the rate of variation of μ to be faster than the other frequencies, viz, the rate of variation of ν and the mean orbital motion. The disturbing function, $\mathcal{H}_1$ can be simplified by neglecting the short-period variation of μ. This is done by averaging the axisymmetric and asymmetric components of the gravity-gradient potential over μ as follows.

$$< \mathcal{V}_{axi} > = \frac{1}{2\pi} \int_0^{2\pi} \mathcal{V}_{axi}(\mu) d\mu \tag{2.126}$$

$$< \mathcal{V}_{asy} > = \frac{1}{2\pi} \int_0^{2\pi} \mathcal{V}_{asy}(\mu) d\mu \tag{2.127}$$

$$\begin{aligned} &< \mathcal{V}_{axi} \\ &> \\ &= 2 \left(3 \sin(J)^2 - 2\right) \left(3 \sin(K)^2 - 2\right) - 6 \sin(K)^2 \left(3 \sin(J)^2 - 2\right) \left(2 \cos(\phi)^2 - 1\right) \end{aligned} \tag{2.128}$$

$$\begin{aligned} &< \mathcal{V}_{asy} \\ &> \\ &= 6 \sin(J)^2 \sin(K)^2 \left(2 \cos(\nu + \phi)^2 - 1\right) \\ &\quad - 4 \sin(J)^2 \left(3 \sin(K)^2 - 2\right) \left(2 \cos(\nu)^2 - 1\right) + 6 \sin(J)^2 \sin(K)^2 \left(2 \cos(\nu - \phi)^2 - 1\right) \end{aligned} \tag{2.129}$$

Utilizing this form of the disturbing function, one can qualitatively analyze the rigid body tumbling motion using phase-space analysis of the $J - \nu$ space. The influence of the small parameter is shown below for the inertia ratios of $B/C = 0.844207$ and $A/C = 0.260936$, which are the inertia ratios of the PEGASUS-A satellite [75].

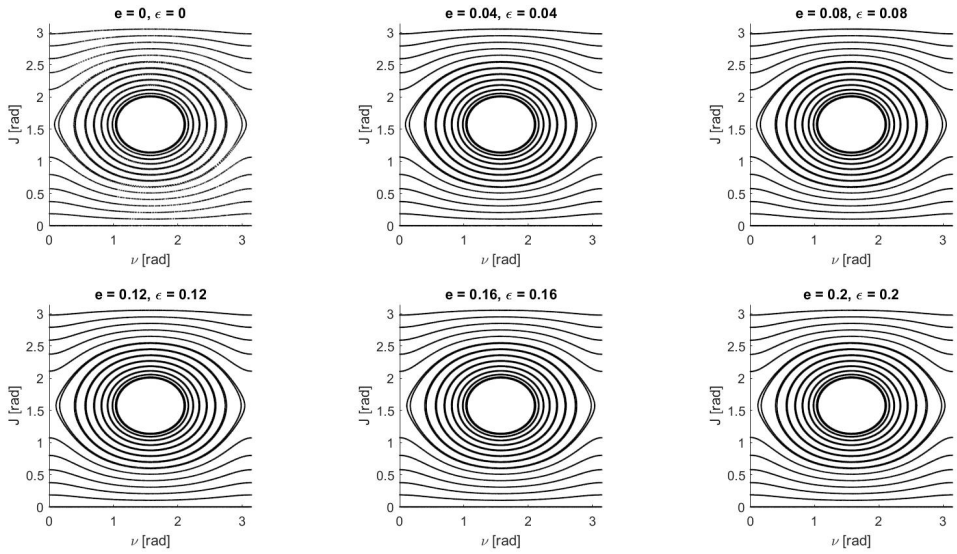

Figure 2.32: Phase-space analysis of tumbling rigid body for $B/C = 0.84$ and $A/C = 0.26$

Furthermore, one can examine the phase-space for different inertia ratios to discern the location of the equilibria as determined analytically in the previous section.

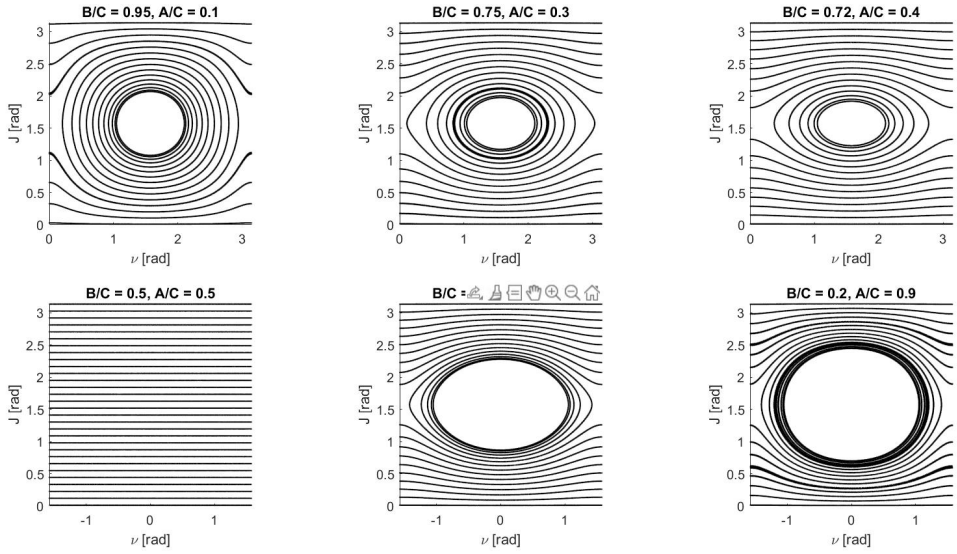

Figure 2.33: Phase-space analysis of tumbling rigid body for $e = 0.1$ and $\epsilon = 0.1$

Note that for the axisymmetric configuration ($A/C = B/C$), J is also a constant, implying that the direction of the angular momentum vector in the body-frame is constant. For $B/C > A/C$, the equilibria is at $\nu = \frac{\pi}{2}$ (and $\frac{3\pi}{2}$) and for $B/C < A/C$, the equilibria is at $\nu = 0$ (and π) as established by Eq. (2.108) . It is evident that the Hamiltonian formulation provides significant insight into the motion of rigid bodies due to its conservative nature and internal symmetries. Such formulations can also be extended to other dynamical systems. The Hamiltonian formulation coupled with perturbation methods will be examined in future chapters dealing with analytical treatment of dynamical systems.

In the past sections, an extensive study of the stability and behavior of motions was studied under the influence of gravity-gradient torques. The expression for the gravity gradient torque was however truncated to second order. This approximation is sufficient because of the assumption that the mass of the rigid body under consideration is much smaller than the primary body, and therefore does not affect the motion of the primary. Meirovitch [37], pointed out that if the rigid body were such that the second order moments of inertia were identical, the effect of gravity-gradient torque would cease to exist. In this context, the higher order moments of inertia would play an important role in the attitude motion or rigid bodies. Thus, it is worthwhile to investigate the cases when the second order contribution to the gravity-gradient torque is zero. Such configurations shall be henceforth termed as inertially symmetric rigid bodies. One particular case where the higher order gravity-gradient torques become prominent is in the study of the cube as a rigid body. In the following section, the disturbing potential for higher-order gravity gradient torque is derived and studied for cuboidal configurations.

2.5 Higher-order gravity-gradient torque formulation

For a rigid body orbiting about a central primary, the potential energy, V, can be written as the sum of all higher order terms of the Taylor expansion of central force field potential. With reference to Fig. 2.34, consider the infinitesimal mass element dm located at a distance **D** from the center of mass B^* of the rigid body B.

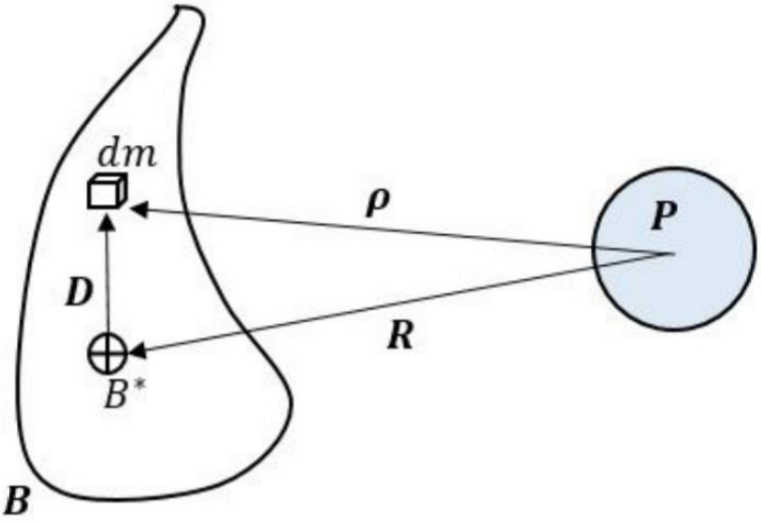

Figure 2.34: Rigid body in a central force field of a primary. B^* is the center of mass of the rigid body, D is the distance from the center of mass to a differential mass element, dm, R locates the rigid body with respect to the primary, P

The potential of the mass element can be written in terms of the gravitational parameter μ and the distance of the mass element from the center of mass of the primary as follows.

$$dV = -\frac{\mu}{|\rho|}\mathrm{d}m = -\frac{\mu}{|\mathbf{R}+\mathbf{D}|}\mathrm{d}m \tag{2.130}$$

The gravitational potential of the rigid body is then formulated by the following integral over B.

$$V = \int_B dV \tag{2.131}$$

Utilizing $|\mathbf{R}+\mathbf{D}|^2 = R^2 + D^2 + 2\mathbf{R}\cdot\mathbf{D}$, one can write $|\mathbf{R}+\mathbf{D}|$ as:

$$|\mathbf{R}+\mathbf{D}| = R\Big(1 + 2\frac{\hat{\mathbf{R}}\cdot\mathbf{D}}{R} + \frac{D^2}{R^2}\Big)^{1/2} \tag{2.132}$$

where, $\hat{\mathbf{R}}$ is the unit vector along $\mathbf{R}$. $|\mathbf{R}+\mathbf{D}|$ can be written in the form of a series using Taylor expansion and truncation of appropriate order using the expression in Eq. (2.132) . Up to fourth

order, the disturbing potential due to gravity is then written as follows.

$$|\mathbf{R}+\mathbf{D}|^{-1} = \frac{1}{R} - \frac{\hat{\mathbf{R}}\cdot\mathbf{D}}{R^2} + \left[\frac{3}{2}\frac{(\hat{\mathbf{R}}\cdot\mathbf{D})^2}{R^3} - \frac{1}{2}\frac{D^2}{R^3}\right] - \left[\frac{5}{2}\frac{(\hat{\mathbf{R}}\cdot\mathbf{D})^3}{R^4} - \frac{3}{2}\frac{D^2(\hat{\mathbf{R}}\cdot\mathbf{D})}{R^4}\right] + \left[\frac{3}{8}\frac{D^4}{R^5} + \frac{35}{8}\frac{(\hat{\mathbf{R}}\cdot\mathbf{D})^4}{R^5} - \frac{15}{4}\frac{D^2(\hat{\mathbf{R}}\cdot\mathbf{D})^2}{R^5}\right] + \mathcal{O}(R^{-6}) \tag{2.133}$$

Using Eq. (2.133) , the leading terms of dV are written as

$$dV^{(0)} = -\frac{\mu}{R}\mathrm{d}m(\mathbf{D}) \tag{2.134}$$

$$dV^{(1)} = \mu\frac{\hat{\mathbf{R}}\cdot\mathbf{D}}{R^2}\mathrm{d}m(\mathbf{D}) \tag{2.135}$$

$$dV^{(2)} = -\mu\left[\frac{3}{2}\frac{(\hat{\mathbf{R}}\cdot\mathbf{D})^2}{R^3} - \frac{1}{2}\frac{D^2}{R^3}\right]\mathrm{d}m(\mathbf{D}) \tag{2.136}$$

$$dV^{(3)} = \mu\left[\frac{5}{2}\frac{(\hat{\mathbf{R}}\cdot\mathbf{D})^3}{R^4} - \frac{3}{2}\frac{D^2(\hat{\mathbf{R}}\cdot\mathbf{D})}{R^4}\right]\mathrm{d}m(\mathbf{D}) \tag{2.137}$$

$$dV^{(4)} = -\mu\left[\frac{3}{8}\frac{D^4}{R^5} + \frac{35}{8}\frac{(\hat{\mathbf{R}}\cdot\mathbf{D})^4}{R^5} - \frac{15}{4}\frac{D^2(\hat{\mathbf{R}}\cdot\mathbf{D})^2}{R^5}\right]\mathrm{d}m(\mathbf{D}) \tag{2.138}$$

Substituting the equations above into Eq. (2.131) gives the leading terms of the gravitational potential V up to fourth order. The zeroth-order gravitational potential is given by

$$V^{(0)} = \int_B -\frac{\mu}{R}\mathrm{d}m(\mathbf{D}) = -\frac{\mu m}{R} \tag{2.139}$$

where m is the mass of the rigid body. Since $\mathbf{D}$ is measured from the center of mass (Fig. 2.34), the first-order contribution is zero.

$$V^{(1)} = \int_B \mu\frac{\hat{\mathbf{R}}\cdot\mathbf{D}}{R^2}\mathrm{d}m(\mathbf{D}) = \int_B \mu\frac{\hat{\mathbf{R}}}{R^2}\cdot\mathbf{D}\mathrm{d}m(\mathbf{D}) = 0 \tag{2.140}$$

For higher-order contributions, the inertia integrals of the rigid body can be defined as.

$$J_{\underbrace{x\cdots x}_{p\text{ times}}\underbrace{y\cdots y}_{q\text{ times}}\underbrace{z\cdots z}_{r\text{ times}}} = \int_B (D^x)^p(D^y)^q(D^z)^r\mathrm{d}m(\mathbf{D}) \tag{2.141}$$

where D^x, D^y, D^z are components of the **D** vector: $D^2 = D^{x^2} + D^{y^2} + D^{z^2}$ and $\hat{\mathbf{R}} \cdot \mathbf{D} = R^x D^x + R^y D^y + R^z D^z$. The higher-order gravity potentials can then be written as follows.

$$V^{(2)} = -\frac{\mu}{2R^3}\left[(1-3(R^x)^2)I_{xx} + (1-3(R^y)^2)I_{yy} + (1-3(R^z)^2)I_{zz}\right] \tag{2.142}$$

where, $I_{xx} = J_{yy} + J_{zz}$, $I_{yy} = J_{xx} + J_{zz}$, and $I_{zz} = J_{yy} + J_{xx}$. On simplification and using $(R^x)^2 + (R^y)^2 + (R^z)^2 = 1$, Eq. (2.142) reduces to Eq. (2.113) as expected. Here, it is assumed that the rigid body reference frame is aligned with the direction of principal moments of inertia. At order three,

$$V^{(3)} = \frac{\mu}{2R^4}\begin{pmatrix} 5\,\mathrm{Rx}^3 - 3\,\mathrm{Rx} \\ 5\,\mathrm{Ry}^3 - 3\,\mathrm{Ry} \\ 5\,\mathrm{Rz}^3 - 3\,\mathrm{Rz} \\ 3\,\mathrm{Ry}\,\left(5\,\mathrm{Rx}^2 - 1\right) \\ 3\,\mathrm{Rx}\,\left(5\,\mathrm{Ry}^2 - 1\right) \\ 3\,\mathrm{Rx}\,\left(5\,\mathrm{Rz}^2 - 1\right) \\ 3\,\mathrm{Rz}\,\left(5\,\mathrm{Rx}^2 - 1\right) \\ 3\,\mathrm{Rz}\,\left(5\,\mathrm{Ry}^2 - 1\right) \\ 3\,\mathrm{Ry}\,\left(5\,\mathrm{Rz}^2 - 1\right) \\ 30\,\mathrm{Rx}\,\mathrm{Ry}\,\mathrm{Rz} \end{pmatrix}^T \begin{pmatrix} \mathrm{Jxxx} \\ \mathrm{Jyyy} \\ \mathrm{Jzzz} \\ \mathrm{Jxxy} \\ \mathrm{Jxyy} \\ \mathrm{Jxzz} \\ \mathrm{Jxxz} \\ \mathrm{Jyyz} \\ \mathrm{Jyzz} \\ \mathrm{Jxyz} \end{pmatrix} \tag{2.143}$$

with (R^x), (R^y), (R^z) being the components of $\hat{\hat{\mathbf{R}}}$. The fourth-order term in the expansion of the gravity-gradient potential is expressed as follows.

$$V^{(4)} = \frac{\mu}{8R^5} \begin{pmatrix} -35\,\mathrm{Rx}^4 + 30\,\mathrm{Rx}^2 - 3 \\ -35\,\mathrm{Ry}^4 + 30\,\mathrm{Ry}^2 - 3 \\ -20\,\mathrm{Rx}\,\mathrm{Rz}\,\left(7\,\mathrm{Rz}^2 - 3\right) \\ -20\,\mathrm{Ry}\,\mathrm{Rz}\,\left(7\,\mathrm{Ry}^2 - 3\right) \\ -20\,\mathrm{Ry}\,\mathrm{Rz}\,\left(7\,\mathrm{Rz}^2 - 3\right) \\ -35\,\mathrm{Rz}^4 + 30\,\mathrm{Rz}^2 - 3 \\ -20\,\mathrm{Rx}\,\mathrm{Ry}\,\left(7\,\mathrm{Ry}^2 - 3\right) \\ -20\,\mathrm{Rx}\,\mathrm{Rz}\,\left(7\,\mathrm{Rx}^2 - 3\right) \\ -210\,\mathrm{Rx}^2\,\mathrm{Ry}^2 + 30\,\mathrm{Rx}^2 + 30\,\mathrm{Ry}^2 - 6 \\ -20\,\mathrm{Rx}\,\mathrm{Ry}\,\left(7\,\mathrm{Rx}^2 - 3\right) \\ -210\,\mathrm{Rx}^2\,\mathrm{Rz}^2 + 30\,\mathrm{Rx}^2 + 30\,\mathrm{Rz}^2 - 6 \\ -210\,\mathrm{Ry}^2\,\mathrm{Rz}^2 + 30\,\mathrm{Ry}^2 + 30\,\mathrm{Rz}^2 - 6 \\ -60\,\mathrm{Ry}\,\mathrm{Rz}\,\left(7\,\mathrm{Rx}^2 - 1\right) \\ -60\,\mathrm{Rx}\,\mathrm{Rz}\,\left(7\,\mathrm{Ry}^2 - 1\right) \\ -60\,\mathrm{Rx}\,\mathrm{Ry}\,\left(7\,\mathrm{Rz}^2 - 1\right) \end{pmatrix}^T \begin{pmatrix} \mathrm{Jxxxx} \\ \mathrm{Jyyyy} \\ \mathrm{Jxzzz} \\ \mathrm{Jyyyz} \\ \mathrm{Jyzzz} \\ \mathrm{Jzzzz} \\ \mathrm{Jxyyy} \\ \mathrm{Jxxxz} \\ \mathrm{Jxxyy} \\ \mathrm{Jxxxy} \\ \mathrm{Jxxzz} \\ \mathrm{Jyyzz} \\ \mathrm{Jxxyz} \\ \mathrm{Jxyyz} \\ \mathrm{Jxyzz} \end{pmatrix} \tag{2.144}$$

Given the explicit expressions for the fourth-order gravity potential expansion, the gravity-gradient torque can be found as follows.

$$\mathbf{L} = \mathbf{R} \times \mathbf{F} = \mathbf{R} \times \left[-\frac{\partial V}{\partial \mathbf{R}} \right] = \hat{\mathbf{R}} \times \left[-\frac{\partial V}{\partial \hat{\mathbf{R}}} \right] \tag{2.145}$$

where $V = V^{(0)} + V^{(1)} + V^{(2)} + V^{(3)} + V^{(4)}$. Substituting them into the equations of attitude motion in terms of the CRPs, one can perform additional qualitative analysis on the behavior of the motions and the stability of equilibria. The expressions above simplify to a considerable extent when the rigid body under consideration is inertially symmetric. In the following section, the attitude behavior is explored for the inertially symmetric cube configuration.

2.5.1 A rigid cube

In this section, we consider specifically a unit cube with the principal directions emanating from the centers of the three mutually perpendicular faces. The origin of the body frame is at the center of mass of the cube. Because of the symmetric nature of the cube, the second-order moment of inertia is identical.

$$J_{xx} = \frac{M}{a^3}\int_{-a/2}^{a/2}\int_{-a/2}^{a/2}\int_{-a/2}^{a/2} x^2 dxdydz = \frac{M}{12}a^2$$

$$J_{yy} = \frac{M}{a^3}\int_{-a/2}^{a/2}\int_{-a/2}^{a/2}\int_{-a/2}^{a/2} y^2 dxdydz = \frac{M}{12}a^2$$

$$J_{zz} = \frac{M}{a^3}\int_{-a/2}^{a/2}\int_{-a/2}^{a/2}\int_{-a/2}^{a/2} z^2 dxdydz = \frac{M}{12}a^2$$

Thus, $I_{xx} + I_{yy} + I_{zz} = \frac{M}{6}a^2$, where a is the length of the side of the cube and M is its mass. Due to this symmetry, our original formulation of the gravity-gradient torque with a truncation of terms at second order results in a torque-free case of attitude motion of the rigid body for which we have analytical solutions: $\omega_1(t) = \omega_{1_0}$, $\omega_2(t) = \omega_{2_0}$, and $\omega_3(t) = \omega_{3_0}$. Therefore, the higher-order moments of inertia become significant in determining the motion.

Taking into account the higher-order moments of inertia for the cube, one can show that there exists only certain non-zero terms in the inertia expansion of Eq. (2.141) [57]. Specifically:

$$J_{\underbrace{x\cdots x}_{p\text{ times}}\underbrace{y\cdots y}_{q\text{ times}}\underbrace{z\cdots z}_{r\text{ times}}} \begin{cases} = 0 & \text{if } p \text{ or } q \text{ or } r \text{ are odd} \\ \neq 0 & \text{otherwise} \end{cases} \tag{2.146}$$

These moments of inertia are denoted as follows:

$$I_{xx} = I_{yy} = I_{zz} = I = \frac{M}{6}a^2 \tag{2.147}$$

$$J_{xxxx} = J_{yyyy} = J_{zzzz} = J_1 = \frac{M}{80}a^4 \tag{2.148}$$

$$J_{xxyy} = J_{yyzz} = J_{xxzz} = J_2 = \frac{M}{144}a^4 \tag{2.149}$$

The equations of motion can then be obtained using the same procedure as in previous sections. Utilizing Eq. (2.64) , we observe that for a general rigid body, the origin is not an equilibrium point anymore since

$$\dot{\mathbf{x}} = \begin{pmatrix} 0 \\ 0 \\ 0 \\ 0 \\ \frac{\Omega^2\,(15\,\mathrm{Jxyyz} - 20\,\mathrm{Jxxxz} + 15\,\mathrm{Jxzzz} - 12\,\mathrm{Jxxz}\,a + 3\,\mathrm{Jyzz}\,a + 3\,\mathrm{Jzzz}\,a)}{4\,a^2} \\ -\frac{\Omega^2\,(15\,\mathrm{Jxyyy} - 20\,\mathrm{Jxxxy} + 15\,\mathrm{Jxyzz} - 12\,\mathrm{Jxyy}\,a + 3\,\mathrm{Jyyz}\,a + 3\,\mathrm{Jzzz}\,a)}{4\,a^2} \end{pmatrix} \neq \mathbf{0} \tag{2.150}$$

for $[\mathbf{q}, \dot{\mathbf{q}}] = \mathbf{0}$ and with $\Omega = \sqrt{\frac{\mu}{a^3}}$. Note however, the origin is an equilibrium point for a cuboidal configuration. To evaluate the stability of the origin, the Jacobian is obtained a follows

$$J = \begin{bmatrix} \mathbf{0} & \mathbf{I}_{3\times 3} \\ -K & -C \end{bmatrix} \tag{2.151}$$

where,

$$K = \begin{pmatrix} 0 & 0 & 0 \\ 0 & -\frac{35\,\Omega^2\,(J_1 - 3\,J_2)}{2\,I\,a^2} & 0 \\ 0 & 0 & -\frac{35\,\Omega^2\,(J_1 - 3\,J_2)}{2\,I\,a^2} \end{pmatrix} \tag{2.152}$$

and

$$C = \begin{pmatrix} 0 & -\Omega & 0 \\ \Omega & 0 & 0 \\ 0 & 0 & 0 \end{pmatrix} \tag{2.153}$$

It is noted here that there may be additional equilibria due to the contribution of the fourth-order gravity-gradient torques. Utilizing the CRPs formulates the attitude motion equations in algebraic form, thereby facilitating the identification of these equilibria through numerical computer-algebra packages. The following equilibria are identified and their linear stability is obtained. A total of 49 equilibrium points are obtained. They are listed along with their linear stability in Tab. 2.2.

Table 2.2: Isolated equilibria for cuboidal configuration and stability

q_1	q_2	q_3	Stability
0	0	0	center
± 1	$\pm(\sqrt{3} \pm 1)$	0	unstable
± 1	$\pm(\sqrt{2})$	0	unstable
± 1	0	$\pm(\sqrt{3} \pm 1)$	unstable
± 1	0	$\pm(\sqrt{2})$	unstable
0	$\pm(1 \pm \sqrt{2})$	0	center
0	± 1	0	center
0	$\pm(\frac{\sqrt{3}}{2} \pm \frac{1}{2})$	$\pm(\frac{\sqrt{3}}{2} \pm \frac{1}{2})$	unstable
0	$\pm\sqrt{2}/2$	$\pm\sqrt{2}/2$	unstable
0	0	± 1	center
0	0	$\pm(1 \pm \sqrt{2})$	unstable

It is noted that each of the above configurations correspond to three particular orientations of the rigid body:

- E_1 The radial vector passing through the center of two opposite faces
- E_2 The radial vector passing through the center of diagonally opposite edges
- E_3 The radial vector passing through diagonally opposite corners

Through linear analysis, the first two equilibrium configurations can be shown to be unstable and the third of center type. These configurations are shown in the figure below.

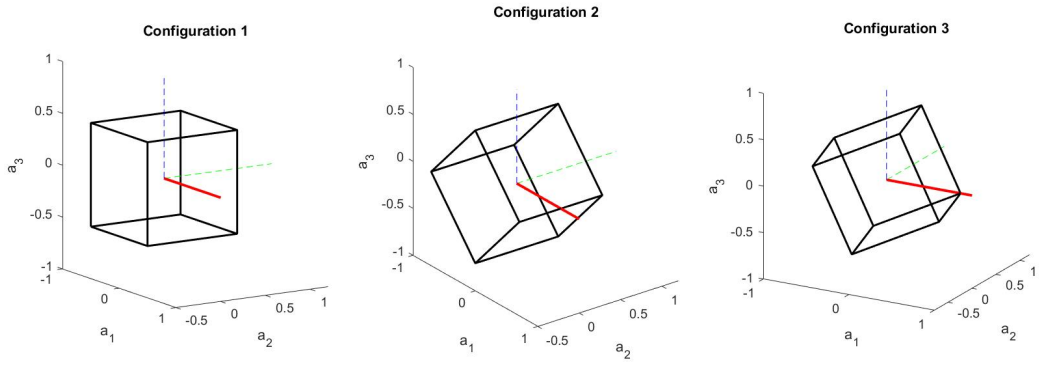

Figure 2.35: Equilibrium configurations for a cube. Configuration 1: The radial vector passes through the center of two opposite faces. Configuration 2: The radial vector passes through the center of diagonally opposite edges. Configuration 3: The radial vector passes through diagonally opposite vertices. The radial vector is shown in red.

2.5.2 Lyapunov stability of equilibrium configurations

One can further analyze Eq. (2.151) for stability. Noting the structure of Eq. (2.152) , one can note that the presence of 0s in the term corresponding to q_1 contribution leads to the conclusion that the Hamiltonian has q_1 as an ignorable coordinate and therefore is cyclic. Additionally, due to the absence of damping terms, asymptotic stability is out of the question. According to Lyapunov's direct method, the motion in the neighborhood of an equilibrium configuration is stable if there exists for the system a Lyapunov function, which is positive definite in that neighborhood and whose time derivative is zero. Noting that the kinetic energy will always be a positive definite quantity due to quadratic terms in the angular velocity, it is sufficient to test the potential of the problem alone. Particularly, since we know that the second-order terms in the potential lead to

stable motions (since $I_1 = I_2 = I_3$), only the higher-order potential terms are required to ascertain stability. The equilibrium configurations can therefore also be obtained by solving the following two algebraic equations:

$$\frac{\partial U}{\partial q_i} = 0 \qquad i = 2, 3 \tag{2.154}$$

where U is the gravity-gradient potential contribution from the third and fourth-order. Note that only two equations determine the complete set of equilibrium configurations. Therefore, to test for stability, the Hessian matrix can be examined for positive definiteness. The Hessian matrix is defined as:

$$H = \left[\frac{\partial^2 U}{\partial q_i \partial q_j}\right] \qquad i = 2, 3 \tag{2.155}$$

For the three configurations, the Hessian matrices are given as:

$$H_{E_1} = K \begin{bmatrix} -70 & 0 \\ 0 & -70 \end{bmatrix} \tag{2.156}$$

$$H_{E_2} = K \begin{bmatrix} 1.5012 & 0 \\ 0 & -\frac{1.5012}{2} \end{bmatrix} \tag{2.157}$$

$$H_{E_3} = K \begin{bmatrix} 1.042 & 0 \\ 0 & 1.042 \end{bmatrix} \tag{2.158}$$

where, $K = \Omega^2(3J_2 - J_1)/R^2$.

These Hessian matrices can be checked for positive definiteness using the Sylvester criterion. If $K > 0$, the method of Lyapunov leads to the conclusion that only the equilibrium position E_3 is stable. Alternatively, if $K < 0$ is stable, which agrees with Tab. 2.2 for $K > 0$ up to a linear analysis.

Therefore, the higher order gravity gradient torques are significant in that they can alter the stability of the equilibrium compared to the second order approximation. Furthermore, the higher-

order gravity gradient approximation may cause the creation or destruction of isolated equilibria, which may not be straightforward through the approximate model used in previous sections. Particularly, when the three principal moments of inertia are equal, terms in the second order inertia integrals cancel out, and higher order integrals are dominant. Also, when the principal moments of inertia are nearly equal, the corresponding terms in the gravitational potential may become comparable in magnitude with the terms in higher-order inertia integrals.

2.6 Qualitative analysis of the planar cirular restricted three body problem

The Global Exploration Roadmap [76, 77, 78, 79] has inspired international interest in a new era of human exploration of the solar system. From among several different efforts, NASA is currently focused on positioning and maintaining an inhabited facility in a long-term and relatively stable orbit in the lunar vicinity. The Earth-Moon libration points offer many options for both storage of propellant and supplies for lunar missions, as well as potential locations for a space-based facility to support future crewed and robotic translunar missions [78, 79]. Beyond the near-vicinity of the Moon, applications are being pursued throughout an expanded Earth neighborhood within lunar orbit. To this end, characterizing the behavior of trajectories in the domain of the relevant phase-volume and identifying dynamical structures existing in the circular restricted three-body problem is of paramount importance for mission design applications.

The pioneering work by Conley [80] on the existence of transit trajectories in the Planar Circular Restricted Three-Body Problem (PCR3BP) led to much attention being devoted to leveraging the collinear points for space missions [81, 82, 83, 84, 85, 86, 87]. Previous research [81, 82, 88] has shown the existence of low-energy transfer trajectories that exploit the natural dynamics from the presence of a fourth body (such as the Sun's gravity). Such ballistic transfers, while very fuel efficient, require a large transfer duration. It is therefore of interest to identify transport opportunities utilizing short duration direct transfers from the Earth to cislunar space. Many such types of transfers exist, and an extensive survey of short-duration transfers can be obtained in Parker and Born [82]. Qualitative analysis tools from dynamical systems theory are often used to identify, generate and categorize transfers in the cislunar space [89, 90, 91, 92, 83, 93, 87, 94].

This section of the dissertation seeks to address two primary challenges:

- Obtain a better understanding of the natural dynamics of a particle under the influence of the gravity field of the Earth and the Moon within the framework of the PCR3BP. The invariant manifolds associated with the planar periodic orbits about the collinear equilibrium points dictate the flow of such particles into and through these orbits in the neighborhood of the equilibria. Understanding this flow will then assist in the characterization of transfers to these periodic orbits. Through qualitative analysis techniques discussed in previous sections, this work seeks to identify key dynamical structures that influence the evolution of the invariant manifolds in the phase-space, and utilize such structures to obtain short-duration direct transfer opportunities to planar periodic orbits.

- Develop a catalog of orbital transfers in the Earth-Moon system identifying the different types of transport opportunities to libration point orbits that can serve in a practical capacity for future mission design applications. This road-map of trajectories can then be used to perform simple geometric analysis to extrapolate the catalog information to identify effective transfer opportunities to other periodic orbits.

The remainder of this section is organized as follows. First, we provide a brief introduction of the PCR3BP and develop the groundwork for describing the zero-momentum surface of section, a special type of Poincaré surface of section developed in this research. Next, the structure of the zero-momentum maps is discussed in detail to explain the flow in the neighborhood of the primary bodies. A new topology is introduced that enables the visualization of the dynamical structure in the phase-space and examines the geometry of the motions obtained. The information from this construction is utilized to find short-duration transfers to the periodic orbits about the libration points. Particularly, the zero-momentum maps provide an upper-bound on the thrust direction for tangential transfers to these orbits. A continuation process is introduced through which multiple families of transfers are identified. Finally, a geometric approach is developed utilizing information from tangential transfers to identify non-tangential transfer opportunities.

2.6.1 PCR3BP and the definition of zero-momentum points

The motion of a particle subjected to the gravitational attraction of two bodies (referred to as primaries) is studied [95, 96, 97]. The underlying assumption that the particle's mass is negligible compared to the primaries allows the treatment of the three-body problem, as restricted in the sense that the primaries are assumed to move on Keplerian orbits around their common barycenter. In this work, a special case of the restricted three-body problem is considered, wherein the primaries move in circular orbits, and the motion of the third body is confined to the plane containing the two primaries. This model is known as the PCR3BP. It is described below.

2.6.1.1 The planar circular restricted three-body model

A rotating reference frame centered at the barycenter of the primaries rotating with the angular velocity of the primaries is considered. The $\hat{x}$-axis is directed from the barycenter to the less-massive primary, and the $\hat{z}$-axis is in the direction of the angular momentum vector of the system. The units of measure are normalized, such that the gravitational constant and the sum of masses of the primaries are unity, and the period of rotation of the primaries is 2π. Denoting $\mu = \frac{m_2}{m_1+m_2}$ as the mass parameter, the more massive primary (with mass m_1) is located at $(-\mu, 0, 0)$ and the other (with mass m_2) at $(1-\mu, 0, 0)$. The set-up of the problem is illustrated in Fig. 2.36.

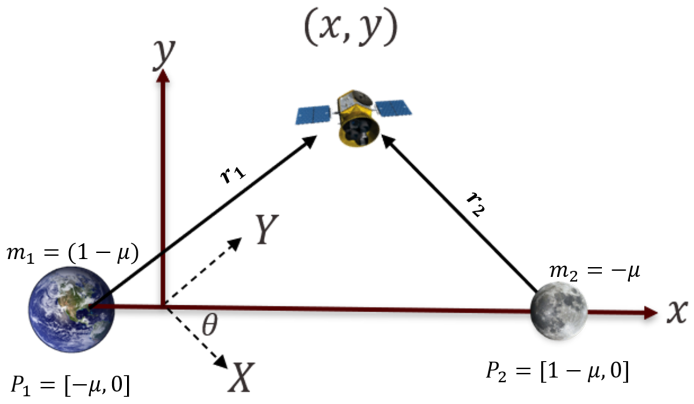

Figure 2.36: The geometry of the planar circular restricted three body problem

The equations of motion for the PCR3BP in the rotating frame can be written in vector form as:

$$\ddot{\mathbf{q}} + 2\boldsymbol{\omega} \times \dot{\mathbf{q}} = \frac{\partial \Omega}{\partial \mathbf{q}} \tag{2.159}$$

where $\boldsymbol{\omega} = [0, 0, 1]^T$ and $\mathbf{q} = [x, y]^T$. $\Omega = \frac{1}{2}(x^2 + y^2) + \frac{1-\mu}{r_1} + \frac{\mu}{r_2}$ is the PCR3BP pseudo-potential obtained by augmenting the inertial potential with the potential of the rotating frame. $r_1 = ((x+\mu)^2 + y^2)^{1/2}$ and $r_2 = ((x-1+\mu)^2 + y^2)^{1/2}$ locates the third body with respect to the first and second primary, respectively. The autonomous and conservative nature of the Hamiltonian admits a constant of motion (the Jacobi constant) as $C = -2\mathcal{H} = -|\dot{\mathbf{q}}|^2 + 2\Omega$ which is commonly used as a measure of energy in the PCR3BP.

Equation (2.159) admits five equilibrium points: the so-called collinear (L_1, L_2, L_3) and triangular (L_4, L_5) points based on its location in the rotating frame [95]. The triangular points are linearly stable for a mass parameterμ less than a critical value ($\mu_c = 0.0385$) and the collinear points are always linearly unstable. The curves of zero-velocity (obtained from the expression for the Jacobi constant for a particular value of μ) denote regions of the phase-space where a particle arrives with zero velocity and therefore cannot penetrate these curves [95]. They partition the phase-space into the regions of motion and the forbidden region. Fig. 2.37 illustrates the libration points and the zero-velocity curves associated with different energy levels.

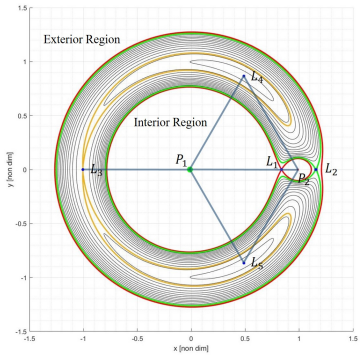

Figure 2.37: Equilibria and Zero-Velocity Curves

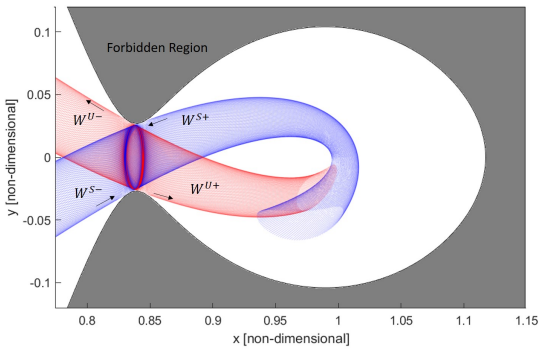

Figure 2.38: Stable and unstable manifolds of a periodic orbit at L_1 ($C = 3.1853$).

The equilibrium points host a variety of periodic orbits in their vicinity, and dynamical systems tools can be employed to construct them. In the PCR3BP, the periodic orbits about the collinear equilibrium points are called Lyapunov orbits. An initial Lyapunov orbit is obtained using the linearized dynamics about the equilibrium point and using the method of differential corrections to ensure closure of the orbit [91, 84, 96]. A continuation process can then be used to obtain other Lyapunov orbits at different energy values[98]. Each periodic orbit can be identified using its time-period (T) and the Jacobi constant (C). Thus, a periodic orbit is represented as $\Gamma(T, C)$. Any specific point on the periodic orbit can be represented using a parameter $\tau \in [0, T)$ where τ is the time elapsed from an initial condition that generates the periodic orbit. Due to periodicity, $\Gamma(\tau + T) = \Gamma(\tau)$.

Similar to an equilibrium point, which are fixed points of a flow, a point on the periodic orbit is represented as a fixed point on a stroboscopic map [85]. The linearized dynamics about this fixed point are obtained from the monodromy matrix $\mathcal{M}$ which is the state transition matrix at one time, and provides insights into the flow near the periodic orbit. The eigenvalues of $\mathcal{M}$ are used to define the stability of the periodic orbit. The Lyapunov orbits about the collinear points are known to be of the type saddle $\times$ center, whose eigenvectors span the saddle and center subspace. The generalization of these eigenspaces are the invariant manifolds. The saddle subspace is then represented by the stable ($W^{S\pm}$) and unstable ($W^{U\pm}$) manifolds. These stable and unstable manifolds act as separatrices to the periodic orbit. Figure 4.3 illustrates the stable and unstable manifold branches of a Lyapunov orbit of Jacobi Constant $C = 3.1853$.

2.6.1.2 The Poincaré map and the zero-momentum surface

Poincaré maps in general refer to the intersection of a flow in the phase-space with a lower-dimensional transverse subspace, called the Poincaré section. It admits a reduction of the dimensionality of the system by at least one. If there exists an integral of motion (as is the case in the PCR3BP), the dimensionality can be further reduced by one. Although Poincaré maps are generally applied to periodic solutions to study the structure of flow in their vicinity, by definition, it only requires the specification of a subspace transversal to the flow in the phase-space [99, 83]. In

this research, we leverage this advantage to generate a Poincaré map that represents points in the phase-space where the specific momentum of the third body is zero. Certain intuitions are obtained by computing a Poincaré map that records the intersections of the flow with a subspace on which the magnitude of the momentum is zero. Such a dynamical construction will provide valuable insights to describe transport in cislunar space.

The magnitude of the specific momentum of the third-body is given by its component along the angular momentum of the primaries, i.e., $L_z = \mathbf{q} \times \dot{\mathbf{q}} = x\dot{y} - y\dot{x} = \pm rv \sin\theta$ (the plus sign being associated with direct motion and the minus sign with retrograde motion). Consequently, a zero-momentum Poincaré surface of section is defined using the condition [100]:

$$\mathbf{q} \times \dot{\mathbf{q}} = 0 \tag{2.160}$$

The expression $\mathbf{q} \times \ddot{\mathbf{q}}$ determines regions of direct and retrograde motions in the phase-space. This expression can be simplified as:

$$\mathbf{q} \times \ddot{\mathbf{q}} = y\frac{\mu(1-\mu)}{r_1^3 r_2^3}[r_2^3 - r_1^3] - 2(\mathbf{q} \cdot \dot{\mathbf{q}}) \tag{2.161}$$

In general, the Poincaré surface of section is defined as:

$$\Sigma = \{(\mathbf{q}, \dot{\mathbf{q}}) : (x-a)\dot{y} - y\dot{x} = 0\} \tag{2.162}$$

where $a = 0$ represents the barycenter, $a = -\mu$ represents the more massive primary, $a = 1 - \mu$ represents the smaller primary. The intersection of the flow with this zero-momentum surface therefore identifies regions in the phase-space where the trajectories twist and change direction with respect to the barycenter or either of the primaries depending on the value of a. These maps are particularly useful in identifying the behavior of flows in the phase-space, especially in the vicinity of the invariant manifolds.

While the insights obtained in this work are valid for any three-body system, the Earth-Moon

system is considered, and the Poincaré map is referred to as a barycentric momentum map for $a = 0$, geocentric momentum map for $a = -\mu$, and selenocentric momentum map for $a = 1 - \mu$. Also, for notational purposes, the Earth neighborhood is defined as the region in the phase-space that contains the Earth at the Jacobi energy level of the L_1 Lagrange point. The Moon neighborhood is the region in the phase-space that contains the Moon for the Jacobi energy levels between the L_1 and L_2 Lagrange points. Transforming from the rotating frame to inertial frame components is straightforward and is given as:

$$L_z = x\dot{y} - y\dot{x} = X\dot{Y} - Y\dot{X} - (X^2 + Y^2) \tag{2.163}$$

$$L_{z_{\text{Inertial}}} = X\dot{Y} - Y\dot{X} = x\dot{y} - y\dot{x} + (x^2 + y^2) \tag{2.164}$$

with $\mathbf{Q} = [X, Y]^T$ denoting the inertial coordinates and $\mathbf{q} = [x, y]^T$ denoting the rotating frame coordinates. Defining $q_1 = x - a$ and $q_2 = y$, the zero-momentum condition is given as $q_1\dot{y} - q_2\dot{x} = 0$. Further, if the velocity components are written as

$$\dot{x} = v\cos\theta \tag{2.165}$$

$$\dot{y} = v\sin\theta \tag{2.166}$$

the zero-momentum condition is obtained as:

$$q_1 v\sin\theta - q_2 v\cos\theta = 0 \Rightarrow \theta = \arctan(q_2, q_1) \tag{2.167}$$

where, v is the velocity magnitude and is obtained as a function of position coordinates directly as: $v = \pm\sqrt{2\Omega - C}$ with Ω as the pseudo-potential. Equation (2.167) is very useful because it states that at the momentum map points, the velocity vector is either towards or away from $[q_1, q_2]^T$, i.e., the barycenter or either of the primaries. The decision on whether it is towards or away can be obtained by looking at the condition $\mathbf{q} \times \ddot{\mathbf{q}}$. A procedure to construct momentum maps constraining the Jacobi energy is as follows:

1. Initial conditions in position (x, y) are chosen in the desired neighborhood on a grid.

2. Initial velocity conditions associated with these positions are chosen so that the zero-momentum condition is satisfied.

3. The trajectories are allowed to evolve under the natural dynamics governed by the PCR3BP, and points of zero-momentum are recorded. (Since each initial condition is already a point on the momentum map, this point is omitted for visualization purposes)

Next, the dynamical structure of these zero momentum Poincaré maps in the Earth and Moon neighborhood is investigated.

2.6.2 Dynamical structure in the Earth-Moon neighborhood

The points on the momentum map denote regions of the phase-space where the flow changes its behavior qualitatively, i.e. exhibits direct and retrograde motions. Many physical insights can be obtained by studying the nature of these momentum maps in the Earth and Moon neighborhood. Particularly, the nature of motion in the vicinity of the invariant manifolds is investigated next.

2.6.2.1 Barycentric momentum maps in the Earth neighborhood

The barycentric momentum maps in the Earth neighborhood are constructed. To begin, the invariant manifold intersections with the zero-momentum surface are obtained. The barycentric momentum map is as shown in Fig. 2.39.

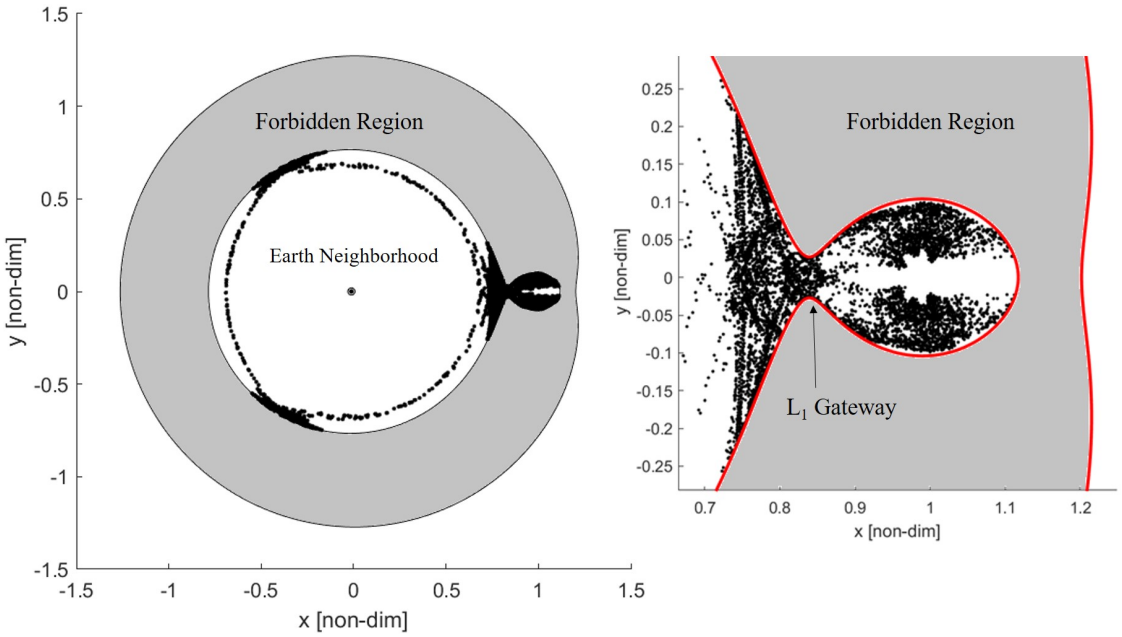

Figure 2.39: Manifold intersections with the zero-momentum surface in the Earth neighborhood. C = 3.1802

Figure 2.39 displays the L_1 gateway which is situated at the neck region of the zero-velocity curves. From Fig. 2.39 and through numerical investigation, it is observed that the invariant manifolds occupy the entire L_1 gateway in the four dimensional space. This is a noteworthy observation because, as shown by Swenson et al.,[101] the observation that the invariant manifolds completely occupy the gateway suggests that only transit trajectories are possible through the periodic orbit located at the gateway. This inference that the invariant manifolds only consist of transit trajectories within them serves as a qualitative validation of that obtained by Swenson et al. [101].

Another observation from Fig. 4.9 is that the invariant manifold intersections with the zero-momentum surface in the Earth neighborhood are located near the zero-velocity curves. This observation implies that the transitions from direct to retrograde motion occur near the boundary of the forbidden region. Following the procedure outlined in the previous section, the complete barycentric momentum map in the Earth neighborhood is obtained. For visualization purposes, each initial condition propagated is color-coded differently to distinguish different trajectories in the map. Prior to this, the inside-out topology is introduced to visualize the dynamical structure in

the vicinity of the invariant manifolds.

2.6.2.2 Inside-out topology:

Motivated by the observation (Fig. 4.9) that the manifold intersections are close to the zero-velocity curves, the following change of coordinates is suggested [100].

$$x = \frac{v}{r}\cos\theta \tag{2.168}$$

$$y = \frac{v}{r}\sin\theta \tag{2.169}$$

Recall that since the angle $\theta = \arctan(y, x)$ can be used to obtain both the position and velocity components on the momentum map, an inverse transform is fairly simple to obtain utilizing the expression for the Jacobi constant. This transformation collapses the zero-velocity curves onto the origin and takes points at the origin to infinity. Therefore, through the inside-out topology, one can visualize how the map appears near the zero-velocity curves. If the invariant manifold momentum map is super-imposed on the momentum map for all trajectories in the Earth neighborhood, it is observed that the manifold momentum map points (in black) lie in the regions surrounded by quasi-periodic motions.

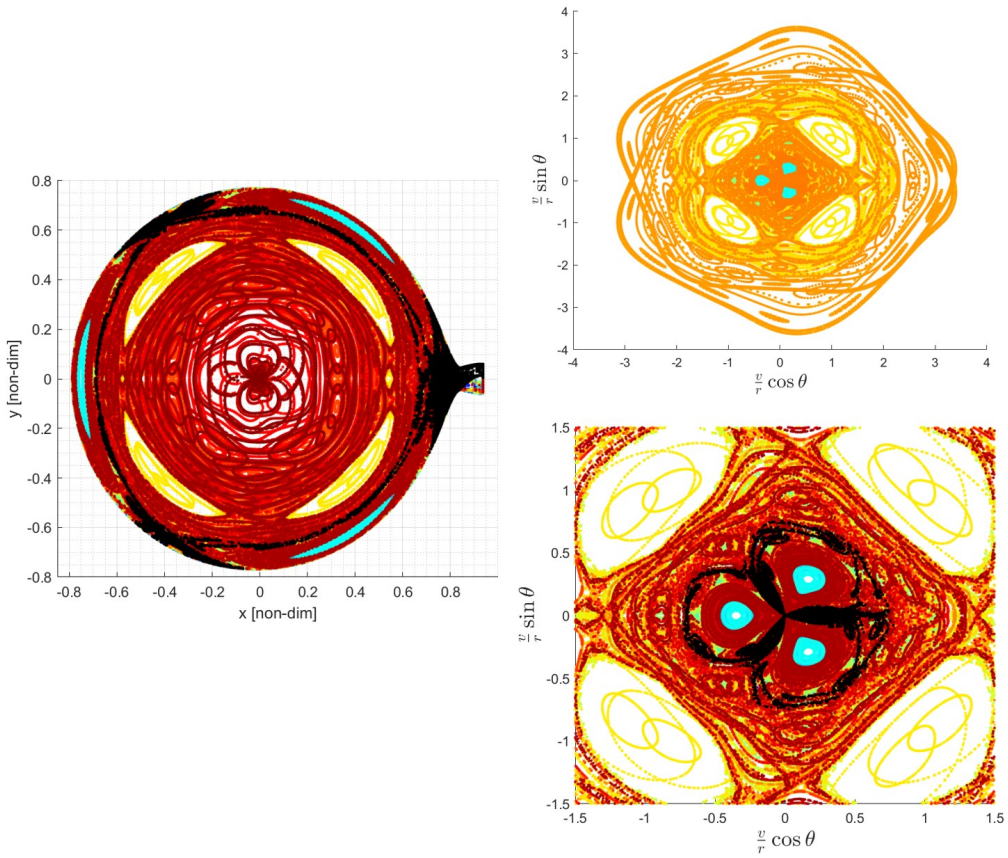

Figure 2.40: Invariant Manifold occupying the spaces between the quasi-periodic regions. $C = 3.1802$. *Left:* Momentum maps in the configuration space, *Right:* Momentum maps through the inside-out topology.

In Fig. 2.40, the stable manifold intersections are overlaid on the momentum map in the configuration space (left). While certain evidence of the behavior of the manifolds is observed, one can infer that the *inside-out transformation* provides better insight (right). It is observed that the manifolds occupy spaces between the quasi-periodic motions. Furthermore, all dynamical structures observed in the position space are captured in the new-coordinate space, albeit with better resolution. Because of the construction of the zero-momentum surface, each point on the map reflects the velocity components of the third-body scaled by the distance to the barycenter. Moreover, information from the color suggests that there are regions in the phase space, which are themselves closed off to many of the trajectories. For example, observe the two sets of quasi-periodic orbits that bound the motion of the manifolds. The color depicted for these orbits in the Fig. 2.40 (i.e. blue,

with three intersections in the phase-space and yellow, with four intersections in the phase-space) indicate that no other set of trajectories approach these quasi-periodic orbits pass through these regions again. Thus, the momentum maps are instrumental in providing a deeper understanding of the nature of transport in the PCR3BP.

2.6.2.3 Barycentric momentum maps in the Moon neighborhood

The momentum maps in the Moon neighborhood are constructed following the procedure outlined in the previous section. The Moon neighborhood is important in the study of the invariant manifold dynamics because of its influence on transfer trajectory design. The dynamical structure in the Moon neighborhood is expected to be drastically different from that in the Earth neighborhood, principally because of its proximity to the collinear equilibrium points and their associated stable, unstable and center subspaces. Just as before, each initial condition propagated is color-coded differently to distinguish different trajectories in the map. The barycentric momentum map is as shown in Fig. 2.41

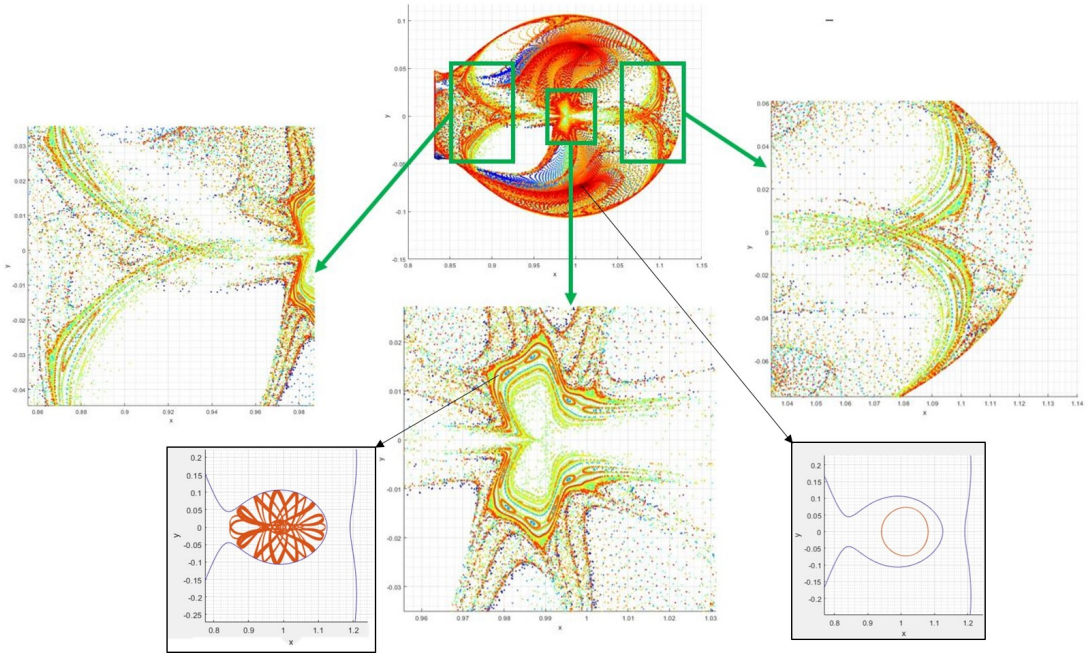

Figure 2.41: Barycentric momentum map in the Moon neighborhood. The expanded regions show the existence of quasi-periodic orbits.

In Fig. 2.41, the presence of quasi-periodic motions in the Moon neighborhood is observed. Two specific sets of quasi-periodic orbits are identified and shown in the figure. Also, it is observed that there are regions of densely populated points and sparsely populated points. One can infer that the initial conditions that originated in these regions did not make it back at a future time. The color associated with these trajectories is also consistent. These initial conditions are identified as those that lie inside the invariant manifold, specifically the unstable manifold. This deduction is intuitive, since the invariant manifold tubes act as separatrices and therefore do not intersect themselves. This observation also validates that the invariant manifold tubes contain transit trajectories. Overlaying the unstable manifold intersections with the zero-momentum surface provides additional insight to this observation. Figure 2.42 illustrates this phenomenon.

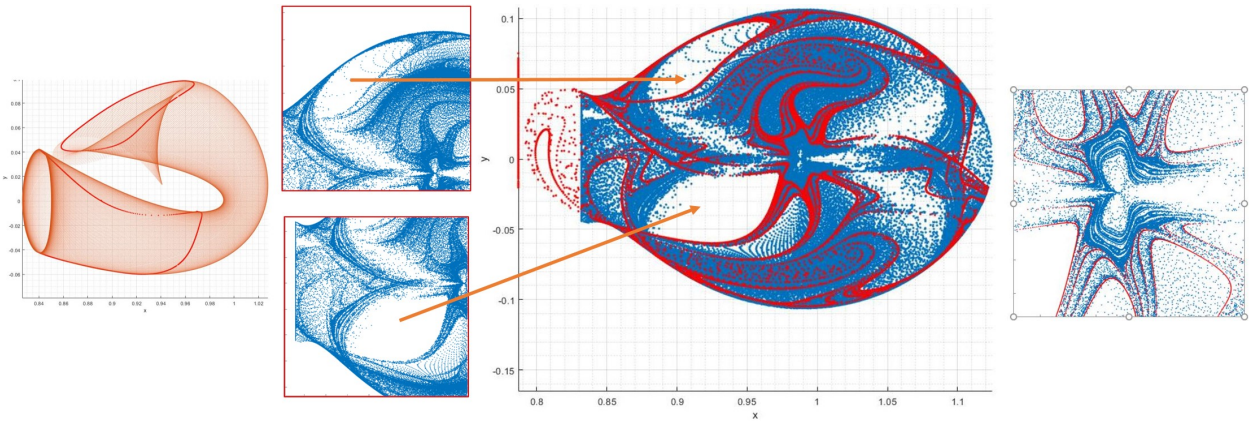

Figure 2.42: Manifold intersections with the Momentum map in the Earth neighborhood. The regions in blue are the momentum map points, while the closed curves in red are the unstable manifold intersections with the zero-momentum surface.

In Fig. 2.42, the regions in blue are the momentum map points, while the closed curves in red are the unstable manifold intersections with the zero-momentum surface. The first two intersections of the unstable manifold are shown. Clearly, the regions in the momentum map give a structure for the evolution of the unstable manifolds. Obtaining multiple intersections of the manifold with the zero-momentum surface makes this structure clearer. The manifold intersections

are observed to be confined to the spaces in between quasi-periodic motions. This is expected, since fundamentally, the manifolds occupy the saddle subspace, while the quasi-periodic motions occupy the center subspace, and the two subspaces do not intersect.

Having analyzed the behavior of the flow in the PCR3BP through the dynamical structure of the momentum maps, the following section focuses on the application of these maps to identify transfer opportunities to planar Lyapunov orbits.

2.6.3 Identification of transport opportunities in the PCR3BP

Direct transfers to Lyapunov orbits at the collinear libration points are investigated. Specifically, the barycentric momentum map in the Moon neighborhood is utilized to find manifold insertion points for the direct transfer. Recall that the points on the momentum map denote regions of the phase-space where the flow twists and changes direction. Therefore, because of the construction of the momentum maps, the direction of the velocity vector is either in the direction of the barycenter or opposite to it. A schematic of such a configuration is shown in the figure below.

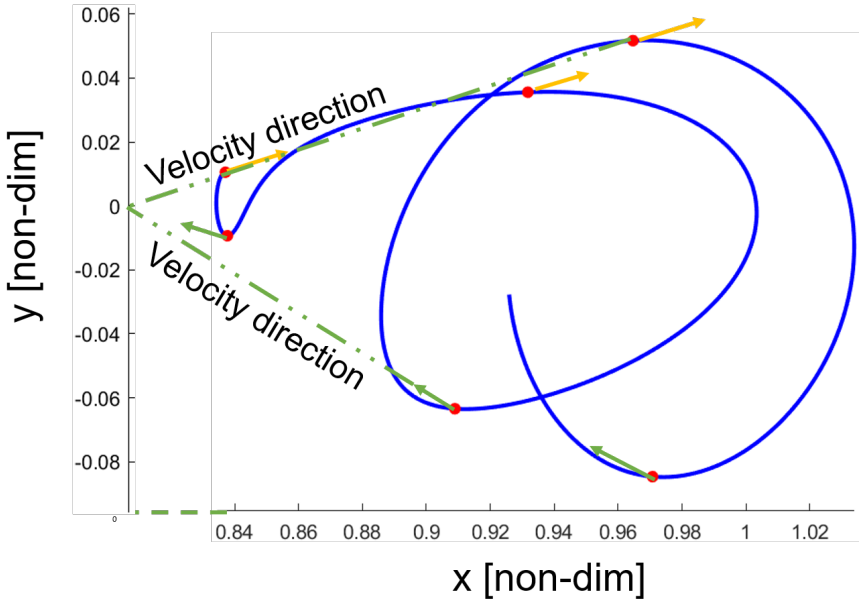

Figure 2.43: Manifold intersections with the Momentum map and directions of velocity. The velocity vector points in the direction of (or away from) the origin.

For the points on the map where the velocity vector is directed away from the position coordinates, a very high delta-v tangential transfer will result in the particle shooting towards the origin (barycenter for a barycentric momentum map and that of the primaries for the Geo/selenocentric momentum map). This information can be leveraged to obtain an upper bound on the possible tangential transfers from an Earth parking orbit (EPO) to the stable manifolds. The procedure to obtain direct tangential transfers to an L_2 Lyapunov orbit using stable manifold intersections with the zero-momentum surface is described next.

2.6.3.1 Direct transfers to Lyapunov orbits

1. Choose the Lyapunov orbit based on mission design parameters. Selecting the target orbit essentially implies fixing the Jacobi constant for the orbit insertion.

2. Generate the stable manifold segments and compute its intersection with the zero-momentum surface. The final state of the propagated stable manifold is the state that a spacecraft would need to obtain in order to inject onto the manifold segment.

3. The transfer trajectory is constructed such that it is tangential to the manifold, and a Δv is applied for manifold insertion. This maneuver is constructed by splitting the initial condition for the transfer into **r** and **v** components. Keeping the initial position (**r**) the same, a Δv is found, such that the initial condition on the transfer trajectory is $\mathbf{x}_{transfer} = [\mathbf{r}^T \quad \Delta v \frac{\mathbf{V}^T}{|\mathbf{V}|}]^T$

4. The transfer trajectory is computed backwards in time, and the state to target is an EPO of desired radius.

A schematic for the transfer trajectory design (to L_1 Lyapunov orbit) is as shown in the Fig. 2.44. This figure illustrates the two maneuvers (trans-lunar injection and manifold injection maneuvers). The black closed curves are the intersections of the stable manifold with the zero-momentum surface. The manifold insertion angle ϕ is also shown.

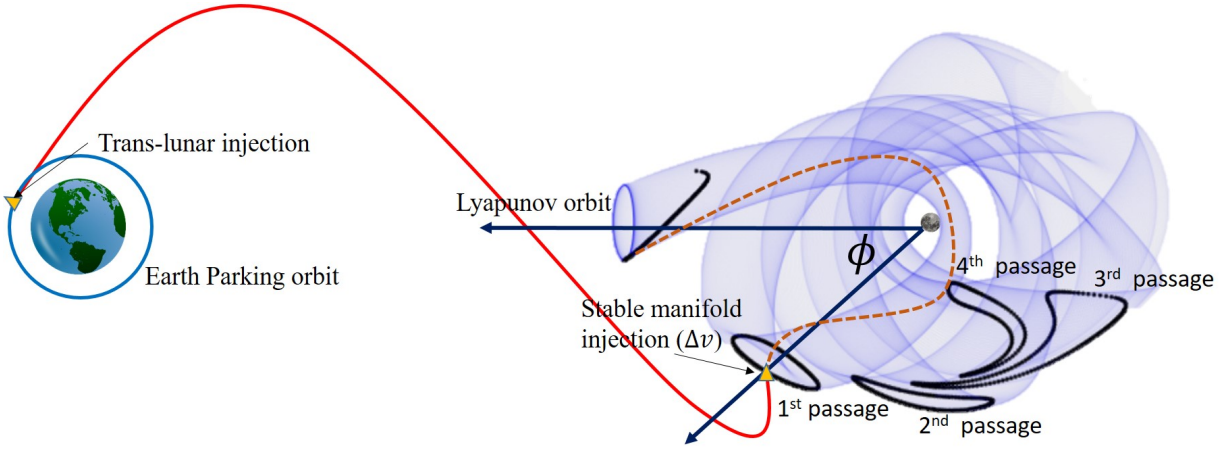

Figure 2.44: Direct transfer design schematic. The red curve shown the translunar segment, the dashed orange curve is the trajectory along the stable manifold (shown in blue). The closed black curves are the intersections of the momentum map with the stable manifold.

Note that since the transfer trajectory must be tangent to the manifold, not all the values of the manifold insertion angle ϕ can be utilized at any time instant as a manifold insertion point. In fact, there exists an upper bound on ϕ given a preference for a particular manifold branch. The points give these bounds on the momentum map. By construction of the barycentric momentum map, the barycenter of the Earth-Moon system lies on the tangent to each of the points in the map. To reach an EPO (in backwards time), one would have to use very high Δv at this momentum map point. A manifold insertion point selected downstream of the flow would then require a lower Δv to accomplish the direct transfer. Also note that any point on the manifold branch occurring upstream to the momentum map point does not result in a tangential transfer trajectory that reaches the EPO. These phenomena are demonstrated using the first three intersections of the manifold with the zero-momentum surface for an L_2 Lyapunov orbit. These three intersections are shown in Fig. 2.45 parameterized using r (computed with respect to the Moon) and ϕ (the manifold insertion angle) for a transfer to an L_2 Lyapunov orbit.

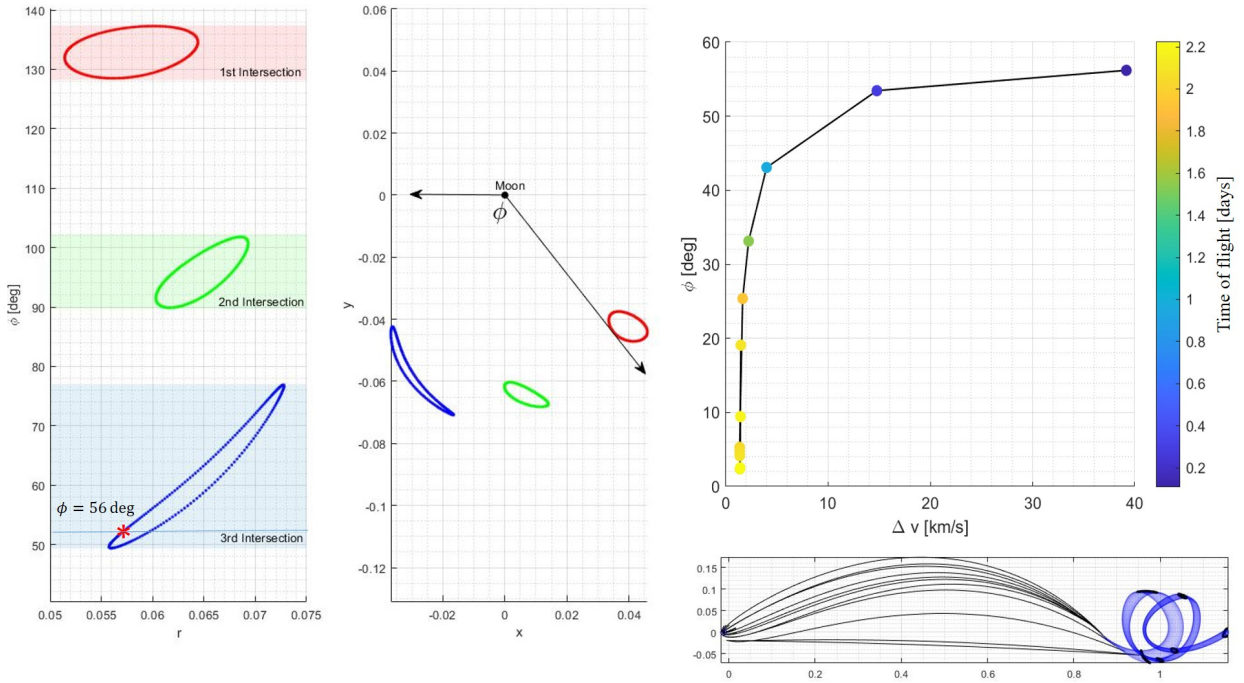

Figure 2.45: Stable manifold intersections with zero-momentum surface and direct transfers to a L_2 Lyapunov orbit.

The manifold insertion angle may be a design parameter for the mission depending on the geometry and time of a stable manifold injection maneuver. Additionally, mission design constraints may dictate the need for multiple revolutions around the Moon before reaching the periodic orbit. Each of these constraints limit the range of the manifold insertion angle, ϕ, that can be used for manifold injection. The upper limit of the bounds of ϕ denotes the maximum possible manifold insertion angle for a tangential transfer. For example, if $\phi = 110$ deg, the only possible manifold insertion would be at the first intersection. Similarly, at $\phi = 90$ deg, the manifold intersection can be chosen, such that the second and first intersection points of the momentum map can be used.

As a particular case, consider the third intersection with a manifold insertion angle of $\phi = 56\,\text{deg}$. The manifold branch chosen and the direct transfer trajectories are shown in Fig. 2.45. The delta-v usage for each of the transfer arcs considered, and the corresponding manifold insertion angle is also shown. Notice here that at $\phi = 56\,\text{deg}$, i.e. the zero-momentum point for the manifold branch, the Δv required is the highest, and the trajectory is nearly a straight line. How-

ever, reducing the manifold insertion angle ϕ under $56\,\mathrm{deg}$, results in lower Δv, as the third-body takes advantage of the natural dynamics of the PCR3BP. It is noted here that the time of transfer is the total time spent on the transfer trajectory, and does not include the time spent on the manifold to reach the periodic orbit. Also, the Δv value is that of the manifold injection maneuver. Since the trans-lunar injection maneuver δv is generally provided by the upper stage of the launch vehicle, this value is not included in the Δv shown in Fig. 2.45. It is worthwhile to note that the dynamical structure of the stable manifold intersects with the zero-momentum surface for a range of Jacobi constant values [100]. This is illustrated in Fig. 2.46.

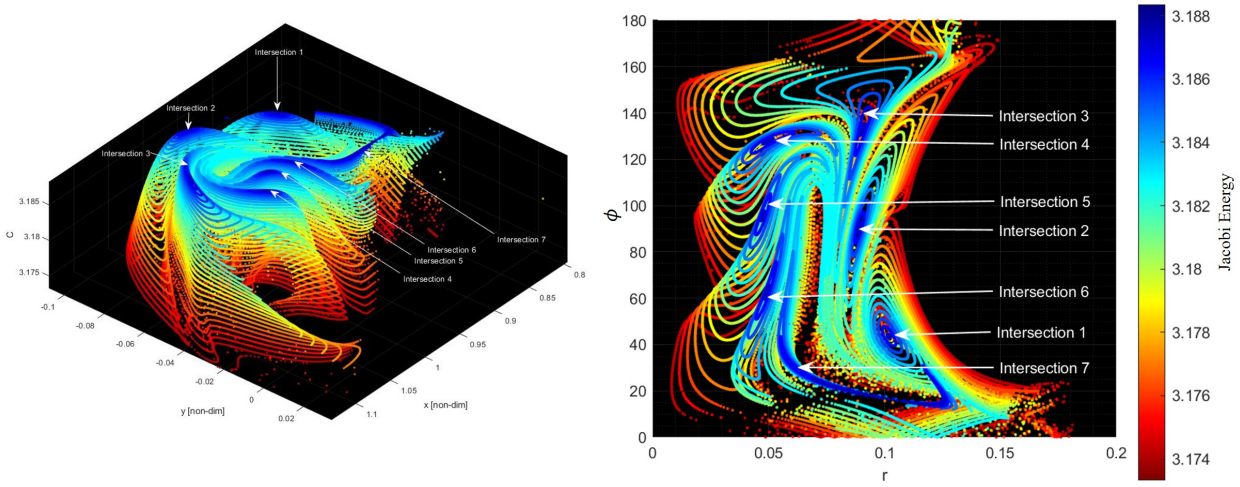

Figure 2.46: Dynamical structure of manifold intersections with zero-momentum surface for a range of Jacobi energies.

In Fig. 2.46, r is the distance of the momentum map point from the less-massive primary (Moon). It is observed that as the Jacobi energy is decreased, the structure of the intersections expands, occupying a larger portion of the phase-space. This behavior is expected because the L_1 gateway opens further, allowing the natural dynamics to extend to larger regions. The topological structure in the configuration space (Fig. 2.46-left) is very interesting. Noting that these are intersections of the invariant manifold, these structures contain within them the trajectories that transit through the L_1 gateway and therefore form a part of the saddle subspace. The regions surrounding

these structures are then the center subspace where quasi-periodic motions exist. Figure 2.46 gives a glimpse of the center and saddle subspace of the PCR3BP for a small range of Jacobi energy.

It is evident from the discussion that the momentum map plays a vital role in identifying direct transfer opportunities to periodic orbits. In the following sections, transfers to L_1 Lyapunov orbits are studied. The momentum map serves as an initial guess for the manifold insertion state, and a continuation process can be used to identify all types of transfers to the periodic orbit. This continuation scheme is presented in the following section to identify the structure of transfers to L_1 Lyapunov orbits. It is noted here that the methodology can be adapted for obtaining transfers to any planar periodic orbit, and the momentum maps serve as a starting point for the classification of these transfers.

2.6.4 Classification of direct transfers to L_1 Lyapunov orbit

The momentum maps have demonstrated their utility to find transfer opportunities in the PCR3BP. As established in the previous sections, the momentum map points serve as a starting point for employing a continuation process to categorically construct transfers with lower Δvs. In this continuation process, the stepping parameter is the propagation time along the stable manifold. Thus, the momentum map points are used as the manifold insertion points to initialize the continuation process. A schematic for the continuation process employed and a converged set of transfers appear in Fig. 2.47.

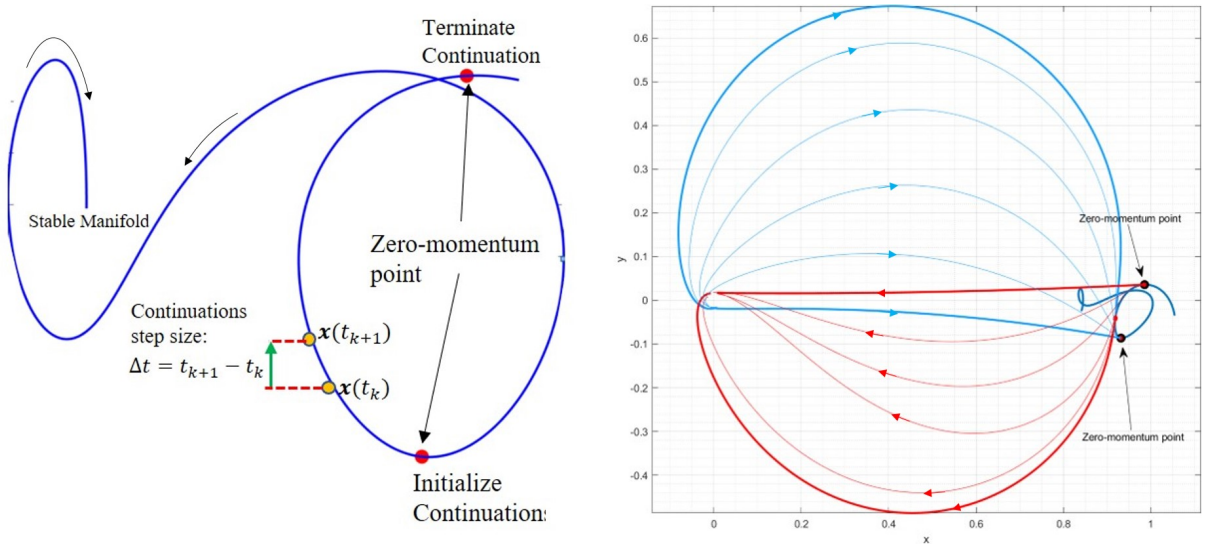

Figure 2.47: Continuation process schematic and direct transfers from a 200 km Earth parking orbit. The curves in blue go from Earth to the Moon and that in red are return transfers.

In the schematic above, the continuation process is initialized at the momentum map point. At this state, the direction of the velocity vector is towards the barycenter of the Earth-Moon system. Therefore, direct transfers can be obtained (in backwards time) from this manifold insertion point to an EPO. The continuation process terminates at the next intersection of the stable manifold with the zero-momentum surface, i.e. when the third-body transitions from direct to retrograde motion. Consequently, the continuation process yields return transfer opportunities near the terminal continuation point. These forward (blue) and return (red) transfers are shown in Fig. 2.47, respectively. Depending on the step size for continuation, multiple families of forward transfers are obtained. Families with similar characteristics are also obtained for return types of transfers [100]. It is noted here that each of the transfers obtained in this work is obtained using a multiple shooting method, which has been extensively discussed in literature [102, 93, 98, 103].

There are no unique parameters that are viable for the description of transfers in the three-body framework. Since the PCR3BP admits only a single constant of the motion (the Jacobi energy), alternative quantities must be introduced to capture significant features of transfers within the PCR3BP to fundamentally assess the realization of the mission requirements. A summary of

such parameters is reported in Table 2.3 along with sample applications.

Table 2.3: Parameters for classifying transfers

Parameter	Sample application
Δv	Transfer cost estimation
Time of transfer	Manifold injection maneuvers
Jacobi constant	Target Periodic orbit determination
Manifold insertion angle (ϕ)	Geometric constraint on maneuvers

2.6.5 Family of direct transfers to L_1 Lyapunov orbit

The continuation process is utilized to obtain a family of direct transfers from an EPO to a Lyapunov orbit at the L_1 libration point. Each transfer trajectory can be classified using the parameters recorded in Table 2.3. Broadly, the types of direct transfer trajectories can be classified using the number of revolutions about the more-massive primary (the Earth) along the trans-lunar segment of the transfer trajectory and the departure direction from the Earth. Particularly, the Δv and the time-of-transfer are used as an indicator of the type of direct transfer trajectory. Seven types of transfer trajectories are observed to exist between two consecutive momentum map points on the stable manifold for the third-body direct motion. It is noted here that such transfers may exist for third-body retrograde motions as well, but those are not investigated in this investigation. The geometry of these transfers is shown in Fig. 2.48.

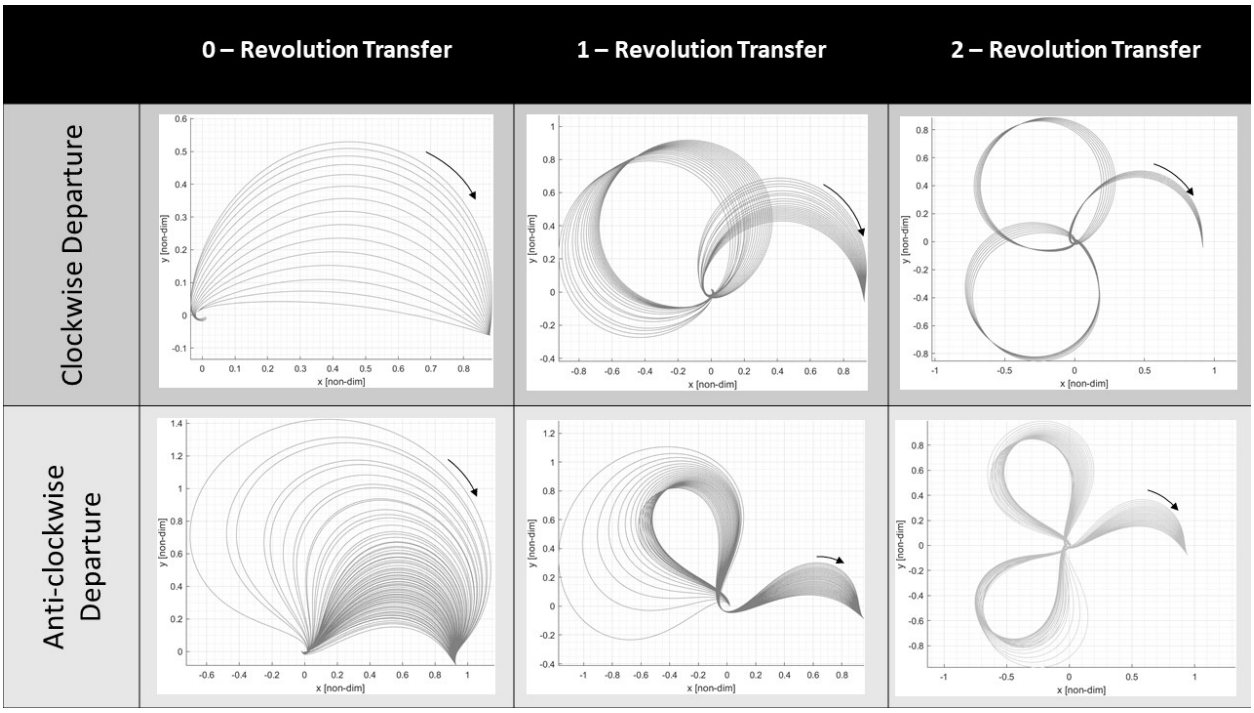

Figure 2.48: Geometry of family of direct transfers and their categories.

For the purposes of this work, these families of direct transfers are named using the convention: **Type C/AC-#**. For example, a zero revolution, clockwise departure transfer is named ***Type C-0*** and a two revolution anti-clockwise departure is named ***Type AC-2***. Another common family of transfers observed are those of the resonant type. The structure of the resonant type of direct transfers is illustrated in Fig. 2.49. These transfers also exhibit both clockwise and anti-clockwise departure directions as shown.

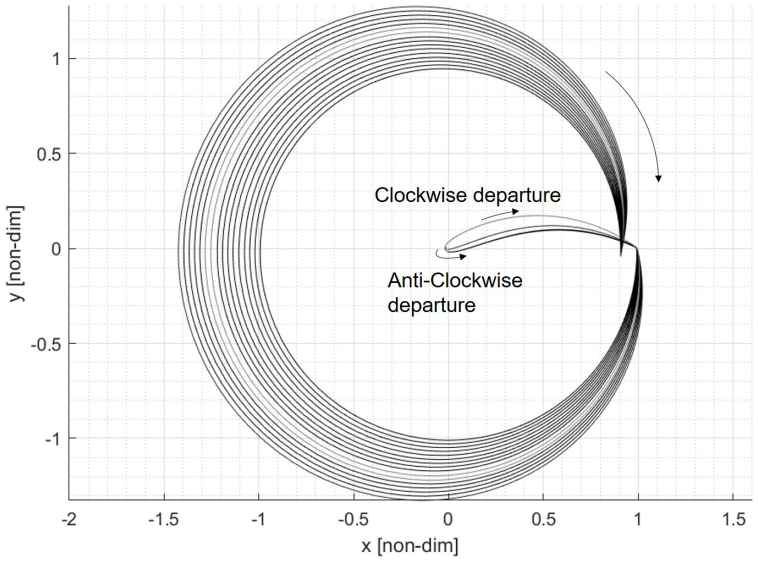

Figure 2.49: Geometry of resonant type transfers

Each family of transfers has a characteristic Δv and a time-of-transfer to enable its identification. An average value for the Δv and a time-of-transfer for each of the families is given in Tab. 2.4:

Table 2.4: Characteristic Δv and time for the family of transfers

Family Type	Mean Δv [km/s]	Mean Transfer Time [days]
Type C-0	1.1	4.56
Type C-1	0.97	7.62
Type C-2	0.95	18.4
Type AC-0	0.69	4.335
Type AC-1	0.57	13.85
Type AC-2	0.62	22.05
Resonant Type	1.82	15.85

It is observed that the Δv for clockwise and anti-clockwise transfers are quite distinct, while the number of revolutions aids in the differentiation of the different families of transfers. It is also noted here that convergence to these transfers is highly dependent on the multiple shooting algorithm and the initial guess supplied. Based on these quantities, there may be additional family

of transfers with as many as five to eight revolutions. These are not particularly studied since the goal is to identify short-duration transfers. Also, note that only the first intersection of the momentum map is used to initialize the continuation process, since higher intersections would imply a longer time spent on the manifold, thereby increasing the duration of the transfers.

Now, having identified the different transport opportunities in the PCR3BP, the continuation methodology, in conjunction with the information from the momentum map, is used to quantify transfers to periodic orbits at different Jacobi energies in the following section.

2.6.6 A roadmap for cislunar transport in PCR3BP

Classification of direct transfers serves as a valuable road-map for cislunar transport (Δv, transfer-time, etc.) in the Earth-Moon PCR3BP. The work done here aids in creating such a catalog for orbital transfers for use in mission design. This work attempts to identify transfers to L_1 Lyapunov orbits over a small range of Jacobi energies. The Jacobi energies chosen such that only the L_1 gateway is open. These transfers are quantified using (a) target Jacobi energy of the periodic orbit, (b) Δv for the transfer and (c) Transfer time. The three quantities are represented using a two-dimensional chart with a color map providing information on the third quantity. The catalog of transfers is presented in Fig. 2.50.

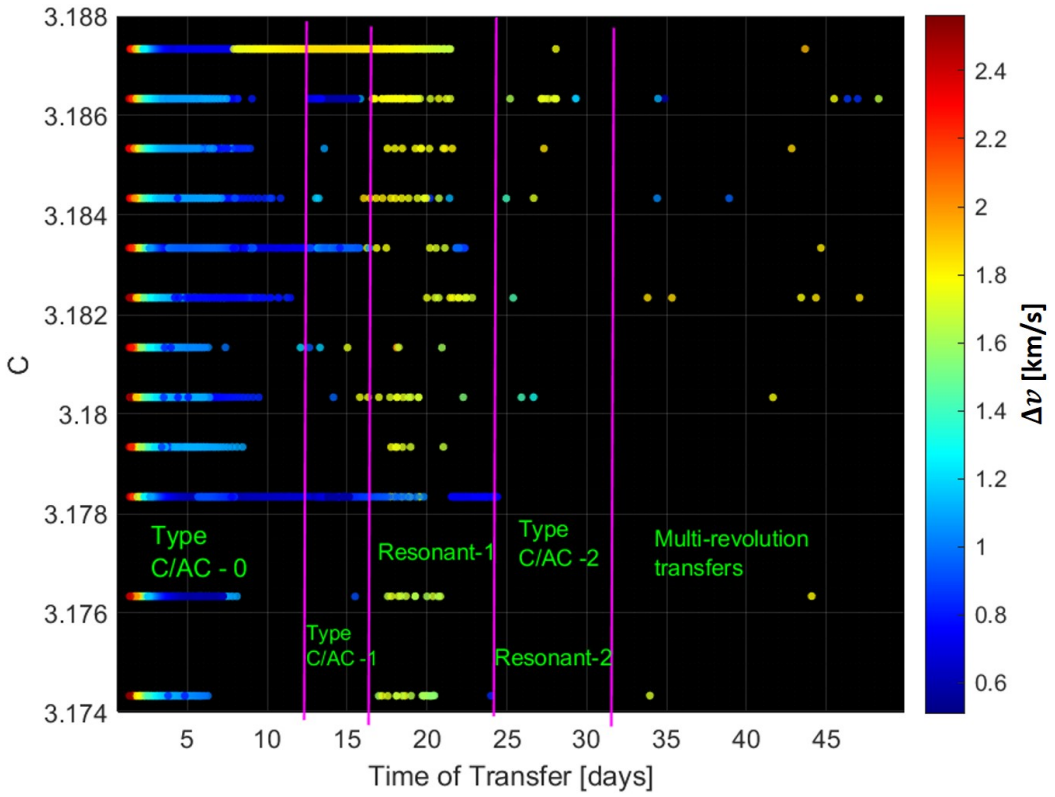

Figure 2.50: Catalog of transfers and an approximate distinction between the family of transfers.

Figure 2.50 gives a look-up table for numerous transfers from an EPO to the L_1 Lyapunov orbit. Additionally, each type of transfer can be identified using the Δv and the transfer time. For example, consider the particular energy level of 3.1833. A close-up of this energy level from the catalog of transfers exhibits the different families (Fig. 2.51).

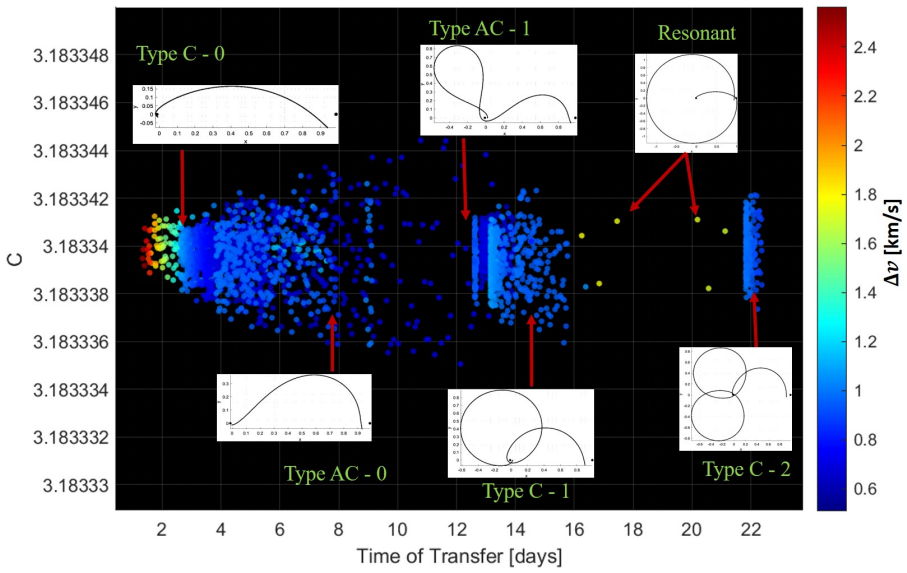

Figure 2.51: Catalog of transfers at $C = 3.1833$

The identification and cataloging of these transfers presents a guide to identifying potential transport opportunities to target periodic orbits at a particular Jacobi energy. This section presents a robust methodology for computing these transfers without manual analysis of Poincaré maps. This process of obtaining the family of direct transfers can be automated for any target Jacobi energy orbit, and the catalog provides a list of transfers to choose from based on mission requirements. This extension to arbitrary Jacobi energy orbits is demonstrated through the use of velocity surfaces, and an example of this application is discussed next.

2.6.7 Application of momentum maps to identifying transport opportunities

To motivate the discussion for this section, recall that the barycentric momentum maps serve as an initial guess for finding suitable manifold insertion points along the stable manifold. The difference in the Jacobi constants between the transfer trajectory and the target periodic provides an estimate of the minimum cost required for the transfer; particularly, those transfers that result from a change in the velocity magnitude and the direction. In the previous sections, only tangential transfers emanating from the first intersection of the momentum map have been considered. However, there may exist non-tangential transfers that result in better Δv savings.

While the difference in Jacobi constant provides an estimate of the transfer cost, an alternate method to visualize the transfers is presented in this section. Here, the velocity is utilized to accomplish this goal. The surface of velocity is defined as:

$$v = \pm\sqrt{2\Omega - C} \tag{2.170}$$

with $\Omega = \frac{1}{2}(x^2+y^2)+\frac{\mu_1}{r_1}+\frac{\mu_2}{r_2}$ and C is the Jacobi constant. Consider only the positive counterpart of the velocity surface. Note here that the velocity surface contains all trajectories at a particular energy level, and therefore the points of zero momentum of any trajectory also lie on this surface. Therefore, one can use these velocity surfaces to define transfers from one energy level to another. The impulse maneuvers will transfer the trajectories from one velocity surface to another. A simple illustration is as follows:

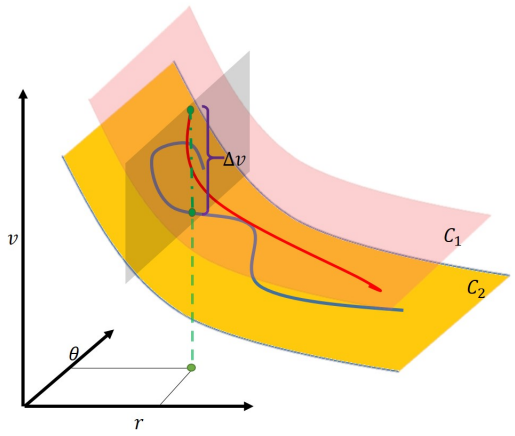

Figure 2.52: Tangential Transfer between two Energy levels: A velocity surface schematic.

The above illustration shows a direct transfer between two energy levels (C_1 and C_2). Note that the position component of the trajectories are the same, and therefore, the height difference between the two points is equal to the Δv.

2.6.7.1 *The geometry of velocity surfaces*

The topology of the velocity surface at a particular energy is as shown in Fig. 2.53. These surfaces are parameterized using polar coordinates with respect to the Moon.

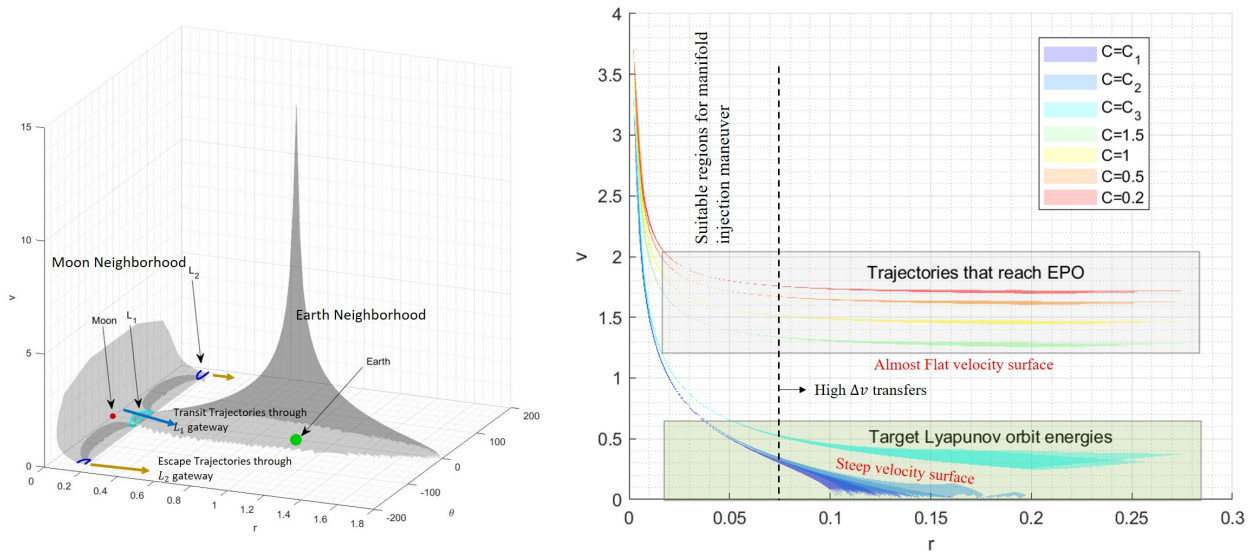

Figure 2.53: Geometry of the velocity surfaces and suitable locations for impulse maneuvers

In the polar coordinates, the L_1 and L_2 gateway are located at $0\,\mathrm{deg}$ and $180\,\mathrm{deg}$, respectively. Also, note the difference in the velocity surfaces for target periodic orbits and for potential transfer trajectories that reach the EPO. This large difference suggests that periodic orbits with Jacobi energies (between C_1 and C_3) lie on velocity surfaces that are close to each other. The Δv required for a sample transfer to a periodic orbit near $C = C_1$ and $C = C_2$ would therefore be very close. This rationale can be utilized when looking up transfer opportunities from the catalog designed in the previous section.

Additionally, this topological visualization technique also enables a geometric analysis of the various transfers in the catalog to determine tangential and non-tangential transport opportunities to periodic orbits. An example of such an application is given below.

2.6.7.2 *Identification of non-tangential transport opportunities*

An application of the geometric visualization technique described above in combination with the catalog of transfers generated in the previous section is developed. Consider the problem of obtaining a transfer to an L_1 Lyapunov orbit at Jacobi constant, $C = 3.17$. Note that at this energy level, the L_2 gateway is open, and the catalog does not contain any transfers to this target energy. Also consider that the Δv budget for the transfer is constrained as: $\Delta v \leq 0.7$. Additionally, the maximum velocity direction change allowed during the manifold injection maneuver is $12\,\mathrm{deg}$. The procedure for finding such a transfer is outlined below:

1. From the catalog, extract transfers that have the Δv within out budget (There are 3785 such transfers in the catalog with $\Delta v \leq 0.7$).

2. Compute the stable manifolds of the target periodic orbit.

3. Compute intersections of the candidate transfers with the manifolds, such that the positions coordinates match up and the velocity vectors are near-tangential ($\alpha = 12\,\mathrm{deg}$). Here, near-tangential is defined by setting a tolerance for the allowed change in velocity direction.

The procedure described above does not require any computational effort due to its purely topological dependence. Each of the above steps is illustrated in Fig. 2.54.

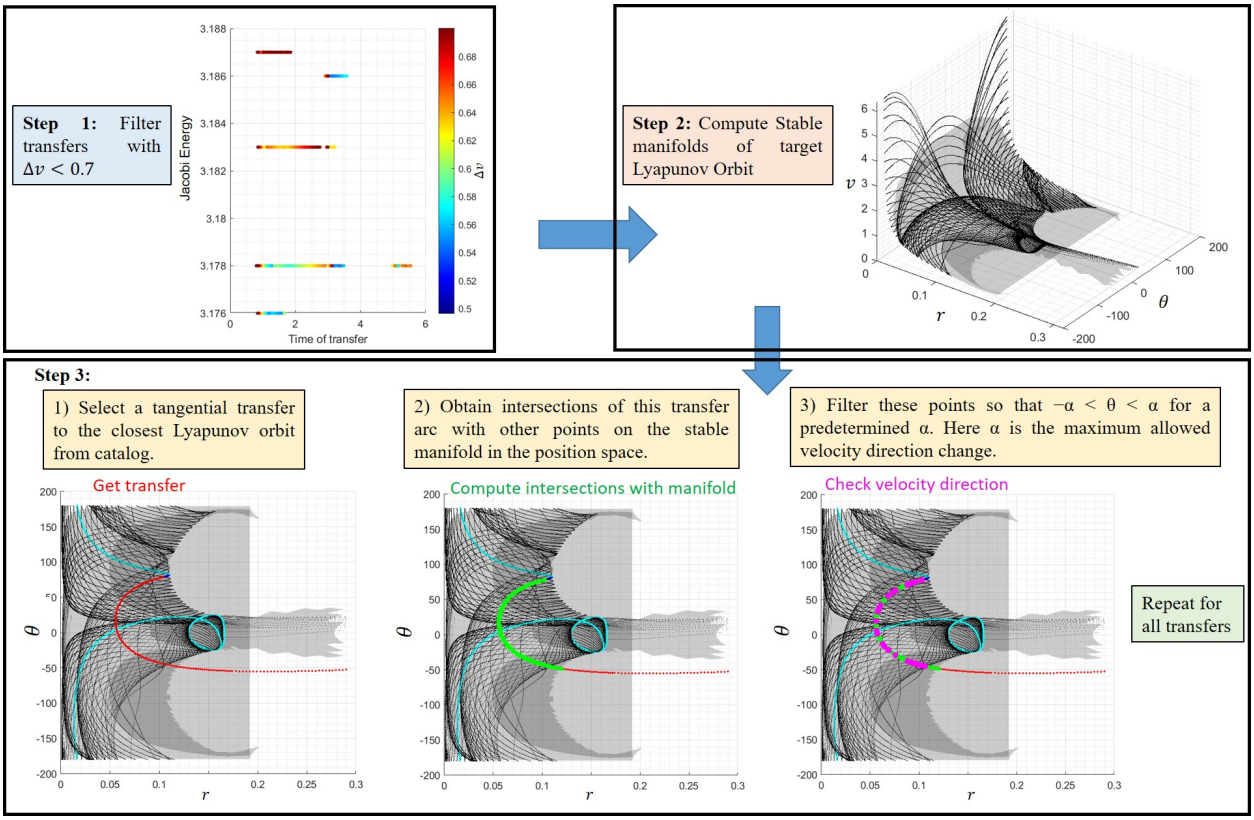

Figure 2.54: Solution procedure for computing transfers to L_1 Lyapunov orbit

The solution procedure described above is completely geometric and can be used as a quick analysis tool to identify possible non-tangential transfers with significant Δv savings. A sample trajectory obtained from the above procedure is as shown in Fig. 2.55

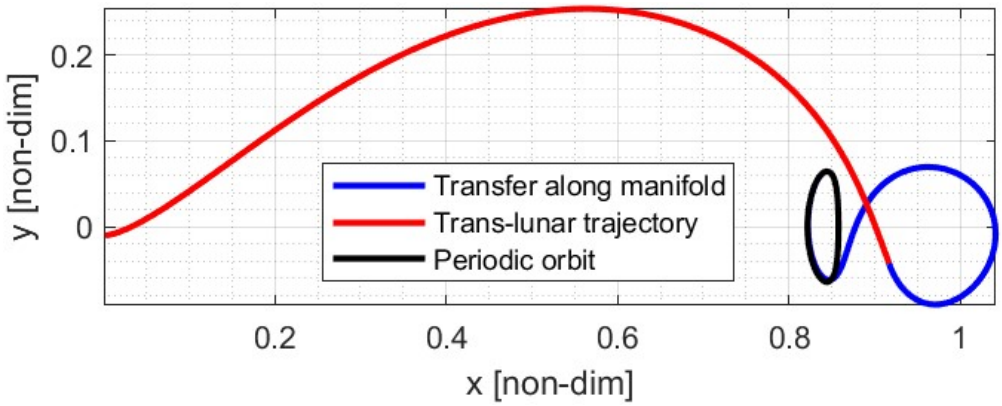

Figure 2.55: Sample transfer obtained from geometric analysis. C = 3.180

A quick analysis with varying maximum change in velocity direction during manifold injection maneuver showed the possibility of finding non-tangential transfers with significant Δv savings. The results of this analysis are shown in Fig. 2.56.

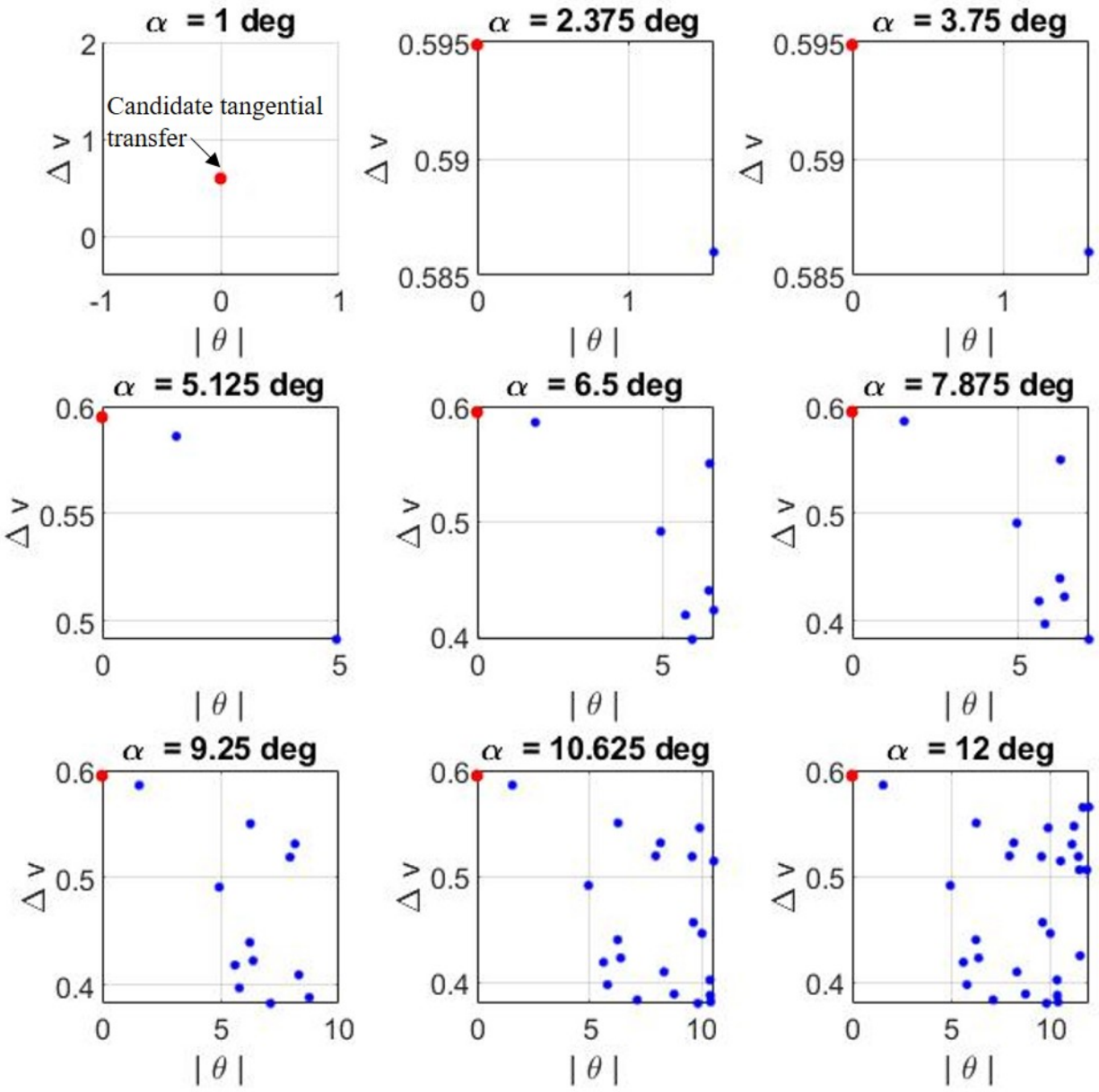

Figure 2.56: Non-tangential transfers to L_1 Lyapunov orbit with $\alpha = [1, 12]$ deg

2.7 Summary

This chapter of the dissertation focuses primarily on various qualitative methods for treating dynamical systems. The tools of dynamical systems theory have been used to obtain geometric insight into the evolution and behavior of the dynamical systems corresponding to the Planar Circular Restricted Three-Body Problem (PCR3BP) and the attitude motion of a rigid body in Keplerian orbit.

The identification and characterization of the dynamical structures within the PCR3BP facilitates comprehensive exploration of the motion of particles in multi-body regimes. The concept of momentum maps in the Earth-Moon system is introduced and explored to offer a deeper understanding of the qualitative properties of the PCR3BP and give a direct physical insight into the global dynamics of the problem. The momentum maps are very intuitive in describing the flow of a particle inside and around the invariant manifolds. Through the use of the inside-out topology, the structure of the invariant manifolds is examined in the Earth neighborhood. The utility of the momentum maps is demonstrated by developing a methodology to construct direct transfers to Lyapunov orbits in the Earth-Moon system. This methodology is employed to generate a catalog of transfers, thereby facilitating the identification of several families of transfers in the PCR3BP. While not requiring more sophisticated mathematics than the study of the velocity surface, a visualization technique is developed that enables the identification of transport opportunities with little computational effort and geometrical analysis. This study then provides an effective approach to analyzing transfers to planar Lyapunov orbits in cislunar space.

The attitude motion of a rigid body in Keplerian orbit is another complex dynamical system that is examined via qualitative methods in this dissertation. This dynamical system serves as a classical example of dynamical behavior being influenced by parametric terms. An alternative method to study the attitude motion of rigid bodies in a Keplerian is introduced. In developing the equations of motion, the parameterization in the Classical Rodrigues Parameters (CRP) is employed. This parameterization provides an advantage in that the equations of motion are in pure algebraic form. The governing equations for attitude dynamics for a general rigid body in a Keplerian orbit are

developed. In the absence of roll-yaw motions, the pitch motion is exclusively studied due to the equations of motion. The analysis of attitude motion is addressed using four specific cases, each developed incrementally, adding complexity to the dynamical system. They are: the planar pitch dynamics of a rigid body in circular orbit, planar pitch dynamics in eccentric orbit, and the three degree-of-freedom dynamics in circular orbit and eccentric orbit, respectively.

The planar pitch motion in circular orbit is completely reduced by obtaining an integral of motion in algebraic form, as a result of using the CRP parameterization. The existence of an integral of motion results in a co-dimension one sub-manifold of the phase space. Eigenvalue analysis gives the analytical limit for motion along the separatrix, thus furnishing the bounding trajectory between libratory and circulatory motions. The planar pitch motion in an eccentric orbit is studied through the use of bifurcation diagrams depending on the eccentricity parameter. Stroboscopic maps are also utilized to discern fascinating dynamical behavior. Many interesting motions are identified, including periodic orbits, quasi-periodic orbits and chaotic pitch motions.

Using the equations of motion, tools to investigate the stability of oscillations about an equilibrium point are developed in the three degree-of-freedom case. Linear analysis of the attitude motion suggests unstable solutions lead to exponential growth. However, the actual motion resulting from nonlinear equations is bounded, and this information is lost in the linearization. Leveraging the conservation principles of gravity-gradient torques, a method of energy balance is used to determine the regions of high energy exchange in the inertia parameter space for a rigid body in a circular orbit. It is shown that these regions (in the parameter space) of high energy exchanges correspond to those near commensurable frequencies in the pitch and roll-yaw motions, specifically at the internal resonance of 2:1 ($\omega_3 = \omega_1$). The apparent instability observed in the Lagrange region of the inertia parameter space is shown to be an exchange of energy between the pitch and roll-yaw motions. This analysis is further extended by investigating the effect of maximum pitch angle on the stability of oscillations. It is shown that an increase in the maximum pitch amplitude is accompanied by an increase in the energy exchange. Thus, the effect of resonant commensurability is shown to envelop a large part of the inertia parameter space.

A method of visualizing the rigid body motion is also developed. The Binet-Poincaré sections developed in this work trace the intersections of the locus of angular momentum vector in the body frame with a reference ellipsoid, resulting in the construction of an osculating polhode. Using this osculating polhode, certain peculiar structures arising from the motion of the angular momentum are observed. It is found that the high energy exchange regions are exclusively due to the 2:1 resonant frequencies. There is no energy pumping, for instance, in the weaker internal resonance condition ($\omega_3 = \omega_2 - \omega_1$). We also observe a monotonous phase shift in the motion of the angular momentum vector about the pitch axis upon crossing the 2:1 commensurability curve. This shift is found to be a function of the inertia properties of the rigid body. A new metric to quantify the coupling between the state variables by utilizing the information in the State Transition Matrix (STM) has been developed. By using the induced two-norm of the sub-matrices in the STM, a quantitative measure of the coupling is obtained. While this metric can be applied to any dynamical system, for the case of a rigid body, this coupling is directly linked to the energy exchange between the pitch and roll-yaw motions.

Noting that the gravity-gradient torque developed for the analysis of rigid body motion is an approximation to second order in the moment of inertia, a higher order gravity-gradient potential is developed. Certain cases are identified where the higher-order gravity-gradient terms become more significant than those at second-order. Relative equilibria and Lyapunov stability analysis are carried out for the special case of the cube as a rigid body. Forty nine equilibrium conditions are found that are identified as conforming to three specific configurations of the cube. Lyapunov stability analysis confirms that only one of the three equilibrium configurations is stable.

The roll-pitch-yaw rigid body motion in an eccentric orbit is investigated from the point of view of the Serret-Andoyer variables. Certain simplifications are introduced that aid in the reduction of the problem and the identification of equilibrium configurations for a triaxial rigid body. Particularly, the long-term behavior of a general triaxial rigid body is investigated utilizing tools of dynamical systems theory, specifically, the phase-plane analysis. This analysis using Serret-Andoyer variables also sets up the preliminaries for the next chapter, where the rigid body attitude

motion is investigated from an analytic perspective.

3. ANALYTIC TREATMENT OF DYNAMICAL SYSTEMS

The name *Analytical Dynamics* is given to that branch of knowledge in which the motions of material bodies, considered as due to the mutual interaction of the bodies, are discussed by the aid of mathematical analysis [31]. Analytical dynamics has been the subject of intense effort over the past two centuries. The modern developments in analytical methods remain in close continuity with classical treatments. Classical mechanics had its roots in the works of Newton, Euler, Lagrange, Gauss, Gibbs, Hamilton, and Jacobi et al., all of whom sought to establish the methodology and understand the behavior of natural dynamical systems under the influence of forces arising in nature. This has evolved to studying artificial and man-made systems under the influence of natural and artificial external forces [29]. Another important aspect is adjusting the analytical methodologies to accommodate the advancement in computational methods and mathematical treatment of a complex class of problems that pose difficulty to applied mathematicians, physicists, and engineers. Such complex dynamical systems preclude the exactness of their solutions. In such situations, an approximation is usually sought. Foremost among the approximation techniques is the systematic method of perturbations (or asymptotic expansions) in terms of a small or a large parameter or coordinate. The solution of the full problem can then be represented by the first few terms of a perturbation expansion. Such methods are proven to be more useful for qualitative as well as quantitative representation of the solutions [104, 105].

Just as in previous chapters, the outline of this chapter will begin with an introduction to different classical analytical techniques and perturbation methods. Again, a bench-test problem is the attitude motion of a rigid body in Keplerian orbit. This problem has been formulated in the previous section but will now garner a more analytical and perturbative approach to its solution. Such a method is extended to include the effects of both orbit on attitude as well as the attitude on orbit. The formulation of the problem itself will bring to light many internal symmetries, and their relation to physical phenomena. Another problem whose solution will be sought is the two-body problem with J_2 geo-potential using the familiar Delaunay variables. The hope of this chapter is

to utilize the information from previous chapters about the geometric insight into the motion of dynamical systems and formulate an analytical solution. Such analytical formulation will form the basis of the next chapter on semi-analytical methods for complex dynamical systems. Starting from the reality that analytical approaches allow for a deeper insight into nonlinear dynamical phenomena, this chapter of the dissertation focuses on emphasizing the recent developments in the analytical investigation of dynamical systems governed by nonlinear differential equations.

3.1 Fundamentals of analytical mechanics

The evolution of analytical mechanics is closely tied to the developments in calculus of variation. The principal developers of variational calculus (Euler, Lagrange, Hamilton, Jacobi, and others) were actively motivated by variational problems arising naturally in analytical mechanics [29]. In this chapter, we begin by outlining the basic concept from variational calculus and move on to Hamilton's principal function, and eventually to the Hamilton-Jacobi theory for canonical transformations. Another aspect that is explored in this chapter is the method of perturbations, specifically the Hori-Lie-Deprit Series method.

3.1.1 Variational calculus fundamentals

The fundamental problem of variational calculus is to determine a space-time trajectory or path $\mathbf{x}(t) \in \mathcal{R}^n$ that causes a given functional $\mathcal{J}(\mathbf{x}(t), t_0, t_f)$ to achieve a local extremum [30, 29]. If $\mathcal{J}$ is expressed as a path integral:

$$\mathcal{J} = \mathcal{J}(\mathbf{x}(t), t_0, t_f) = \int_{t_0}^{t_f} \mathcal{F}(\mathbf{x}(t), \dot{\mathbf{x}}(t), t)dt \tag{3.1}$$

with $\mathbf{x}(t) = [x_1(t), \cdots, x_n(t)]^T$. It is assumed that both $\mathcal{F}$ and $\mathbf{x}$ are functions of class C_2 i.e. continuous and twice differentiable with respect to all arguments [30]. Suppose that $\mathbf{x}(t)$ is the extremizing path with t_0 and t_f as extremizing initial and final times. Let $[\tilde{\mathbf{x}}(t), \tilde{t_0}, \tilde{t_f}]$ represent any differentially neighbouring path and initial/final times which also belong to class C_2. The first path variation is then given as

$$\delta\mathbf{x}(t) = \tilde{\mathbf{x}}(t) - \mathbf{x}(t) \tag{3.2}$$

is of differential magnitude and class C_2. Since $\dot{\mathbf{x}} = d/dt(\mathbf{x}(t))$ and $\dot{\tilde{\mathbf{x}}} = d/dt(\tilde{\mathbf{x}}(t))$,

$$\delta\dot{\mathbf{x}}(t) = \dot{\tilde{\mathbf{x}}}(t) - \dot{\mathbf{x}}(t) = \frac{d}{dt}(\delta\mathbf{x}) \tag{3.3}$$

Thus, the $\delta()$ and $d/dt()$ operations are interchangeable. These variations are introduced for the sake of analysis. Such analysis will lead to the necessary conditions for extremizing the functional mentioned above. The path integral evaluated along the varied path is

$$\tilde{\mathcal{J}} = \mathcal{J}(\tilde{\mathbf{x}}(t), \tilde{t_0}, \tilde{t_f}) = \int_{\tilde{t_0}}^{\tilde{t_f}} \mathcal{F}(\mathbf{x}(t) + \delta\mathbf{x}(t), \dot{\mathbf{x}}(t) + \delta\dot{\mathbf{x}}(t), t)dt \tag{3.4}$$

Defining the variation $\mathcal{J}$ as

$$\delta\mathcal{J} = \tilde{\mathcal{J}} - \mathcal{J} \tag{3.5}$$

$$= \int_{t_0+\delta t_0}^{t_f+\delta t_f} \mathcal{F}(\mathbf{x}(t) + \delta\mathbf{x}(t), \dot{\mathbf{x}}(t) + \delta\dot{\mathbf{x}}(t), t)dt - \int_{t_0}^{t_f} \mathcal{F}(\mathbf{x}(t), \dot{\mathbf{x}}(t), t)dt \tag{3.6}$$

Expansion in Taylor series and retaining the first order terms results in a cancellation with the second term leaving the form:

$$\delta\mathcal{J} = \int_{t_0}^{t_f} \left[\left[\frac{\partial\mathcal{F}}{\partial\mathbf{x}(t)} \right]^T \delta\mathbf{x}(t) + \left[\frac{\partial\mathcal{F}}{\partial\dot{\mathbf{x}}(t)} \right] \right] dt + \mathcal{F}(\ , t_f)\delta t_f - \mathcal{F}(\ , t_0)\delta t_0 \tag{3.7}$$

After some mathematical manipulation and integrating by parts, the final form of the functional $\mathcal{J}$ can be written as:

$$\delta\mathcal{J} = \left[\left[\frac{\partial\mathcal{F}}{\partial\mathbf{x}} \right]^T - \frac{d}{dt} \left[\frac{\partial\mathcal{F}}{\partial\dot{\mathbf{x}}} \right]^T \right] \delta\mathbf{x}(t)dt + \left[\frac{\partial\mathcal{F}}{\partial\dot{\mathbf{x}}(t_f)} \right]^T \delta\mathbf{x}(t_f) - \left[\frac{\partial\mathcal{F}}{\partial\dot{\mathbf{x}}(t_0)} \right]^T \delta\mathbf{x}(t_0) + \mathcal{F}(\ , t_f)\delta t_f - \mathcal{F}(\ , t_0)\delta t_0 \tag{3.8}$$

The final four boundary terms are referred to as transversality conditions. We draw out atten-

tion, particularly to the first term. This term gives us the Euler-Lagrange equations:

$$\left[\frac{\partial \mathcal{F}}{\partial \mathbf{x}}\right] - \frac{d}{dt}\left[\frac{\partial \mathcal{F}}{\partial \dot{\mathbf{x}}}\right] = 0 \tag{3.9}$$

Notice here that the Euler-Lagrange equations look very similar and are identical to Lagrange's equations:

$$\frac{d}{dt}\left[\frac{\partial \mathcal{L}}{\partial \dot{q}_j}\right] - \frac{\partial \mathcal{L}}{\partial q_j} = 0 \tag{3.10}$$

Since Eq. (3.9) is the necessary condition for

$$\mathcal{J} = \int_{t_0}^{t_f} \mathcal{F} dt$$

to be an extremum, it can be inferred that

$$\mathcal{S} = \int_{t_0}^{t_f} \mathcal{L} dt \tag{3.11}$$

is an extremum for a large class of dynamical systems. For these class of systems, $\delta\mathcal{S} = 0$. The scalar $\mathcal{S}$ is known as *Hamilton's principal function* and $\delta\mathcal{S} = 0$ is the most simple version of *Hamilton's principle*. The reader is referred to the following extensive texts for further reading on the topic [29, 27, 51, 106, 70, 99]. In the following section, we shall take a look at the Hamiltonian function and derive the basics for the Hamilton-Jacobi theory.

3.1.2 The Hamiltonian function

The Hamiltonian function is closely related to the Lagrangian ($\mathcal{L}$) and is defined in terms of the Lagrangian as follows:

$$\mathcal{H} = \sum_{i=1}^{n} \frac{\partial \mathcal{L}}{\partial \dot{\mathbf{q}}} \dot{\mathbf{q}} - \mathcal{L} = \mathcal{H}(\mathbf{q}, \dot{\mathbf{q}}, t) \tag{3.12}$$

The first term in the above equation can be used to define the generalized (or conjugate) momenta p_i as:

$$p_i \equiv \frac{\partial \mathcal{L}}{\partial \dot{\mathbf{q}}} \tag{3.13}$$

Thus, the Hamiltonian can be written as follows in terms of the coordinates (q_i) and their conjugate momenta (p_i) as:

$$\mathcal{H} = \sum_{i=1}^{n} p_i \dot{\mathbf{q}}_i - \mathcal{L} = \mathbf{p}^T \dot{\mathbf{q}} - \mathcal{L} \tag{3.14}$$

Because of the definition of the Lagrangian ($\mathcal{L} \equiv T - V$), it has a quadratic dependence on $\dot{\mathbf{q}}$. This leads to a familiar kinematic form of the above equation, and elucidates the fact that $[\mathbf{p}, \dot{\mathbf{q}}]$ are alternative velocity (or momentum) descriptions of the dynamical system's motion [51, 28]. Differentiating the Hamiltonian and collecting terms give us the conditions under which the Hamiltonian is a constant of motion.

$$\frac{d\mathcal{H}}{dt} = \sum_{i=1}^{n} \left[\frac{d}{dt} \left(\frac{\partial \mathcal{L}}{\partial \dot{\mathbf{q}}_i} \right) - \frac{\partial \mathcal{L}}{\partial q_i} \right] \dot{\mathbf{q}}_i - \frac{\partial \mathcal{L}}{\partial t} \tag{3.15}$$

The term in the bracket is Lagrange's equations which vanish for conservative external forces. Thus, the conditions under which the Hamiltonian is a constant of motion are: (a) External forces are conservative, and (b) The Lagrangian is not an explicit function of time. It is noted here that the second condition may be satisfied for systems with explicit time dependence by rewriting the dynamical equations in an extended phase-space. One such example will be discussed in the following sections and the description of the extended phase-space will be provided then. Therefore, in Hamiltonian dynamics, the variables are the canonical coordinates, usually $\mathbf{q}$, and the canonical momenta, $\mathbf{p}$. The paths of these variables are governed by the Hamiltonian, $\mathcal{H}$. These paths render a certain functional stationary[27, 51]:

$$\delta \int \mathbf{p} \cdot d\mathbf{q} - \mathcal{H} dt = 0 \tag{3.16}$$

Using the calculus of variations and expanding Eq. (3.16) , we obtain Hamilton's equations of motion.

$$\dot{\mathbf{q}} = \frac{\partial \mathcal{H}}{\partial \mathbf{p}}, \qquad \dot{\mathbf{p}} = -\frac{\partial \mathcal{H}}{\partial \mathbf{q}} \tag{3.17}$$

Introducing the canonical state-vector:

$$\mathbf{x} \equiv \begin{bmatrix} \mathbf{q} \\ \dots \\ \mathbf{p} \end{bmatrix}, \qquad \frac{\partial \mathcal{H}}{\partial \mathbf{x}} \equiv \begin{bmatrix} \frac{\partial \mathcal{H}}{\partial \mathbf{q}} \\ \dots \\ \frac{\partial \mathcal{H}}{\partial \mathbf{p}} \end{bmatrix} \tag{3.18}$$

Thus, Hamilton's canonical equations assume the symplectic form:

$$\dot{\mathbf{x}} = -[J]\frac{\partial \mathcal{H}}{\partial \mathbf{x}} = -[J]\nabla_{\mathbf{x}}\mathcal{H} \tag{3.19}$$

with $J = \begin{bmatrix} \mathbf{0} & -I_{n\times n} \\ I_{n\times n} & \mathbf{0} \end{bmatrix}$ and $I_{n\times n}$ being a $n-$dimensional identity matrix. The following section extends these developments to formally introduce the Hamilton-Jacobi theory.

3.1.3 Hamilton-Jacobi theory

The Hamilton-Jacobi theory plays a crucial role in the development of mathematical physics. It serves as a bridge between classical mechanics and other branches of dynamical systems theory in understanding the evolution of a system, particularly in the presence of internal symmetries and conserved quantities. This relation between topology and motion represents the culmination of Lagrangian and Hamiltonian mechanics [27, 107, 24, 106]. These action functions are the solutions of a nonlinear, first-order, hyperbolic partial differential equation (PDE), called the Hamilton-Jacobi equation (HJE). The characteristic equations of this differential equation are the extended Hamilton's equations. The potential of the HJE arises from the fact that the solution of mechanics problems is thus reduced to the solution of a single partial differential equation. It serves as a map from the original (nonlinear) equation into another equation that is more tractable. The beauty of HJE is to uncover the canonical transformations leading to a simplified, more manageable set of equations for dynamical systems. In the words of Arnold[22], *"The technique of generating functions for canonical transformations, developed by Hamilton and Jacobi, is the most powerful method available for integrating the differential equations of dynamics."*

From Eq. (3.16) , the addition of a path-independent term to $\mathbf{p} \cdot d\dot{\mathbf{q}} - \mathcal{H}dt$ does not affect the dynamics. If one were to introduce new coordinates and momenta (**Q**,**P**) which are expressed in terms of the old coordinates and momenta: (**q**,**p**).

$$Q_i = Q_i(\mathbf{q}, \mathbf{p}, t) \qquad\qquad P_i = P_i(\mathbf{q}, \mathbf{p}, t) \tag{3.20}$$

Equation (3.20) ensures that there exists a function $\mathcal{K}(\mathbf{Q}, \mathbf{P}, t)$ for which the new equations of motion are given by

$$\dot{Q}_i = \frac{\partial}{\partial P_i}\mathcal{K}(\mathbf{Q}, \mathbf{P}, t) \tag{3.21}$$

$$\dot{P}_i = -\frac{\partial}{\partial Q_i}\mathcal{K}(\mathbf{Q}, \mathbf{P}, t) \tag{3.22}$$

where, $\mathcal{K}$ is known as the new Hamiltonian or '*Kamiltonian*'. Transformations (Eq. (3.20)) for which these equations hold are called canonical transformations. These Hamilton's equations lead to the conditions[108]:

$$\delta \int_{t_1}^{t_2} \Big[\sum_{i=1}^{n} p_i \dot{q}_i - \mathcal{H}(\mathbf{q}, \mathbf{p}, t) \Big] dt = 0 \tag{3.23}$$

$$\delta \int_{t_1}^{t_2} \Big[\sum_{i=1}^{n} P_i \dot{Q}_i - \mathcal{K}(\mathbf{Q}, \mathbf{P}, t) \Big] dt = 0 \tag{3.24}$$

Thus, given Eq. (3.23) , there exists an arbitrary function $\mathcal{S}$ such that

$$\sum_{i=1}^{n} p_i \dot{q}_i - \mathcal{H}(\mathbf{q}, \mathbf{p}, t) = \sum_{i=1}^{n} P_i \dot{Q}_i - \mathcal{K}(\mathbf{Q}, \mathbf{P}, t) + \frac{dS}{dt} \tag{3.25}$$

is satisfied in order for Eq. (3.24) to hold. For a different set of variables $(\mathbf{P}, \mathbf{Q})$ and a different Hamiltonian, $\mathcal{K}$, the dynamics is same if the integrand differs by a path independent term, $d\mathcal{S}$, such that

$$\mathbf{p}^T \dot{\mathbf{q}} - \mathcal{H}(\mathbf{q}, \mathbf{p}, t) = \mathbf{P}^T \dot{\mathbf{Q}} - \mathcal{K}(\mathbf{Q}, \mathbf{P}, t) + \frac{d\mathcal{S}}{dt} \tag{3.26}$$

Equation (3.26) gives a functional form of the perfect differential criterion that leads to [**Q,P**] satisfying the canonical differential equations of Hamilton. The variable changes that preserve $\oint \mathbf{p} \cdot d\mathbf{q}$ also preserve dynamics (with appropriately modified Hamiltonian). Such variable changes are known as canonical transformations [22, 109]. One can leverage this freedom to add path-independent terms (of type $\mathcal{S}$) to specify canonical transformations that simplify the motion of dynamical systems and bring out the inherent symmetries of the system. Since S generates a transformation from the old variable space (**q,p**) to the new variable space (**Q,P**), it is called the generating function and is written as a function of mixed variables. Arnold [110] has shown that there are 2^n possible forms of the generating function of which the four possible forms of the generating function are of interest:

$$\mathcal{S} = \mathcal{S}_1(\mathbf{q}, \mathbf{Q}, t) \qquad \mathcal{S} = \mathcal{S}_2(\mathbf{q}, \mathbf{P}, t) \qquad \mathcal{S} = \mathcal{S}_3(\mathbf{p}, \mathbf{Q}, t) \qquad \mathcal{S} = \mathcal{S}_4(\mathbf{p}, \mathbf{P}, t)$$

Taking $S = S_1(\mathbf{q}, \mathbf{Q}, t)$ as an example and expanding the total time derivative of $\mathcal{S}$ in Eq. (3.17) ,

$$(\mathbf{p} - \frac{\partial S_1}{\partial \mathbf{q}})^T \dot{\mathbf{q}} - \mathcal{H} = (\mathbf{P} + \frac{\partial S_1}{\partial \mathbf{Q}})^T \dot{\mathbf{Q}} - \mathcal{K} + \frac{\partial S_1}{\partial t} \tag{3.27}$$

Since the old and new coordinates are independent, Eq. (3.27) can only hold if each coefficient of $\dot{\mathbf{q}}$ and $\dot{\mathbf{Q}}$ is zero. This enables us to obtain a relation for the old and new momenta as:

$$\mathbf{p} = \frac{\partial S_1}{\partial \mathbf{q}}, \qquad \mathbf{P} = -\frac{\partial S_1}{\partial \mathbf{Q}} \tag{3.28}$$

and

$$\frac{\partial S_1}{\partial t} + \mathcal{H} = \mathcal{K} \tag{3.29}$$

Similarly, we can obtain the relations for S_2, S_3, and S_4 as follows:

$$\mathcal{S}_2 : \frac{\partial \mathcal{S}_2}{\partial t} + \mathcal{H} = \mathcal{K}, \qquad \mathbf{p} = \frac{\partial \mathcal{S}_2}{\partial \mathbf{q}}, \qquad \mathbf{Q} = \frac{\partial \mathcal{S}_2}{\partial \mathbf{P}} \tag{3.30}$$

$$\mathcal{S}_3 : \frac{\partial \mathcal{S}_3}{\partial t} + \mathcal{H} = \mathcal{K}, \qquad \mathbf{q} = -\frac{\partial \mathcal{S}_3}{\partial \mathbf{p}}, \qquad \mathbf{P} = -\frac{\partial \mathcal{S}_3}{\partial \mathbf{Q}} \tag{3.31}$$

$$S_4 : \frac{\partial \mathcal{S}_4}{\partial t} + \mathcal{H} = \mathcal{K}, \qquad \mathbf{q} = -\frac{\partial \mathcal{S}_4}{\partial \mathbf{p}}, \qquad \mathbf{Q} = \frac{\partial \mathcal{S}_4}{\partial \mathbf{P}} \tag{3.32}$$

When a canonical transformation ensues such that the new Hamiltonian, $\mathcal{K}$, is a constant, which without loss of generality can be taken as zero, we obtain the Hamilton-Jacobi equation [27].

$$\mathcal{H}(\mathbf{q}, \mathbf{p}) + \frac{\partial \mathcal{S}}{\partial t} = 0 \tag{3.33}$$

Now, let us assume that $\mathcal{S} = \mathcal{S}_2(\mathbf{q}, \mathbf{P})$. Taking the time derivative of $\mathcal{S}$, we get:

$$\frac{d\mathcal{S}}{dt} = \frac{\partial \mathcal{S}}{\partial q_i}\dot{q}_i + \frac{\partial \mathcal{S}}{\partial P_i}\dot{P}_i + \frac{\partial \mathcal{S}}{\partial t} \tag{3.34}$$

Using expressions in Eq. (3.30) , $\dot{P}_i = 0$, and using Hamilton-Jacobi equation, we get:

$$\frac{d\mathcal{S}}{dt} = p_i \dot{q}_i - \mathcal{H} \tag{3.35}$$

However, note that the right hand side of the above equation is the Lagrangian. Thus,

$$\dot{\mathcal{S}} = \mathcal{L} \quad \Rightarrow \mathcal{S} = \int \mathcal{L} \tag{3.36}$$

Thus, the generating function is actually Hamilton's principal function. We see that Hamilton's principal function, $\mathcal{S}$, is the generator of canonical transformations of constant $(\mathbf{Q}, \mathbf{P})$, and provides a method of obtaining solutions to classical mechanics problems by way of finding a transformation. Classical examples of canonical set of variables are the Delaunay variables for the two-body problem, phase and amplitude variables for the simple harmonic oscillator, and the Serret-Andoyer

variables for the torque-free attitude motion of a rigid body. Certain situations require finding appropriate transformations and then checking for canonicity. In such situations, the Poisson bracket of the new and old variables serves as a useful tool in establishing canonicity. A brief description of Poisson brackets and the symplectic condition is given below.

3.1.4 Poisson brackets and the symplectic condition

In classical mechanics, the Poisson brackets are defined as:

$$\{u, v\}_{q,p} = \sum_i \left(\frac{\partial u}{\partial q_i} \frac{\partial v}{\partial p_i} - \frac{\partial v}{\partial q_i} \frac{\partial u}{\partial p_i} \right) \tag{3.37}$$

The following fundamental properties of Poisson brackets are listed:

$$\{q_i, q_j\}_{q,p} = \{p_i, p_j\}_{q,p} = 0 \tag{3.38}$$

$$\{q_i, p_j\}_{q,p} = \delta_{ij} \tag{3.39}$$

$$\{u, v\} = 0 \tag{3.40}$$

$$\{u, v\} = -\{v, u\} \tag{3.41}$$

$$\{au + bv, w\} = a\{u, w\} + b\{u, w\} \tag{3.42}$$

$$\{uv, w\} = u\{v, w\} + \{u, w\}v \tag{3.43}$$

$$\{u\{v, w\}\} + \{v\{w, u\}\} + \{w\{u, v\}\} = 0 \tag{3.44}$$

Utilizing the above formulae, we can prove the statement:

Theorem. *A transformation $Q_j = Q_j(p, q, t)$ and $P_j = P_j(q, p, t)$ is canonical if and only if*

$$\{Q_i, Q_j\}_{q,p} = \{P_i, P_j\}_{q,p} = 0 \quad \textit{and} \quad \{Q_i, P_j\}_{q,p} = \delta_{ij}$$

Let the canonical state vectors be given by:

$$\mathbf{x} = [q_i, p_i]^T \qquad i = 1, \cdots n \tag{3.45}$$

$$\mathbf{y} = [Q_i, P_i]^T \qquad i = 1, \cdots n \tag{3.46}$$

We know that Hamilton's equations of motion give us: $\dot{\mathbf{x}} = [J]\frac{\partial \mathcal{H}}{\partial \mathbf{X}}$. Also, one can write $\mathbf{y} = \mathbf{y}(\mathbf{x})$. Now, consider the derivative of $\mathbf{y}$

$$\frac{d\mathbf{y}}{dt} = \frac{\partial y_i}{\partial x_i}\dot{x}_i \Rightarrow \dot{\mathbf{y}} = M\dot{\mathbf{x}} \quad \text{where, } M_{ij} = \frac{\partial y_i}{\partial x_j} \tag{3.47}$$

Expanding the equation above, we obtain:

$$\dot{y}_i = \frac{\partial y_i}{\partial x_j}\dot{x}_j = \frac{\partial y_i}{\partial x_j}J_{jk}\frac{\partial \mathcal{H}}{\partial x_k} = \frac{\partial y_i}{\partial x_j}J_{jk}\frac{\partial y_l}{\partial x_k}\frac{\partial \mathcal{H}}{\partial y_l} \Rightarrow \dot{y}_i = MJM^T\frac{\partial \mathcal{H}}{\partial \mathbf{y}} \tag{3.48}$$

for any $\mathcal{H}$. This is known as the symplectic condition. Furthermore,

$$MJ = J(M^T)^{-1} \quad \text{and} \quad J^2 = -I \tag{3.49}$$

we can the write

$$J(MJ)J = -JM = J(J(M^T)^{-1})J = -(M^T)^{-1}J \Rightarrow MJM^T = J \Rightarrow M^TJM = J \tag{3.50}$$

Now, from the fundamental Poisson brackets:

$$\{x_i, x_j\}_{\mathbf{x}} = J_{ij} \tag{3.51}$$

Therefore,

$$\{y_i, y_j\}_{\mathbf{x}} = \left(\frac{\partial y_i}{\partial x_j}\right)^T J \left(\frac{\partial y_i}{\partial x_j}\right) = (M^TJM)_{ij} \tag{3.52}$$

Equation 3.52 is the same as Eq. (3.50) . Thus, the new variables satisfy the Poisson brackets

relationship if and only if

$$M^T J M = J$$

which is only true if the transformation: $\mathbf{y} = \mathbf{y}(\mathbf{x})$ is canonical. Thus, the statement of the theorem is proved. Two important facts arise from this theorem:

1. Poisson brackets are canonical invariants

$$\{u, v\}_{\mathbf{x}} = \{u, v\}_{\mathbf{y}} = \{u, v\} \tag{3.53}$$

2. The phase volume elements are preserved by canonical transformations.

$$\det(M^T J M) = \det(J) = \det(M^2)\det(J) \Rightarrow |\det(M)| = 1 \tag{3.54}$$

This property of the Poisson brackets becomes very useful when a transformation is obtained and its canonicity has to be checked. The Poisson brackets can be used in place of finding an explicit generating function for the transformation. A simple example is the set of canonical variables introduced by Fukushima [111] for both orbit and attitude motions : $\mathcal{T} : (x, y, X, Y) \Rightarrow (u, v, U, V)$. The transformations are given as:

$$\begin{aligned} U &= X \\ V &= \sqrt{X^2 - Y^2}\sin y \\ u &= x + \tan^{-1}\left(\frac{Y}{X}\tan y\right) \\ v &= \tan^{-1}\left(\frac{\sqrt{X^2 - Y^2}}{Y}\cos y\right) \end{aligned} \tag{3.55}$$

While a generating function of any kind for the above transformation cannot be found explicitly, the Poisson brackets are used to test for canonicity. Thus

$$\{U, u\} = \{V, v\} = 1 \qquad \{U, v\} = \{U, V\} = \{V, u\} = \{u, v\} = 0$$

The transformation above is therefore canonical and are used to replace (L, l, G, g) and (G, g, H, h) in the Delaunay variables for a new non-singular canonical set for orbital mechanics problems, and similarly for attitude dynamics problems as well. More often than not, under the effect of perturbations, many dynamical systems exhibit non-integrability. In such cases, a perturbation solution is sought out depending on a small parameter, and a chain of Poisson brackets. In the following section, one such method is highlighted.

3.1.5 Perturbation theory based on Lie transforms

In the presence of a perturbation, many dynamical systems exhibits non-integrability. Non-integrable systems do not exhibit a canonical set of variables that completely satisfy the Hamilton-Jacobi Theory. Perhaps, this is why the HJ theory is seldom used for solving dynamical systems since most problems can be treated by the Lagrangian and Hamiltonian approach. Felix Klein [112] quotes: "*the HJ method does not bring anything to the engineer and very little to the physicist*". However, while a complete solution cannot be obtained, many of the qualitative properties of the dynamical system can be discerned using a perturbations method that depend on a small parameter. Specifically, canonical transformations are obtained by seeking a generating function that depends explicitly on the small parameter. Lie transforms define naturally a class of canonical mappings in the form of a power series in the small parameter [74]. Perturbation theories based on this method of Lie series provide a significant advantage in that they yield the transformation of state variables in explicit form; in a function of the original variables, the substitution of the new variables consists simply of an iterative process involving explicit chains of Poisson brackets [113, 114, 74, 104].

Consider the dynamical system with vector differential equations as:

$$\dot{\mathbf{q}} = \mathcal{H}_{\mathbf{p}}, \qquad \dot{\mathbf{p}} = \mathcal{H}_{\mathbf{q}} \tag{3.56}$$

derived from the Hamiltonian

$$\mathcal{H}(\mathbf{q}, \mathbf{p}; t; \epsilon) = \mathcal{H}_0(\mathbf{q}, \mathbf{p}; t) + \epsilon \mathcal{H}_1(\mathbf{q}, \mathbf{p}; t) + \frac{1}{2!}\epsilon^2 \mathcal{H}_2(\mathbf{q}, \mathbf{p}; t) + \cdots \tag{3.57}$$

The essence of the technique is in constructing a canonical transformation $(\mathbf{q}, \mathbf{p}, t, \epsilon) \rightarrow (\mathbf{Q}, \mathbf{P})$ analytic in ϵ at $\epsilon = 0$ so as to achieve in the transformed Hamiltonian

$$\mathcal{K}(\mathbf{Q}, \mathbf{P}; t; \epsilon) = \mathcal{K}_0(\mathbf{Q}, \mathbf{P}; t) + \epsilon \mathcal{K}_1(\mathbf{Q}, \mathbf{P}; t) + \frac{1}{2!}\epsilon^2 \mathcal{K}_2(\mathbf{Q}, \mathbf{P}; t) + \cdots \tag{3.58}$$

satisfies specific requirements: suppression of periodic terms of assigned type, elimination of some or all angle coordinates, normalization, etc. The difference from von Zeipel's method[105] is to build the mapping explicitly in the form of a power series in the new variables.

$$\begin{aligned} \mathbf{q} &= \mathbf{Q} + \epsilon \mathbf{Q}^{(1)}(\mathbf{Q}, \mathbf{P}; t) + \frac{1}{2!}\mathbf{Q}^{(2)}(\mathbf{Q}, \mathbf{P}; t) + \cdots \\ \mathbf{p} &= \mathbf{P} + \epsilon \mathbf{P}^{(1)}(\mathbf{Q}, \mathbf{P}; t) + \frac{1}{2!}\mathbf{P}^{(2)}(\mathbf{Q}, \mathbf{P}; t) + \cdots \end{aligned} \tag{3.59}$$

together with its inverse:

$$\begin{aligned} \mathbf{Q} &= \mathbf{q} + \epsilon \mathbf{q}^{(1)}(\mathbf{q}, \mathbf{p}; t) + \frac{1}{2!}\mathbf{q}^{(2)}(\mathbf{q}, \mathbf{p}; t) + \cdots \\ \mathbf{P} &= \mathbf{p} + \epsilon \mathbf{p}^{(1)}(\mathbf{q}, \mathbf{p}; t) + \frac{1}{2!}\mathbf{p}^{(2)}(\mathbf{q}, \mathbf{p}; t) + \cdots \end{aligned} \tag{3.60}$$

and its remainder function

$$R(\mathbf{Q}, \mathbf{P}; t) = \epsilon R^{(1)}(\mathbf{Q}, \mathbf{P}; t) + \frac{1}{2!}R^{(2)}(\mathbf{Q}, \mathbf{P}; t) + \cdots \tag{3.61}$$

The scheme is recursive in that it is based on the principle that with respect to the transformation in Eq. (3.59) , the canonical system in Eq. (3.56) is equivalent to the system

$$\dot{\mathbf{Q}} = \mathcal{K}_{\mathbf{P}}, \qquad \dot{\mathbf{P}} = \mathcal{K}_{\mathbf{Q}} \tag{3.62}$$

derived from the Hamiltonian

$$\mathcal{K}(\mathbf{Q}, \mathbf{P}; t; \epsilon) = \mathcal{H}(\mathbf{q}(\mathbf{Q}, \mathbf{P}; t; \epsilon), \mathbf{p}(\mathbf{Q}, \mathbf{P}; t; \epsilon); t; \epsilon) + R(\mathbf{Q}, \mathbf{P}; t) \tag{3.63}$$

Thus, the problem of finding a canonical transformation is reduced to finding the generating function $\mathcal{S}$ and the Hamiltonian $\mathcal{K}$ to satisfy the prescribed requirements in Eq. (3.62) . The recursion is entered by putting

$$\mathcal{K}_0(\mathbf{Q}, \mathbf{P}, t) = \mathcal{H}_0(\mathbf{Q}, \mathbf{P}, t) \tag{3.64}$$

The operations at higher orders is accomplished using a Lie triangle which is shown in Fig. 3.1 [115, 74]

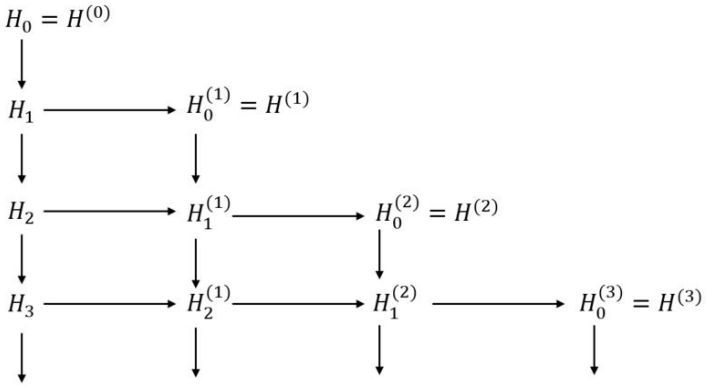

Figure 3.1: The Lie triangle: Recursive transformation of the Hamiltonian under a Lie transform.

To use the Lie triangle, one starts at a vertex, goes one step to the right, and then steps up and

performs the L_n operator on the quantity at each step as one moves up top. To illustrate this:

$$f^{(1)} = f_1 + L_1 f_0 \tag{3.65}$$

$$f_1^{(1)} = f_2 + L_1 f_1 + L_2 f_0 \tag{3.66}$$

$$f^{(2)} = f_1^{(1)} + L_1 f^{(1)} \tag{3.67}$$

$$= f_2 + L_1 f_1 + L_2 f_0 + L_1 f^{(1)} \tag{3.68}$$

$$= f_2 + L_1 f_1 + L_2 f_0 + L_1 (f_1 + L_1 f_0) \tag{3.69}$$

$$= f_2 + 2L_1 f_1 + L_2 f_0 + L_1 (L_1 f_0) \tag{3.70}$$

$$f_2^{(1)} = f_3 + L_1 f_2 + L_2 f_1 + L_3 f_0 \tag{3.71}$$

$$\vdots \tag{3.72}$$

where $L_n f$ is a linear operator called the Lie derivative generated by W_n and is the Poisson bracket given by

$$L_n f = \{f, W_n\} = \frac{\partial f}{\partial(\mathbf{q}, \mathbf{p})} \frac{\partial W_n}{\partial(\mathbf{Q}, \mathbf{P})} - \frac{\partial f}{\partial(\mathbf{Q}, \mathbf{P})} \frac{\partial W_n}{\partial(\mathbf{q}, \mathbf{p})} \tag{3.73}$$

A recursive formula exists for $\mathcal{H}_n^{(k)}$ as:

$$\mathcal{H}_n^{(k)}(\mathbf{q}, \mathbf{p}, t) = \mathcal{H}_{n+1}^{(k-1)} + \sum_{0 \leq m \leq n} C_m^n L_{m+1} \mathcal{H}_{n-m}^{(k-1)} \tag{3.74}$$

Utilizing this recursive formulation, one can obtain to arbitrary order, the perturbation solution of a dynamical system. The key point to note here is that the problem of finding the transformation has now been reduced to the problem of finding a generating function that serves our purpose. As an example, the Duffing oscillator is considered next and a fourth-order Lie series perturbation solution is found by averaging over the periodic variable to fourth-order.

3.1.5.1 Lie series solution of a nonlinear oscillator

The differential equation governing the Duffing oscillator is:

$$\ddot{z} + z + \epsilon z^3 = 0 \tag{3.75}$$

The Hamiltonian for the nonlinear oscillator can therefore be written as the sum of kinetic energy and the potential in the nonlinear spring as:

$$\mathcal{H} = \frac{1}{2}\dot{z}^2 + \frac{1}{2}z^2 + \frac{1}{4}\epsilon z^4 = \mathcal{H}_0 + \epsilon\mathcal{H}_1 \tag{3.76}$$

First, a simple canonical transformation is made as follows. It can be checked using Poisson brackets that the transformation preserves canonicity.

$$z = \sqrt{2X}\sin x, \qquad Z = \sqrt{2X}\cos x \tag{3.77}$$

In the new variables, (x, X), the Hamiltonian is rewritten as:

$$\mathcal{K} = \mathcal{K}_0 + \epsilon\mathcal{K}_1 = X + \epsilon\frac{X^2}{8}(3 - 4\cos 2x + \cos 4x) \tag{3.78}$$

On averaging up to fourth-order, we obtain the following expression for the Hamiltonian:

$$\mathcal{K} = -\frac{10689\,X^5\,\epsilon^4}{16384} + \frac{375\,X^4\,\epsilon^3}{1024} - \frac{17\,X^3\,\epsilon^2}{64} + \frac{3\,X^2\,\epsilon}{8} + X \tag{3.79}$$

The generating function that results in the averaged Hamiltonian is:

$$W_1 = -\frac{X^2 \left(4 \sin\left(2\,X\right) - \frac{\sin(4\,X)}{2}\right)}{16} \tag{3.80}$$

$$W_2 = \frac{X^3 \sin\left(2\,X\right) \left(-8\sin\left(X\right)^4 + 26\sin\left(X\right)^2 + 39\right)}{96} \tag{3.81}$$

$$W_3 = -\frac{X^4 \cos\left(X\right) \sin\left(X\right) \left(368\cos\left(X\right)^6 - 2088\cos\left(X\right)^4 + 1598\cos\left(X\right)^2 + 2333\right)}{512} \tag{3.82}$$

$$W_4 = \frac{3\,X^5 \cos\left(X\right) \sin\left(X\right)}{1024} \tag{3.83}$$

$$\frac{\left(640\cos\left(X\right)^8 + 1768\cos\left(X\right)^6 - 18124\cos\left(X\right)^4 + 19710\cos\left(X\right)^2 + 9017\right)}{1024} \tag{3.84}$$

Noting that the resulting averaged Hamiltonian is only a function of the momenta X, Hamilton's equation gives the evolution of X to be constant for all time ($\dot{X} = -\frac{\partial \mathcal{K}}{\partial x}$). The original solution for z, Z can be obtained straightforwardly from literature [104, 74, 114, 70]. Also, note here that the Lie series procedure is used to obtain a canonical transformation. The canonical transformation that we desire is to have the Hamiltonian be a function of only the momenta. Therefore, the angle is eliminated by averaging. On the other hand, if one wanted to solve the Hamilton-Jacobi equation exactly, we could ask the question of what the generating function should be to obtain the new Hamiltonian as zero. Of course, one may not be able to obtain an analytic form for the integral for the generating function to achieve this. All in all, note that the Lie series procedure results in a transformation of variables

$$(x, X) \to (x', X')$$

where the Hamiltonian expressed in the primed variables are a function of only the momenta. The equations above are all in primed variables and the *prime* is dropped for simplicity.

In the following sections, we shall specifically address the case of the attitude motion of a rigid body from the point of view of Hamiltonian formulations and averaging techniques using perturbation methods discussed above. The dynamical model will be built up hierarchically starting

from a simple axisymmetric rigid body in a torque-free environment to a slow rotating triaxial rigid body in Keplerian orbit.

3.2 Hamiltonian formulation of the free motion of a rigid body

The Euler-Poinsot problem is one of the classical problems of mechanics and describes the torque-free motion of a rigid body. The solution of any classical problem has broadly two steps: First: *Kinematics*, which is used to describe the orientation of the rigid body with respect to a spatial inertial frame. Second: *Dynamics*, which is represented by differential equations for the angular rates and the angular velocity rates. The study of this classical problem has led to and facilitated the use of various analytic methods. The description of the dynamics through the use of space and body cones, the observation that the polhode rolls without slipping on the herpolhode that lies on the invariable plane [31, 70, 69] are all methods developed by dynamicists to gain a deeper understanding of the Euler-Poinsot problem. The study of these analytic techniques eventually led to taking advantage of the internal symmetries to reduce the Euler-Poinsot problem to a one degree of freedom problem and using a perturbation method to obtain a solution [71]. While this method is used by most engineers, astronomical scholars prefer a formulation that takes advantage of the internal symmetries that reduce the Euler-Poinsot problem to a one degree of freedom problem and use a perturbations method to solve the problem [71].

The Hamiltonian form is useful in performing this reduction since perturbed Hamiltonian systems can be solved analytically to any order through many methods such as the one used by Deprit [3], and discussed above. The full reduction of the Euler-Poinsot problem has been offered by Deprit & Elipe [71]. To perform this reduction, one must resort to solving the Hamilton-Jacobi equation to obtain a generating function responsible for the canonical transformation from the action-angle variables to the Serret-Andoyer variables. These constants became the attitude-dynamics analogs of the Delaunay variables in the theory of orbits. Now, while Serret [72] had come up with a full reduction of the problem, Andoyer [73] suggested a partial reduction. Much later, the study by Andoyer was amended by Deprit and it was shown that canonicity may be proven by using differential forms and without resorting to explicitly finding a generating function [3, 4].

In this section, the free motion of a rigid body is discussed and the Hamiltonian is formulated. Note that the Hamiltonian formulation of the motion of a rigid body has been addressed in Sec. 2.4.6.2 using the Serret-Andoyer variable description. This description is briefly recalled here.

3.2.1 Serret-Andoyer description

Consider the orientation of the body frame with respect to an inertial frame written in terms of a coordinate frame aligned with the invariable plane [4]. An invariable plane is a plane whose normal is in the direction of the rotational angular momentum vector. This is illustrated in figure 3.2. The body frame is obtained through a $3-1-3-1-3$ rotation with respect to the inertial frame as

$$\hat{\mathbf{b}} = R_3(\nu)R_1(J)R_3(\mu)R_1(K)R_3(\lambda)\,\hat{\mathbf{s}}$$

where K denotes how the invariable plane is inclined with respect to the inertial frame and J denotes how the invariable plane is inclined with respect to the body frame. We can observe from Fig. 3.2 that K is the angle between the rotational angular momentum vector M and its inertial third component, L. Similarly, J is the angle between the rotational angular momentum vector M and its body-fixed third component, N.

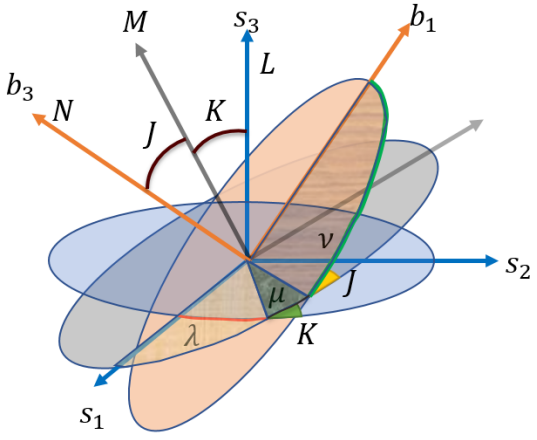

Figure 3.2: Body frame representation using the invariable frame [3, 4]

Here, the momenta conjugate to the coordinates (λ, ν, μ) are (L,N,M), respectively. From geometry, we can relate the angles K and J to the conjugate momenta as follows:

$$\cos K = \frac{L}{M} \qquad\qquad \cos J = \frac{N}{M} \tag{3.85}$$

Given these relations, the torque-free Hamiltonian can be rewritten in terms of the Serret-Andoyer variables as:

$$\mathcal{H} = \frac{1}{2}\Big(\frac{s_\nu^2}{A} + \frac{c_\nu^2}{B}\Big)(M^2 - N^2) + \frac{N^2}{2C} \tag{3.86}$$

where, A, B, and C are the moments of inertia of the rigid body. The Hamiltonian does not explicitly depend on μ and λ. Then Eq. (3.86) is simplified into the Hamiltonian of a two-dimensional system with a single independent coordinate ν. Since the number of degrees of freedom of the torque-free motion is reduced to one, the motion is solved by quadrature with the use of elliptic functions. Many [116, 117, 31] have given analytical expressions of the solution with the use of action-angle variables. Deprit [3] discussed the global and quantitative features of the torque-free motion with the use of the isoenergetic curves without using the analytical solution.

3.2.2 Axisymmetric rigid body simplification

As observed from Eq. (3.86) , if $A = B$, i.e. the body is axisymmetric, the explicit dependence on ν is also eliminated. Thus, the torque-free motion of an axisymmetric rigid body can be completely reduced and solved using the method of quadrature [4, 75, 118, 3]. The resulting Hamiltonian is:

$$\mathcal{H} = \frac{1}{2A}(M^2 - N^2) + \frac{N^2}{2C} \tag{3.87}$$

Hamilton's equations of motion the gives:

$$\frac{d\lambda}{dt} = 0 \qquad \frac{dL}{dt} = 0 \tag{3.88}$$

$$\frac{d\mu}{dt} = \frac{M}{A} \qquad \frac{dM}{dt} = 0 \tag{3.89}$$

$$\frac{d\nu}{dt} = \frac{N}{C} - \frac{N}{A} \qquad \frac{dN}{dt} = 0 \tag{3.90}$$

the solutions for which are very straightforward. The solution for a triaxial rigid body in torque-free environment is given next.

3.2.3 Free motion of a triaxial rigid body

The kinetic energy can be expressed explicitly in terms of the Serret-Andoyer variables as done previously. (Eq. (3.86)). Hamilton's equations of motion then give:

$$\frac{d\lambda}{dt} = 0 \tag{3.91}$$

$$\frac{d\mu}{dt} = 2\,M\,\left(\frac{\cos(\nu)^2}{2\,B} + \frac{\sin(\nu)^2}{2\,A}\right) \tag{3.92}$$

$$\frac{d\nu}{dt} = \frac{N}{C} - 2\,N\,\left(\frac{\cos(\nu)^2}{2\,B} + \frac{\sin(\nu)^2}{2\,A}\right) \tag{3.93}$$

$$\frac{dL}{dt} = 0 \tag{3.94}$$

$$\frac{dM}{dt} = 0 \tag{3.95}$$

$$\frac{dN}{dt} = -\left(M^2 - N^2\right)\,\left(\frac{\cos(\nu)\,\sin(\nu)}{A} - \frac{\cos(\nu)\,\sin(\nu)}{B}\right) \tag{3.96}$$

The torque-free solution for a tri-axial rigid body has been obtained in closed form by Kinoshita. [119, 120, 121] and is expressed here for completeness. The new variables are describes as follows.

$$N = N_0 \mathrm{dn}(u,k) \tag{3.97}$$

$$M = M_0 \tag{3.98}$$

$$L = L_0 \tag{3.99}$$

$$\nu = \tan^{-1}\left(\frac{\mathrm{cn}(u,k)}{\gamma \mathrm{sn}(u,k)}\right) \tag{3.100}$$

$$\mu = \mu_0 + \frac{M_0}{C}(t-t_0) + \frac{M_0\gamma}{L_0}\Pi(\mathrm{am}(u,k),\alpha^2,k) \tag{3.101}$$

$$\lambda = \lambda_0 \tag{3.102}$$

where

$$\gamma = \sqrt{\frac{a}{b}}, \quad u = \frac{N_0}{C}\sqrt{ab}(t-t_0), \quad k = \sqrt{\gamma^2-1}\frac{\sqrt{M_0^2-N_0^2}}{N_0} \tag{3.103}$$

$$\alpha^2 = 1-\gamma^2, \quad a = \frac{C}{A}-1, \quad b = \frac{C}{B}-1 \tag{3.104}$$

and $L_0, M_0, N_0, \lambda_0, \mu_0, \nu_0$ are the six integration constants of the torque-free motion and are the initial values of the state-space variables at the epoch t_0 defined as the instant $l = \pi/2$. Here the functions am (amplitude), sn (sine-amplitude), dn (delta-amplitude), cn (cosine amplitude) are Jacobi's elliptic functions with the argument u and modulus k. Also,

$$\Pi(\psi,\alpha^2,k) = \int_0^{\psi} \frac{1}{(1-\alpha^2\sin^2\theta)\sqrt{1-k^2\sin^2\theta}} d\theta \tag{3.105}$$

is the incomplete elliptic integral of the third kind with the argument ψ, the modulus k, and the parameter α^2 [122, 123] (see [111, 120] for details). There are additional sets of variables such as the ones introduced by Lara and Ferrer [75, 124, 125, 121], that offer a complete reduction of the torque-free Hamiltonian and expresses it in terms of momenta variables only. This is left to the reader to verify and study. In the following sections, the influence of gravity gradient torques is studied for an axisymmetric rigid body in Keplerian orbit.

3.3 Hamiltonian formulation of the motion of a fast-rotating rigid body in Keplerian orbit

The torque-free rotation of artificial satellites may be perturbed by a variety of effects such as gravity, solar radiation pressure, drag, magnetic field effects, etc. [126]. Due to the complexity of the force models, the problem of attitude perturbation is most commonly approached using numerical and qualitative methods as described in the previous chapter. Nevertheless, the problem can also be approached analytically using perturbation methods as discussed previously. This analytical alternative takes the Euler-Poinsot problem as the unperturbed part, and the other effects are added as perturbations to the torque-free motion [127, 121, 128]. The gravity-gradient torque can be identified as one of the most important perturbing torques affecting the motion of the rigid body [129, 130]. This model of rigid body motion therefore is treated as a basic, nonintegrable dynamical system used in the study of attitude motion of artificial satellites. Furthermore, the utility of this model is not restricted to the case of artificial satellites but can also be extended to fit the description of rotational motion of celestial bodies [120, 117].

In the remainder of this section, we shall treat two specific cases of rigid body motion: a fast-rotating/ tumbling rigid body and a slow rotating rigid body. Each case can be individually attributed to the motion of artificial satellites and that of celestial bodies, respectively. While interesting dynamics exist in the consideration of triaxial rigid bodies, of particular interest is that of an axisymmetric rigid body when specifically applied to the natural motion of celestial objects due to symmetry or near-symmetry rotations exhibited by them.

3.3.1 The Hamiltonian formulation : problem set-up

The Hamiltonian of the rigid body rotation in the presence of conservative gravity-gradient torques is

$$\mathcal{H} = \mathcal{T} + \mathcal{V} \tag{3.106}$$

where $\mathcal{T}$ is the kinetic energy of rigid body motion about its center of mass and $\mathcal{V}$ is the potential due to gravity. The Hamiltonian formulation of the rigid body in Keplerian orbit has been discussed previously in Sec. 2.4.6.3. We shall borrow the preliminary results from there. The complete

Hamiltonian can be written ignoring the orbital energies since they are always constant because of the assumption that the attitude motion does not affect the orbit. This Hamiltonian is the sum of the torque-free Hamiltonian from equation 2.104 and the gravity-gradient potential.

$$\mathcal{H} = \frac{1}{2}\Big(\frac{s_\nu^2}{A} + \frac{c_\nu^2}{B}\Big)(M^2 - N^2) + \frac{N^2}{2C} - \frac{k^2}{2r^3}\Big((C-B)(1-3r_3^2) - (B-A)(1-3r_1^2)\Big) \quad (3.107)$$

where k^2 is the gravitational parameter. To bring this expression to a form that can enable the use of perturbation theory, Eq. (3.107) is modified as follows. First, we rearrange the Hamiltonian of the torque-free case as follows.

$$\mathcal{H}_0 = \Big(\frac{\sin^2\nu}{A} + \frac{\cos^2\nu}{B}\Big)\Big(\frac{M^2 - N^2}{2}\Big) + \frac{N^2}{2C} \quad (3.108)$$

$$= \frac{M^2}{2C}\Big[1 + \Big(\frac{\sin^2\nu}{A/C} + \frac{\cos^2\nu}{B/C} - 1\Big)\sin^2 J\Big] \quad (3.109)$$

where, $\sin^2 J = \frac{M^2 - N^2}{M^2}$. The gravity-gradient potential is rewritten as:

$$\mathcal{V}_{ggt} = -\frac{M^2}{2C}\Big(\frac{n}{M/C}\Big)^2\frac{(1+e\cos f)^3}{(1-e^2)^3}\Big[(1-\frac{B}{C})(1-3r_3^2) - (\frac{B}{C} - \frac{A}{C})(1-3r_1^2)\Big)\Big] \quad (3.110)$$

where n is the constant orbital mean motion, and the eccentricity (e) and true anomaly (f) enter through the expansion of the radius vector $r = \frac{a(1-e^2)}{1+e\cos f}$. Utilizing expressions for r_1 and r_3 from Eq. (2.113) , we can expand the above expression. Further, we note from the torque-free Hamiltonian that for an axisymmetric body ($A = B$), ν is cyclic. Therefore, we can split the total Hamiltonian into an axisymmetric part (independent of ν) and a symmetric part (containing ν).

$$\mathcal{V}_{ggt} = -\frac{M^2}{2C}\Big(\frac{n}{M/C}\Big)^2\frac{(1+e\cos f)^3}{(1-e^2)^3}\frac{1}{16}\Big(\Big(2 - \frac{B}{C} - \frac{A}{C}\Big)\mathcal{V}_{axi} + \frac{3}{2}\Big(\frac{B}{C} - \frac{A}{C}\Big)\mathcal{V}_{asy}\Big) \quad (3.111)$$

where, the expressions for $\mathcal{V}_{axi}$ and $\mathcal{V}_{asy}$ are given in Eq. (2.123) and Eq. (2.124) , respectively. A simplification to the above expression of the potential is possible if we consider an axisymmetric rigid body, i.e. $A = B$.

3.3.2 Axisymmetric rigid body simplification

Equation 3.112 gives the complete expression of the gravity-gradient potential for a triaxial rigid body. After application of the axisymmetric assumption, the expression for the potential becomes:

$$\mathcal{V}_{ggt} = -\frac{M^2}{2C}\Big(\frac{n}{M/C}\Big)^2 \frac{(1+e\cos f)^3}{(1-e^2)^3}\frac{1}{16}\Big(\Big(2-\frac{B}{C}-\frac{A}{C}\Big)\mathcal{V}_{axi}\Big) \tag{3.112}$$

The total Hamiltonian is then given as

$$\mathcal{H} = \frac{M^2}{2C}\left[1+\frac{1}{A/C}\left(1-\frac{A}{C}\right)\frac{M^2-N^2}{M^2}\right] - \epsilon\frac{M^2}{2C}\left[\frac{1}{8}\left(\frac{a}{r}\right)^3\left(1-\frac{A}{C}\right)\right]\mathcal{V}_{axi} \tag{3.113}$$

where $\epsilon = \left(\frac{n}{M/C}\right)^2$. The representation of the Hamiltonian in Eq. (3.113) is non-autonomous because of the explicit time-like variable, the true anomaly through expressions in $\mathcal{V}_{axi}$ and explicit dependence on r. The following discussion, therefore, aims to alleviate this undesirability by introducing the mechanics through which the true anomaly is added into the extended phase-space thus rendering the Hamiltonian autonomous.

3.3.3 Extended phase-space mechanics

The following discussion is inspired from Alfriend et. al [131, 132]. With the introduction of the true anomaly in the expression for the gravity-gradient potential, we now have a system with the Hamiltonian in the form:

$$\mathcal{H} = \mathcal{H}(\mathbf{q}, \mathbf{p}, f) \tag{3.114}$$

where $\mathbf{q} = [\lambda, \mu, \nu]^T$ and $\mathbf{p} = [L, M, N]^T$ are the coordinates and their conjugate momenta, respectively. Let, q_0, be the coordinate that coincides with the true anomaly f, and p_0 be its conjugate

momenta.

$$\mathcal{H} = \mathcal{H}(q_0, \mathbf{q}, \mathbf{p}) + p_0 \tag{3.115}$$

The solution of the system governed by Eq. (3.115) must coincide with the one governed by Eq. (3.114) . This is accomplished by prescribing the following conditions at $t = 0$:

$$q_0(0) = 0; \qquad p_0(0) = -\mathcal{H}|_{t=0} \tag{3.116}$$

Now, recall that the expression for $\mathcal{V}_{axi}$ has the true anomaly appearing explicitly through the angle $\phi = \lambda - f$. This is done because of the construction of a rotating frame moving at the same rate as that of the orbital motion. Let us, therefore, introduce a new variable, $l = \lambda - f$ as a new coordinate, and its conjugate momenta can remain L. The torque-free Hamiltonian is then written as

$$\mathcal{H}_{TF} = \mathcal{H}_0 + L\frac{df}{dt} \tag{3.117}$$

This follows form the fact that:

$$\frac{dl}{dt} = \frac{d\lambda}{dt} - \frac{df}{dt} = \frac{\partial \mathcal{H}_0}{\partial L} \tag{3.118}$$

$$= \frac{\partial}{\partial L}\left(\mathcal{H}_0 + L\frac{df}{dt}\right) \tag{3.119}$$

$$\frac{dL}{dt} = -\frac{\partial \mathcal{H}_0}{\partial l} = 0 \tag{3.120}$$

Now, to set $q_0 = f$, another term has to be added to the Hamiltonian. The complete Hamiltonian is written as follows:

$$\mathcal{H} = \mathcal{H}_0 + L\frac{h}{r^2} + \mathcal{V}_{ggt} + p_0\frac{h}{r^2} \tag{3.121}$$

where h is the orbital angular momentum. The relation $\frac{df}{dt} = \frac{h}{r^2}$ is also utilized [50]. Using this, we also obtain that the value of p_0 at $t = 0$ must be

$$p_0(t = 0) = -(\mathcal{H}_0 + L\frac{h}{r^2} + \mathcal{V}_{ggt})\frac{r^2}{h} \tag{3.122}$$

Using this value, we have the Hamiltonian at the initial time to be zero. In the extended phase-space, the Hamiltonian is constant ($= 0$) for all time. Note here the usefulness of the extended phase space. The extended phase-space is utilized to include the independent variable of time as a dependent variable. For the independent variable that is a function of time ($g = \alpha(t)$)), the addition to the extended phase-space is done by adding a dummy momenta scaled by $\frac{dg}{dt}$. We also note here that the extended phase-space is not limited to the dynamical model under consideration, i.e. the axisymmetric rigid body. However, the extended phase-space can be used for any non-autonomous dynamical system to remove explicit time dependence.

Note here that there are two ways to remove the true anomaly dependence: (a) Moving into the extended phase-space, and (b) Defining the new variable $(l = \lambda - f)$. Both these methods will result in the Hamiltonian being autonomous. Using method (a), the state-space is eight-dimensional while using method (b) the state-space is only six-dimensional. However, using method (b) requires solving Kepler's relation for the true anomaly at every time instant. This can be avoided by adding one additional differential equation for the evolution of the true anomaly. In the remainder of this chapter, the extended phase-space methodology is used.

3.3.4 Higher-order Lie series averaging

For the axisymmetric case, we rewrite the components of the Hamiltonian as follows:

$$\mathcal{H}_0 = \frac{M^2}{2C}\left[\frac{\sin^2 J}{A/C} + \cos^2 J\right] \tag{3.123}$$

$$\mathcal{H}_1 = \frac{M}{C}\left[\frac{a}{r}\right]^2 \sqrt{1-e^2}\;\; p_0 \tag{3.124}$$

$$\mathcal{H}_2 = -\frac{M^2}{C}\left[\frac{a}{r}\right]^3 \left(1 - \frac{A}{C}\right)(1 - 3r_3^2) \tag{3.125}$$

The total Hamiltonian is then given as:

$$\mathcal{H} = \mathcal{H}_0 + \epsilon\mathcal{H}_1 + \frac{\epsilon^2}{2!}\mathcal{H}_2 \tag{3.126}$$

with $\epsilon = \frac{n}{M/C}$ where n is the mean motion. Note here that the coefficient of p_0 in $\mathcal{H}_1$ is simply $\frac{df}{dt} = \frac{h}{r^2}$. Similarly, we have already expanded $(1 - A/C)(1 - 3r_3^2)$ in previous sections. It is expressed as follows:

$$(1 - A/C)(1 - 3r_3^2) = \begin{pmatrix} -\frac{3\cos(J)\sin(J)\sin(K)(\cos(K)-1)(A-C)}{2C} \\ -\frac{3\cos(J)\sin(J)\sin(K)(\cos(K)+1)(A-C)}{2C} \\ -\frac{\sin(J)^2\sin(K)^2(3A-3C)}{4C} \\ \frac{\sin(K)^2(3A-3C)\left(3\sin(J)^2-2\right)}{4C} \\ -\frac{3\sin(J)^2(\cos(K)-1)^2(A-C)}{8C} \\ -\frac{3\sin(J)^2(\cos(K)+1)^2(A-C)}{8C} \\ \frac{3\cos(J)\cos(K)\sin(J)\sin(K)(A-C)}{C} \\ -\frac{(A-C)\left(3\sin(J)^2-2\right)\left(3\sin(K)^2-2\right)}{4C} \end{pmatrix}^T \begin{pmatrix} \cos(2f - 2\lambda + \mu) \\ \cos(2\lambda - 2f + \mu) \\ \cos(2\mu) \\ \cos(2f - 2\lambda) \\ \cos(2f - 2\lambda + 2\mu) \\ \cos(2\lambda - 2f + 2\mu) \\ \cos(\mu) \\ 1 \end{pmatrix} \tag{3.127}$$

Also note that the secular terms come in at the second order. The two critical inclinations are:

$$J = \cos^{-1} \pm\sqrt{\frac{1}{3}} \qquad K = \cos^{-1} \pm\sqrt{\frac{1}{3}} \tag{3.128}$$

The secular terms reveal special configurations (the critical inclinations) of the satellite in which the satellite's attitude under gravity-gradient torque evolves, on average, as in the torque-free state, but with a slightly modified angular momentum. Now, a fast-rotating rigid body has the rate of change of the angle μ much higher than the rate of change of the true anomaly. With this information, we can use a perturbations method to obtain an approximate solution in the powers of the small parameter, ϵ. Using this approach and averaging over the fast angle μ, we obtain the averaged Hamiltonian up to fourth-order as follows. Certain qualitative insights are also provided.

1. At first order:

$$\begin{aligned} \mathcal{H}_{0,1} &= \mathcal{H}_{1,0} \\ < \mathcal{H}_{0,1} > &= \frac{1}{2\pi}\int_0^{2\pi} \mathcal{H}_{0,1} = \frac{M}{C}\left[\frac{a}{r}\right]^2 \sqrt{1-e^2} \quad p_0 = \mathcal{H}_{1,0} \\ W_1 &= \int (\mathcal{H}_{0,1} - < \mathcal{H}_{0,1} >) d\mu = 0 \end{aligned} \tag{3.129}$$

This is not a surprise since $\mathcal{H}_{0,1}$ arises due to the use of the extended phase-space. The homological equation using standard Lie-Deprit solution procedure is:

$$\mathcal{H}_{0,1} = \mathcal{H}_{1,0} - \frac{\partial V_1}{\partial t}$$

Since the use of the extended phase-space removes any explicit dependence on the time-like variable, $\frac{\partial V_1}{\partial t} = 0$. In addition, $\mathcal{H}_{0,0}$ is purely a function of the Momenta and completely reduced. Because of these reasons, $\mathcal{L}_1\mathcal{H}_{0,0}$ reduces to zero. So, $\mathcal{H}_{0,1} = \mathcal{H}_{1,0}$ and the generating function, $W_1 = 0$.

2. At second order

$$\begin{aligned} \mathcal{H}_{1,1} =& \mathcal{H}_{2,0} + \mathcal{L}_1(\mathcal{H}_{1,0}) + \mathcal{L}_2(\mathcal{H}_{0,0}) \\ \mathcal{H}_{2,0} =& \mathcal{H}_{1,1} + \mathcal{L}_1(\mathcal{H}_{0,1}) \\ < \mathcal{H}_{0,2} > =& \frac{1}{2\pi}\int_0^{2\pi} \mathcal{H}_{0,2} = \frac{M^2}{2C}\left(1 - \frac{A}{C}\right)\left(\frac{a}{r}\right)^3 \left(3\sin^2 J - 2\right) \\ & \left(1 - 3\sin^2 K \sin^2\phi\right) \end{aligned} \tag{3.130}$$

with $\phi = f - \lambda$. Note here the secular term corresponding to $(3\sin^2 J - 2)$. Thus, one can obtain the critical inclination at which the secular drift of the coordinates is zero. In fact, at this critical inclination, the second-order contribution to the Hamiltonian itself vanishes.

This critical inclination is obtained as:

$$J = \pm \cos^{-1}\left(\frac{1}{\sqrt{3}}\right) \tag{3.131}$$

Therefore, at the critical inclination, the first-order averaged attitude motion of the rigid body under the influence of gravity-gradient torques (up to second-order moment of inertia approximation) behaves like that of the free motion of the rigid body (torque-free motion).

3. At third-order

$$\begin{aligned} \mathcal{H}_{2,1} &= \mathcal{H}_{3,0} + \mathcal{L}_1(\mathcal{H}_{2,0}) + \mathcal{L}_2(\mathcal{H}_{1,0}) + \mathcal{L}_3(\mathcal{H}_{0,0}) \\ \mathcal{H}_{1,2} &= \mathcal{H}_{2,1} + \mathcal{L}_1(\mathcal{H}_{1,1}) + \mathcal{L}_2(\mathcal{H}_{0,1}) \\ \mathcal{H}_{0,3} &= \mathcal{H}_{1,2} + \mathcal{L}_1(\mathcal{H}_{0,2}) \\ < \mathcal{H}_{0,3} > &= \frac{1}{2\pi}\int_0^{2\pi} \mathcal{H}_{0,3} = 0 \end{aligned} \tag{3.132}$$

4. At fourth-order

$$\begin{aligned} \mathcal{H}_{0,4} = M^2 \frac{-9A(A-C)^2}{64C^4}\left[\frac{a}{r}\right]^6 \Bigg(& 3(4\cos 2\phi + \cos 4\phi + 3) \\ & + (4\cos 2\phi - \cos 4\phi - 3)\cos^4 K \\ & + 85(4\cos 2\phi - \cos 4\phi - 3)\cos^4 K \cos^4 J \\ & + (-4\cos 2\phi - 17\cos 4\phi + 16)\cos^4 J \\ & + 2(-4\cos 2\phi - 9\cos 4\phi + 5)\cos^2 J \\ & + 4(16\cos 2\phi - 9\cos 4\phi - 7)\cos^2 K \cos^2 J \\ & + 54(-4\cos 2\phi + \cos 4\phi + 3)\cos^4 K \cos^2 J \\ & + 6(-32\cos 2\phi + 17\cos 4\phi + 15)\cos^2 K \cos^4 J \\ & + 2(1 - \cos 4\phi)\cos^2 K \Bigg) \end{aligned} \tag{3.133}$$

with $\phi = f - \lambda$. One can observe that the critical inclinations are only valid for a second-order approximation. In the fourth-order, the critical inclinations do not exist anymore. It is to be noted here that the variables in the above expressions are averaged variables i.e. the Lie series process results in a canonical transformation from

$$(\lambda, \mu, \nu, fL, M, N, F) \rightarrow (\lambda', \mu', \nu', f', L', M', N', F')$$

where the Hamiltonian expressed in the primed variables have the structure

$$\mathcal{K} = \mathcal{K}(\lambda', \sim, \sim, f', L', M', N', F') \tag{3.134}$$

The Kamiltonian is in the primed variables with the coordinate μ' has been eliminated. Additionally, one can notice that the coordinate ν' is also cyclic due to the assumption of an axisymmetric rigid body.

This method of averaging is very useful for a fast-rotating rigid body. However, for slow rotations of the rigid body, the rate of change of the attitude angle, μ, is of the same order as that of the orbital variables, the mean anomaly. The following section presents the methodology for treating the motion of slow-rotating rigid bodies.

3.4 Hamiltonian formulation of the motion of a slow-rotating rigid body in Keplerian orbit

The rigid body motion is formulated in the Serret-Andoyer variables: $(\lambda, \mu, \nu, L, M, N)$ [4]. Recall that they are defined as:

1. M is the magnitude of the rotational angular momentum

2. N is the component of the rotational angular momentum projected onto the z-axis of a coordinate frame fixed to the rigid body and aligned with the principal moments of inertia.

3. L is the component of the rotational angular momentum projected on to the z-axis of a coordinate frame fixed to the central body, also termed as the inertial frame.

4. λ is the angle measured from the inertial x-axis along the xy plane up to a node (N) defined by the intersection of the xy plane and the invariable plane (plane perpendicular to the rotational angular momentum vector).

5. μ is the angle measured from the node N along the invariable plane up to another node (M) defined by the intersection of the invariable plane with the xy plane of the body-fixed coordinate system.

6. ν is the angle measured from the node M along the xy plane of the body-fixed frame up to the x-axis.

The auxiliary angles J and K are also defined as in Eq. (3.85) .

$$\cos K = \frac{L}{M} \qquad\qquad \cos J = \frac{N}{M}$$

Although the Serret-Andoyer variables are suitable for studies of general rotational motion, they have some of the same deficits as that of the Delaunay variables in orbital motion: in the limit, $N \to M$, the angles ν and μ cannot be defined definitely. Similarly, in the limit, $L \to M$, the angles λ and μ cannot be defined definitely. Such an analogous condition occurs in the Delaunay variables for small eccentricities and inclinations of the orbit. Note that at these auxiliary angles, $J = 0$ and $K = 0$, while the angles are not well defined, their sum: $\lambda + \mu + \nu$ is well defined. This leads to the definition of the modified Serret-Andoyer variables. The transformation from the Serret-Andoyer variables to its modified variant can be obtained through a generating function of the second kind. Let us define this generating function as follows:

$$\mathcal{S}(\lambda, \mu, \nu, \Lambda_1, \Lambda_2, \Lambda_3) = \Lambda_1(\lambda + \mu + \nu) + \Lambda_2(-\nu) + \Lambda_3(-\lambda) \tag{3.135}$$

where, $\mathcal{S}$, a generating function of the second type is expressed in terms of the old coordinates

(λ, μ, ν) and new momenta $(\Lambda_1, \Lambda_2, \Lambda_3)$. The new coordinates can then be obtained as:

$$\lambda_1 = \frac{\partial \mathcal{S}}{\partial \Lambda_1} = \lambda + \mu + \nu \tag{3.136}$$

$$\lambda_2 = \frac{\partial \mathcal{S}}{\partial \Lambda_2} = -\nu \tag{3.137}$$

$$\lambda_3 = \frac{\partial \mathcal{S}}{\partial \Lambda_3} = -\lambda \tag{3.138}$$

The relation between the old and new momenta can also be obtained using the expressions from HJ theory as shown below :

$$L = \frac{\partial \mathcal{S}}{\partial \lambda} = \Lambda_1 - \Lambda_3 \tag{3.139}$$

$$M = \frac{\partial \mathcal{S}}{\partial \mu} = \Lambda_1 \tag{3.140}$$

$$N = \frac{\partial \mathcal{S}}{\partial \nu} = \Lambda_1 - \Lambda_2 \tag{3.141}$$

which gives:

$$\Lambda_1 = M \tag{3.142}$$

$$\Lambda_2 = M - N \tag{3.143}$$

$$\Lambda_3 = M - L \tag{3.144}$$

These pair of coordinates $(\lambda_1, \lambda_2, \lambda_3)$ and conjugate momenta $(\Lambda_1, \Lambda_2, \Lambda_3)$ are canonical and the Hamiltonian for the torque-free rigid body motion can be written as:

$$\mathcal{H}_0 = \frac{1}{2}\left(\frac{\sin^2\lambda_2}{A} + \frac{\cos^2\lambda_2}{B}\right)(\Lambda_1^2 - (\Lambda_1 - \Lambda_2)^2) + \frac{1}{2C}(\Lambda_1^2 - \Lambda_3^2) \tag{3.145}$$

which is rewritten as:

$$\mathcal{H}_0 = \frac{\Lambda_1^2}{2C}\left[1 + \left(\frac{\sin^2\lambda_2}{A/C} + \frac{\cos^2\lambda_2}{B/C} - 1\right)\sin^2 J\right] \tag{3.146}$$

Having obtained the torque-free Hamiltonian, the gravity-gradient potential can be formulated. Recall that this section deals with the attitude motion of a slow-rotating rigid body wherein the rates of the attitude angles are commensurable to that of the orbital rates. Therefore, the gravity-gradient potential is written in terms of both the attitude and orbital variables. The radius vector in the body frame is expressed relative to the inertial frame as follows:

$$\begin{bmatrix} r_1 \\ r_2 \\ r_3 \end{bmatrix} = R_3(-\lambda_2)R_1(J)R_3(\lambda_1+\lambda_2+\lambda_3)R_1(K)R_3(-\lambda_3)R_3(-h_o)R_1(-i_o)R_3(-g_o) \begin{bmatrix} \cos f \\ \sin f \\ 0 \end{bmatrix} \tag{3.147}$$

where, R_i are rotation matrices, where the subscript denotes the rotation axis. Here, note that the first five rotations: $R_3(-\lambda_2)R_1(J)R_3(\lambda_1+\lambda_2+\lambda_3)R_1(K)R_3(-\lambda_3)$ orients the body frame relative to the inertial frame and the remaining transformation: $R_{313}(-h_o,-i_o,-g_o)$ orients the inertial frame relative to the orbit frame. h_o is the Right Ascension of the Ascending Node (RAAN), i_o is the orbital inclination and g_o is the Argument of Perigee (AOP). Thus, the expression for the radius vector has dependence on both the orbital and attitude variables. The gravity-gradient torque is given by:

$$\mathcal{V}_{ggt} = -\frac{\mu}{2r^3}\left((C-B)(1-3r_3^2)-(B-A)(1-3r_1^2)\right) \tag{3.148}$$

Equation 3.148 can be modified after some mathematical simplifications to the following form:

$$\mathcal{V}_{ggt} = -\frac{\mu}{a^2}\left(\frac{a}{r}\right)^3\left(\frac{1}{2}\frac{A+B-2C}{2}(2r_3^2-r_1^2-r_2^2)+3\frac{B-A}{4}(r_1^2-r_2^2)\right) \tag{3.149}$$

which is written in a form similar to Eq. (3.112) . Comparing to Eq. (3.112) , the axisymmetric part ($\mathcal{V}_{axi}$) is given by $(2r_3^2-r_1^2-r_2^2)$ and the triaxial part ($\mathcal{V}_{asy}$) is given by $(r_1^2-r_2^2)$. One can note that the coefficient of the axisymmetric term ($\mathcal{V}_{axi}$) can be written in terms of the J_{20} term for large celestial bodies and the triaxial term ($\mathcal{V}_{asy}$) can be written in terms of the C_{22} term [133, 134, 12]

through the relations:

$$\begin{aligned} C_2^0 &= \frac{2C - (A+B)}{2} = -mJ_2R_e^2 \\ C_2^2 &= \frac{A-B}{4} = mC_{22}R_e^2 \end{aligned} \tag{3.150}$$

with m as the mass of the rigid body and R_e as the mean equatorial radius of the rigid body. Therefore, $\mathcal{V}_{ggt}$ takes the form:

$$\mathcal{V}_{ggt} = -\frac{\mu}{a^2}\left(\frac{a}{r}\right)^3\left(\frac{C_2^0}{2}(2r_3^2 - r_1^2 - r_2^2) + 3C_2^2(r_1^2 - r_2^2)\right) \tag{3.151}$$

in terms of the spherical harmonics of the rigid body.

Note that Eq. (3.148) and Eq. (3.149) are functions of the true anomaly. One can express the true anomaly as a coordinate in the extended phase space. However, this adds an additional variable to the combined attitude-orbit variables. Alternatively, if one were to express the true anomaly as a function of the mean anomaly, the gravity-gradient potential can be written as a function of the mean anomaly and its corresponding momenta from the Delaunay variables.

Using the developments in eccentricity [123] up to a required order of accuracy, we can write the gravity-gradient potential as a function of the mean anomaly, semi-major axis and eccentricity using the following expressions:

$$\begin{aligned} \frac{a}{r} &= 1 + 2\sum_{v=1}^{\infty} J_v(ve)\cos(vl_o) \\ \cos f &= \frac{2(1-e^2)}{e}\sum_{v=1}^{\infty} J_v(ve)\cos(vl_o) - e \\ \sin f &= 2\sqrt{1-e^2}\sum_{v=1}^{\infty}\frac{dJ_v(ve)}{de}\frac{\sin(vl_o)}{v} \end{aligned} \tag{3.152}$$

where, J_v are the Bessel functions of the first kind [35] with eccentricity as a parameter. Using these equations in the expression for the potential function, we can eliminate the presence of true

anomaly from the Hamiltonian expression. If we further require that the mean anomaly be a coordinate, an additional term equivalent to the orbital energy is added to the torque-free Hamiltonian.

$$\mathcal{H} = \mathcal{H}_0 + nL_o \tag{3.153}$$

where L_o is the momentum conjugate to the mean anomaly and $\frac{dl_o}{dt} = n$. If we choose L_o to be the same as that of the Delaunay variable, i.e. $L_o = \sqrt{\mu a}$, then we have:

$$\mathcal{H} = \mathcal{H}_0 - \frac{\mu^2}{2L_o^2} \tag{3.154}$$

3.4.1 Resonant Hamiltonian

To understand spin-orbit resonance, as a first approximation, ignore the shape of the rigid body and consider the angular momentum vector to be aligned with the third principal axis of inertia, i.e. $\Lambda_2 = 0$ and $J = 0$, and that the orbital motion of the rigid body is Keplerian. Under such approximations, the Hamiltonian is just the sum of the two-body Hamiltonian and the torque-free Hamiltonian. This is a completely uncoupled problem with two degrees of freedom: (λ_1, l_o) and (Λ_1, L_o)

$$\dot{\lambda}_1 = \frac{\Lambda_1}{C} \tag{3.155}$$

$$\dot{l}_o = \frac{\mu^2}{L_o^3} = n_o \tag{3.156}$$

The frequencies above are associated with the orbital and rotational motions of the rigid body. For a slow-rotating rigid body, these frequencies are of the same order. Now, one can relax the previous assumption of $J = 0$ and introduce the complete Hamiltonian including the gravity-gradient potential so as to couple both the orbital and attitude motions. To capture the essence of the slow-rotation of a rigid body, the spin and orbital rates are expressed using the following relation:

$$\dot{\lambda}_1 = \kappa \dot{l}_o \tag{3.157}$$

What we have is two variables λ_1 and l_o moving at comparable rates given by the commensurability, κ. Therefore, a new variable is introduced to combine the orbital and attitude variables. Let,

$$\sigma = \lambda_1 - \kappa l_o \tag{3.158}$$

Note that for the above expression, for a particular value of κ such that $\dot{\lambda}_1 = \kappa \dot{l}_o$, $\dot{\sigma}$ is zero and near to this commensurability, σ varies very slowly. This is an important development because, through σ, the orbital and attitude motions are linked. Thus, change in attitude motion due to change in the orbital variable is captured nicely. However, in order to see this effect, the transformation must be made canonical. This is reflected by a change in the Hamiltonian structure. Consider the generating function of the second type as follows:

$$\mathcal{S} = \Lambda_1(\lambda_1 - \kappa l_o) + \Lambda_2(\lambda_2) + \Lambda_3(\lambda_3) + \Lambda_o l_o \tag{3.159}$$

This ensures that the momenta Λ_1 remains associated to the new variable σ. However, $p_i = \frac{\partial S}{\partial q_i}$ gives:

$$L_o = \Lambda_o - \kappa \Lambda_1 \tag{3.160}$$

To make this transformation canonical, we have to reassign the momenta conjugate to the mean anomaly to be:

$$\Lambda_o = L_o + \kappa \Lambda_1$$

We can then write the complete Hamiltonian as:

$$\mathcal{H} = \mathcal{H}_{TF} - \frac{\mu^2}{2(\Lambda_o - \kappa\Lambda_1)^2} + \mathcal{V}_{ggt} \tag{3.161}$$

where,

$$\mathcal{V}_{ggt} = -\frac{1}{2}\frac{\mu^4}{(\Lambda_o - \kappa\Lambda_1)^6}\left[\frac{a}{r}\right]^3 \left((C-B)(1-3r_3^2) - (B-A)(1-3r_1^2)\right)$$

and μ is the gravitational parameter. The Hamiltonian formulation above is that of the resonant condition i.e. $\mathcal{H} = \mathcal{H}(\sigma_1, \lambda_2, \lambda_3, l_o, \Lambda_1, \Lambda_2, \Lambda_3, \Lambda_o)$. Note that the non-resonant Hamiltonian is simply: $\mathcal{H} = \mathcal{H}_o + \mathcal{H}_{TF} + \mathcal{V}_{ggt}$ where $\mathcal{H}_o$ is the orbital energy, $\mathcal{H}_{TF}$ is the torque-free Hamiltonian of the rigid body and $\mathcal{V}_{ggt}$ is the gravity-gradient potential with $\mathcal{H} = \mathcal{H}(\lambda_1, \lambda_2, \lambda_3, l_o, \Lambda_1, \Lambda_2, \Lambda_3, L_o)$. Having formulated the Hamiltonian for slow-rotating rigid bodies, we shall now look at some simplifications to better understand the dynamics at play.

3.4.2 A simplification and averaging

The case of a fast-rotating rigid body was simplified under the assumption of an axisymmetric rigid body. While it is prudent to use the same simplification for slow-rotating rigid bodies, since most celestial bodies can be approximated as oblate spheroids, we shall retain the triaxial nature of the mass distribution. We can once again use the method of averaging to obtain an approximate solution. However, because of the slow-rotating rigid body assumption, we average over the mean anomaly. The averaged Hamiltonian is obtained as follows:

$$< \mathcal{H} >= \mathcal{H}_o + \mathcal{H}_{TF} + < \mathcal{V}_{ggt} > \tag{3.162}$$

Since there are over a thousand terms in the expansion of $< \mathcal{V}_{ggt} >$, they are not mentioned in this dissertation. The symbolic code in MATLAB is used to generate these terms.

3.4.2.1 Resonant commensurabilities and relative equilibria

Having obtained the averaged form of the gravity-gradient potential, one can identify all the resonant commensurabilities in the dynamical model. The resonant commensurabilities are identified at the value of κ that results in a zero divisor, i.e. at these values of κ, $< \mathcal{V}_{ggt} >= \infty$. By truncating the approximation of $\cos f$, $\sin f$ and $\frac{a}{r}$ at the third power of eccentricity (from Eq. (3.152)), we obtain the following commensurabilities at which the averaged dynamics are in resonance[135].

$$\kappa = \frac{1}{2}, \quad \frac{1}{1}, \quad \frac{3}{2}, \quad \frac{2}{1}, \quad \frac{5}{2} \qquad \text{at order } \mathcal{O}(e^3) \tag{3.163}$$

The following resonant commensurabilities were obtained by truncating the expansion of the true anomaly terms at the third order of eccentricity. However, truncating at different orders identifies different resonant commensurabilities. It is very important to note the role of orbital eccentricity in higher-order resonances. However, its effects could be relegated for lower-order resonances such as that of Earth-Moon 1:1 spin-orbit resonance for which the first approximation of the orbital motion could be a circular orbit. For completeness, the resonant commensurabilities identified at lower orders are:

$$\kappa = \frac{1}{2}, \quad \frac{1}{1}, \quad \frac{3}{2}, \quad \frac{2}{1} \qquad \text{at order } \mathcal{O}(e^2) \tag{3.164}$$

$$\kappa = \frac{1}{2}, \quad \frac{1}{1}, \quad \frac{3}{2} \qquad \text{at order } \mathcal{O}(e^1) \tag{3.165}$$

$$\kappa = \frac{1}{1}, \qquad \text{at order } \mathcal{O}(e^0) \tag{3.166}$$

These resonances are quite easily obtained from the pitch equation of motion studied in Eq. (2.81) . Rewriting Eq. (2.81) in terms of Euler angles and expanding the true anomaly in terms of eccentricity and the mean anomaly:

$$\ddot{\theta} = -K_3 \frac{\mu}{r^3} \cos 2(\theta - f) \tag{3.167}$$

$$= -K_3 n^2 \left[\sin 2(\theta - nt) - \frac{1}{2} e \left(\sin(2\theta - nt) - 7 \sin(2\theta - 3nt) \right) + \mathcal{O}(e^2) \right] \tag{3.168}$$

with $K_3 = \frac{3(B-A)}{2C}$. At the first-order in eccentricity, we can confirm that there are two new terms corresponding to the $1 : 2$ and $3 : 2$ spin-orbit resonances. Note that since we averaged over the mean anomaly l_o, in the resonant Hamiltonian, $< \mathcal{H} >$, l_o is cyclic. Thus, from Hamilton's equations, Λ_o is a constant of (averaged) motion. Let us further consider a simplified motion of $J = 0$. For the free motion of an axisymmetric rigid body, $J = 0$ is an equilibrium. Furthermore, this assumption is very close to reality for many celestial bodies (eg. Mercury [136, 137] and the Moon [138, 139]). Physically, this means that the rotational angular momentum vector is aligned with the third principal axis of inertia. Within this framework, we now have $\Lambda_2 = 0$ The torque-free

Hamiltonian is completely reduced to the form:

$$\mathcal{H}_{TF} = \frac{\Lambda_1^2}{2C} \tag{3.169}$$

For the gravity-gradient torque formulation, the coordinate change becomes:

$$\begin{bmatrix} r_1 \\ r_2 \\ r_3 \end{bmatrix} = R_3(\lambda_1 + \lambda_3)R_1(K)R_3(-\lambda_3)R_3(-h_o)R_1(-i_o)R_3(-g_o) \begin{bmatrix} \cos f \\ \sin f \\ 0 \end{bmatrix} \tag{3.170}$$

Observe the absence of λ_2 in the expression for the gravity-gradient potential. λ_2 is now a cyclic quantity which makes the momenta associated with it, $\Lambda_2(=0)$ an integral of motion rendering the Hamiltonian two-dimensional. We can now obtain the relative equilibria for this system from Hamilton's equations of motion as follows:

$$\frac{d\mathbf{q}}{dt} = \frac{\partial < \mathcal{H} >}{\partial \mathbf{p}} = 0 \qquad\qquad \frac{d\mathbf{p}}{dt} = -\frac{\partial < \mathcal{H} >}{\partial \mathbf{q}} = 0 \tag{3.171}$$

with, $\mathbf{q} = [\sigma, \lambda_3]$ and $\mathbf{p} = [\Lambda_1, \Lambda_3]$. Specifically, the equations of motion lead to

$$\dot{\sigma}_1 = \frac{\partial < \mathcal{H} >}{\partial \Lambda_1} + \frac{\partial < \mathcal{H} >}{\partial (\cos K)} \frac{\partial (\cos K)}{\partial \Lambda_1} \tag{3.172}$$

$$\dot{\lambda}_3 = \frac{\partial < \mathcal{H} >}{\partial \Lambda_3} + \frac{\partial < \mathcal{H} >}{\partial (\cos K)} \frac{\partial (\cos K)}{\partial \Lambda_3} \tag{3.173}$$

$$\dot{\Lambda}_1 = -\frac{\partial < \mathcal{H} >}{\partial \sigma_1} \tag{3.174}$$

$$\dot{\Lambda}_3 = -\frac{\partial < \mathcal{H} >}{\partial \lambda_3} \tag{3.175}$$

The first two equations lead to

$$\frac{\partial < \mathcal{H} >}{\partial \Lambda_1} = 0 \tag{3.176}$$

$$\frac{\partial < \mathcal{H} >}{\partial (\cos K)} = 0 \tag{3.177}$$

The remaining two equations lead to the following equilibrium states in the angles. These are given by:

$$(\sigma_1, \lambda_3) = (0,0), \qquad (\pi/2, 0), \qquad (0,\pi), \qquad (\pi/2,\pi) \tag{3.178}$$

The last two configurations are the same as the first two. For each of these equilibrium configurations, the value of ecliptic obliquity (K) can be found. The value of the ecliptic obliquity for different resonant conditions is obtained and is given in Tab. 3.1.

Table 3.1: Relative equilibria and ecliptic obliquity

Resonant Commensurability	Equilibrium Configuration	Ecliptic Obliquity
$3:2$	$(0,0)$, $(\pi/2,0)$, $(0,\pi)$, $(\pi/2,\pi)$	$\pm i_o, \cos^{-1}\alpha^{3:2}$
$1:1$	$(0,0)$, $(\pi/2,0)$, $(0,\pi)$, $(\pi/2,\pi)$	$\pm i_o, \cos^{-1}\alpha^{1:1}$
$1:2$	$(0,0)$, $(\pi/2,0)$, $(0,\pi)$, $(\pi/2,\pi)$	$\pm i_o, \cos^{-1}\alpha^{1:2}$
$2:1$	$(0,0)$, $(\pi/2,0)$, $(0,\pi)$, $(\pi/2,\pi)$	$\pm i_o, \cos^{-1}\alpha^{2:1}$
$5:2$	$(0,0)$, $(\pi/2,0)$, $(0,\pi)$, $(\pi/2,\pi)$	$\pm i_o, \cos^{-1}\alpha^{5:2}$

where,

$$\alpha^{3:2} = \frac{C_2^2 e(253e^2 - 168)}{\sqrt{1-e^2}(C_2^0(120e^2+48) \pm C_2^2(359e^3 - 168e))} \tag{3.179}$$

$$\alpha^{1:1} = \frac{2C_2^2(2e^2-1)}{\sqrt{1-e^2}(C_2^0(5e^2+2) \pm C_2^2(12e^2-2))} \tag{3.180}$$

$$\alpha^{1:2} = \frac{C_2^2 e(5e^2+12)}{\sqrt{1-e^2}(C_2^0(60e^2+24) \pm C_2^2(179e^3+84e))} \tag{3.181}$$

$$\alpha^{2:1} = \frac{17C_2^2 e^2}{\sqrt{1-e^2}(C_2^0(5e^2+2) \pm 17C_2^2 e^2)} \tag{3.182}$$

$$\alpha^{5:2} = \frac{239C_2^2 e^3}{\sqrt{1-e^2}(C_2^0(40e^2+16) \pm 239C_2^2 e^3)} \tag{3.183}$$

Note here the principal moments of inertia $[A, B, C]$ are expressed through functions of the spherical harmonics of the rigid body, C_2^0 and C_2^2 (Eq. (3.150)) and are valid for expressions of the gravity-gradient potential truncated at the third power of eccentricity. The value for Λ_1 is a constant and is a function of the inertia parameters, orbit parameters, and the commensurability, κ.

The values of $K = i_o$ and $K = 180 - i_o$ can be interpreted physically as the configuration when the orbit normal is aligned along the rotational angular momentum vector. We further observe that these equilibria are of stability type center and the separatrix occurs at $K = 2i_o$ and $K = 180 - 2i_o$, respectively, for the pair of equilibrium configurations. This is illustrated in the figure below.

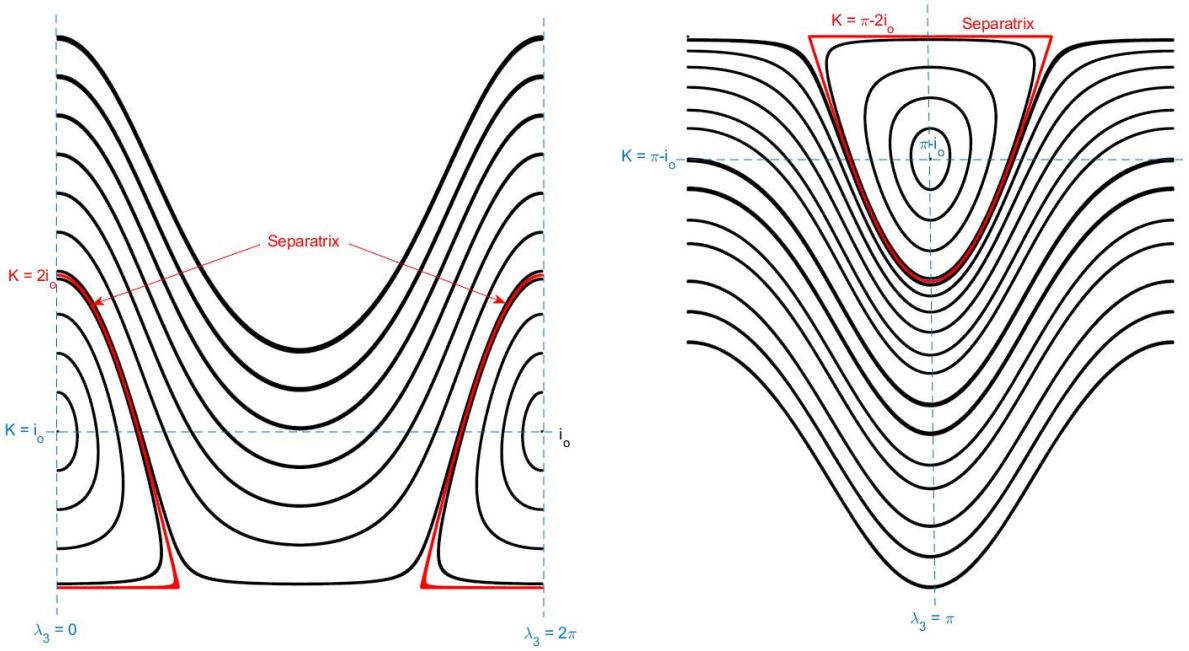

(a) Relative equilibria for (σ, λ_3) = (0,0) and (π,0) (b) Relative equilibria for (σ, λ_3) = (0,π) and (π,π)

Figure 3.3: Relative equilibria and isoenergetic curves of the averaged motion in the $K - \lambda_3$ phase-space

The periodic motions exhibited about the equilibria show how the body librates as the orbital angular momentum is no longer aligned with the rotational angular momentum. Beyond the separatrix, the body performs circulatory motions. The angle $(K - i_o)$ and $(180 - (K - i_o))$ can be interpreted as analogues to the ecliptic obliquity of a planetary body.

3.4.3 Another canonical transformation combining the attitude and orbital variables

The angle J can be reintroduced into the expansion of the $\mathcal{V}_{ggt}$ thereby reintroducing the angle λ_2. This results in the following form of the Hamiltonian.

$$\mathcal{H} = \mathcal{H}_o(\Lambda_o, \Lambda_1) + \mathcal{H}_{TF}(\lambda_2, \Lambda_1, \Lambda_2) + \mathcal{V}_{ggt}(\sigma, \lambda_2, \lambda_3, \Lambda_1, \Lambda_2, \Lambda_3, l_o, g_o, h_o, \Lambda_o, G_o, H_o) \quad (3.184)$$

To get rid of the short-period terms, we can average over the mean anomaly (l_o) in $\mathcal{V}_{ggt}$. We have performed this before and after the averaging process, the Hamiltonian can be written as:

$$\mathcal{H} = \mathcal{H}_o(\Lambda_o, \Lambda_1) + \mathcal{H}_{TF}(\lambda_2, \Lambda_1, \Lambda_2) + \mathcal{V}_{ggt}(\sigma, \lambda_2, \lambda_3, \Lambda_1, \Lambda_2, \Lambda_3, \sim, g_o, h_o, \Lambda_o, G_o, H_o) \quad (3.185)$$

We know from our previous discussion that the ecliptic obliquity depends on the inclination of the rigid body in orbit. So we attempt to perform a canonical transformation that couples the orbital variables and the attitude variables. Specifically, we are looking for combinations of $(\sigma_1, \lambda_2, \lambda_3, g_o, h_o)$ variables. On expanding Eq. (3.147) , we find that certain combinations of the orbit and attitude angles can be isolated. These combinations are used to define a canonical transformation whose generating function (of type 2) is given by:

$$\mathcal{S} = \Sigma_1(\sigma_1 - g_o - h_o) + \Sigma_2(\lambda_2) + \Sigma_3(\lambda_3 + h_o) + \Sigma_h h_o + \Sigma_g g_o \quad (3.186)$$

The new coordinates and their conjugate momenta are:

$$\sigma_1 = \sigma_1 - g_o - h_o \qquad \Sigma_1 = \Lambda_1 \quad (3.187)$$

$$\sigma_2 = \lambda_2 \qquad \Sigma_2 = \Lambda_2 \quad (3.188)$$

$$\sigma_3 = \lambda_3 + h_o \qquad \Sigma_3 = \Lambda_3 \quad (3.189)$$

$$\sigma_g = g_o \qquad \Sigma_g = G_o - \Lambda_1 \quad (3.190)$$

$$\sigma_h = h_o \qquad \Sigma_h = H_o + \Lambda_3 - \Lambda_1 \quad (3.191)$$

Since we are considering Keplerian motion, the Hamiltonian is not an explicit function of Σ_g and Σ_h thereby resulting in $\dot{h}_o = 0$ and $\dot{g}_o = 0$. However, with the formulation above, one could

introduce a constant precession of the ascending node and precession of the pericenter quite easily.

3.4.3.1 Precession of the ascending node and pericenter

To introduce a constant precession of the ascending node and pericenter, let us define the following:

$$\dot{h}_o = \dot{\sigma}_h = \eta_1 \tag{3.192}$$

$$\dot{g}_o = \dot{\sigma}_g = \eta_2 \tag{3.193}$$

The Hamiltonian is then simplify modified as:

$$\mathcal{H}_\eta = \mathcal{H} + \eta_1\Sigma_h + \eta_2\Sigma_g = \mathcal{H} + \eta_1 H_o + \eta_2 G_o - (\eta_1 + \eta_2)\Lambda_1 + \eta_1\Lambda_3 + \eta_2\Lambda_2 \tag{3.194}$$

Note that we are still working in averaged variables i.e. the Hamiltonian is not an explicit function of l_o. Utilizing the following form of the Hamiltonian, we can now investigate the nature of equilibria and the effects of precession on the equilibria for various slow-rotating rigid bodies.

3.4.3.2 Evolution of the relative equilibria

Using the Hamiltonian formulation above and the process used in the previous section, the equilibrium configurations can now be found. It is found that specifically, the angle equilibria remain the same, i.e.:

$$(\sigma_1, \sigma_3) = (0,0) \qquad (0,\pi) \qquad (\pi/2, 0) \qquad (\pi/2, \pi) \tag{3.195}$$

At each of the equilibrium conditions, the obliquity (K) and Σ_1 are computed so as to equate the right hand side of Hamilton's equations of motion to zero. These can be classified as those that depend on the inclination of the rigid body and those that depend on the principal moments of inertia (or C_2^2 and C_2^0) of the rigid body as seen before. The nodal precession results in a drift in the equilibrium obliquity. The following results are obtained for the rigid body with inertia parameters:

$K_1 = 1/3$, and $K_2 = 1/5$ inertia parameters or equivalently: $A = 300, B = 400, C = 500$. The orbital parameters are taken as: $i_o = 7\,\text{deg}$, $g_o = 0\,\text{deg}$, $h_o = 0\,\text{deg}$, $a = 13,000$ km. The rigid body is considered to be in $1:1$ spin-orbit resonance. The units of nodal precession are radians per seconds. The figure below (Fig. 3.4) shows increments of 10^{-5} [rad/s] in nodal precession, μ_1 i.e. approximately 1.8 deg/hr.

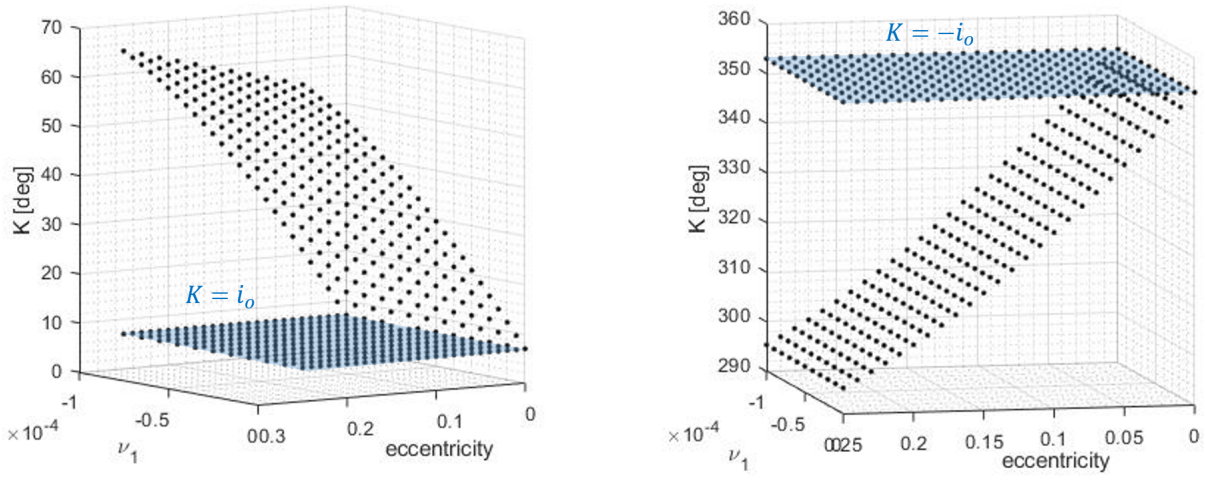

Figure 3.4: Variation in the equilibrium obliquity due to eccentricity and nodal precession for $1:1$ spin-orbit resonance equilibrium: (σ_1, σ_3) = (0,0).

A similar result is documented for the $3:2$ spin-orbit resonance keeping the same parameters describing the rigid body and the orbit. This is illustrated in Fig. 3.5

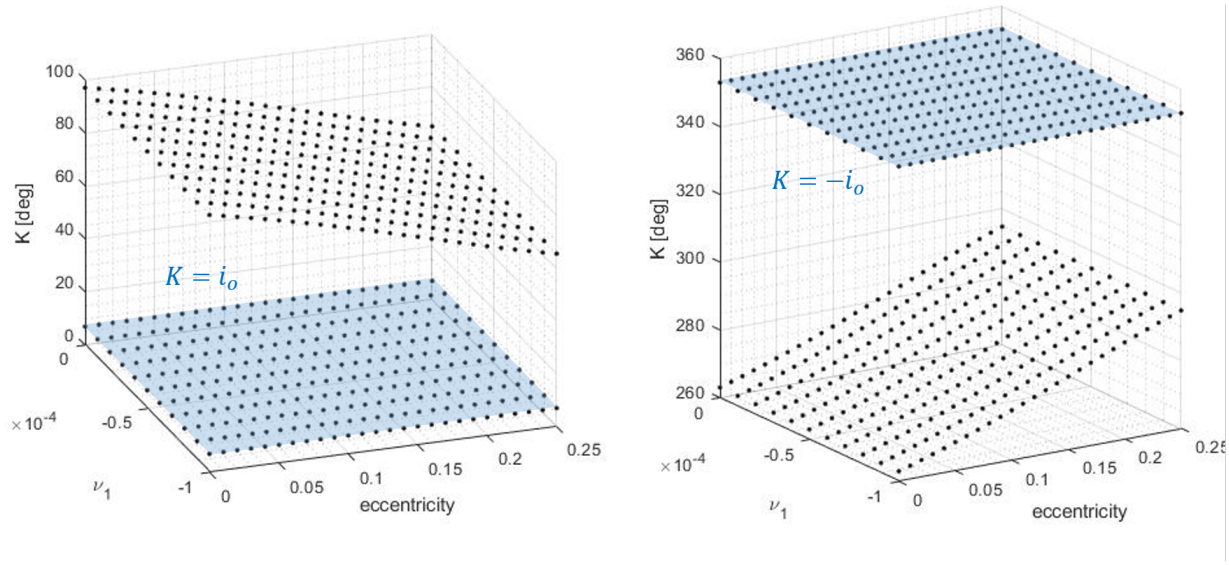

Figure 3.5: Variation in the equilibrium obliquity due to eccentricity and nodal precession for $3:2$ spin-orbit resonance equilibrium: (σ_1, σ_3) = (0,0).

As seen from the problem formulation, there are many parameters to track such as eccentricity, inclination, moments of inertia, precession rates, etc. An extensive study can be performed using these parameters with the Hamiltonian formulation presented in this section. We shall reserve that for future work. The main application of the Hamiltonian formulation of the slow-rotating rigid body is to apply it towards studying planetary body librations. As a first step, we shall verify that the Hamiltonian formulation holds for planetary bodies as well.

3.5 Validation of Hamiltonian formulation for planetary bodies

The Hamiltonian formulation for planetary bodies is very similar to that of artificial satellites. The primary difference is that now the mass of the rigid body becomes significant as compared to the primary. The Hamiltonian is only slightly modified, specifically in the Hamiltonian contribution from orbital mechanics $\mathcal{H}_o$ and the coefficient of gravity-gradient potential. They are as shown below

$$\mathcal{H}_o = \frac{-m^3\mu^2}{2\left(\Lambda_o - \kappa\Lambda_1\right)^2} \tag{3.196}$$

$$\mathcal{V}_{ggt} = -\frac{\mu^4}{2\left(\Lambda_o - \kappa\Lambda_1\right)^6}\left((C-B)(1-3r_3^2) + (B-A)(1-3r_1^2)\right) \tag{3.197}$$

where G is the gravitational constant, m is the mass of the planetary rigid body, M is the mass of the primary body, and $\mu = G(M+m)$. A, B and C are the moments of inertia of the planetary rigid body which can be expressed as a function of the spherical harmonics (C_2^2 and C_2^0). The gravity-gradient potential then takes the form

$$\mathcal{V}_{ggt} = -\frac{GMm^6\mu^3R_e^2}{\left(\Lambda_o - \kappa\Lambda_1\right)^6}\left(\frac{C_2^0}{2}(2r_3^2 - r_1^2 - r_2^2) + 3C_2^2(r_1^2 - r_3^2)\right) \tag{3.198}$$

In order to validate this model, we have attempted to study the motion of Mercury around the Sun. Mercury is observed in a stable state, close to a 3:2 spin-orbit resonance. It is considered as a rigid body in this framework. Using the Hamiltonian formalism, the long-term behavior of the spin of Mercury is examined. For validation, we compare our formulation of the Hamiltonian with that of [140, 10, 141, 137]. It is observed that our formulation gives a reasonably close value of the final equilibrium state that is obtained by D'Hoedt et al.[134, 140]. The discrepancy in the value obtained is due to the truncation of the eccentricity terms and the possible use of different constants of orbital and attitude motion. We begin by outlining the orbital and rotational parameters of Mercury in the table below.

Table 3.2: The numerical values of the parameters for the Hamiltonian formulation. The gravity coefficients is taken from [6]. The value of Mercury's radius R_e was borrowed from [7]. The values of both the semimajor axis a and the eccentricity, are derived from the secular planetary theory of [8]

Parameter	Numerical Value
Semimajor axis (a_o)	5.791 $\times 10^7$ km
Eccentricity (e_o)	0.206
Inclination (i_o)	7 deg
Radius of Mercury (R_e)	2440 km
$C_{20} = -J_2$	-5.031×10^{-5}
C_{22}	8.088×10^{-6}

Mercury is located at the equilibrium $(\sigma_1, \sigma_2, \sigma_3) = (0, 0, 0)$ with $K = i_o$. Utilizing these parameters, the equilibrium value for Σ_1 is obtained to be:

$$\Sigma_1 = 13.5475 \quad mR_e^2/\text{year} \tag{3.199}$$

Contrastingly, the value obtained by D'Hoedt et al. [136, 10] was $\Sigma_1 = 13.303\, mR_e^2/$year. Using Hamilton's equations of motion, we can study the evolution of the state-space variables. They are as shown below.

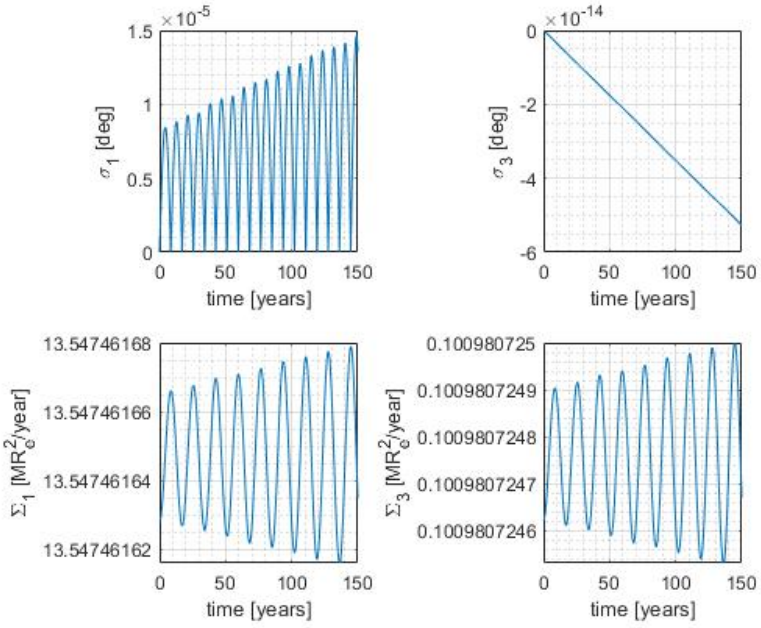

Figure 3.6: Evolution of the state-space variables for slightly off equilibrium configuration.

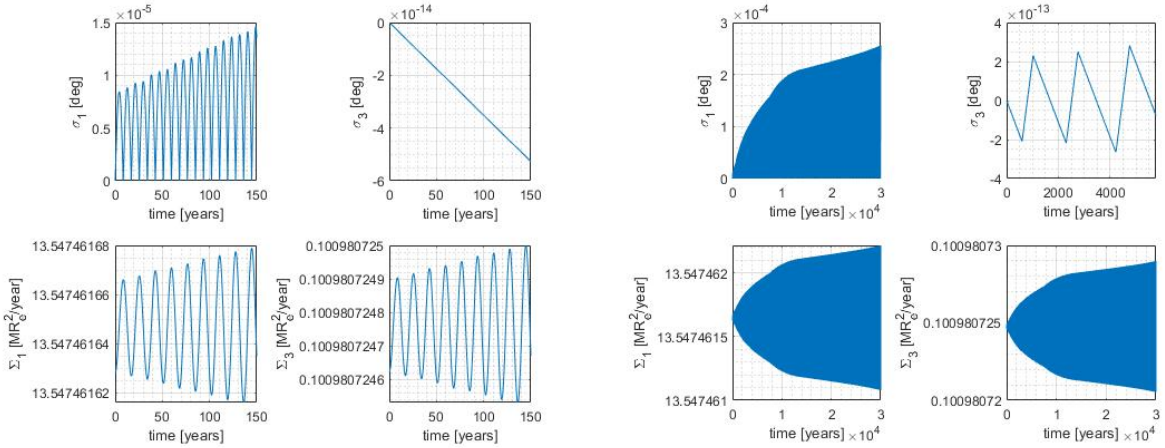

Figure 3.7: Evolution of the state-space variables for slightly off equilibrium configuration for simulation period of 150 and 30000 years, respectively

The slightly off equilibrium configuration is obtained by using a low integration tolerance and thereby introducing (on purpose) numerical errors in the states that cause it to move away from equilibrium. We can observe from Fig. 3.7 that the simulation results in constant values up to 10^{-7} which was the tolerance of integration set. Using spectral analysis, the frequency of σ_1 and σ_3 can be obtained thereby giving its periodicity. The period of σ_1 is obtained to be $T_1 = 16.6$ years which is close to the value obtained by [142, 10] of 15.857 years. Similarly, through spectral analysis, the frequency of σ_3 is also obtained. It is observed that the spectrum of σ_3 has multiple frequencies. The second strongest one corresponding to a time period of $T_3 = 1034.4$ years. This value is also close to the one obtained by [142, 10] of 1065.05 years.

Having validated the Hamiltonian formulation for planetary rotational dynamics, we move to examine the librations exhibited by the Moon in the next section.

3.6 Application to examining the free librations of the Moon

The resonant motion of the moon was one of the earliest optical discoveries. Cassini developed an elegant description of the motion of the Moon in 1693 through his observation that the telescopic observations of the librations are in fact the sum of two uniform motions moving synchronously with the orbital period and precession of the orbit ([143, 144, 9]). Fundamentally, there are three modes of free libration: The dynamical mode of the Moon in spin-orbit resonance when the spin is displaced from its dynamical equilibrium, the longitudinal mode (optical measurements resulting in seeing more of the east side than the west sometimes and other times seeing the west more than the east side of the Moon first observed by Hevelius) and the latitudinal mode (optical measurements resulting in seeing more of the north side than the south sometimes and other times seeing the south more than the north side of the Moon first observed by Galileo). The libration in longitude results because while the orbital motion of the Moon is variable, the rotation is uniform and the latitude librations result because the lunar equator has a small inclination with respect to the lunar orbit i.e. the obliquity (K) [9]. The table below provides a brief history of the development of lunar theory and the approaches taken to obtain the free-librations of the Moon.

Table 3.3: Brief history of lunar libration theories [9, 10, 11, 12, 13, 14]

Contributor	Contribution
Cassini's Laws (1721)	Based on observations and theory of superposition: Moon's rotations which govern its librations as the sum of two uniform motions which are synchronized with the period and precession of its orbit.
Tobias Mayer (1750)	Observational proof of Cassini's Laws.
Lagrange (1780)	Dynamical explanation of Cassini's rules.
Hayn (1902)	Lunar libration theory based on Hansen's lunar theory of orbital motion. Semi-analytic based on Fourier series expansions of the lunar coordinates within framework of linear approximation of Euler's equations of motion.
Keziel (1948)	Lunar libration theory based on Brown's lunar theory of orbital motion Semi-analytic based on Fourier series expansions of the lunar coordinates within framework of linear approximation of Euler's equations of motion.
Williams (1977) and Cappallo et al.	Direct approach based on numerical simulations from lunar laser ranging.
Eckhardt (1981), Moons (1982), Williams et al. (2001), Varadi et al. (2005)	Linear first order theory from Euler's equations of motion.
Chapront et al. (1999), Newhall and Williams (1997)	Compared analytical representation to Euler angles in JPL ephemeris through data fitting.

An elegant yet simple descriptive explanation of the librations is given by Donald Eckhardt [9] which is concisely paraphrased as follows. Under the assumption of a uniform triaxial ellipsoid and moments of inertia $A < B < C$ for the Moon, to keep one of its axes constantly facing the Earth and in a stable manner, this axis must be the axis of minimum moment of inertia (A) and the rotation axis must be the that of greatest (or least, but this axis is pointing towards the Earth) principal moment of inertia to maintain stability. The axis of rotation of the Moon cannot be in the direction of orbit normal because then the Earth would always be in the plane of the lunar equator and could not torque it so as to maintain the precession of the rotation axis. For small inclination and nearly similar principal moments of inertia, the rotation axis will precess at the same rate as the orbit if it is oriented at the same value of the inclination of the lunar orbit i.e. the

obliquity $K = i_o$. This was shown to be the case for the $1:1$ commensurability discussed in the previous section. Lunar ranging and differential VLBI have been providing observations for lunar librations. These have been confirmed by the numerical simulation of the lunar motion to extract the libration frequencies ([145, 146]). In this section, the Hamiltonian formulation of the $1:1$ spin-orbit resonance condition of the rigid body (developed previously) will be used to examine lunar free librations.

Let us recall the reference frames used in the Serret-Andoyer representation. Figure 3.8 illustrates the coordinate and momenta for the Serret-Andoyer variables as well as the Euler 3-1-3 minimal representation.

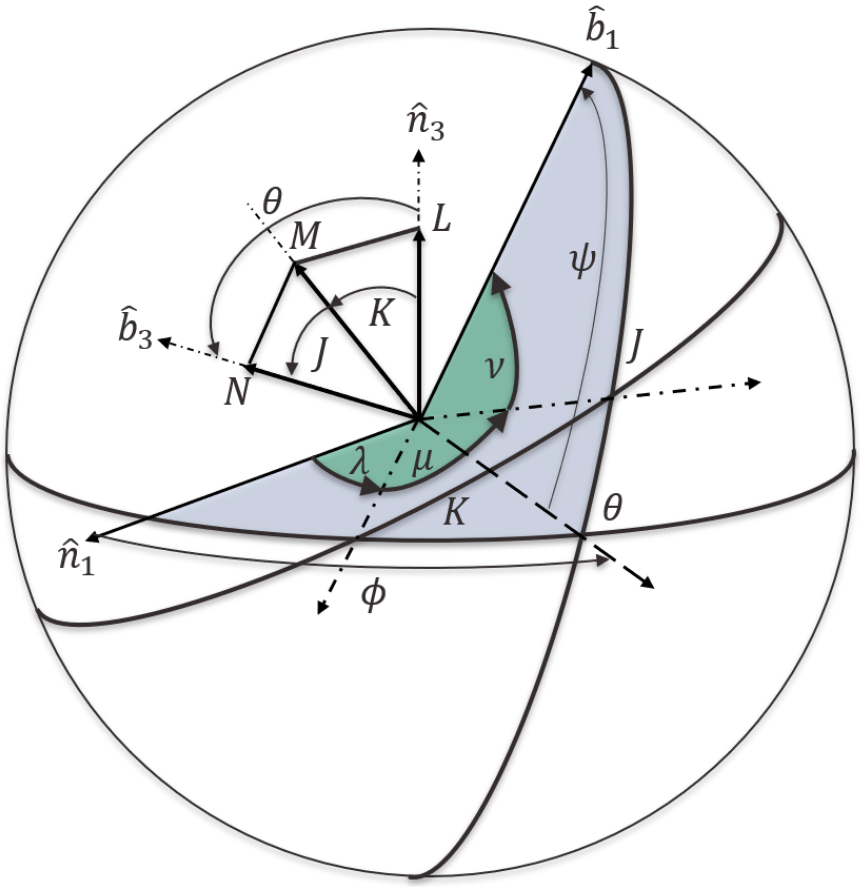

Figure 3.8: Body frame representation using the invariable frame [3, 4]. $[\lambda, \mu, \nu]$ are the coordinates and their corresponding momenta are $[L, M, N]$.

Cassini described the laws [144, 143] that govern spin-orbit resonant motions. While he presented the laws for the motion of the Moon, it was found later that these laws hold valid for any rigid body with near axial symmetry. In the literature, Cassini's laws are taken as a nominal motion and the physical librations imply the departure of the rotational motion from that defined by Cassini's laws. Cassini's laws for the Moon's rotational motion is described below:[143]

1. The Moon rotates uniformly about its polar axis with a rotational period equal to the mean sidereal period of its orbit about the earth.

2. The inclination of the Moon's equator to the ecliptic is a constant angle.

3. The ascending node of the lunar orbit on the ecliptic coincides with the descending node of the lunar equator on the ecliptic.

One can interpret these laws using the Serret-Andoyer formulation from Fig. 3.8. With reference to Fig. 3.8, let b_1 be the axis coinciding with the minimum principal moment of inertia, A. b_3 coincides with the maximum principal moment of inertia, C. In Fig. 3.8, let θ be the inclination of the lunar equator to the ecliptic, ϕ is the longitude of ascending node and ψ is the angle between the ascending node and b_3. Let us decipher each of these laws with respect to the equilibrium configurations that we obtained in the previous sections. To have an exact coincidence with Cassini's laws, one must have:

$$\theta = K, \qquad \phi = h_o, \qquad \phi + \psi = \pi + (h_o + g_o + l_o) \tag{3.200}$$

with h_o being the longitude of the ascending node, g_o the argument of periapse, l_o the mean anomaly. This is then traced back to the Serret-Andoyer formulation. Recall that the coordinates

and momenta derived in the previous section are as follows:

$$\sigma_1 = \lambda + \mu + \nu - l_o - g_o - h_o \qquad \Sigma_1 = M \tag{3.201}$$

$$\sigma_2 = -\nu \qquad \Sigma_2 = M - N \tag{3.202}$$

$$\sigma_3 = -\lambda + h_o \qquad \Sigma_3 = M - L \tag{3.203}$$

$$\sigma_4 = l_o \qquad \Sigma_4 = L_o + \Sigma_1 \tag{3.204}$$

$$\sigma_5 = g_o \qquad \Sigma_5 = G_o + \Sigma_1 \tag{3.205}$$

$$\sigma_6 = h_0 \qquad \Sigma_6 = H_o + \Sigma_1 - \Sigma_3 \tag{3.206}$$

with L_o, G_o, H_o are the Delaunay variables momenta conjugate to l_o, g_o, h_o. We can now relate the Serret-Andoyer variables to the Cassini laws as follows:

1.
$$\theta = K \Rightarrow J = 0 \Rightarrow \lambda = \phi \Rightarrow \mu + \nu = \psi \Rightarrow K = i_o$$

2.
$$\phi = h_o \Rightarrow \lambda = h_o \Rightarrow \sigma_3 = 0$$

3.
$$\phi + \psi = \pi + (l_o + g_o + h_o) \Rightarrow \sigma_1 = \phi + \psi - (\phi + \psi - \pi) \Rightarrow \sigma_1 = \pi$$

Thus, Cassini's laws give us the following equilibrium condition for the Serret-Andoyer variables.

$$\sigma_1 = \pi \qquad \sigma_3 = 0 \qquad K = i_o \tag{3.207}$$

Since Cassini's laws are not exact, one can assume the above equilibrium to be the nominal motion and therefore we can proceed to investigate perturbations about this nominal orientation. Our main hypothesis is introduced as follows: The Moon is assumed to move on a fixed elliptic orbit with the orbital and rotational parameters as follows (NASA Fact sheet):

Table 3.4: The numerical values of the parameters for the Hamiltonian formulation. The gravity coefficients are taken from Williams et. al [12, 15]

Parameter	Numerical Value
Semimajor axis (a_o)	384400 km
Eccentricity (e_o)	0.0549
Inclination to ecliptic (i_o)	5.145 deg
Obliquity to the orbit	6.68 deg
Equatorial radius (R_e)	1738.1 km
$C_{20} = -J_2$	$-203.21568 \times 10^{-6}$
C_{22}	22.38184×10^{-6}

The mass of the Moon is 7.3463×10^{22} kg and the obliquity to the orbit is 6.68 deg. giving us the inclination of the lunar equator to the ecliptic as 1.5350 deg. The principal moments of inertia for the Moon are obtained using the un-normalized coefficients J_2 and C_{22} along with the relations of the inertia parameters from Eq. (2.48) and relations from Eq. (3.150) using expressions from Williams et. al [12, 15].

In this approach, the simple resonant model constructed in previous sections is used to evaluate the frequency of free librations of the Moon. The assumptions are listed below.

1. A simplified Hamiltonian model is considered. To avoid the uncertainty associated with the Laplace plane (mean or reference plane about whose axis the instantaneous orbital plane of that satellite precesses), the averaged Hamiltonian is considered.

2. The wobble motion of the Moon (optical libration) is neglected i.e. the maximum axis of inertia is considered as the axis of rotation. Thus, J is set to zero and the torque-free Hamiltonian is reduced to
$$\mathcal{H}_{TF} = \frac{\Sigma_1^2}{2C} \tag{3.208}$$

3. The effect of the rotation of the Moon on its orbital motion is neglected, i.e. the phase-space under consideration is only two dimensional: (σ_1, σ_3). This also implies that the orbital parameters are constants and known quantities.

4. Next, the short period effects are neglected. Thus, the potential is averaged over the mean anomaly as:

$$< \mathcal{V}_{ggt} >= \frac{1}{2\pi} \int_0^{2\pi} \mathcal{V}_{ggt}(\sigma_1, \sigma_3, \Sigma_1, \Sigma_3) dl_o \tag{3.209}$$

Because of such averaging, the potential becomes independent of the mean anomaly, l_o (or σ_4). Thus, Σ_4 is a constant of motion which leads to the semimajor axis (function of the momenta conjugate to l_o) being a constant. Note that this averaging procedure is the first step of the Lie-series averaging that was discussed in the previous sections. Since we are interested in the dynamical evolution of the averaged variables, we do not need the generating function that averaged the motion but only the averaged potential.

Under such assumptions, we can now examine the averaged dynamical system. We already know the equilibria for σ_1, σ_3 and K as

$$(\sigma_1, \sigma_3, K) = (\pi, 0, i_o)$$

using these quantities, the equilibria for Σ_1 can be obtained by finding its value that results in the right-hand side of Hamilton's equations to go to zero. For the sake of simplicity, the numerical values are scaled so that the equatorial radius of the Moon (R_e), the mass of the Moon (M), and the terrestrial year are chosen as units of length, mass, and time. The value of Σ_1 is obtained to be

$$\Sigma_1 = 33.0327 \ \ \frac{MR_e^2}{year} \tag{3.210}$$

Assuming the above model, variation of the coordinates and momenta of the reduced phase-space is shown to be as follows.

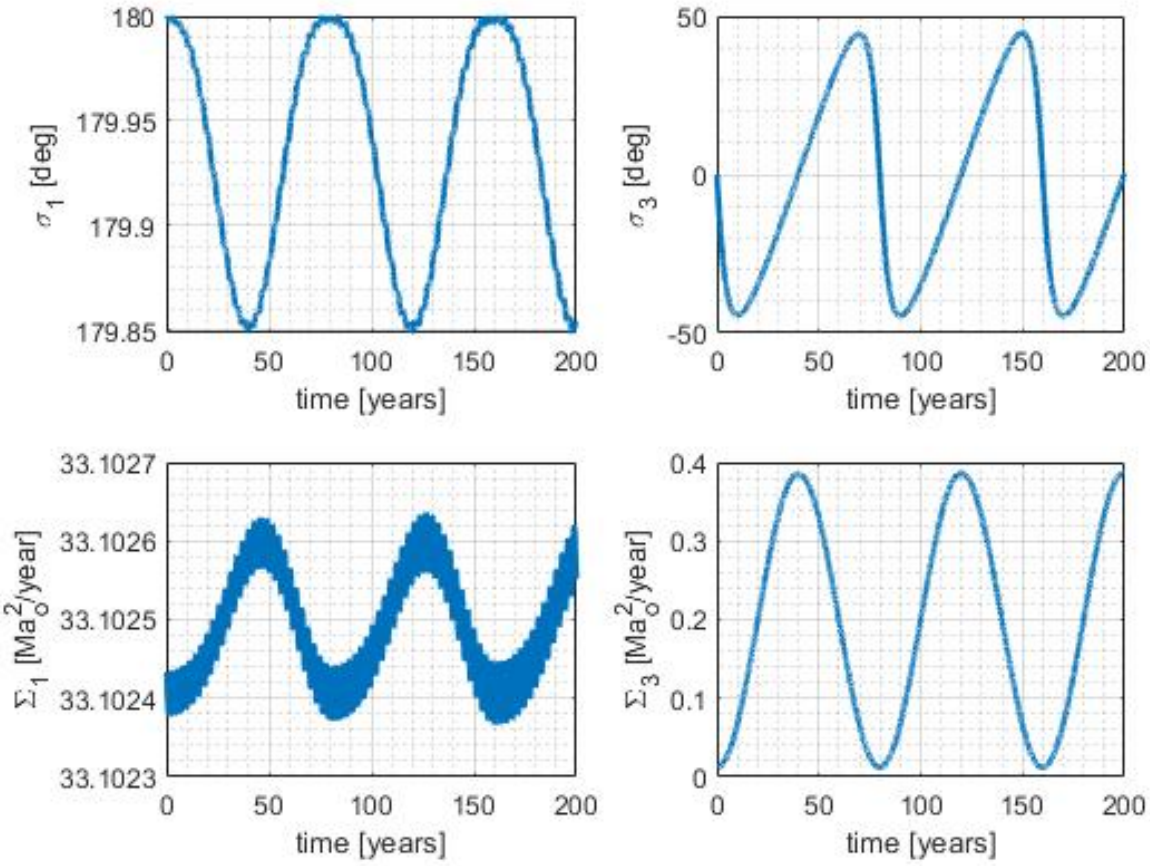

Figure 3.9: Long-term evolution of coordinates and momenta

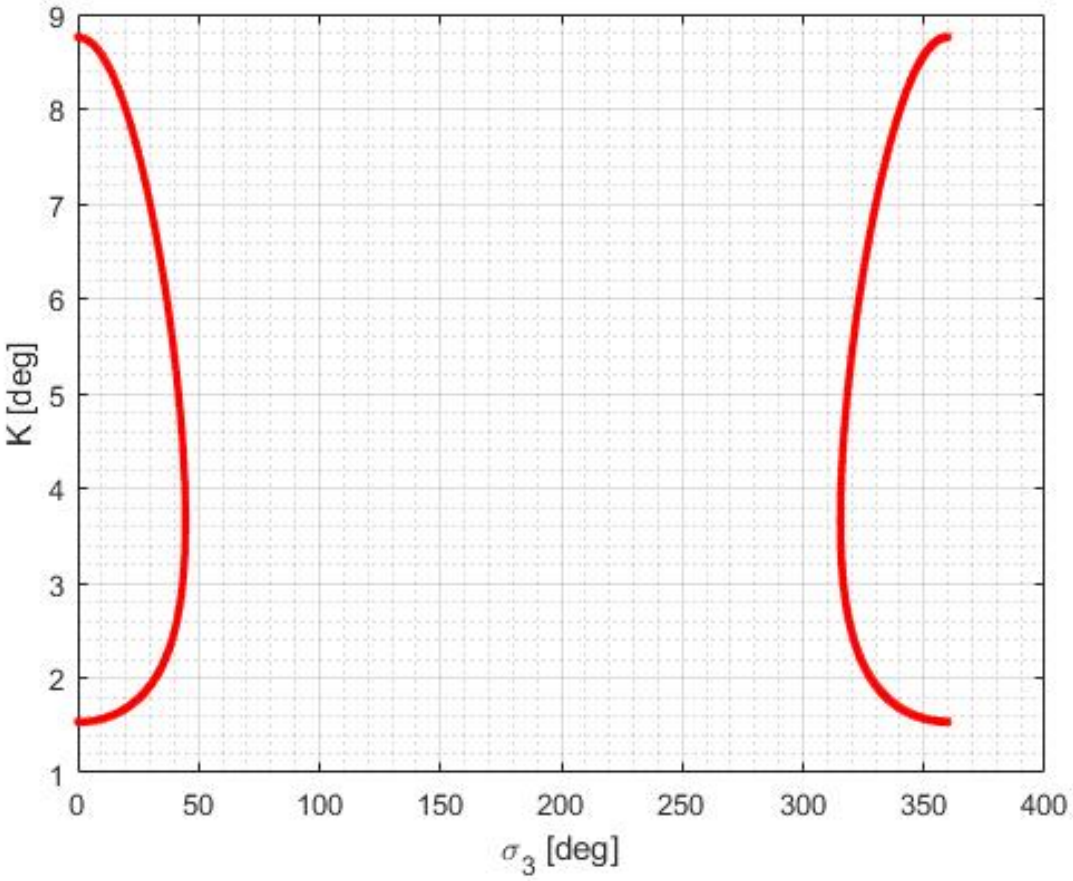

Figure 3.10: $\sigma_3 - K$ phase-space for the Moon

It is known that there are three modes for free libration of the Moon. They correspond to the dynamical normal modes of the Moon in spin-orbit resonance when its spin is displaced from its dynamical equilibrium position. The period of the free rotational modes of the solid Moon can be calculated in linear first-order theory (see works by Eckhardt [9], Moons [139], Williams et al. [146], Varadi et al. [13]). They are listed as follows [146]:

1. *In longitude with the rotation parallel to the equatorial plane of the Moon, and has a period of 2.9 years.* Recall from Fig. 3.8, for $J = 0$, this angle corresponds to ϕ i.e. rotation about the angular momentum vector Σ_1.

2. *In the latitude mode, the axis normal to the lunar equatorial plane traces out a small cone. That motion in space is retrograde with a period near 81 years.* This denotes the period of evolution of the obliquity, K.

3. *The third mode of free libration is related to the motion of the axis of figure* [1] *As seen from the reference frame, the axis of figure traces out an elliptical path with a period of around 75 years.* This axis then corresponds to Σ_3, the inertial component of the angular momentum vector.

If we are to do a spectral analysis of the data in Fig. 3.9, i.e. take the Fourier transform of the interested variables, we can then extract all the different frequencies of the dynamical system. A note on the sampling and simulation of the dynamical system is given next and the dynamical model simulation results are discussed after.

3.6.1 A note on sampling

In order to ascertain the frequencies of free libration, the dynamical system governed by the Hamiltonian discussed in the previous sections is propagated using initial conditions of the equilibrium state of the Moon and noting that the Moon performs small librations about the equilibrium configuration by a value equal to the difference between the inclination to the ecliptic and the

[1] The term "axis of figure" is adopted from the Russian translation of E. P. Bullard's monograph - Theory of Earth's rotation about its center of mass. It is also referred to as the inertial axis [147]

obliquity to the orbit. During the propagation tests performed as a part of this work, it is found that to obtain an accurate estimate of the frequency, the sampling of the time-domain evolution of the reduced phase-space variables is crucial. The results obtained below correspond to a sampling interval of one orbital period of the Moon (27 days) and sampling time of 5000 years. It is also found that propagating for longer time periods results in the accumulation of numerical error, and propagation for shorter time periods precludes the state-space variables to evolve sufficiently.

3.6.2 Frequencies associated with the longitudinal mode

The Fourier transform of Σ_1 is shown below. We can see that there are two particular frequencies that stand out.

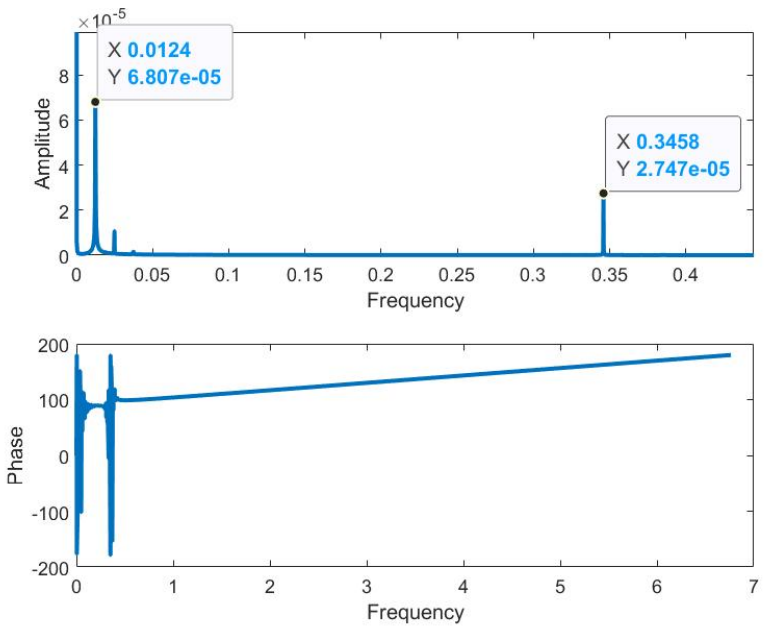

Figure 3.11: Spectral analysis of Σ_1 frequencies

The time period corresponding to these frequencies are 2.89184 years and 80.64529 years. Note that these correspond to the free libration in longitude and the latitude mode. Next, the spectral decomposition of the obliquity K is performed.

3.6.3 Frequencies associated with the latitudinal mode

The Fourier transform of K is shown below. We can see that there are multiple frequencies that stand out.

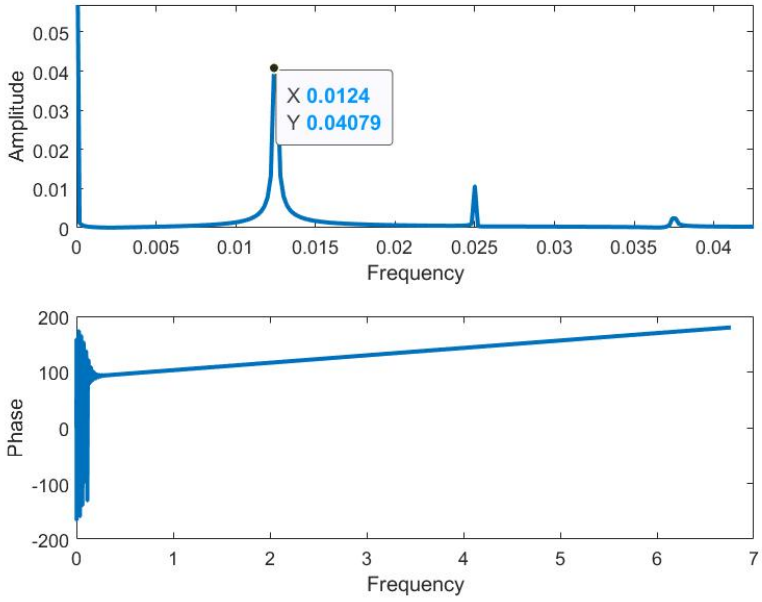

Figure 3.12: Spectral analysis of the obliquity evolution $K = \cos^{-1}\left(1 - \frac{\Sigma_3}{\Sigma_1}\right)$ frequencies

The time period corresponding to the most dominant frequency (i.e. the one with the largest amplitude) is 80.64529 years. Note that this corresponds to the free libration in the latitude mode. Next, the spectral decomposition of Σ_3 is performed.

3.6.4 Frequencies associated with the wobble mode

The Fourier transform of Σ_1 is shown below. We can see that there are two particular frequencies that stand out. They are not as discernible in the amplitude plot and hence, the information is extracted from the phase plot.

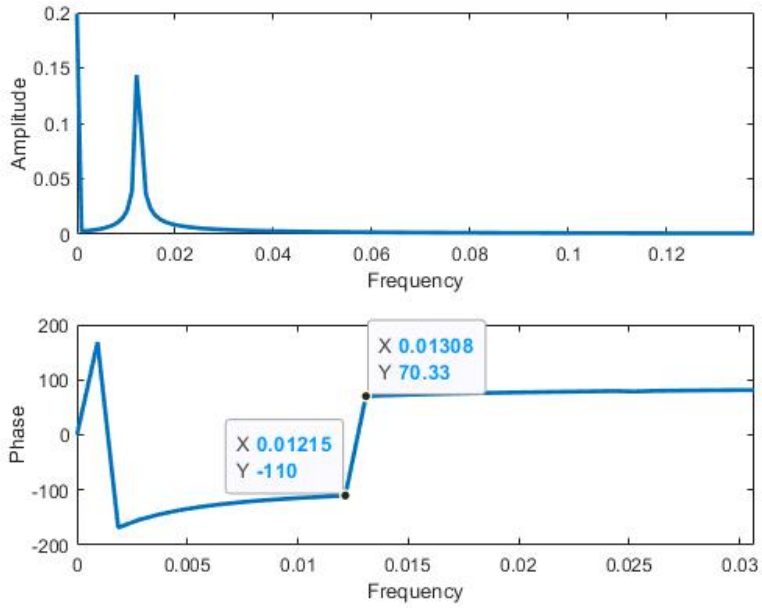

Figure 3.13: Spectral analysis of Σ_3 frequencies

The first frequency is the familiar libration in the latitude mode. The second one has a time period of 76.4526 years. This corresponds to the free libration in the motion of the axis of figure about the rotational axis. Therefore, the Hamiltonian formulation of the slow-rotating rigid body is utilized to discern the frequency of modes of free libration of the Moon. The simple dynamical model captures information on all the three main modes of libration. Additionally, other modes of libration are also captured. As emphasized in Bois [14], the free librations at 2.9 and 81 years are the result of the spin-orbit resonance problem of the Moon around the Earth and do not correspond to the free Eulerian modes of rotation of a body alone in space. While the periods of the free modes can be calculated analytically, the determination of their amplitudes requires data analysis. However, using the spectral decomposition of the evolution of the angles, one can obtain a reasonable starting guess to match data to a dynamical model.

3.7 Summary

This chapter of the dissertation explores the various analytic methods for treating dynamical systems. The attitude motion of a rigid body is exclusively studied from an analytic perspective.

Two broad cases for the rigid body motion are considered: the case of a fast-rotating rigid body, and that of a slow-rotating rigid body. The former case ensues the development of a dynamical system targeted at studying the long-term dynamics of a rigid body and is comparable to that of the motion of artificial satellites. The latter case is studied specifically to treat the attitude motion of large celestial bodies that rotate slowly as compared to artificial satellites.

In this work, the Hamiltonian formulation of the attitude motion of a rigid body in a Keplerian orbit has been developed. This formulation has been done in the Serret-Andoyer variables. A Lie-series perturbation approach is used to average out the short-period terms and the averaged Hamiltonian up to fourth-order is obtained. The short-period terms for the fast-rotating rigid body dynamical system are associated with the coordinate corresponding with the angular momentum conjugate momenta, and that for the slow-rotating rigid body dynamical system is associated with the orbital mean anomaly. Physical insights are obtained into the attitude motion of the rigid body such as relative equilibria, and critical inclinations. Certain simplifying assumptions (such as axisymmetric oblate rigid body assumption) enable us to reduce the dynamical system so as to allow its treatment from an analytic viewpoint.

It is noticed that the averaged motions of a rigid body in a circular orbit may behave as if they were in a torque-free motion at the critical inclinations. These effects of critical inclinations, however, vanish at fourth-order. For eccentric orbits, only the second-order terms of the averaged Hamiltonian vanish at the critical inclinations. The extended phase-space mechanics is introduced to preserve the constant nature of the Hamiltonian and treat the external periodic forcing introduced due to the eccentricity. This averaged Hamiltonian is then used to obtain an analytical model of the attitude motion of a fast-rotating rigid body.

A systematic procedure to treat slow-rotating rigid bodies in eccentric orbits has also been presented. The slow-rotating case arises from the coupling between the orbital and attitude variables of the dynamical system. Several interesting insights have been discussed such as the development of the resonant Hamiltonian, the existence of resonant commensurabilities, and relative equilibria for commensurable frequencies of spin-orbit coupling. The effects of the precession of the ascend-

ing node and that of the precession of the pericenter and introduced in the Hamiltonian to facilitate a one-way coupling between the orbital and attitude variables. Thus, under this development, only the orbital variables are allowed to affect the attitude of the rigid body while the orbital motion is assumed to be a known constant. The dynamical system developed is legitimized by investigating the 3:2 spin-orbit coupling of Mercury and the frequency of librations are found to match those in literature. A major contribution of this work is the development of a theory for lunar librations under the framework of the simplified Hamiltonian developed in this dissertation. The three primary modes of lunar librations of the moon: The longitudinal mode (with a frequency of 2.9 years), latitudinal mode (with a frequency of 81 years), and the wobble mode (with a frequency of 75 years) are studied and their frequencies are obtained with very close agreements with experimental data thereby bridging the gap between analytic and experimental results.

4. SEMI-ANALYTIC TREATMENT OF DYNAMICAL SYSTEMS

Mathematical modeling of physical phenomena in all branches of science often results in solving a set of nonlinear differential equations. For most phenomena occurring in nature, these differential equations do not admit a closed-form solution. Evidence of such situations has been explored in the previous chapters, where the dynamical system is treated using qualitative or analytical techniques to simplify them to a more tractable form, so as to extract information about the physical phenomena from them. Primarily, the treatment of dynamical systems in the previous chapters has involved the following approaches: (a) mathematical modeling of the dynamical system using physically interpretive quantities (such as Euler angles for attitude description, and position-velocity for spatial description), (b) simplification of mathematical models using internal symmetry and derived quantities (such as the Serret-Andoyer description for the attitude, *inside -out* topology for description of the PCR3BP, phase and amplitude description for oscillators), (c) qualitative insights from employing a bundle of trajectories in the relevant phase volume (such as tools and techniques from DST or Monte Carlo methods), and (d) analytical insights from examining the structure of the resulting differential equations. These approaches have been used separately and together to provide valuable information in understanding the underlying physics at work. Numerical methods are strictly approximate solutions, and therefore can be used to ascertain the qualitative behavior of the dynamical system. They involve reformulating the problem such that their solutions can be approximated with arithmetic operations whose error can be estimated [148, 149]. Analytical solutions are more symbolic in nature, thereby allowing symbolic manipulation to extract information. The primary difference between a numerical solution and an analytical solution is that an analytical solution can provide complete information about the behavior of all trajectories in the dynamical system, while a numerical solution can only provide information on a particular trajectory because of its dependence on initial conditions. Therefore, equivalence between numerical and analytical solutions is only obtained in the limit as the number of initial conditions simulated using numerical methods approaches infinity.

For practical implementations, most dynamical systems do not admit a closed-form analytical solution, and numerical methods to decipher its complete behavior may prove computationally expensive. In order to overcome the limitation of numerical and analytical techniques, semi-analytic approaches have been developed. In a semi-analytic framework, the knowledge of the system under analysis is exploited to reduce the computational load and complexity that numerical simulations would require. In this way, the strengths of both analytical and numerical methods are effectively combined. Semi-analytic techniques are a powerful tool for the analysis of complex systems [148]. Among such methods are the variational iteration method [150], the homotopy perturbation method [150], the homotopy analysis method [151], the Adomian decomposition method [152], and the differential transformation method [153]. These methods have been extensively used in recent years, and several texts and articles have been devoted to investigating their application to solve differential equations in numerous engineering applications from diverse fields including astrodynamics, solid mechanics, heat transfer, fluid mechanics, and biomedicine [154, 11, 155, 154, 156]. The advantages of many of these semi-analytical approaches over numerical methods are their direct application to both linear and nonlinear equations without requiring linearization, discretization, or perturbation [157]. Additionally, they can be used to prove the existence of solutions. A potential efficient and accurate alternative to semi-analytical and traditional numerical methods for treating dynamical systems is the method of variation of parameters (VPM) (Section 3.1). Lagrange developed this method to solve linear, non-homogeneous ordinary differential equations [158, 27]. However, it can also be implemented to solve nonlinear differential equations in which the nonlinearity is found in the inhomogeneity [159, 160, 149, 161].

This chapter of the dissertation is devoted to developing a semi-analytical approach to treating dynamical systems of all classes. Contrasting to existing techniques, the methodology developed to produce the solution in symbolic or functional form. This methodology combines the power of the VPM, insights from the analytical structure of equations, and different numerical approaches to decipher physical phenomena in a wide variety of engineering problems. The fundamental difference between the methodology developed in this chapter and those discussed in previous chapters

is that previous chapters developed methods that use numerical simulations on a simplified and/or reduced analytical form of the dynamical system to extract information, while the current chapter utilizes numerical simulations to provide an analytical form of the solution of the dynamical system. Another difference is that while previous chapters focused on extracting and examining particular behavior of trajectories (or particular solutions), the current chapter will focus on methods to capture the complete dynamical behavior. This process is accomplished by finding solutions to the Hamilton-Jacobi (HJ) equation. The HJ theory is briefly discussed in the context of obtaining canonical transformations in Sec. 3.1.3. In the following section, the HJ theory is discussed in greater detail.

4.1 Fundamentals of the HJ Theory

The HJ theory is the culmination of classical mechanics, serving as a bridge to other branches of dynamical systems theory by introducing relevant topological structure for the description of motion [162]. The deepest problems of classical mechanics can be investigated by HJ theory and it has led to the formulation of multiple methods of treating dynamical systems, such as the perturbation theory, KAM theorem, action-angle variables, and the theory of adiabatic invariants [163]. The mechanics is reduced to action functions that encode all the possible trajectories of a mechanical system satisfying conservation principle [164, 70, 51]. These action functions are the solutions of a nonlinear, first-order, hyperbolic partial differential equation (PDE), called the HJ equation. The characteristic equations of this differential equation are the extended Hamilton's equations. The power of the HJ equations arises from the fact that the solution of a class of mechanics problems is thus reduced to the solution of a single partial differential equation. The use of the HJ equation is not guaranteed to lead to a solution. It serves as a map from the original (nonlinear) equation into another equation, linear or nonlinear, which is more tractable. This method consists of obtaining a suitable canonical transformation, which leads to equilibrium [28, 62, 27, 70, 165], and is given by its generating function. This function is the so-called HJ equation. Section 3.1.3 provides the derivation of the HJ equation and introduces the different types of generating functions. To recall, the HJ equation is given as follows:

$$\frac{\partial \mathcal{S}}{\partial t} + \mathcal{H}\left(\frac{\partial \mathcal{S}}{\partial q_i}, q_i, t\right) = 0 \tag{4.1}$$

where, q_i are the generalized coordinates and $p_i = \frac{\partial \mathcal{S}}{\partial q_i}$ are the generalized momenta of the dynamical system, $\mathcal{S}$ is the generating function, and $\mathcal{H}$ is the Hamiltonian. To obtain a feel for what the generating function means physically, consider the general form of the HJ equation and that the generating function is separable

$$a^*\left(\frac{\partial \mathcal{S}}{\partial q_i}\right)^2 + b^*\left(\frac{\partial \mathcal{S}}{\partial q_i}\right) + V(q,t) + \frac{\partial \mathcal{S}}{\partial t} = 0 \tag{4.2}$$

where, V is the potential. Taking $b^* = 0$ (which is valid for a large class of dynamical systems), and $a^* = 1$ the HJ equation can be written as:

$$\frac{\partial \mathcal{S}}{\partial t} = -(\nabla \mathcal{S})^2 - V \tag{4.3}$$

Noting that $\mathcal{S}$ is a function of time, and of the coordinates x, y, z, a real solution for $\mathcal{S}$ may exist only over part of the space. This implies that the real solution of $\mathcal{S}$ exists over a region, and not just at a single point. Contrast this with a single moving particle, which only exists at one point. Therefore, $\mathcal{S}$ must be associated with many paths, not just one [166]. Since each of the particles is moving in the same potential, the momentum of the particles is given by a function of the position and time by:

$$\mathbf{p} = \nabla \mathcal{S} \tag{4.4}$$

Equation (4.3) tells us how $\mathcal{S}$ changes with time at a given point in space. The rate of change of $\mathcal{S}$ with time is given by:

$$\frac{d\mathcal{S}}{dt} = \mathcal{L} = T - V = (\nabla \mathcal{S})^2 - V \tag{4.5}$$

By using either Eq. (4.3) or Eq. (4.5) , one can follow the change of $\mathcal{S}$ with time. At each instant, $\nabla \mathcal{S}$ gives the momentum distribution in space. Knowing $\mathcal{S}$ as a function of the position

and time then gives us the possible set of paths that can be taken by a particle. Then, based on the initial condition of the particle itself, the true path of the particle can be obtained. Thus, the generating function is actually Hamilton's principal function. We recognize that Hamilton's principal function $\mathcal{S}$ is the generator of canonical transformations of constant coordinates and momenta, and provides a method of obtaining solutions to classical mechanics problems by way of finding a transformation. These constants are obtained from the initial conditions at time $t = t_0$.

While the HJ equation is generally difficult to solve, and often no closed-form solution can be found, numerical techniques can be employed within a domain of interest to solve the HJ equation to a reasonable tolerance. In the 1980s, Crandall and Lions [167, 168] obtained existence and/or uniqueness results for the HJ equation. These results were extended to HJ equation stemming from optimal control problems [169]. Beard et.al [170] studied the convergence of Galerkin approximation methods applied to the generalized Hamilton-Jacobi-Bellman (GHJB) equations. Sakamoto and van der Schaft [171] obtained an approximate stabilizing solution of the HJE using symplectic geometry and the Hamiltonian perturbation technique for feedback infinite time optimal control problems. Many numerical techniques exist to solve the HJB equation, in particular [172, 173]; to solve the PDE directly, Graijne [174] proposed an adaptive finite-difference method to solve the discrete HJB equation. Apart from finite difference methods, Finite Element Methods [172] can also be used to approximate the solution to the GHJB equation. Recently, sparse approximation techniques were employed to find solutions to the GHJB solutions applied to optimal control problems [175]. In this dissertation, we focus specifically on perturbed Hamiltonian systems, for which the unperturbed Hamiltonian already admits a canonical set of constant coordinates and momenta that then renders the Hamiltonian zero. Utilizing such a formulation allows for the use of VPM approach to solve the HJ equation. This is discussed in the following section.

4.2 Perturbations-based approach to solving the HJ equation

The existence of action-angles which admit solutions of the form $\mathbf{P}(t) =$ constant (constant momenta) and $\mathbf{Q}(t) =$ constant (constant coordinate) are only valid for integrable systems as defined by Liouville-Arnold theorem [28, 176, 177]. Integrable systems are rare, and therefore only

a few dynamical systems have analytical solutions for the HJ equation and admit constant action-angle variables. Examples of such systems include the simple harmonic oscillator (with phase and amplitude being the action-angle variables) and the two-body problem (with the Delaunay variables being the action-angle pair). The methodology proposed in this chapter utilizes the dominant physics, i.e. HJ solutions to the unperturbed Hamiltonian, to simplify the dynamics of nearby Hamiltonians. To see this, let us consider the formulation of the Hamiltonian using the dominant term ($\mathcal{H}_0$) and a perturbation ($\Delta\mathcal{H}$).

$$\mathcal{H} = \mathcal{H}_0 + \Delta\mathcal{H} \tag{4.6}$$

Assuming the integrability of the unperturbed system, the Hamiltonian at first order reduces to exactly the perturbation. This is seen as follows:

$$\text{HJE}: \qquad \mathcal{K}(\mathbf{Q},\mathbf{P},t) = \mathcal{H}_0 + \Delta\mathcal{H} + \frac{\partial S}{\partial t} = \mathcal{H}_0 + \frac{\partial S}{\partial t} + \Delta\mathcal{H} = \Delta\mathcal{H} \tag{4.7}$$

since $\mathcal{H}_0 + \frac{\partial S}{\partial t} = 0$ from the HJ solution of the dominant term. We then seek to find a transformation from the (**Q**,**P**) space to a new space, say (**X**,**Y**) such that in the new state-space variables, the new Hamiltonian, $\tilde{\mathcal{K}}(X,Y)$ is zero through the HJ equation

$$\frac{\partial \tilde{S}}{\partial t} + \mathcal{K} = 0 \tag{4.8}$$

In general, for a generating function of type 2, the solution to Eq. 4.8 can be written as

$$\tilde{S} = \tilde{S}_2(\mathbf{Q}, \boldsymbol{\alpha}, t) \tag{4.9}$$

where $\boldsymbol{\alpha} \in \Re^n$ is a column vector, whose elements are constants of integration. Without loss of generality, we can take $\boldsymbol{\alpha}$ to be the momenta (**P**) of the unperturbed problem, which are constants. Since the following relations

$$\mathbf{P} = \frac{\partial S_2}{\partial \mathbf{Q}} \qquad \mathbf{X} = \frac{\partial S_2}{\partial \mathbf{Y}}$$

hold for all time,

$$\mathbf{Y} = \mathbf{P}(t_0) = \frac{\partial S_2(\mathbf{Q}, \mathbf{P}_0, t)}{\partial \mathbf{Q}}\Big|_{t=t_0} \tag{4.10}$$

which gives us $S_2(\mathbf{Q}, \mathbf{P}_0, t) = \mathbf{P}_0^T\mathbf{Q}$ Also we have,

$$\mathbf{X}(t_0) = \frac{\partial S_2(\mathbf{Q}, \mathbf{P}_0, t)}{\partial \mathbf{P}_0}\Big|_{t=t_0} = \frac{\partial \mathbf{P}_0^T\mathbf{Q}_0}{\partial \mathbf{P}_0} = \mathbf{Q}_0 \tag{4.11}$$

Thus, the new variables in the canonical transformation are simply the coordinates and momenta of the unperturbed Hamiltonian (which are constant, provided the unperturbed Hamiltonian is zero).

Another consequence of the formulation above is the addition of multiple perturbations. Since we are finding complete solutions (and not averaging), the perturbations can be added in any order and also solved separately, with the difference being the addition of new canonical transformations at every step. Each canonical transformation stems from the previously solved HJ equation. Since the new action-angle variables are always initial conditions of the unperturbed problem, they can be solved independently (and in parallel, from a computational standpoint).

$$\mathcal{H}^{(1)} = \mathcal{H}_0^{(1)} + \epsilon_1\mathcal{H}_1^{(1)} + \epsilon_2\mathcal{H}_2^{(1)} + \epsilon_3\mathcal{H}_3^{(1)} + \cdots + \epsilon_k\mathcal{H}_k^{(1)} \tag{4.12}$$

$$\mathcal{H}^{(2)} = \mathcal{H}_0^{(2)} + \epsilon_2\mathcal{H}_2^{(1)} + \epsilon_3\mathcal{H}_3^{(1)} + \cdots + \epsilon_k\mathcal{H}_k^{(1)} \tag{4.13}$$

$$\mathcal{H}^{(3)} = \mathcal{H}_0^{(3)} + \epsilon_3\mathcal{H}_3^{(1)} + \cdots + \epsilon_k\mathcal{H}_k^{(1)} \tag{4.14}$$

$$\vdots \tag{4.15}$$

$$\mathcal{H}^{(k)} = \mathcal{H}_0^{(k)} + \epsilon_k\mathcal{H}_k^{(1)} \tag{4.16}$$

Here, $\mathcal{H}_0^{(2)}$ is the Hamiltonian resulting from solving the HJE: $\frac{\partial \mathcal{S}_1}{\partial t} + \epsilon_1\mathcal{H}_1^{(1)} = 0$ and $\mathcal{H}_0^{(3)}$ is the Hamiltonian resulting from solving the HJE: $\frac{\partial \mathcal{S}_2}{\partial t} + \epsilon_2\mathcal{H}_2^{(1)} = 0$, and so on. Since the new canonical variables are always constants, and the resulting new Hamiltonian is zero (i.e. $\mathcal{H}_0^{(i)} = 0, i = 1, \cdots, k$), the HJE results in a separate PDE independent of any previous or upcoming HJE solutions. The only care to be taken in this formulation is the transformation of coordinates

between each HJ solution.

$$(\mathbf{Q}^{(0)}, \mathbf{P}^{(0)}) \rightarrow (\mathbf{Q}^{(1)}, \mathbf{P}^{(1)}) \rightarrow (\mathbf{Q}^{(2)}, \mathbf{P}^{(2)}) \rightarrow \cdots \rightarrow (\mathbf{Q}^{(k)}, \mathbf{P}^{(k)}) \tag{4.17}$$

Such perturbed dynamical systems do not generally admit analytical solutions for the generating functions ($\mathcal{S}$). Thus, the search for the solution of the dynamical system has been decomposed to two steps:

1. Formulating the problem using VPM coupled with a perturbation-based approach
2. Solving a nonlinear, first-order, hyperbolic partial differential equation with initial conditions P_0 and Q_0, which are known quantities from the dominant physics.

It is important to note that these known quantities, P_0 and Q_0, need not be numerical values and can retain their symbolic or functional form. By doing so, the solution to the HJ PDE is obtained in functional form and is therefore valid for a region of the phase-space, and not just for a single trajectory. Since (1) above involves using analytic techniques and (2) utilizes numerical methods, the methodology is termed semi-analytic. In the next section, we will specifically address the methodology used in solving the HJ equation.

4.3 Numerical approaches for solving the HJ equation

There are multiple methods in literature to solve the HJ equation, both numerically and analytically. Since the primary purpose of solving the HJ equation is to facilitate a canonical transformation, the formulation of the problem can be achieved using methods like von Zeipel [104] and that of Lie Series [178, 113, 74]. Both of these methods are examples of perturbation-based approaches in the literature. Other methods to solve the HJ equation stem from numerical approaches, including using finite difference methods and finite element methods [172, 174, 173], collocation, Galerkin methods [170, 5, 179], and others. Often, PDE collocation methods are solved on regular grids. While this is feasible when the dimensionality d of the problem is low, regular grids suffer from the curse of dimensionality. In this work, we shall use the Galerkin approximation method in

conjunction with sparse collocation techniques. Sparse grids are very useful when such methods prove inadequate. The use of a Galerkin approximation is motivated by the non-autonomous nature of the HJ equation. The overall lack of global solution for the generating function $\mathcal{S}$ in Eq. (4.1) makes it necessary to define a "weak" solution for the HJ equation, that is, a solution $\mathcal{S}$ which may not satisfy the PDE in Eq. (4.1) point-wise at every point. Before diving into the solution procedure, a brief outline on the numerical discretization procedure based on sparse grids is given.

4.3.1 Numerical descretization based on sparse grids

Sparse grids are a numerical discretization technique used to speed up the solution formulation of PDEs. They defeat the curse of dimensionality at the cost of slightly deteriorated errors [180, 181]. The main idea of sparse grids is to evaluate a scalar valued function u, which maps some parameters $\mathbf{x}$ to an output value $u(\mathbf{x})$. u is usually a computationally expensive function, and it is therefore replaced with another function $f : [a, b]^d \to \mathbf{R}$ that approximates u well and is cheaper to evaluate. f is constructed by evaluating u at a small number of points $\mathbf{x}_k$, and these $u(\mathbf{x}_k)$ are used to define f. These points $\mathbf{x}_k$ are the sparse grids points. We begin with the definition of full grids as:

$$\sigma_n := x_{n,i} | i = 0, \cdots, 2^n, \quad x_{n,i} := ih_n, \quad h_n := 2^{-n} \tag{4.18}$$

where n is the level of the grid, $x_{n,i}$ are the grid points of index i and h_n is the grid spacing. For example, the 1D grid $\sigma_1 = 0, 0.5, 1$ with $h_1 = 0.5$. In higher dimensions, the tensor product of grid points through all dimensions is used to construct the grid points. Thus, $\sigma_{\mathbf{n}}$ consists of all combinations of σ_n.

$$\sigma_{\mathbf{n}} := \sigma_{n_1} \otimes \cdots \otimes \sigma_{n_d} \tag{4.19}$$

It is evident that the size of $\sigma_{\mathbf{n}}$ grows exponentially with dimension, and evaluations of u on these grids are expensive and will exhaust the available memory even on large computers. Thus, sparse grids aim to reduce the number of grid points to perform function evaluations on. One such example of sparse grids are those arising from Clenshaw-Curtis quadrature, where the 1D grid points are nested in the sense that σ_{n-1} is contained in σ_n. For each level, only the odd-indexed grid

points are new. It is also noted that the Clenshaw-Curtis quadrature also used Chebyshev node points, which are not equally spaced like the full grids. Extension to higher dimension is achieved by tensor product of 1D grids. Fig. 2.37 illustrates the decomposition of 1D grid of level 3.

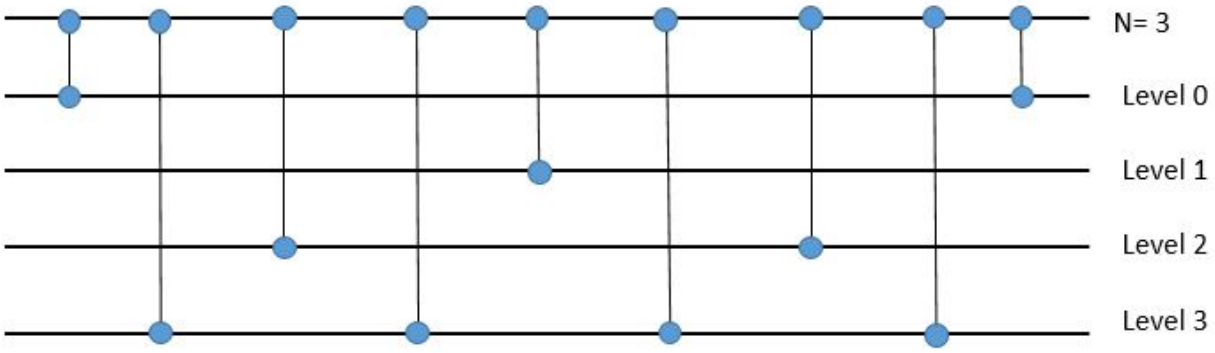

Figure 4.1: Sparse grid decomposition: 1D grid of level $n = 3$ [5]

Specifically, for two-dimensions, the sparse grids are computed and illustrated in the figure below.

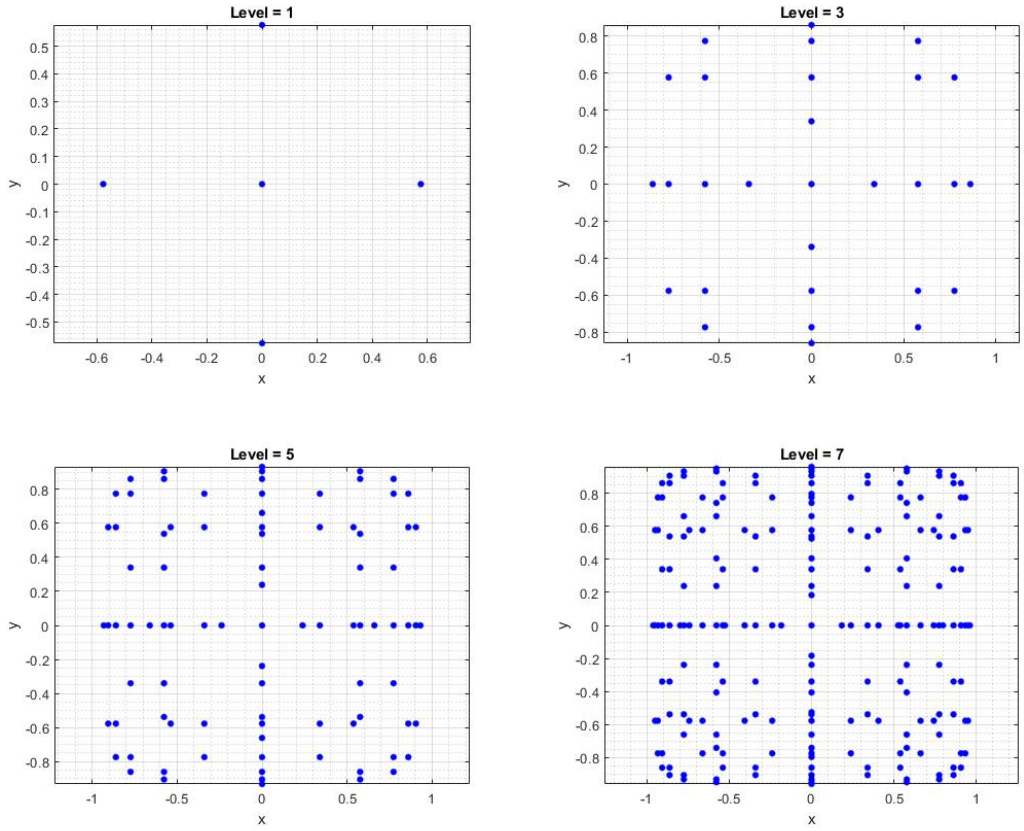

Figure 4.2: Sparse grid points for two-dimensional phase-space for different levels $n = 1, 3, 5, 7$.

The sparse grids are computed based on the Smolyak rule for sparse-grid method [180]. The number of points in a Smolyak grid grows polynomially with dimensionality d, meaning that the Smolyak method is not subject to the curse of dimensionality. This becomes particularly helpful when dealing with large dynamical systems of dimensions $d \geq 4$.

4.3.1.1 The basis function space

With the sparse grid defined above, the generating function ($\mathcal{S}$) is approximated as a linear combination of basis functions evaluated at each grid point. In 1D, these are defined as:

$$\tilde{\mathcal{S}} := \sum_{i=0}^{m} c_i \phi_i(x), \quad c_i \in \mathbf{R} \tag{4.20}$$

where m is the number of basis functions, and $\tilde{\mathcal{S}}$ is the approximate generating function. The simplest choice of basis functions are monomials of a certain degree, i.e $\phi_i = x^i$. Extension to higher dimensions is given by the tensor product of basis functions in each dimension. There are other choices of basis functions, like the Legendre polynomials, Chebyshev polynomials, b-splines, radial basis functions and so on. Since the HJ equation stems from the Hamiltonian definition, there are always $2N$ dimensions, and therefore the minimum dimensionality for any dynamical system is two.

Now, while the tensor product spans the entire space, not all basis functions are required to characterize the dynamical system. Also, the exhaustive use of all tensor products may result in a large number of basis functions that may cause additional computational expenses and even lead to Gibbs phenomenon [182] . To alleviate this burden, we define a basis function space defined by certain rules as a function of the highest degree of basis function used. For an N-dimensional problem, the approximate value function is defined as:

$$f := \sum_{g(\alpha_1,\cdots,\alpha_{2N})\leq L} c_i \beta_{\alpha_1}(x_1)\cdots\beta_{\alpha_{2N}}(x_{2N}) \tag{4.21}$$

where $\beta_{\alpha_z}(x_1)$ denotes the basis function corresponding to the x_1 variable, and L is the degree of basis functions required for truncation. These βs could be monomials: $\beta_2(x_1) = x_1^2$, or Legendre Polynomials: $\beta_3(x_1) = P_3(x_1)$, or Chebychev polynomials of the first kind: $\beta_1(x_1) = T_1(x_1)$, or any other basis function. The rules for truncating the approximation are listed as follows:

1. Total Degree: $g(\alpha_1, \cdots, \alpha_{2N}) = \alpha_1 + \cdots + \alpha_{2N}$
2. Maximum Degree: $g(\alpha_1, \cdots, \alpha_{2N}) = \max(\alpha_1, \cdots, \alpha_{2N})$
3. Hyperbolic Cross: $g(\alpha_1, \cdots, \alpha_{2N}) = \alpha_1 \times \cdots \times \alpha_{2N}$
4. Hybrid: Specifically selected choice of basis from the basis function space.

The basis function space for a 2D scenario can be visualized as in Fig. 4.3. We can immediately perceive the utility of using different rules for characterizing the basis functions along each

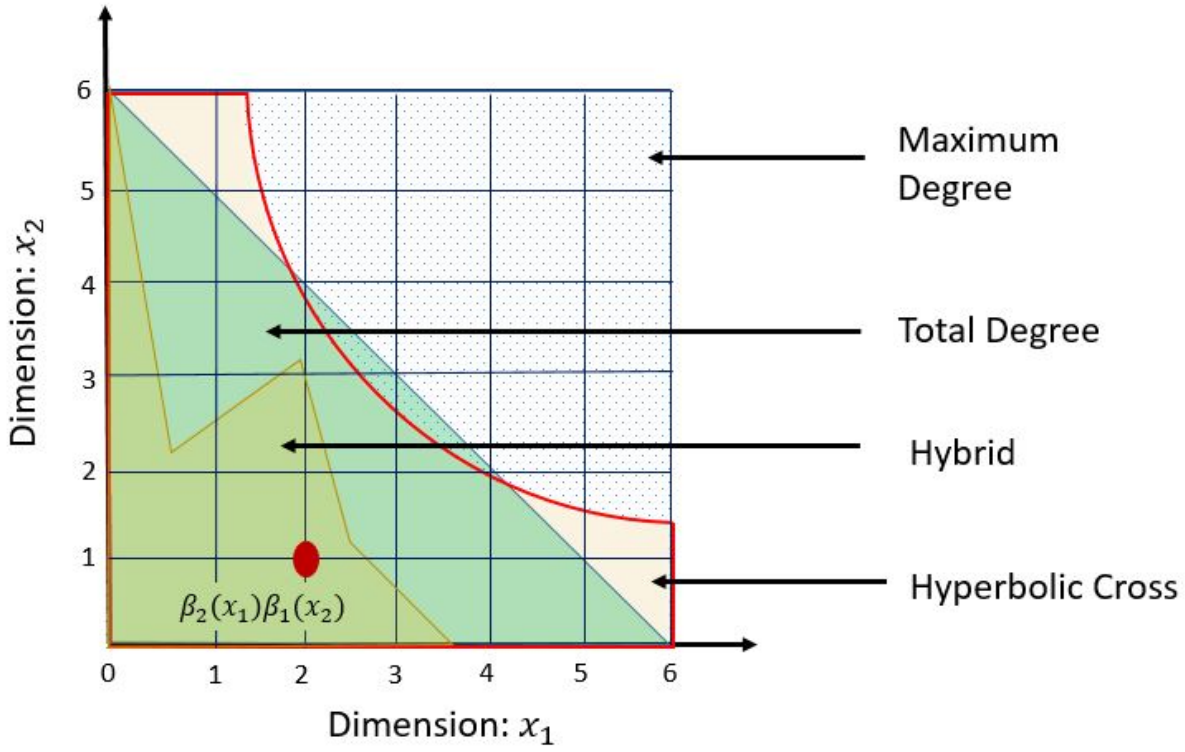

Figure 4.3: Basis Function Space for 2D representation. The figure shows a geometric representation of the rules defining the generating function approximation.

dimension. The maximum degree chooses the entire basis function space, while the total degree rule utilizes less. The hyperbolic cross rule results in basis functions that combine high-low degree ($\beta_6(x_1)\beta_1(x_2)$ and $\beta_6(x_2)\beta_1(x_1)$) along each dimension instead of lower degree combinations. The use of these rules becomes significant when one dimension becomes more important than the other. A simple example would be

$$u(\mathbf{x}) = \sin(0.2x_1)\cos(200x_2)$$

where the second dimension is more important than the first, since it is highly oscillating. Therefore, to resolve the fast oscillating terms, one may need more basis functions along the second dimension than the first. The Hybrid rule in Fig. 4.3 comes in handy here. In the case of the HJ equation, we know that the generating function subspace is composed of some old variables and some new variables. Noting that the new variables are constants for a particular problem, one

might consider assigning more basis functions to old variable dimensions, since they vary under the effect of the perturbing Hamiltonian.

In the following section, a systematic procedure is formulated to solve the HJE for a dynamical system, using tools developed in the previous sections. For the purposes of demonstration, we limit ourselves to considering a two-dimensional Hamiltonian system. It is however noted that the method can also be extended to non-Hamiltonian systems in a way similar to that shown by Kamel [115].

4.3.2 Formulation and solution procedure for *rectifying* dynamical systems

The objective of this research is to present a systematic procedure to determine the motion of a complex dynamical system by viewing it from the perspective of a canonical set of coordinates obtained by solving the HJ equation. Consider a dynamical system whose motion is governed by a Hamiltonian $\mathcal{H}(q_i, p_i, t)$, $i = 1, \cdots, d$. The solution of the HJ equation (Eq. (4.1)) is a generating function that facilitates a canonical transformation to a set of coordinates and momenta that display the most simplest dynamical structure (constant or linear time evolution). This process of transforming the state-space variables so as to ensure constant or linear time evolution is termed as *Rectification.* This is done by specifying a generating function of type-2: $\tilde{\mathcal{S}}(\mathbf{Q}, \mathbf{Y}, t)$, such that the other variables hold the relation:

$$X_i = \frac{\partial \tilde{\mathcal{S}}}{\partial Y_i} \tag{4.22}$$

$$P_i = \frac{\partial \tilde{\mathcal{S}}}{\partial Q_i} \tag{4.23}$$

Recall that the resulting dynamics would remain the same under this change of variables if the HJ equation is

$$\tilde{\mathcal{K}}(\mathbf{X}, \mathbf{Y}, t) = 0 = \mathcal{K}(\mathbf{Q}, \mathbf{P}, t) + \frac{\partial \tilde{\mathcal{S}}}{\partial t} \tag{4.24}$$

The problem then reduces to finding the generating function $\tilde{\mathcal{S}}$ that satisfies the HJE in Eq. 4.24. Now, while the HJE may not admit closed-form solutions for the generating function, within

a domain of interest, a sparse collocation based approach along with a Galerkin-like approximation can be employed to obtain an approximate analytic form of the generating function. Next, the solution procedure for a two-dimensional dynamical system is outlined. Extension to higher-order dimensional system is straight-forward.

4.3.3 Solution procedure for a 2D dynamical system

Consider a two-dimensional dynamical system with coordinate Q and conjugate momenta P. The aim is to solve the HJ equation given by:

$$\mathcal{H}(Q,P) + \frac{\partial \mathcal{S}}{\partial t} = 0$$

Let us assume that the generating function is of type 2, i.e. $\mathcal{S} = \mathcal{S}_2(Q, Y, t)$, where Y is the conjugate momenta of the coordinate X of the canonically transformed variables (Q, P). Following the definition of the approximate generating function, the solution to the HJ equation is assumed to be of the form:

$$\tilde{\mathcal{S}}(Q,Y,t) = \sum_{i=1}^{m} c_i(t)\phi_i(Q,Y) \tag{4.25}$$

The basis functions $\Phi_k(Q,Y) = [\phi_1, \cdots, \phi_m]$, $k = 1, \cdots, N$ are assumed to have at least continuous first-order derivatives. Note here that since the Kamiltonian, $\tilde{\mathcal{K}}$ is non-autonomous, the approximate value function is written in a way that the basis functions are in the spatial variables, and its coefficients are temporal. It is noted here that alternatively, the basis functions could also be expressed in the temporal variable, leaving c_i to be constants for all time. However, assuming separability in the temporal and spatial variables enables us to use a Galerkin-like method to convert the HJ PDE to a set of ODE in the coefficients of the basis function. Because of this separability, we have

$$\frac{\partial \tilde{\mathcal{S}}}{\partial t} = \sum_{i=1}^{m} \frac{c_i(t)}{dt}\phi_i(Q,Y) \tag{4.26}$$

On evaluating Eq. (4.26) at the sparse grid points, the HJ PDE is converted to a set of coupled ODE as follows:

$$\Phi\dot{\mathbf{c}} = \begin{bmatrix} \phi_1^{(1)} & \dots & \phi_m^{(1)} \\ \vdots & \ddots & \vdots \\ \phi_1^{(N)} & \dots & \phi_m^{(N)} \end{bmatrix} \begin{bmatrix} \dot{c}_1 \\ \vdots \\ \dot{c}_m \end{bmatrix} = \begin{bmatrix} b_1 \\ \vdots \\ b_N \end{bmatrix} = \mathbf{b} \tag{4.27}$$

where $\mathbf{b} = [b_1, ..., b_N]^T$ are expressions for $-\mathcal{K}$ from Eq. 4.24 evaluated at the N sparse grid points. The L_2-norm error is reduced in Eq. 4.27 to obtain m-coupled ODEs $\dot{\mathbf{c}} = (\Phi^T\Phi)^{-1}\Phi^T\mathbf{b}$

The Galerkin-like approximation is effective because it reduces the addition of the temporal dimension in the sparse grid collocation. Also, the coefficients of the basis functions capture all information about the evolution of the variables, i.e. periodic and secular behavior. This eliminates the need for using a large number of basis functions in the generating function phase-space. Recall that at the initial time, both the old and new variables are exactly the same. This implies that the contact transformation at initial time between old and new variables is completely separable and they take the form:

$$\tilde{\mathcal{S}}(\mathbf{Q}, \mathbf{Y}, t_0) = \mathbf{Q}^T\mathbf{Y} \tag{4.28}$$

for arbitrary dimensional problem giving the initial conditions for the ODEs. This reduces to $\tilde{\mathcal{S}} = QY$ for the two-dimensional case. Note that these conditions do not depend on the boundary conditions of a specific problem. Therefore, the ODE in Eq. (4.27) must be propagated only once to obtain the time-varying coefficients of the basis functions, and a functional form of the generating function can be achieved.

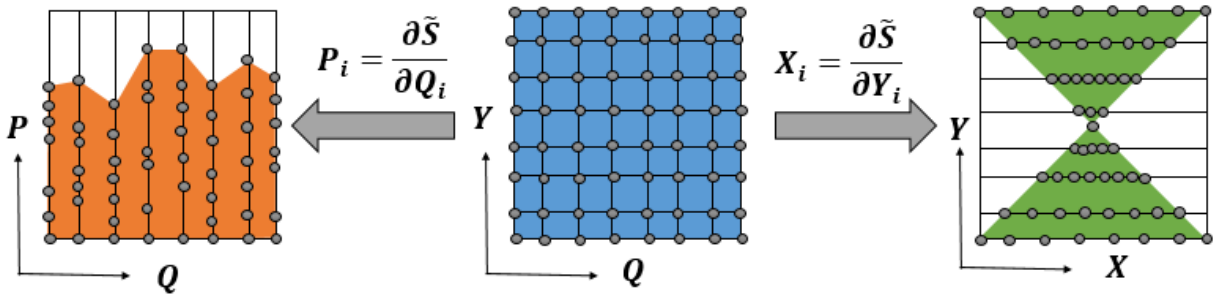

Figure 4.4: Mapping to the old (Q,P) and new (X,Y) space from the generating function space (Q,Y)

One can then obtain an analytical expression for a time-varying generating function from a numerically propagated ODE for the coefficients. Thus, a semi-analytic representation of the time-varying generating function is obtained. Once such a functional is obtained, transformation to the old coordinates is straightforward from HJ theory [164, 62, 183, 108] and is illustrated in Fig. 4.9. The only condition on $\tilde{\mathcal{S}}$ to ensure an inverse transformation exists is that

$$\frac{\partial^2 \tilde{\mathcal{S}}}{\partial Q \partial Y} \neq 0 \tag{4.29}$$

Note that this condition is motivated from geometry [184]. At an initial epoch, the canonical transformation is identity, and the variables are exactly separable [185, 183, 186]. However, as these variables evolve with time, Eq. (4.29) prevents the inverse transformation from becoming degenerate, and the mapping between the old and new coordinates is bijective. In the following section, we demonstrate the methodology through the example of the Duffing oscillator.

4.4 Semi analytical solution to the Duffing oscillator

It is seen from the HJ theory that a transformation can be carried out on the Hamiltonian, which leaves Hamilton's equations of motion in canonical form. The equations of motion after the transform become

$$\dot{Q}_i = \frac{\partial K}{\partial P_i}, \qquad \dot{P}_i = -\frac{\partial K}{\partial Q_i}, \qquad K = H + \frac{\partial \mathcal{S}}{\partial t} \tag{4.30}$$

where Q_i and P_i are the new variables, K is the new Hamiltonian, and $\mathcal{S}$ is the generating function, which is a function of the old and new variables [27]. If the approach is to transform the canonical coordinates at time t to that at t_0, the transformation equations are the desired solution to the problem.

$$q = q(q_0, p_0, t) \quad and \quad p = p(q_0, p_0, t)$$

Such a procedure applies to both autonomous and non-autonomous systems and corresponds to the method of Hamilton-Jacobi. Selecting the constant at a fixed time renders the canonical equations of motion as $\dot{Q} = 0, \dot{P} = 0$ and the new Hamiltonian, K, a constant which can be set to zero without loss of generality. The Duffing oscillator is a two-dimensional dynamical system obtained by adding a perturbative nonlinear spring to the simple harmonic oscillator. The Hamiltonian is given as:

$$\mathcal{H} = \frac{1}{2}p^2 + \frac{1}{2}kq^2 + \frac{1}{4}\epsilon q^4 \tag{4.31}$$

where p is the momenta conjugate to q and is physically equal to the velocity of the particle ($\dot{q}$). We can write the Hamiltonian of the the Duffing oscillator as [187]

$$\mathcal{H} = \mathcal{H}_0 + \epsilon\mathcal{H}_1 = \left(\frac{1}{2}p^2 + \frac{1}{2}kq^2\right) + \epsilon\left(\frac{1}{4}q^4\right) \tag{4.32}$$

where $\mathcal{H}_0$ is identified as the Hamiltonian of the simple harmonic oscillator. As per the methodology discussed in the previous sections, let us first treat the dynamical system corresponding to the dominant term, i.e. the simple harmonic oscillator. Using a generating function of type-2, the HJ equation for the simple harmonic oscillator is given as:

$$\frac{1}{2}\left(\frac{\partial\mathcal{S}}{\partial q}\right)^2 + \frac{1}{2}kq^2 + \frac{\partial\mathcal{S}}{\partial t} = 0 \tag{4.33}$$

where $\mathcal{S} = \mathcal{S}(q, \alpha, t$ and α is the new constant momenta. At this stage, we can assume separability in the spatial and temporal variables in the generating function and can write them as

$$\mathcal{S}(q, \alpha, t) = W(\alpha, q) + V(\alpha, t) \tag{4.34}$$

Knowing that the Hamiltonian is conservative gives a simple form for V as

$$V = -\alpha t$$

Therefore, the HJ equation can now be written as

$$\frac{1}{2}\left(\frac{dW}{dq}\right)^2 + \frac{1}{2}kq^2 = \alpha t \tag{4.35}$$

which is simplified as

$$\frac{dW}{dq} = \sqrt{2\alpha - kq^2} = \sqrt{2\alpha}\left(\sqrt{1 - \frac{kq^2}{2\alpha}}\right) \tag{4.36}$$

Thus, the generating function can be obtained as

$$W = \sqrt{2\alpha}\int\left(\sqrt{1 - \frac{kq^2}{2\alpha}}\right)dq \tag{4.37}$$

Now, from the relations of the generating function of type-2 we know that

$$\beta = \frac{\partial \mathcal{S}}{\partial \alpha} = \frac{dW}{d\alpha} - t \Rightarrow \frac{dW}{d\alpha} = \beta + t \tag{4.38}$$

Therefore, taking the derivative before the integral, we obtain

$$\beta + t = \frac{1}{\sqrt{2\alpha}}\int \frac{1}{\sqrt{1 - \frac{kq^2}{2\alpha}}}dq \tag{4.39}$$

We can therefore obtain the coordinate q as:

$$q = \sqrt{\frac{2\alpha}{k}} \sin\left(\sqrt{k}(\beta + t)\right) \tag{4.40}$$

The momenta is then obtained as:

$$p = \frac{\partial \mathcal{S}}{\partial q} = \sqrt{2\alpha} \cos\left(\sqrt{k}(\beta + t)\right) \tag{4.41}$$

Thus, we have solved the HJ equation for the simple harmonic oscillator completely to obtain the new variables, α and β, which are functions of the phase and amplitude of the simple harmonic oscillator. Let us denote these new variables as $(\alpha, \beta) = (P, Q)$ to keep up with the notations. Thus, for the simple Harmonic oscillator, P and Q are constants for all time. Now, since we have found the solution of the dynamical system, i.e. we have solved the HJ equations completely, let us look at tEq. (4.30) for the Duffing oscillator

$$\frac{1}{2}\left(\frac{\partial \mathcal{S}}{\partial q}\right)^2 + \frac{1}{2}kq^2 + \frac{1}{4}\epsilon q^4 + \frac{\partial \mathcal{S}}{\partial t} = \mathcal{K} \tag{4.42}$$

If $\mathcal{S}$ is taken as the generating function that treats the simple harmonic oscillator, then

$$\mathcal{K} = \frac{1}{4}\epsilon q^4 = \frac{1}{k^2}\epsilon P^2 \sin^4\left(\sqrt{k}(\beta + t)\right) \tag{4.43}$$

since $\frac{1}{2}\left(\frac{\partial \mathcal{S}}{\partial q}\right)^2 + \frac{1}{2}kq^2 + \frac{\partial \mathcal{S}}{\partial t} = 0$ from the HJ solution of the simple harmonic oscillator. Then, the evolution of the phase and amplitude variables P and Q for the Duffing oscillator are given by Hamilton's equations of motion as:

$$\dot{Q} = \frac{\partial \mathcal{K}}{\partial P} = \frac{2\,P\,\epsilon \sin\left(\sqrt{k}\ (Q + t)\right)^4}{k^2} \tag{4.44}$$

$$\dot{P} = -\frac{\partial \mathcal{K}}{\partial Q} = -\frac{4\,P^2\,\epsilon\,\cos\left(\sqrt{k}\ (Q + t)\right)\ \sin\left(\sqrt{k}\ (Q + t)\right)^3}{k^{3/2}} \tag{4.45}$$

where $P = \frac{1}{2}p_0^2 + \frac{1}{2}q_0^2$ and $Q = \frac{1}{\sqrt{k}}\tan^{-1}\left(\sqrt{k}\frac{q_0}{p_0}\right) - t_0$, q_0, p_0, t_0 are the initial position, velocity and time for the simple harmonic oscillator. Now, in order to treat the Duffing oscillator dynamical system, we hope to find a canonical transformation from the old space (Q, P) to a new space (say (X, Y)), such that in these new canonical coordinates, the resultant Hamiltonian is zero. We do so by numerically solving the HJ equation. We again choose the generating function of type-2, i.e. old coordinate and new momenta: $\mathcal{S} = \mathcal{S}(Q, Y, t)$. For the sake of demonstration, we approximate the generating function using monomials as the basis functions. The total degree of the approximate generating function is taken as two. This corresponds to the minimal set of basis functions that is required to avoid degeneracy and ensure a one-to-one transformation from the generating function space to the old and new space following Eq. (4.29) . Using the total degree rule, there are six basis functions, and the generating function is given by:

$$\tilde{\mathcal{S}} = c_1 + c_2 Q + c_3 Y + c_4 Q^2 + c_5 QY + c_6 Y^2 \tag{4.46}$$

From the relations of type-2 generating function, we know that

$$\begin{aligned} P &= \frac{\partial \tilde{\mathcal{S}}}{\partial Q} = c_2 + 2c_4 Q + c_5 Y \Rightarrow Y = \frac{1}{c_5}(P - c_2 - 2c_4 Q) = f(P, Q) \\ X &= \frac{\partial \tilde{\mathcal{S}}}{\partial Y} = c_3 + c_5 Q + 2c_6 Y = c_3 + c_5 Q + 2\frac{c_6}{c_5}(P - c_2 - 2c_4 Q) = f(P, Q) \end{aligned} \tag{4.47}$$

We can check for canonicity using the Poisson brackets as:

$$\{X, Y\} = \frac{\partial X}{\partial Q}\frac{\partial Y}{\partial P} - \frac{\partial X}{\partial P}\frac{\partial Y}{\partial Q} = 1 \tag{4.48}$$

with

$$\frac{\partial X}{\partial Q} = c_5 - \frac{4c_4c_6}{c_5} \qquad \frac{\partial X}{\partial P} = \frac{2c_6}{c_5} \tag{4.49}$$

$$\frac{\partial Y}{\partial Q} = -\frac{-2c_4}{c_5} \qquad \frac{\partial Y}{\partial P} = \frac{1}{c_5} \tag{4.50}$$

$$\tag{4.51}$$

Therefore, following the procedure in the previous section, we can find the ODE for evaluating the coefficients as:

$$\Phi\dot{\mathbf{c}} = \begin{bmatrix} \phi_1^{(1)} & \dots & \phi_m^{(1)} \\ \vdots & \ddots & \vdots \\ \phi_1^{(N)} & \dots & \phi_m^{(N)} \end{bmatrix} \begin{bmatrix} \dot{c}_1 \\ \vdots \\ \dot{c}_m \end{bmatrix} = \begin{bmatrix} b_1 \\ \vdots \\ b_N \end{bmatrix} = \mathbf{b} \tag{4.52}$$

with the initial condition on the ODE being $c_5 = 1$. Here, Φ are the basis functions evaluated on the sparse grid and b_i is given by

$$\mathbf{b} = -\frac{1}{k^2}\epsilon \left(\frac{\partial \tilde{\mathcal{S}}}{\partial Q}\right)^2 \sin^4\left(\sqrt{k}(\beta + t)\right) \tag{4.53}$$

evaluated at the sparse grid points. Note here the dependence of **b** on time, which is still a symbolic variable. Thus, the ODE for the coefficients is non-autonomous. The coefficients are obtained by solving the ODEs. They are shown below for the following values: $k = 1, \epsilon = 0.1$.

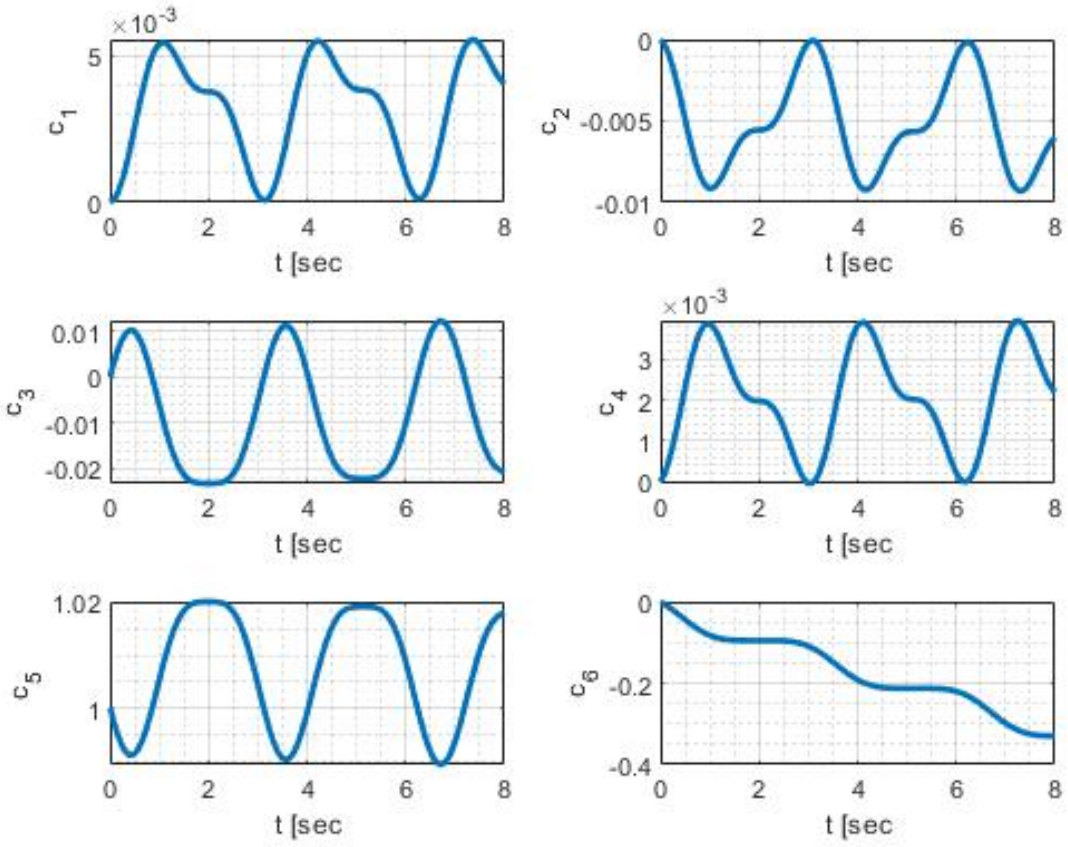

Figure 4.5: Coefficients for the Generating function approximation for the Duffing equation.

Note that the only coefficient with a secular drift is in c_6. Therefore, from Eq. (4.47) and with constant X and Y, the only variable with a secular drift is Q. This is not surprising since we know that the phase exhibits a secular drift for the Duffing Oscillator. The periodic behavior of the other coefficients suggests that the amplitude of the Duffing oscillator is periodic. After obtaining the generating function in functional form, the phase and amplitude can be extracted through regular algebra as:

1. Q is obtained by setting

$$X - \frac{\partial \tilde{\mathcal{S}}}{\partial Y} = 0 \tag{4.54}$$

and solving for Q, and $X = Q_0$, $Y = P_0$

2. P is then obtained using the converged value of Q using

$$P = \frac{\partial \tilde{\mathcal{S}}}{\partial Q} \tag{4.55}$$

with $X = Q_0, Y = P_0$

Note that because of the quadratic nature of the approximating function, the equations for Q and P are linear polynomials. For a general approximate generating function, the equations for Q and P will be of degree $N - 1$ where N is the degree of the approximate generating function. The solutions for Q and P are found to be as follows.

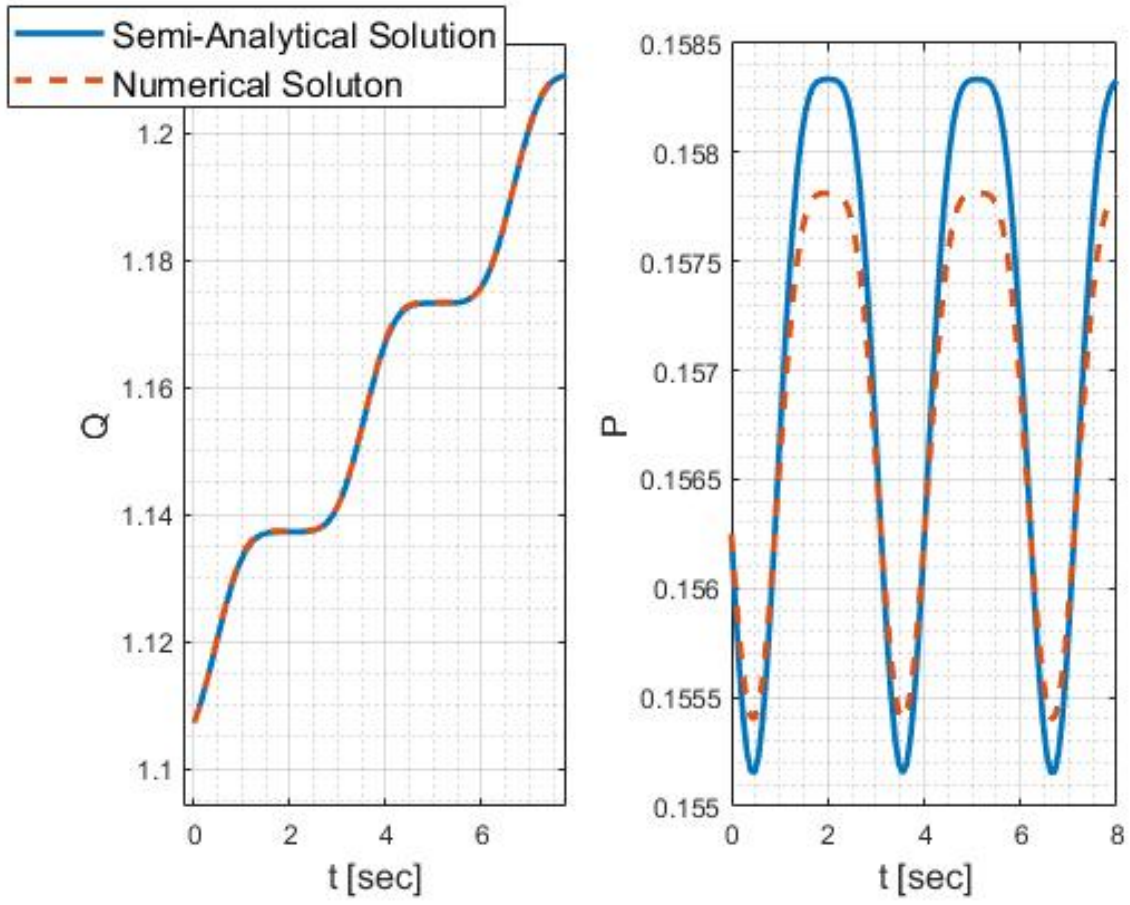

Figure 4.6: Comparison between numerical and semi-analytical solution for the Duffing equation. $\epsilon = 0.1$

The methodology is therefore very useful in both approximating the solution of a dynamical system and obtaining qualitative information on the evolution of the variables from the evolution of the coefficients. One can also consider using the Lie series perturbation method developed in the previous chapter. It is observed that the Lie series formulation results in the same HJ equation for the generating function, albeit in new variables.

4.4.1 Relation to Lie series solution

It is important to note here that using the method of Lie series, one arrives at the exact same step as the HJ equation for the perturbation. To see this, note that

$$\mathcal{H}_0 = 0 \tag{4.56}$$

$$\mathcal{H}_1 = \epsilon \frac{1}{k^2} P^2 \sin^4(\sqrt{k}(Q+t)) \tag{4.57}$$

We are interested in finding the generating function that solves the HJ equation i.e. we require $\mathcal{H}_0^{(1)} = \mathcal{H}^{(1)} = 0$. Therefore at first order, the generating function is given using the Lie triangle relations as [74]:

$$\mathcal{H}^{(1)} = 0 = \mathcal{H}_1 + \mathcal{L}_1 \mathcal{H}_0 = \mathcal{H}_1 + \left(\frac{\partial \mathcal{H}_0}{\partial Q} \frac{\partial W_1}{\partial P} - \frac{\partial \mathcal{H}_0}{\partial P} \frac{\partial W_1}{\partial Q} \right) + \frac{\partial W_1}{\partial t} \tag{4.58}$$

Thus, we are left with the HJ equation (relating W_1 to $\mathcal{S}$):

$$\frac{\partial W_1}{\partial t} + \mathcal{H}_1 = 0 \tag{4.59}$$

However, noting that $\mathcal{H}_1$ is in terms of new variables (X, Y), which are constants, the generating function at first order can be obtained exactly as:

$$W_1 = -\int \epsilon \frac{1}{k^2} Y^2 \sin^4(\sqrt{k}(X+t)) \tag{4.60}$$

$$= -\epsilon \frac{Y^2}{32k^{5/2}} \left(\sin(4\sqrt{k}(X+t)) - 8\sin(2\sqrt{k}(X+t)) + 12\sqrt{k}t \right) + \tilde{W}_1 \tag{4.61}$$

where $\tilde{W}_1$ is a constant of integration which is determined from the initial conditions. Notice the first order secular term coefficient is $3/8$ which is the same as we obtained in the averaging of the Duffing oscillator in Eq. (3.79) . The transformation of coordinates to the old variables are directly given as:

$$Q(t) = Q_0 - \frac{\partial W_1}{\partial Y} \tag{4.62}$$

$$P(t) = P_0 + \frac{\partial W_1}{\partial X} \tag{4.63}$$

and the errors are of the order of $\mathcal{O}(\epsilon^2)$. The difference between using Lie series and our current approach is that the solution obtained using the Lie series perturbation method is a series solution in powers of ϵ and our methodology attempts to find the generating function that solves the HJ equation directly. The errors in our approach are primarily due to the domain of discretization and the basis function (or lack thereof) used in the generating function. Some of the sources of the error in the numerical solution of the HJ equations is discussed below.

4.4.2 Sources of error in the numerical solution of the HJ equation

The error in the semi-analytical solution is of the order of $1e-4$. Some of the sources of the errors are the size of the domain of discretization and the basis functions used. The errors can be computed exactly because the HJ equation has to be exactly satisfied. Thus, the error in the semi-analytical solution is of the same order as that in the generating function. Because the coefficients are a function of time, the errors are also functions of time. The section below discusses the different sources of error in the HJ solution.

4.4.2.1 Error sources: Discretization domain

The major source of error is observed to be the domain size. For reference, the figure below illustrates the error in the generating function space (Q, Y) at different time intervals for different domain sizes. The size of the domain can be extracted from the abscissa and ordinate of the plots.

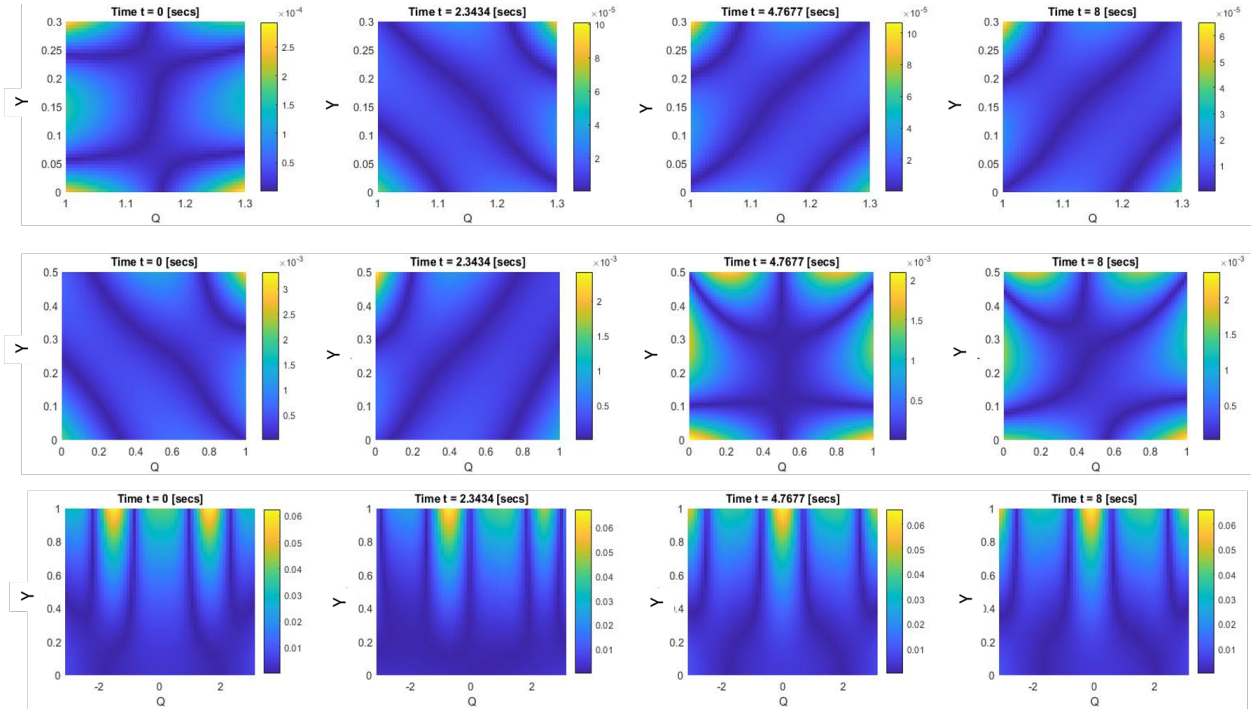

Figure 4.7: Error in the HJ equation solution for different domain sizes expressed in the generating function space for the Duffing oscillator. Since the coefficients are time-varying, the error is shown at different time instances.

Recall that the new variables X and Y capture the variation in the old variables Q and P, respectively. Therefore, depending on the value of ϵ, the domain size need not be large. Further, note that since Y is a constant, the domain of Y corresponds to different initial conditions of the dominant term in the Hamiltonian, i.e. the simple harmonic oscillator. Note how the trajectories of the Duffing oscillator move in the generating function phase-space.

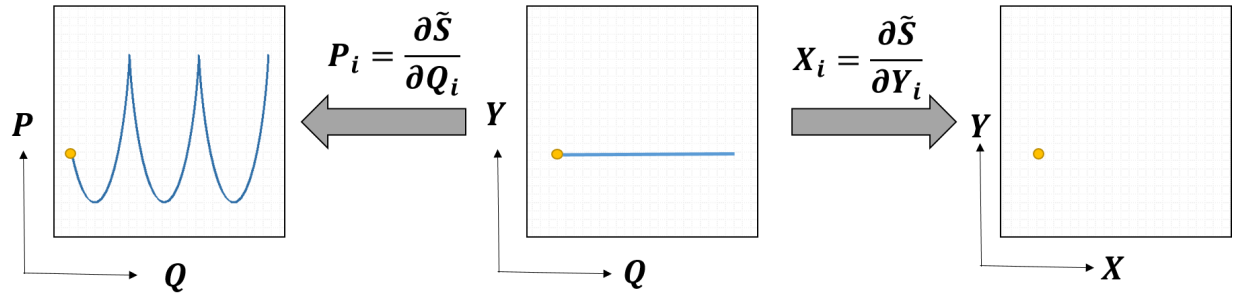

Figure 4.8: Mapping of trajectory to the old (Q,P) and new (X,Y) space from the generating function space (Q,Y). IN the old space, the phase (Q) and amplitude (P) have secular and periodic variations. In the new space, the motion is rectified and the new variables (X,Y) are constants for all time.

Thus, shrinking the domain of discretization down to the exact region of the generating function phase-space results in a better approximation of the trajectory. The errors in the state-space variables are observed to decrease only by an order of magnitude of one. This domain-shrinking is however not the goal of the methodology, since we are interested in finding the solution of all trajectories in the phase-volume. Next, the effect of adding additional basis functions is discussed.

4.4.2.2 Error sources: Total degree of approximating polynomial

The total degree of the approximating polynomial has a significant effect on the error in the HJ solution. It is observed that the magnitude of the error is proportional to the degree of the polynomial used. One can obtain up to machine precision if the degree of the approximate generating function is high enough. This would also constitute a higher computational time in finding the coefficients, such as stiff ODE equations for the coefficients. The figure below illustrates how the total degree of the approximate generating function affects the error in the approximation of the HJ solution.

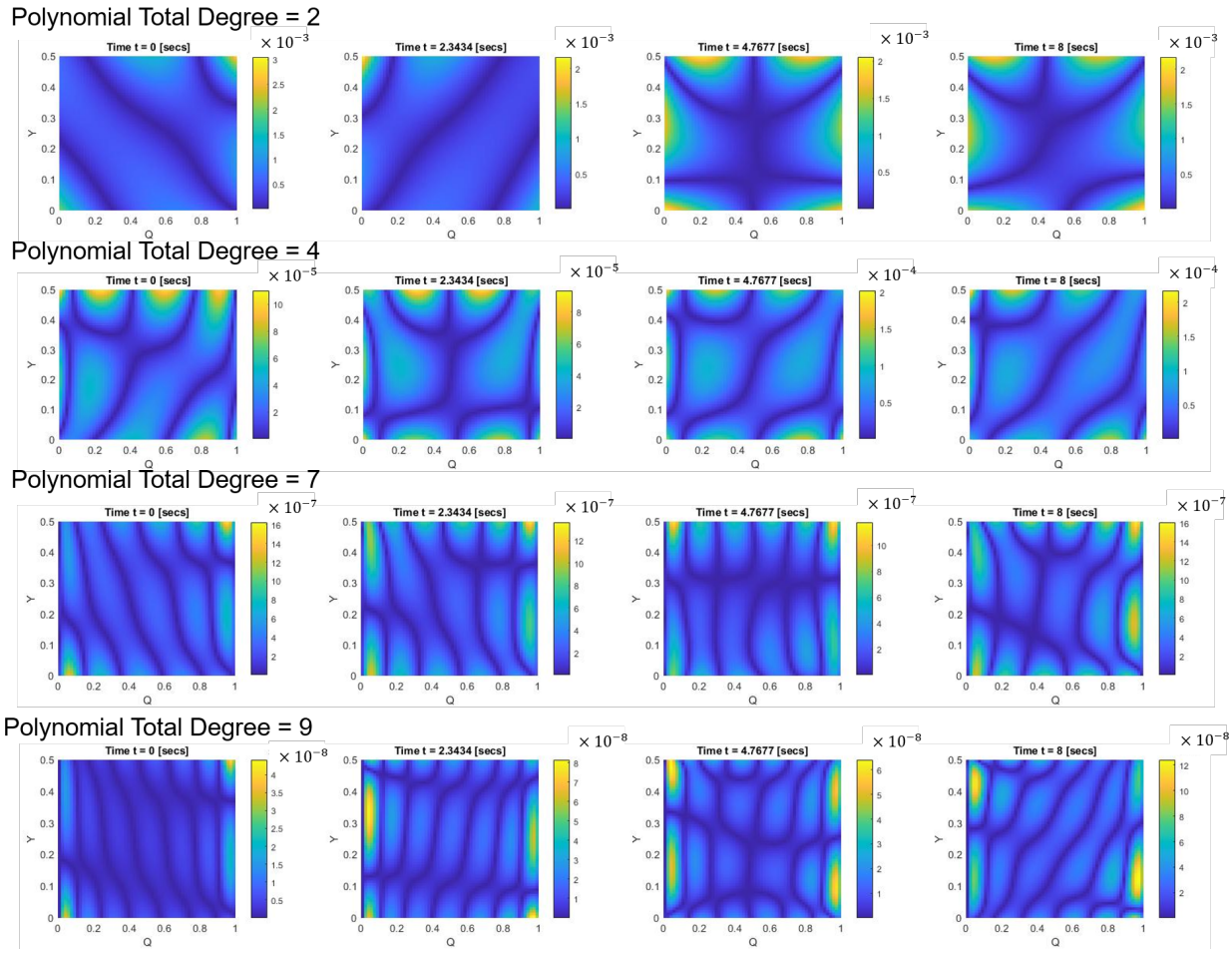

Figure 4.9: Error in the HJ equation solution for different degree approximations of the generating function of the Duffing oscillator.

This method proves very useful in investigating the effect of variation of coordinates in a perturbed dynamical system, particularly from a numerical standpoint. Another advantage of having a semi-analytical solution is that once the error grows significantly, the problem can be reinitialized to continue the process. Insight from the qualitative analysis of the dynamical system can be utilized to design the domain of discretization. Furthermore, the semi-analytic formulation leads to the development of the semi-analytic State Transition Matrix. This is discussed next.

4.4.3 Semi-analytical state transition matrix

The perturbations approach results in a transformation of coordinates from the unperturbed action-angle set $(\mathbf{Q}, \mathbf{P})$ to constant action-angle variables $(\mathbf{X}, \mathbf{Y})$ of the perturbed problem. These variables are the initial conditions of a specific problem under consideration. Once we determine the functional form of the generating function following the procedure in the previous section, we can obtain the inverse relations as:

$$\mathbf{Q} = \mathbf{Q}(\mathbf{X}, \mathbf{Y}, t) = \mathbf{Q}(\mathbf{Q}_0, \mathbf{P}_0, t) \tag{4.64}$$

$$\mathbf{P} = \mathbf{P}(\mathbf{X}, \mathbf{Y}, t) = \mathbf{P}(\mathbf{Q}_0, \mathbf{P}_0, t) \tag{4.65}$$

Also, from the HJ solution of the unperturbed problem, we can write the position and velocity variables and their inverse relations as:

$$\mathbf{q}_0 = \mathbf{q}_0(\mathbf{Q}_0, \mathbf{P}_0, t_0) \qquad \text{and} \qquad \mathbf{Q}_0 = \mathbf{Q}_0(\mathbf{q}_0, \mathbf{p}_0, t_0) \tag{4.66}$$

$$\mathbf{p}_0 = \mathbf{p}_0(\mathbf{Q}_0, \mathbf{P}_0, t_0) \qquad \text{and} \qquad \mathbf{P}_0 = \mathbf{P}_0(\mathbf{q}_0, \mathbf{p}_0, t_0) \tag{4.67}$$

Using Eqs. 4.64 and 4.65, we get:

$$\mathbf{q} = \mathbf{q}(\mathbf{Q}, \mathbf{P}, t) = \mathbf{q}(\mathbf{Q}_0, \mathbf{P}_0, t) = \mathbf{q}(\mathbf{q}_0, \mathbf{p}_0, t) \tag{4.68}$$

$$\mathbf{p} = \mathbf{p}(\mathbf{Q}, \mathbf{P}, t) = \mathbf{p}(\mathbf{Q}_0, \mathbf{P}_0, t) = \mathbf{p}(\mathbf{q}_0, \mathbf{p}_0, t) \tag{4.69}$$

Therefore, given the forward and inverse canonical transformations, we can formulate a semi-analytical form of the state transition matrix as:

$$\Phi(t, t_o) = \begin{bmatrix} \frac{\partial \mathbf{q}}{\partial \mathbf{q}_0} & \frac{\partial \mathbf{q}}{\partial \mathbf{p}_0} \\ \frac{\partial \mathbf{p}}{\partial \mathbf{q}_0} & \frac{\partial \mathbf{p}}{\partial \mathbf{p}_0} \end{bmatrix} \tag{4.70}$$

Such form of the State Transition matrix has immense utility for many applications involving

sensitivity studies, stable, unstable, and center manifold detection, etc. Many of such applications have been discussed in the previous chapters. Therefore, the methodology developed for a semi-analytical solution to dynamical systems holds water under both numerical and analytical scrutiny. The primary use of such a methodology is to examine larger dynamical systems exhibiting complex motions. To this effect, the Main problem in artificial satellite theory is treated next. The following section provides the formulation and solution of the problem.

4.5 Hamilton-Jacobi formalism for the main problem in artificial satellite theory

The late 50s and early 60s witnessed an enormous rise in analytic orbit theories for estimating orbits of space objects [188, 189, 190, 191]. Brouwer [188] used von Zeipel's method to obtain a perturbation solution to the artificial satellite problem by incorporating zonal harmonics from J_2 to J_5 of the geopotential. The main problem in artificial satellite theory is the perturbed two-body problem with inclusion of only the J_2 geopotential. We begin our discussion by considering the unperturbed two-body problem using the Hamiltonian formalism. The Hamiltonian for the two-body problem is given in Eq. 4.71.

$$\mathcal{H} = \frac{1}{2}\mathbf{p} - \frac{\mu}{r} \tag{4.71}$$

To represent the action-angle variables, one can associate an action with each of the spherical polar coordinates. In terms of the orbital elements, they are:

$$P_\phi = \sqrt{\mu a(1-e^2)}\cos I \tag{4.72}$$

$$P_\theta + P_\phi = \sqrt{\mu a(1-e^2)} \tag{4.73}$$

$$P_r + P_\theta + P_\phi = \sqrt{\mu a} \tag{4.74}$$

and the Hamiltonian in terms of these actions is:

$$\mathcal{H} = -\frac{1}{2(P_r + P_\theta + P_\phi)^2} \tag{4.75}$$

The Hamiltonian can be written in terms of the Delaunay variables which are associated with the action variables in spherical polar coordinates as:

$$P_1 = L = P_r + P_\theta + P_\phi \qquad l = M \quad \text{(mean anomaly)} \tag{4.76}$$

$$P_2 = G = P_\theta + P_\phi \qquad g = \omega \quad \text{(argument of perigee)} \tag{4.77}$$

$$P_3 = H = P_\phi \qquad h = \Omega \quad \text{(right ascension)} \tag{4.78}$$

$$\mathcal{H} = -\frac{\mu^2}{2L^2} \tag{4.79}$$

From Hamilton's equations of motion, we see that the two angles, g, and h, are cyclic, and therefore, their corresponding momenta are constants of motion. Physically, they are the magnitude of the angular momentum vector and the z-component of the angular momentum in the inertial frame. The angle l varies with time, and its rate is given by the mean motion. We can perform another canonical transformation to a new set of variables, so that the two-body Hamiltonian is zero. In these new variables, the mean anomaly is replaced with the initial mean anomaly given by the relation:

$$l_0 = l - n(t - t_0)$$

The Hamiltonian with J_2 geopotential is written in terms of the Delaunay variables as follows:

$$\mathcal{H} = \mathcal{H}_0 + \Delta\mathcal{H} \tag{4.80}$$

$$\mathcal{H}_0 = 0 \tag{4.81}$$

$$\Delta\mathcal{H} = J_2\Big(\frac{\mu^4 R_e^2}{4}\Big)\Big(\frac{1 + e\cos f}{G^2}\Big)^3\Big[\Big(1 - 3\frac{H^2}{G^2}\Big) - 3\Big(1 - \frac{H^2}{G^2}\Big)\cos(2f + 2g)\Big] \tag{4.82}$$

where f is the true anomaly and an approximation in terms of the initial mean anomaly l_0 is used as [50, 123]:

$$\begin{aligned} f = l + \Big(2e - \frac{1}{4}e^3 + \frac{5}{96}e^5\Big)\sin l + \Big(\frac{5}{4}e^2 - \frac{11}{24}e^4 + \frac{17}{192}e^6\Big)\sin 2l + \Big(\frac{13}{12}e^3 \\ - \frac{43}{64}e^5\Big)\sin 3l + \Big(\frac{103}{96}e^4 - \frac{451}{480}e^6\Big)\sin 4l + \Big(\frac{1097}{960}e^5\Big)\sin 5l + \Big(\frac{1223}{960}e^6\Big)\sin 6l \end{aligned} \tag{4.83}$$

where $l = l_0 + n(t - t_0)$. The eccentricity and mean notion is written in terms of the Delaunay variables as $e = \sqrt{1 - G^2/L^2}$ and $n = \mu^2/L^3$. We now look for a transformation $(l, g, h, L, G, H) \rightarrow (x, y, z, X, Y, Z)$ to a new set of variables such that in these variables, the resulting Hamiltonian is zero. The HJ equation is given as:

$$\frac{\partial \mathcal{S}}{\partial t} + \mathcal{K} = 0 \tag{4.84}$$

where $\mathcal{S} = \mathcal{S}(x, y, z, L, G, H)$ is a generating function of type-3. The reason for choosing type-3 is to take advantage of the fact that the angle h is cyclic and one can avoid complex equations arising from the $\frac{H^2}{G^2}$ and $\frac{G^2}{L^2}$ terms which for a type-2 generating function would result in

$$\frac{H^2}{G^2} = \frac{\left(\frac{\partial \mathcal{S}}{\partial h}\right)^2}{\left(\frac{\partial \mathcal{S}}{\partial g}\right)^2} \qquad \frac{G^2}{L^2} = \frac{\left(\frac{\partial \mathcal{S}}{\partial g}\right)^2}{\left(\frac{\partial \mathcal{S}}{\partial l_0}\right)^2}$$

A further simplification can be made if one notes that since h is cyclic, H is a constant of motion. Therefore, the generating function admits a separability in the variables (h, H). The generating function can be approximated as

$$\mathcal{S} = \mathcal{S}_1(x, y, L, G) + \mathcal{S}_2(z, H) \tag{4.85}$$

The solution procedure remains same as before. The six-dimensional space is discretized into subdomains based on the orbital parameters. For the purposes of demonstration, we choose three such domains:

1. A near circular Low Earth Orbit (LEO) at near equatorial inclination
2. A Molniya orbit: highly elliptical Medium Earth Orbit (MEO) at critical inclination
3. A Geostationary Earth orbit (GEO)

The discretization of the domain is crucial to avoid large errors in the approximation of the gen-

erating function. For the main problem, the phase space is normalized, such that the gravitational parameter (μ) and the Earth equatorial radius (R_e) are taken as unity. Using this normalization, the perturbation is taken to be of the order of $1e-4$ and is given by $\epsilon = J_2 \frac{\mu^4 R_e^2}{4}$. The generating function is approximated using Legendre polynomials and monomials using the "total degree" rule for the basis functions space in the discretized phase volume. The effect of domain size, basis functions and sparse-grids is conducted for each case of LEO, MEO, and GEO.

We restrict ourselves to using the minimal degree for approximating the generating function, i.e. total degree of two. As evidenced from the previous discussion on the duffing oscillator, adding a higher degree basis functions gives us additional order of accuracy. Note that the generating function phase volume is divided into two phase volumes, i.e. one belonging to $\mathcal{S}_1(x, y, L, G)$ and the other belonging to $\mathcal{S}_2(z, H)$. One can see the advantage in leveraging this separability by looking at the number of basis functions in the approximating polynomial. The total number of basis functions of degree d in n variables is given by:

$$N = 1 + \sum_{D=1}^{d} \binom{n+D-1}{n-1} \tag{4.86}$$

Thus, for $d = 2$ and six variables, we would have 28 basis functions, while for $d = 2$ and (4+2) variables we would have 20 basis functions. Having this advantage reduces the computational time, as well as the number of ODE to solve for the coefficients. The following sections outline the results for each case. The orbital parameters chosen are as follows:

Table 4.1: Orbital parameters for LEO, MEO, and GEO cases

Orbit	a	e	i	Ω	ω	l_o
LEO	8000 km	0.05	3.665 deg	46.95 deg	7.85 deg	24
MEO	26554 km	0.72	63.4 deg	12 deg	270 deg	20
GEO	42000 km	0.1	15 deg	35 deg	12 deg	95

4.5.1 Case 1: Low Earth orbit example

The orbital elements phase volume is discretized as shown in the table below. The time period for propagation is taken to be 25 reference orbits i.e. $25 \times 2\pi$ where the reference orbit is an orbit with the normalizing parameters.

Table 4.2: Orbital elements phase-volume discretization

Cases	a	e	i	Ω	ω	l_0
1	100 km	0.05	7 deg	5 deg	5 deg	6 deg
2	200 km	0.1	20 deg	20 deg	20 deg	10 deg

The error in the approximate generating function is obtained as follows for monomial basis functions on a sparse-grid with depth two. It is noted here that the units of L, G, H are normalized while those of x, y, z are the same as l_0, g, h, i.e., in radians.

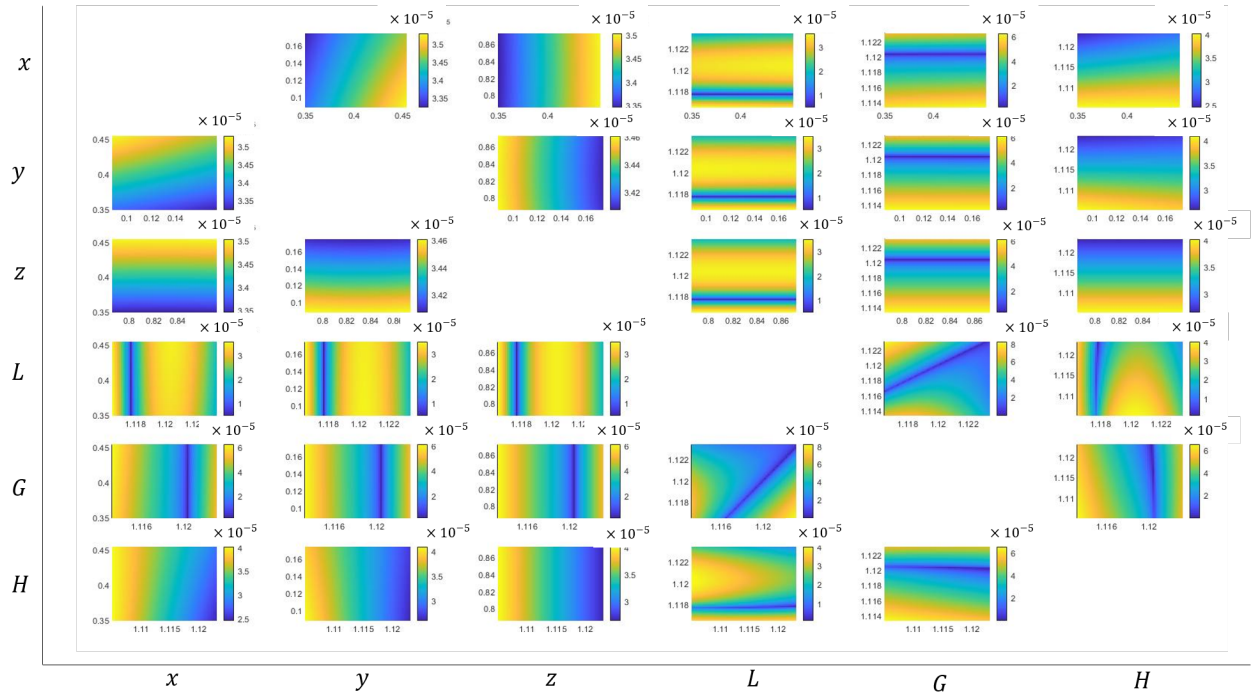

Figure 4.10: LEO: Error in the approximate generating function for the phase-volume.

The error is of the order of ϵ^2, as anticipated. The same order of error was obtained for basis functions with Legendre polynomials and with sparse-grid of depth three. Therefore, these plots are not shown here. The size of the domain chosen seems to have a bigger effect on the error characterization. For the domain discussed above, a representative trajectory is propagated and compared with a numerical solution. This is as shown below.

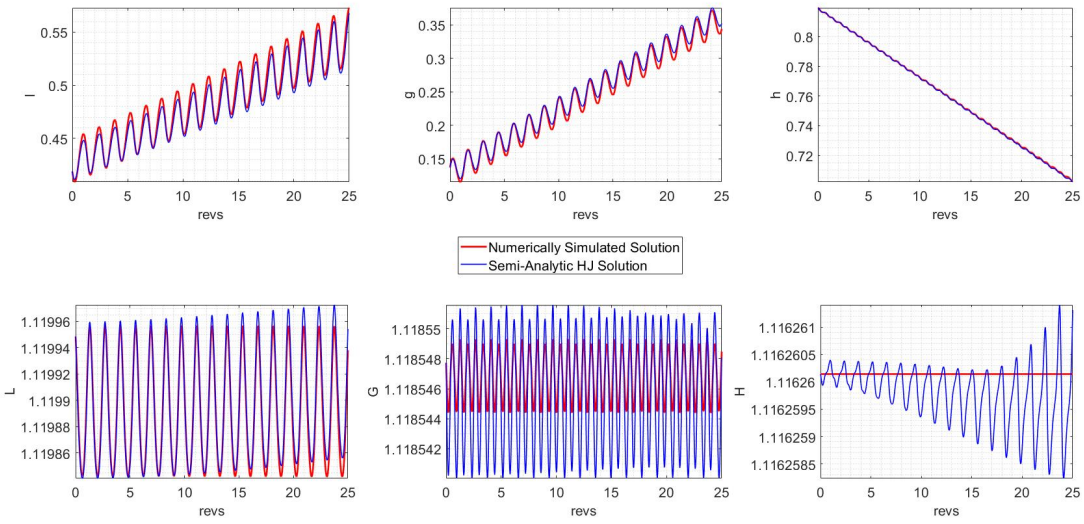

Figure 4.11: Representative trajectory for LEO.

Note that the secular drift in the variables are captured quite nicely. Similarly, the periodic variations are also captured. The errors in the approximated trajectory is found to be of the order of ϵ^2 in the conjugate momenta and ϵ in the angles. This is as shown in the figure below.

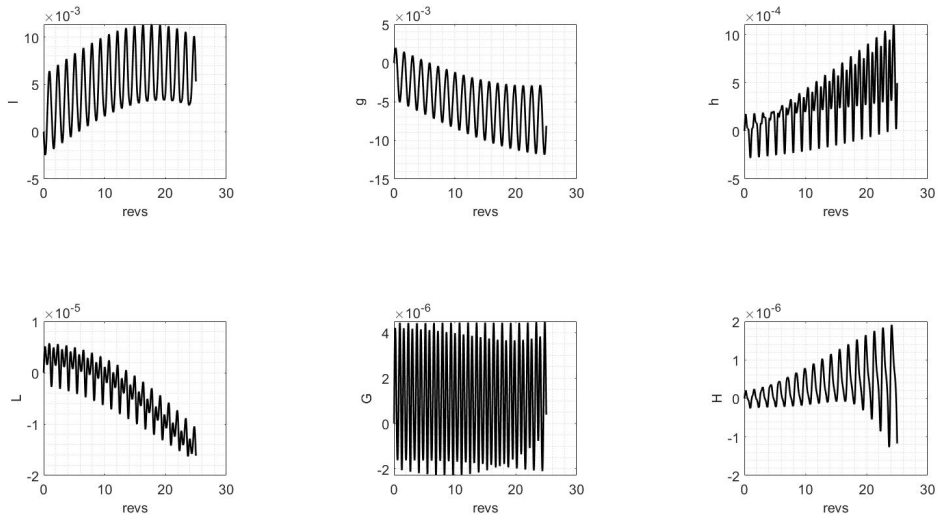

Figure 4.12: Error in the representative trajectory for LEO for case 1 domain discretization

When a larger domain size is chosen, the errors are found to be larger. This is shown as:

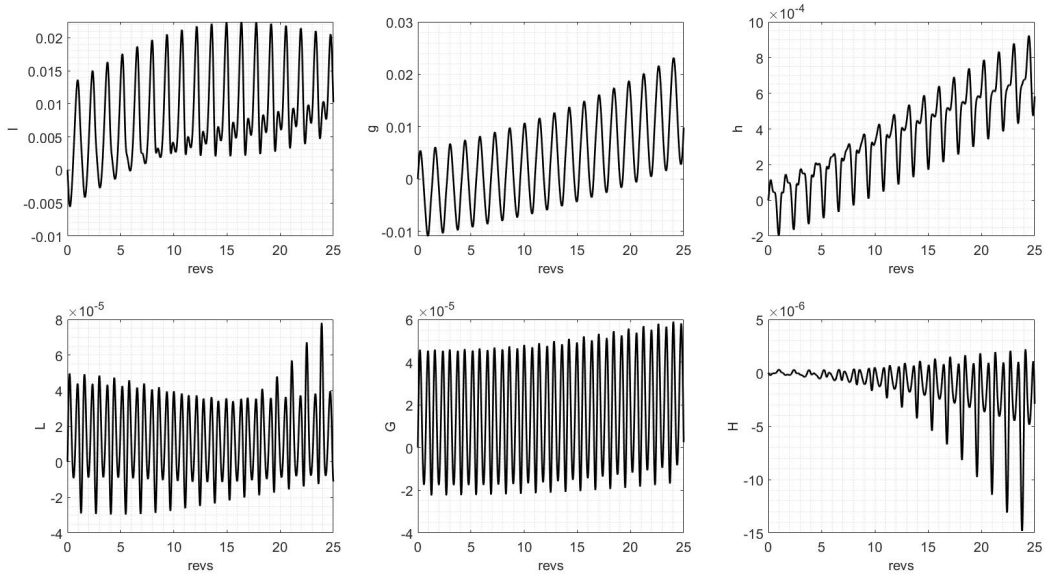

Figure 4.13: Error in the representative trajectory for LEO for case 2 domain discretization

4.5.2 Case 2: Molniya orbit example

The orbital elements phase volume is discretized as shown in the table below. The time period for propagation is taken to be 25 reference orbits i.e. $25 \times 2\pi$ where the reference orbit is an orbit with the normalizing parameters.

Table 4.3: Orbital elements phase-volume discretization

Cases	a	e	i	Ω	ω	l_0
1	100 km	0.1	10 deg	10 deg	10 deg	10 deg
2	300 km	0.2	30 deg	30 deg	30 deg	20 deg

The error in the approximate generating function is obtained as follows for monomial basis functions on a sparse-grid with depth two.

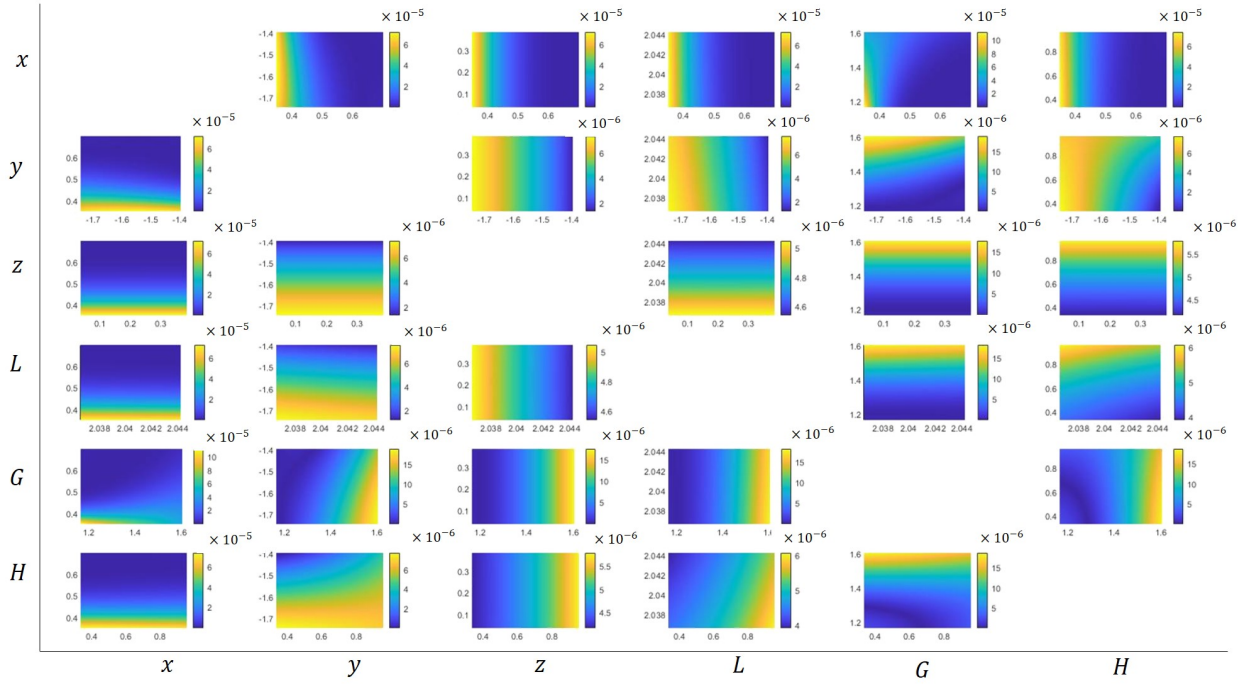

Figure 4.14: MEO: Error in the approximate generating function for the phase-volume

The error is of the order of ϵ^2, as seen. The same order of error was obtained for basis functions with Legendre polynomials and with sparse-grid of depth three. Therefore, these plots are not shown here. The size of the domain chosen seems to have a bigger effect on the error characterization. For the domain discussed above, a representative trajectory is propagated and compared with a numerical solution. This is as shown below.

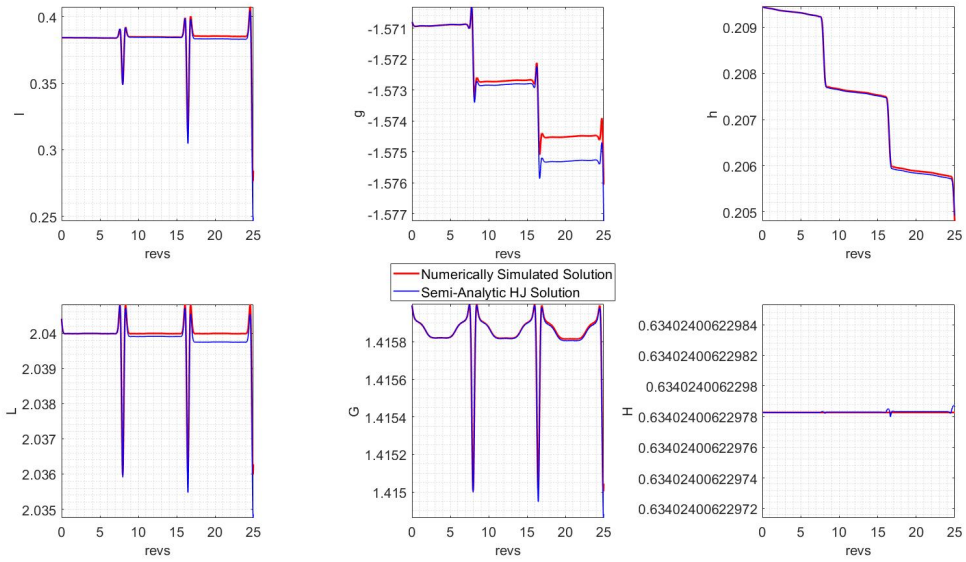

Figure 4.15: Representative trajectory for Molniya orbit

Note that the secular drift in the variables is captured quite nicely. Similarly, the periodic variations are also captured. The errors in the approximated trajectory are found to be of the order of ϵ^2 in the conjugate momenta and ϵ in the angles. This is as shown in the figure below.

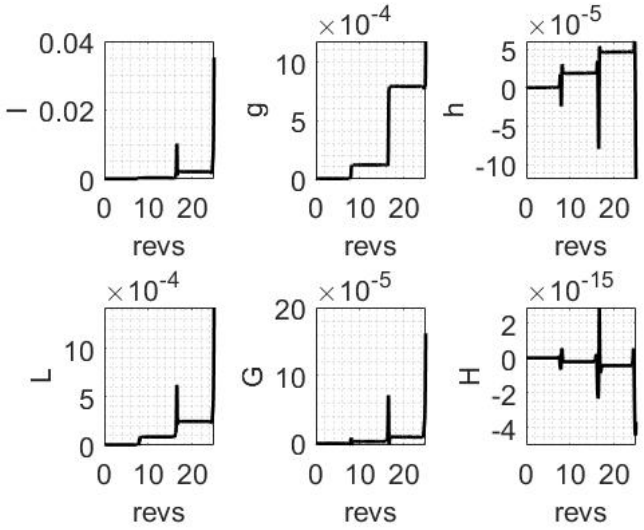

Figure 4.16: Error in the representative trajectory for MEO for case 1 domain discretization

When a larger domain size is chosen, the errors are found to be larger. This is shown as:

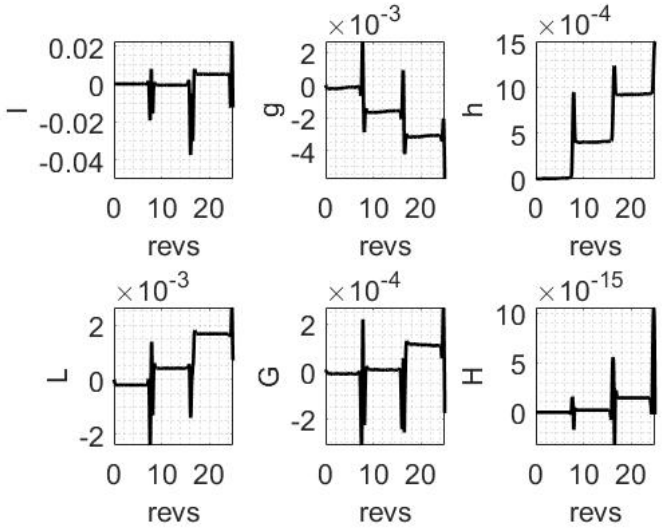

Figure 4.17: Error in the representative trajectory for MEO for case 2 domain discretization

4.5.3 Case 3: Geostationary Earth orbit example

The orbital elements phase volume is discretized as shown in the table below. The time period for propagation is taken to be 25 reference orbits i.e. $25 \times 2\pi$ where the reference orbit is an orbit with the normalizing parameters.

Table 4.4: Orbital elements phase-volume discretization

Cases	a	e	i	Ω	ω	l_0
1	200 km	0.1	20 deg	20 deg	20 deg	10 deg
2	400 km	0.4	40 deg	40 deg	40 deg	20 deg

The error in the approximate generating function is obtained as follows for monomial basis functions on a sparse-grid with depth two.

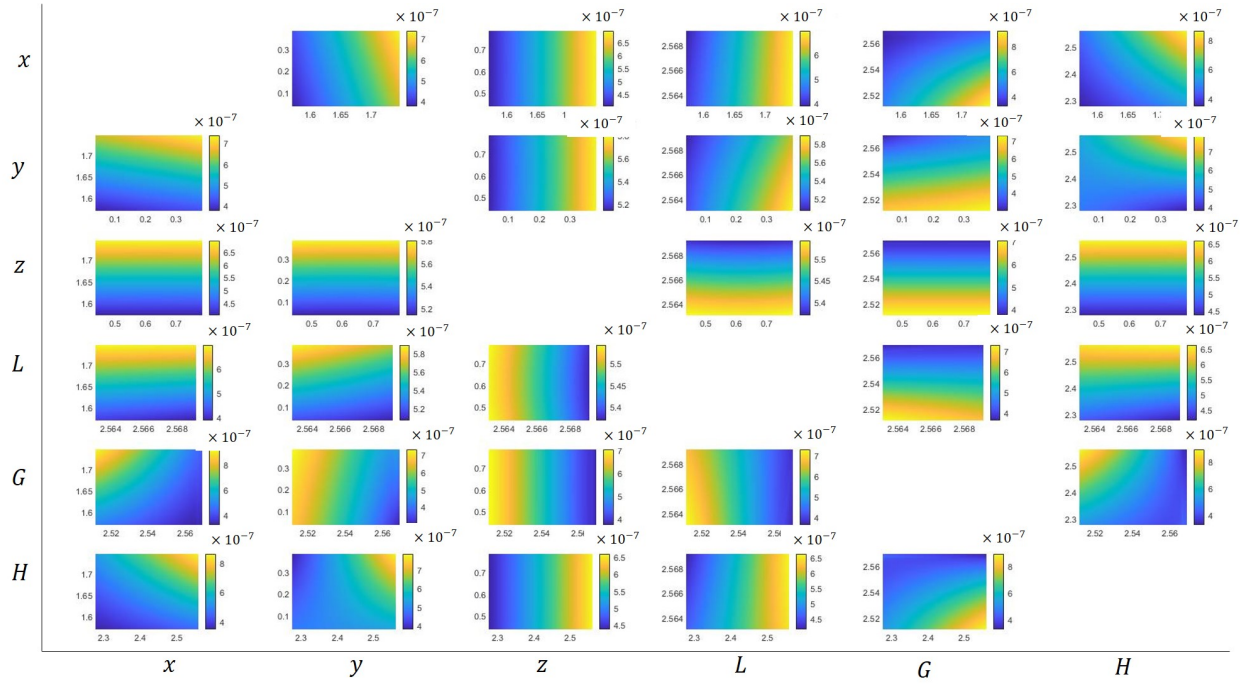

Figure 4.18: GEO: Error in the approximate generating function for the phase-volume

The error is of the order of ϵ^2, as expected. The same order of error was obtained for basis functions with Legendre polynomials and with sparse-grid of depth three. Therefore, these plots are not shown here. The size of the domain chosen seems to have a bigger effect on the error characterization. For the domain discussed above, a representative trajectory is propagated and compared with a numerical solution. This is as shown below.

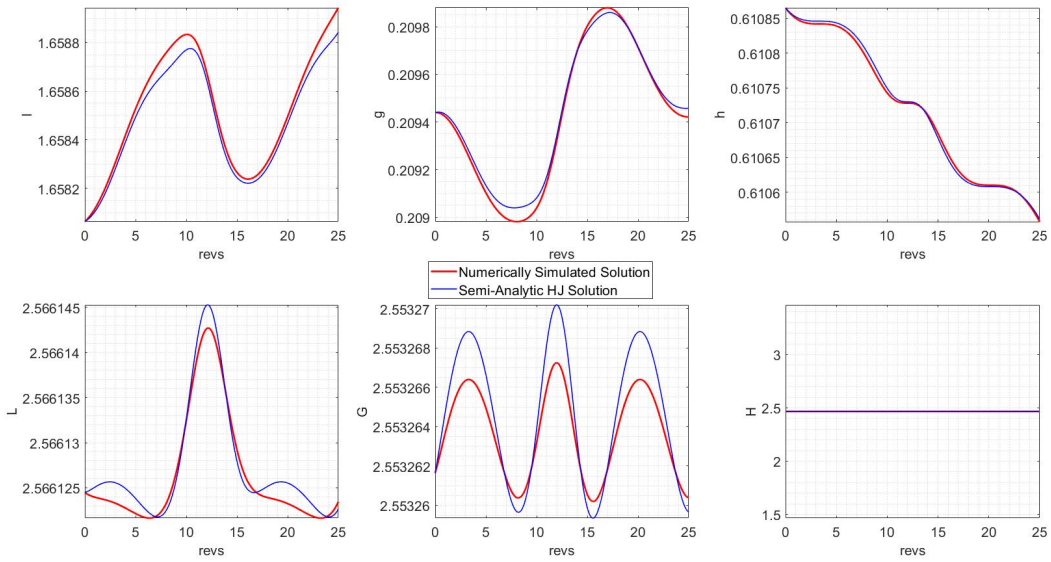

Figure 4.19: Representative trajectory for GEO

Note that the secular drift in the variables is captured quite nicely. Similarly, the periodic variations are also captured. The errors in the approximated trajectory are found to be of the order of ϵ^2 in the conjugate momenta and ϵ in the angles. This is as shown in the figure below.

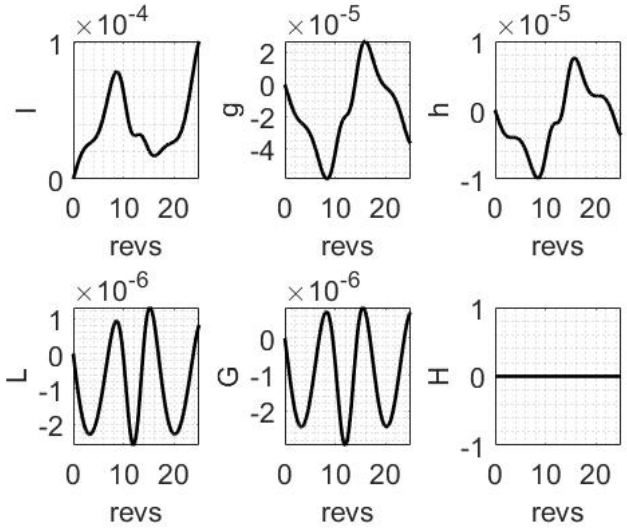

Figure 4.20: Error in the representative trajectory for GEO for case 1 domain discretization

When a larger domain size is chosen, the errors are found to be larger. This is shown as:

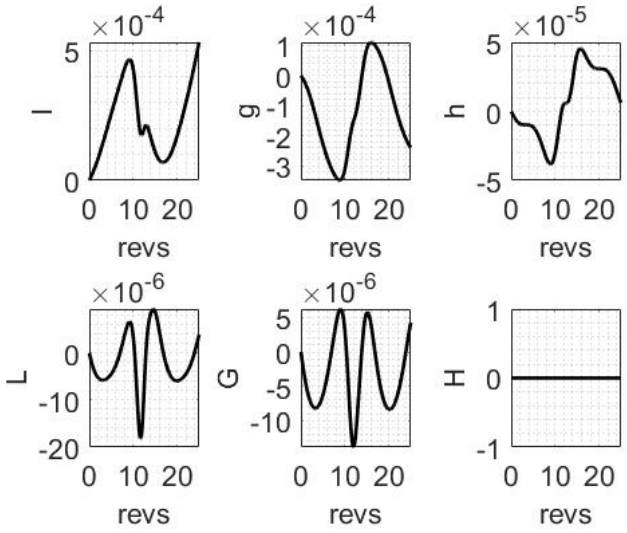

Figure 4.21: Error in the representative trajectory for GEO for case 2 domain discretization

One can notice how the error in the generating function approximation reduces as the orbit semi-major axis increases. This is due to the fact that for LEO, MEO, and GEO orbits considered

here, the time for propagation was the same, i.e. 25 revolutions of the reference orbit. While 25 revolutions of the reference orbit may correspond to 18, 3 and 1.5 revolutions of the LEO, MEO, and GEO orbit, respectively. Errors corresponding to 1.5 revolutions of the LEO and MEO orbit would also result in lower errors, as that observed in GEO. The error in the generating function builds up with time. This is possibly due to the accumulation of numerical error in the solution of the ODE, as well as insufficient basis functions. However, despite these drawbacks, a semi-analytical solution to the Main problem in artificial satellite theory is obtained to close correspondence with a fully numerical solution.

In this investigation, a systematic procedure is described to study conservative systems. In the following sections, this method is extended to develop a canonical perturbation method for non-conservative dynamical systems. We have briefly glimpsed this procedure in Sec. 3.3.3 when the non-conservative Hamiltonian was modified to a conservative Hamiltonian using the extended phase space mechanics. While the extended phase space was utilized to take care of the non-autonomous nature of the Hamiltonian, general non-conservative dynamical systems can also be treated using this approach. The extension is obtained by embedding the $n-$dimensional non-conservative dynamical system in a $2n-$dimensional phase-space to render the coordinates and momenta canonical [115, 192].

4.6 The extended canonical perturbation method for non-conservative dynamical systems

In this section, the methodology developed in the previous sections is extended to treat non-conservative Hamiltonian systems. This methodology is inspired by the works of Kamel [115], and Choi and Tapley [192]. Consider the problem of describing the motion of a dynamical system as

$$\dot{\mathbf{x}} = f(\mathbf{x}) \tag{4.87}$$

where $\mathbf{x} = [x_1, \cdots, x_n]^T$ and $f(\mathbf{x}) = [f_i(\mathbf{x}), \cdots, f_n(\mathbf{x})]^T$. It the dynamical system is non-autonomous, one can follow the procedure described in Sec. 3.3.3 to make the dynamics follow $\mathbf{x}_{n+1} = t$ and adding an associated dummy momenta to make the equations canonical. Or, in non-canonical co-

ordinates, this is done by expressing $\dot{x}_{n+1} = 1$ and $x_{n+1}(0) = 0$. Now, introducing a set of adjoint variables **y** which satisfy the differential equation:

$$\dot{\mathbf{y}} = -\frac{\partial f(\mathbf{x})}{\partial \mathbf{x}}\mathbf{y} \tag{4.88}$$

where, $\mathbf{y} = [y_1, \cdots, y_n]^T$. The Hamiltonian then takes the form

$$\mathcal{H}(x, y) = \mathbf{y}^T f(\mathbf{x}) \tag{4.89}$$

Note that in this formulation, the adjoint variables (**y**) act like conjugate dummy momenta to x. Hamilton's equations of motion can then be written as:

$$\begin{aligned} \frac{d\mathbf{x}}{dt} &= \frac{\partial \mathcal{H}}{\partial \mathbf{y}} \\ \frac{d\mathbf{y}}{dt} &= -\frac{\partial \mathcal{H}}{\partial \mathbf{x}} \end{aligned} \tag{4.90}$$

In this formulation, the solution of the $n-$dimensional dynamical system is embedded into the solution of a $2n-$dimensional canonical differential equations. Once the problem is formulated in this manner, the procedure to treat the dynamical system follows that developed in previous sections. For demonstrating the formulation and solution of the methodology developed, we shall look at two examples: (a) The simple harmonic oscillator with cubic damping, and (b) the van der Pol oscillator. Let us take a look at the simple harmonic oscillator with cubic damping.

4.6.1 The simple harmonic oscillator with cubic damping

Consider the dynamical system of the simple harmonic oscillator with cubic damping. The differential equations governing the motion is given as follows:

$$\ddot{x} + x + \epsilon \dot{x}^3 = 0 \tag{4.91}$$

We can write this as a set of first order ordinary differential equations using $x_1 = x$ and $x_2 = \dot{x}$ as

$$\dot{x}_1 = x_2 \tag{4.92}$$

$$\dot{x}_2 = -x_1 - \epsilon x_2^3 \tag{4.93}$$

Note that the dynamical system cannot be written in a Hamiltonian form with canonical variables in its current coordinate representation. The energy is not conservative due to the presence of the velocity-dependent perturbation. However, for $\epsilon = 0$, the dominant physics is due to the simple harmonic oscillator, which has a complete reduction in terms of its phase and amplitude variables. The simple harmonic oscillator with cubic damping has been treated in Choi and Tapley [192] using the methods developed by Kamel [115]. In this work, we will use a slightly different methodology to treat this non-Hamiltonian dynamical system. Recognizing that the simple harmonic oscillator has canonical coordinates defined using the phase and amplitude variables as

$$q_1 = a_1 \sin(b_1 + t) \tag{4.94}$$

$$q_2 = a_1 \cos(b_1 + t) \tag{4.95}$$

with substituting $(q_1, q_2) = (x_1, x_2)$ and (a_1, b_1) are the constants of motion for the simple harmonic oscillator. We can obtain the variation of these constants under the influence of the perturbation using variation of parameters methods as

$$\dot{a}_1 = -\frac{\epsilon}{8} a_1^3 \left(3 + \cos 4(b_1 + t) + 4 \cos 2(b_1 + t)\right) \tag{4.96}$$

$$\dot{b}_1 = -\frac{\epsilon}{8} a_1^2 \left(\sin 4(b_1 + t) + 2 \sin 2(b_1 + t)\right) \tag{4.97}$$

At this stage, we introduce the adjoint variables (y_1, y_2) so that the Hamiltonian is written as:

$$\mathcal{H} = y_1 \left[-\frac{\epsilon}{8} a_1^3 \left(3 + \cos 4(b_1 + t) + 4\cos 2(b_1 + t)\right)\right] + y_2 \left[-\frac{\epsilon}{8} a_1^2 \left(\sin 4(b_1 + t) + 2\sin 2(b_1 + t)\right)\right] \tag{4.98}$$

These **y** can be considered as the dummy momenta conjugate to the coordinates (a_1, b_1). From Hamilton's equations of motion:

$$\begin{aligned}
\frac{da_1}{dt} &= \frac{\partial \mathcal{H}}{\partial y_1} = -\frac{\epsilon}{8} a_1^3 \left(3 + \cos 4(b_1 + t) + 4\cos 2(b_1 + t)\right) \\
\frac{db_1}{dt} &= \frac{\partial \mathcal{H}}{\partial y_2} = -\frac{\epsilon}{8} a_1^2 \left(\sin 4(b_1 + t) + 2\sin 2(b_1 + t)\right) \\
\frac{dy_1}{dt} &= -\frac{\partial \mathcal{H}}{\partial a_1} = 3\epsilon a_1^2 y_1 \cos^4(b_1 + t) - \frac{1}{4}\left(a_1 \epsilon y_2 (2\sin 2(b_1 + t) + \sin 4(b_1 + t))\right) \\
\frac{dy_2}{dt} &= -\frac{\partial \mathcal{H}}{\partial b_1} = -4a_1^3 \epsilon y_1 \cos^3(b_1 + t)\sin(b_1 + t) - \frac{1}{8}\left(a_1^2 \epsilon y_2 (4\cos 2(b_1 + t) + 4\cos 4(b_1 + t))\right)
\end{aligned} \tag{4.99}$$

By combining the variation of parameters method and the introduction of the dummy momenta, we have the Hamiltonian as a pure function of the perturbation. Thus, the total Hamiltonian can be written as:

$$\mathcal{H} = \mathcal{H}_0 + \epsilon \mathcal{H}_1 \tag{4.100}$$

$$\mathcal{H}_0 = 0 \tag{4.101}$$

$$\mathcal{H}_1 = -\frac{1}{8} a_1^2 \left[a_1 y_1 \left(3 + \cos 4(b_1 + t) + 4\cos 2(b_1 + t)\right) + y_2 \left(\sin 4(b_1 + t) + 2\sin 2(b_1 + t)\right)\right] \tag{4.102}$$

For simplicity and to maintain familiarity of notations, we rewrite the Hamiltonian in terms of the familiar (q_1, q_2, p_1, p_2) coordinates and momenta as follows

$$\mathcal{H} = -\frac{1}{8} q_1^2 \left[q_1 p_1 \left(3 + \cos 4(q_2 + t) + 4\cos 2(q_2 + t)\right) + p_2 \left(\sin 4(q_2 + t) + 2\sin 2(q_2 + t)\right)\right] \tag{4.103}$$

Certain patterns can be observed in the Hamiltonian, which gives insights into the structure of the generating function. Since **y** was a linear multiplier to $f(\mathbf{x})$ in the Hamiltonian, **p** is also a linear multiplier in the new Hamiltonian and the generating function as well. Therefore, the complete solutions for $\mathbf{p}(t)$ are not necessary to obtain the complete solutions for $\mathbf{q}(t)$. They are only of interest as the conjugate solutions to **q** in the $4-$dimensional topological space. This observation is valid for any general $2n-$dimensional Hamiltonian system formed using the procedure above. The linear multiplier condition can be enforced (as done by Hori [113]) that **p** be a linear multiplier by taking $\mathcal{S} = \mathbf{p}^T T(\mathbf{q})$ or its equivalent form (where T is an approximating generating function). This form of the generating function will then ensure that solutions of **p** are not required for the solutions of **q**.

At this point, we can revert back to our methodology of solving the HJ equation using an approximate generating function. To recall, we are seeking a transformation from the old space of (q_1, q_2, p_1, p_2) to a new space (Q_1, Q_2, P_1, P_2) through a generating function of mixed variables. Assuming the generating function of type-2 is used, it takes the form: $\mathcal{S} = \mathcal{S}(q_1, q_2, P_1, P_2)$. The functional for $\mathcal{S}$ can be obtained by solving the HJ equation given by:

$$\frac{\partial \mathcal{S}}{\partial t} + \mathcal{K} = 0 \tag{4.104}$$

with

$$\mathcal{K} = -\epsilon \frac{\partial \mathcal{S}}{\partial q_1} q_1^3 \cos^4(t + q_2) + \frac{\epsilon}{8} \frac{\partial \mathcal{S}}{\partial q_2} q_1^2 \left(\sin 4(q_2 + t) + 2 \sin 2(q_2 + t)\right) \tag{4.105}$$

The methodology for solving the HJ equation is similar to that in previous sections. Since **P** appears only linearly, we limit the degree of **P** in the basis function approximation to 1. So, the generating function is approximated using n basis functions as:

$$\mathcal{S} = \mathcal{S}(q_1, q_2, P_1, P_2) = c_1 + c_2 q_1 P_1 + c_3 q_2 P_2 + c_4 q_1 P_2 + c_5 q_2 P_1 + \sum_{i=6}^{n} c_i \phi_i(q_1, q_2) \tag{4.106}$$

The initial conditions for the set of ODE for the coefficients are given using $c_2 = 1$, $c_3 = 1$, and all

other $c_j = 0$. To demonstrate the accuracy of this method, an example simulation is shown below. The evolution of the phase and amplitude variables under the influence of the perturbation and the error in the semi-analytical solution is shown below.

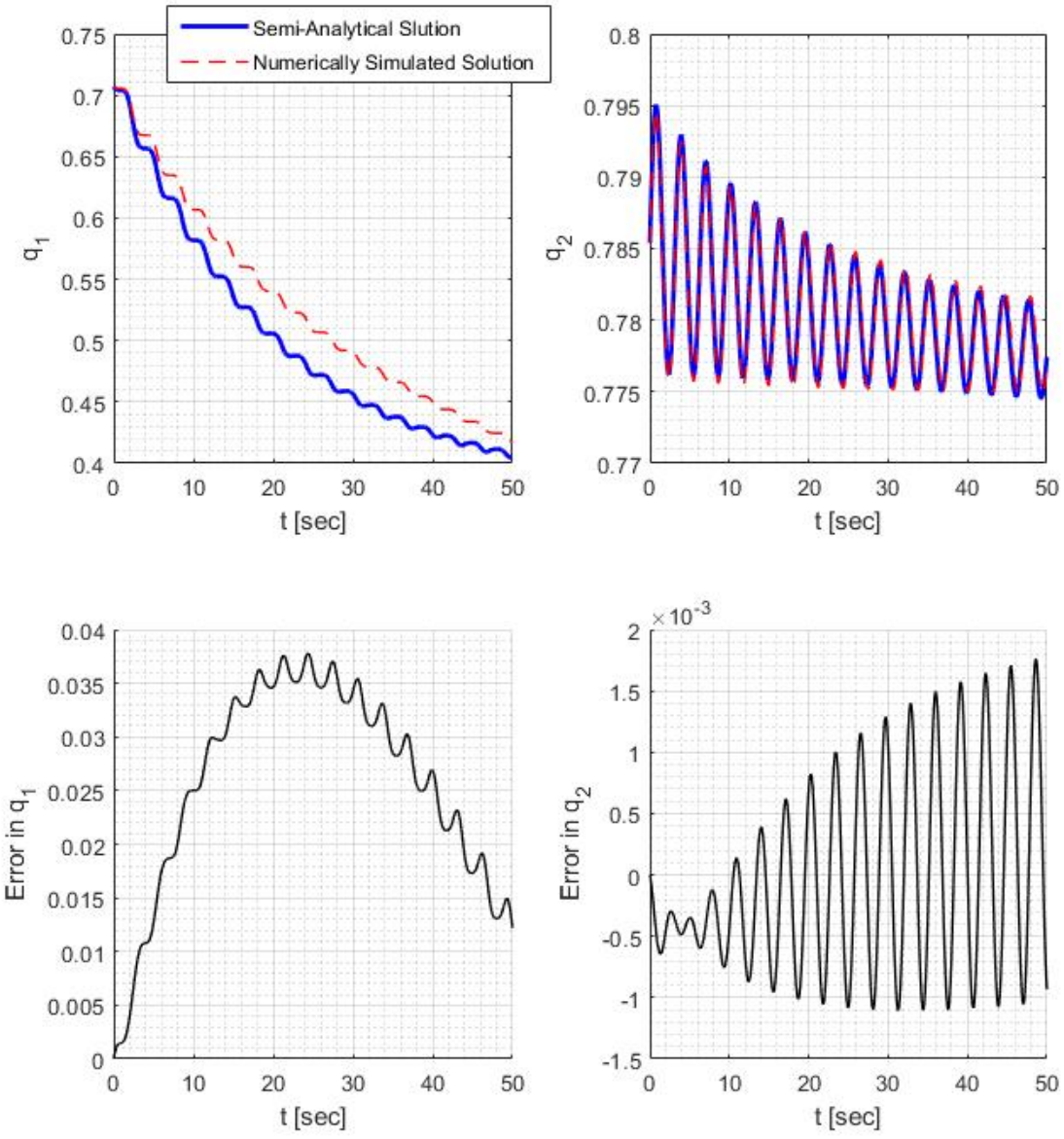

Figure 4.22: Semi-analytical solution to the simple harmonic oscillator with cubic damping; $\epsilon = 0.1$

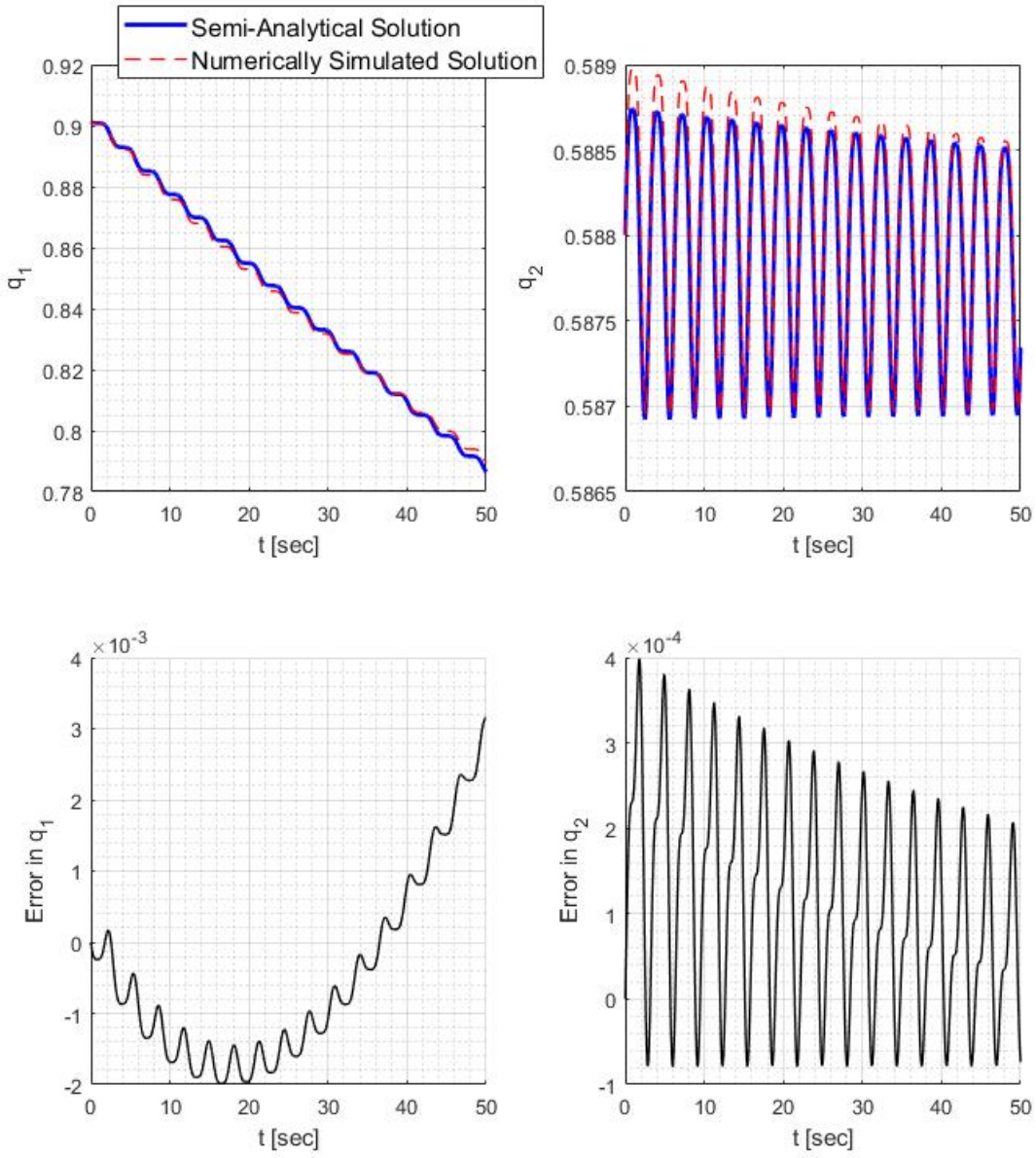

Figure 4.23: Semi-analytical solution to the simple harmonic oscillator with cubic damping; $\epsilon = 0.01$

The errors are of the order of ϵ^2 in the periodic coordinate i.e. q_2. Because of the damping nature of the coordinate q_1, one cannot get away with a small domain for (q_1, q_2) as we could for Hamiltonian systems. Nevertheless, the semi-analytical solution is found to conform to the

expectations anticipated from Hamiltonian dynamical systems. Thus, this methodology aids in the Hamiltonianization of non-Hamiltonian systems from a semi-analytical framework. From a qualitative perspective, the secular and periodic variations are captured quite nicely. Since the dummy momenta do not appear in the evaluation of q_1 and q_2, their domain doesn't affect the solution. Another application to the semi-analytical extended canonical perturbation method is to the van der Pol oscillator. This is discussed next.

4.6.2 The van der Pol oscillator

Consider the dynamical system of the van der Pol oscillator. The differential equations governing the motion is given as follows:

$$\ddot{x} + x - \epsilon(1 - x^2)\dot{x} = 0 \tag{4.107}$$

We can write this as a set of first order ordinary differential equations using $x_1 = x$ and $x_2 = \dot{x}$ as

$$\dot{x}_1 = x_2 \tag{4.108}$$

$$\dot{x}_2 = -x_1 + \epsilon(1 - x_1^2)x_2 \tag{4.109}$$

Note that the dynamical system cannot be written in a Hamiltonian form with canonical variables in its current coordinate representation. The energy is not conservative due to the presence of the velocity-dependent perturbation. However, for $\epsilon = 0$, the dominant physics is due to the simple harmonic oscillator, which has a complete reduction in terms of its phase and amplitude variables.

$$q_1 = a_1 \sin(b_1 + t) \tag{4.110}$$

$$q_2 = a_1 \cos(b_1 + t) \tag{4.111}$$

with substituting $(q_1, q_2) = (x_1, x_2)$ and (a_1, b_1) are the constants of motion for the simple harmonic oscillator. We can obtain the variation of these constants under the influence of the pertur-

bation, using variation of parameters methods as

$$\dot{a}_1 = a_1\,\epsilon\,\left(\sin\left(b_1+t\right)^2-1\right)\,\left({a_1}^2\sin\left(b_1+t\right)^2-1\right) \tag{4.112}$$

$$\dot{b}_1 = \frac{\epsilon\,\sin\left(2\,b_1+2\,t\right)\,\left({a_1}^2\sin\left(b_1+t\right)^2-1\right)}{2} \tag{4.113}$$

At this stage, we introduce the adjoint variables (y_1, y_2) so that the Hamiltonian is written as:

$$\mathcal{H} = y_1\left[a_1\,\epsilon\,\left(\sin\left(b_1+t\right)^2-1\right)\,\left({a_1}^2\sin\left(b_1+t\right)^2-1\right)\right] \tag{4.114}$$

$$+\,y_2\left[\frac{\epsilon\,\sin\left(2\,b_1+2\,t\right)\,\left({a_1}^2\sin\left(b_1+t\right)^2-1\right)}{2}\right] \tag{4.115}$$

These adjoint variables (**y**) can be considered as the dummy momenta conjugate to the coordinates (a_1, b_1). From Hamilton's equations of motion:

$$\begin{aligned}\frac{da_1}{dt} &= \frac{\partial\mathcal{H}}{\partial y_1} = a_1\,\epsilon\,\left(\sin\left(b_1+t\right)^2-1\right)\,\left({a_1}^2\sin\left(b_1+t\right)^2-1\right)\\ \frac{db_1}{dt} &= \frac{\partial\mathcal{H}}{\partial y_2} = \frac{\epsilon\,\sin\left(2\,b_1+2\,t\right)\,\left({a_1}^2\sin\left(b_1+t\right)^2-1\right)}{2}\end{aligned} \tag{4.116}$$

By utilizing VPM and the introduction of dummy momenta, we have the Hamiltonian as a pure function of the perturbation. Thus, the total Hamiltonian can be written as:

$$\mathcal{H} = \mathcal{H}_0 + \epsilon\mathcal{H}_1 \tag{4.117}$$

For simplicity and to maintain familiarity of notations, we rewrite the Hamiltonian in terms of the familiar (q_1, q_2, p_1, p_2) coordinates and momenta as follows

$$\begin{aligned}\mathcal{H} =&\epsilon\,p_1\,q_1\cos\left(q_2+t\right)^2\,\left({q_1}^2\cos\left(q_2+t\right)^2-{q_1}^2+1\right)\\ &-\frac{\epsilon\,p_2\,\left(4\,\sin\left(2\,q_2+2\,t\right)-2\,{q_1}^2\,\sin\left(2\,q_2+2\,t\right)+{q_1}^2\,\sin\left(4\,q_2+4\,t\right)\right)}{8}\end{aligned} \tag{4.118}$$

Certain structure can be observed in the Hamiltonian, which gives insights into the structure of the generating function. Since **y** was a linear multiplier to $f(\mathbf{x})$ in the Hamiltonian, **p** is also a linear multiplier in the new Hamiltonian and the generating function as well. Therefore, the complete solutions for $\mathbf{p}(t)$ are not necessary to obtain the complete solutions for $\mathbf{q}(t)$. They are only of interest as the conjugate solutions to **q** in the $4-$dimensional topological space. We can then revert back to our methodology of solving the HJ equation using an approximate generating function. To recall, we are seeking a transformation from the old space of (q_1, q_2, p_1, p_2) to a new space (Q_1, Q_2, P_1, P_2) through a generating function of mixed variables. Assuming the generating function of type-2 is used, it takes the form: $\mathcal{S} = \mathcal{S}(q_1, q_2, P_1, P_2)$. To functional for $\mathcal{S}$ can be obtained by solving the HJ equation given by:

$$\frac{\partial \mathcal{S}}{\partial t} + \mathcal{K} = 0 \tag{4.119}$$

with $\mathcal{K}$ as the Hamiltonian having $p_1 = \frac{\partial \mathcal{S}}{\partial q_1}$ and $p_2 = \frac{\partial \mathcal{S}}{\partial q_2}$. The methodology for solving the HJ equation is similar to that in previous sections. Since **P** appears only linearly, we limit the degree of **P** in the basis function approximation to 1. So, the generating function is approximated using n basis functions as:

$$\mathcal{S} = \mathcal{S}(q_1, q_2, P_1, P_2) = c_1 + c_2 q_1 P_1 + c_3 q_2 P_2 + c_4 q_1 P_2 + c_5 q_2 P_1 + \sum_{i=6}^{n} c_i \phi_i(q_1, q_2) \tag{4.120}$$

The initial conditions for the set of ODE for the coefficients are given using $c_2 = 1$, $c_3 = 1$, and all other $c_j = 0$. To demonstrate the accuracy of this method, an example simulation is shown below. The evolution of the phase and amplitude variables under the influence of the perturbation and the error in the semi-analytical solution is as shown.

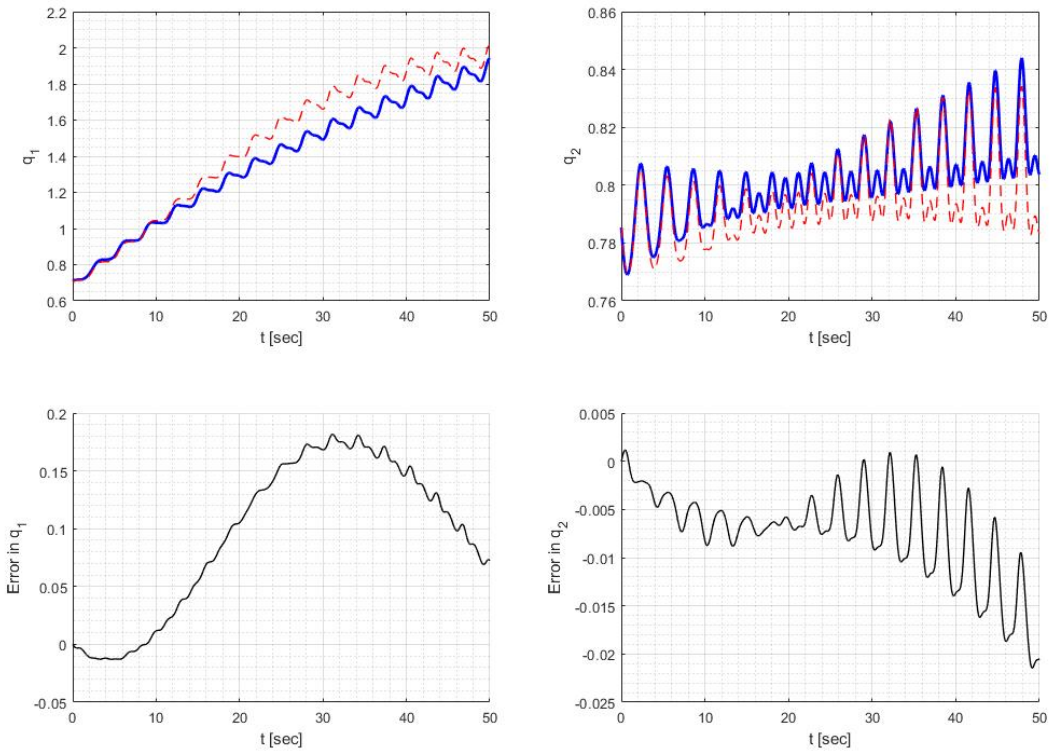

Figure 4.24: Semi-analytical solution to the van der Pol equation; $\epsilon = 0.1$

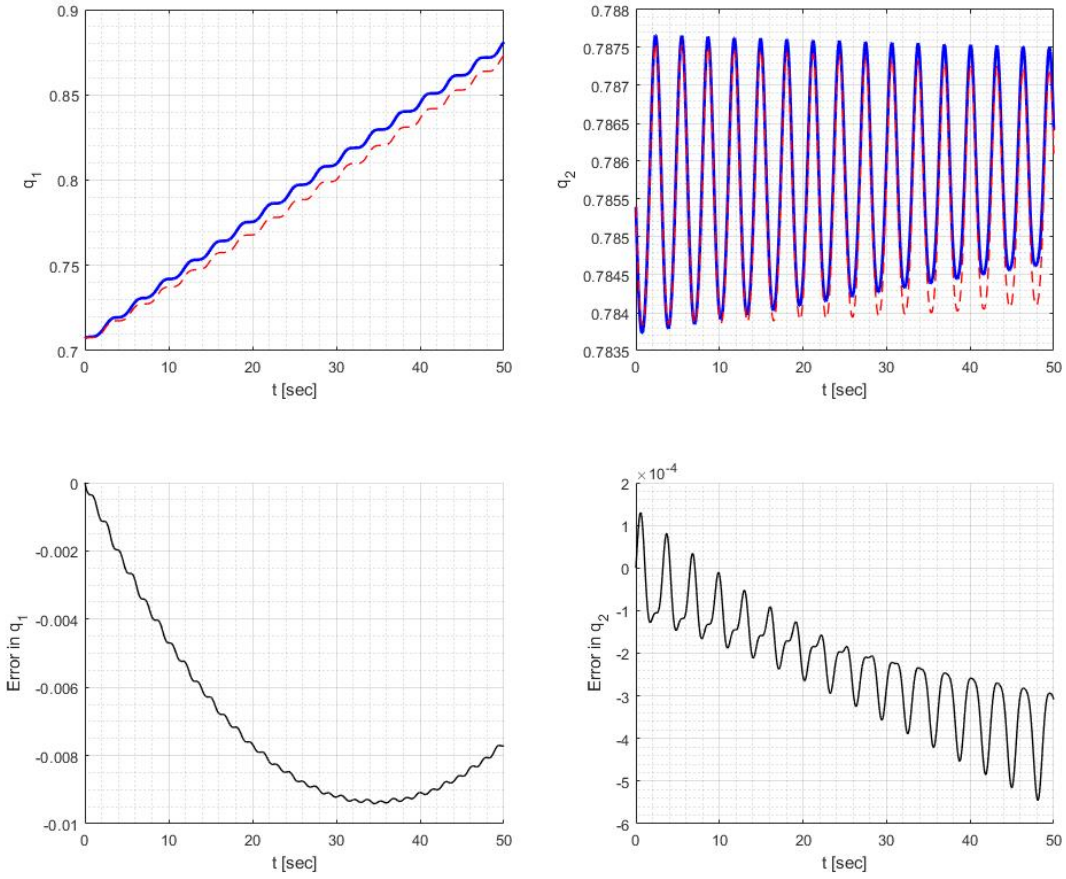

Figure 4.25: Semi-analytical solution to the van der Pol equation; $\epsilon = 0.01$

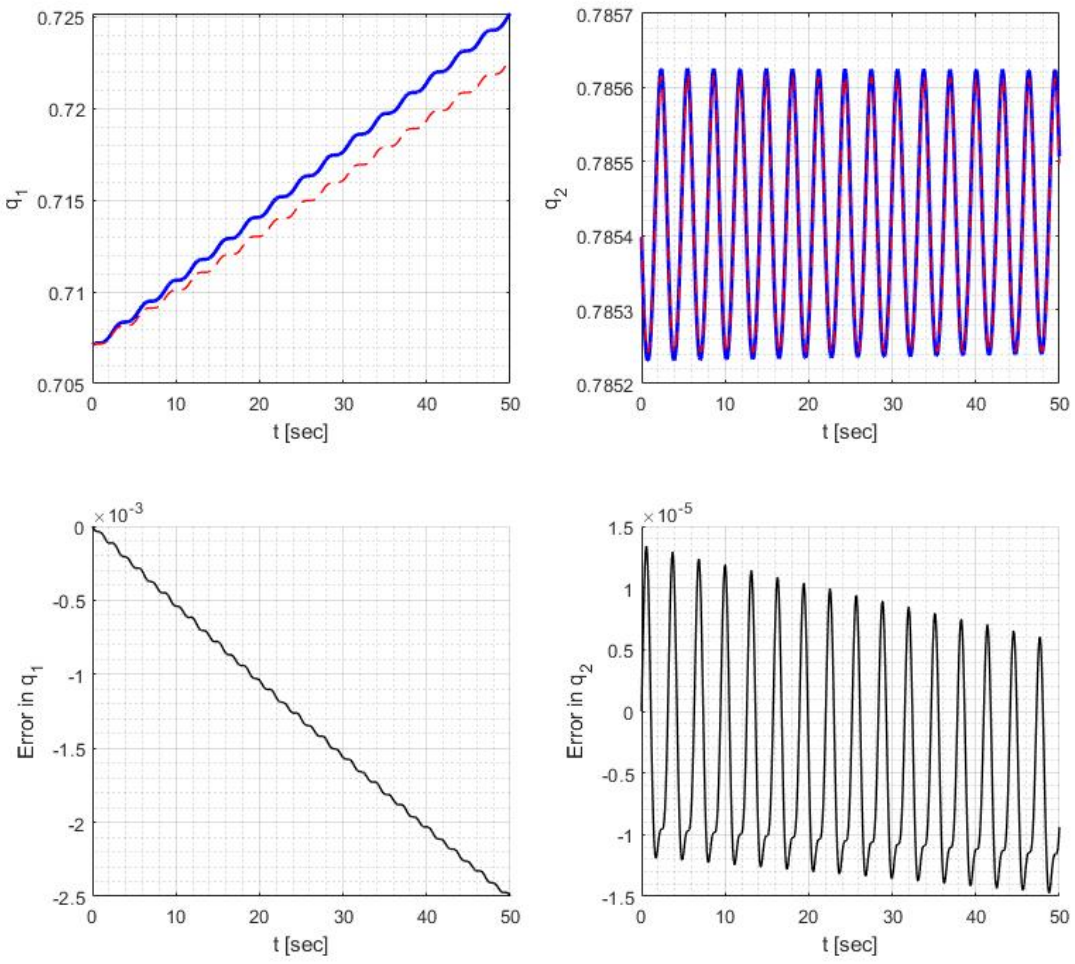

Figure 4.26: Semi-analytical solution to the van der Pol equation; $\epsilon = 0.001$

The errors are of the order of ϵ^2 in the periodic coordinate, i.e. q_2. Because of the phenomenon of the limit cycle, one cannot get away with a small domain for (q_1, q_2) as we could for Hamiltonian systems. The errors in the $q_1 - q_2$ phase-space of the generating function phase volume are as shown below, for different degrees of approximating polynomial is shown in the figures below.

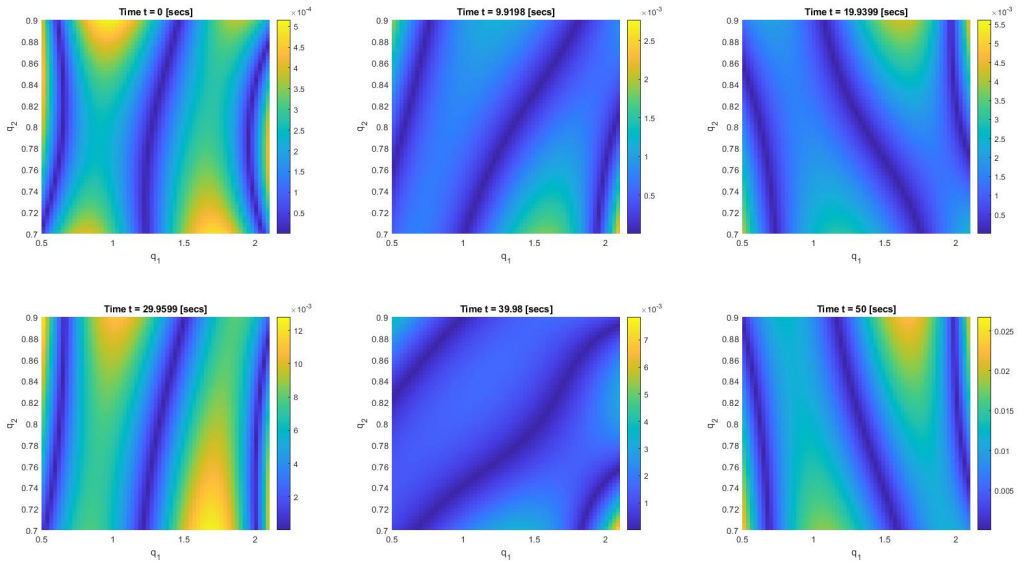

Figure 4.27: Error in $q_1 - q_2$ phase space for $\epsilon = 0.1$ and approximate generating function of degree 2 of the van der Pol oscillator.

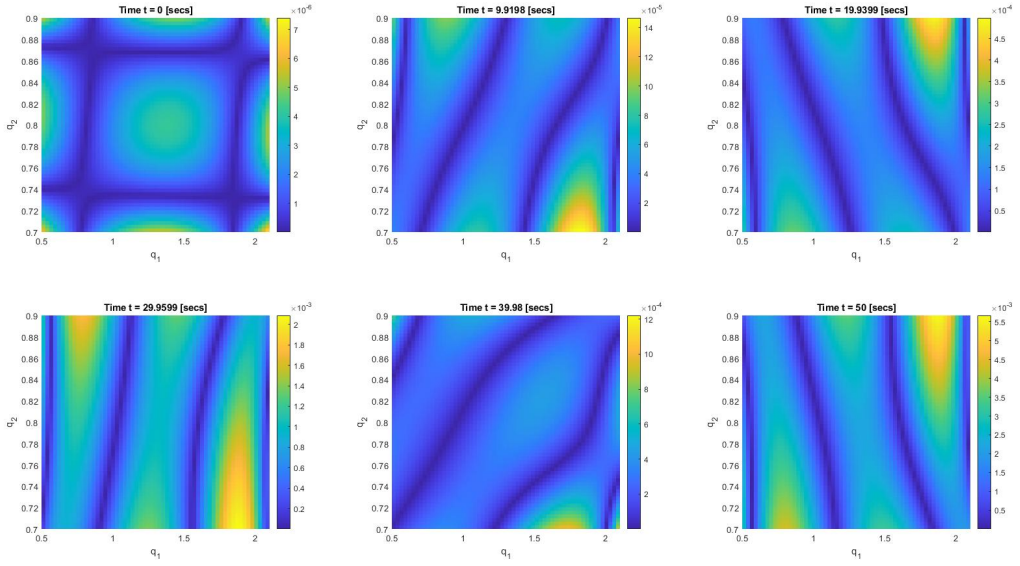

Figure 4.28: Error in $q_1 - q_2$ phase space for $\epsilon = 0.1$ and approximate generating function of degree 3 of the van der Pol oscillator.

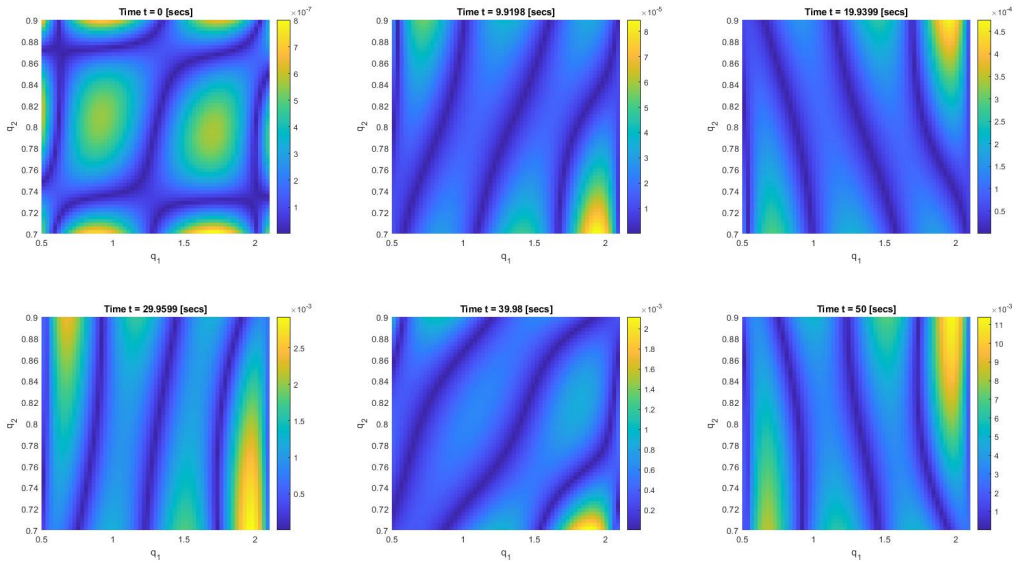

Figure 4.29: Error in $q_1 - q_2$ phase space for $\epsilon = 0.1$ and approximate generating function of degree 4 of the van der Pol oscillator.

The semi-analytical solution is found to conform to the expectations anticipated from Hamiltonian dynamical systems. From a qualitative perspective, the secular and periodic variations are captured quite nicely. Since the dummy momenta do not appear in the evaluation of q_1 and q_2, their domain doesn't affect the solution.

It is interesting to note that the Formulation of the problem using expressions from Eqs. (4.88-4.90) is related in a direct manner to the equations which govern the optimal motion of a dynamical system subjected to effects of an optimal control input [193, 194, 192, 185, 186, 195]. The adjoint variables in Eq. (4.88) are analogous to the Lagrange multipliers (or costates) which are used to define the optimal control. In such situations, the evolution of the adjoint variables also becomes important, and therefore one cannot get away with an arbitrary domain for the adjoint variables. The following section discusses this analogous behavior for optimal control problems.

4.7 Applications of semi-analytic HJ theory to optimal control problems

The formulation of the problem for solving the HJ equation for non-Hamiltonian dynamical systems has a stark similarity to that of optimal control problems through the analogous nature of

the adjoint variables and the Lagrange multipliers. In this section, the methodology of a Two-Point Boundary Value Problem (TPBVP) is developed using canonical transformations to derive general semi-analytic solutions. Since the generating function contains all the relevant information of the dynamical system, simple manipulations of the generating function equations provide exact solutions (provided the generating function is exact) to the control for arbitrary boundary conditions, thereby giving a significant advantage over some classical methods. To motivate this discussion, let us recall the TPBVP of a Hamiltonian system.

4.7.1 The two-point boundary value problem

Consider the minimization of a general performance index given by

$$J = \phi(\mathbf{x}(t_f), t_f) + \int_{t_0}^{t_f} \mathcal{L}(\mathbf{x}(t), \mathbf{u}(t), t)dt \tag{4.121}$$

subject to a dynamical system governed by

$$\dot{\mathbf{x}} = \mathbf{f}(\mathbf{x}(t), \mathbf{u}(t), t) \tag{4.122}$$

satisfying the boundary conditions

$$\begin{aligned} \mathbf{x}(t_0) &= x_0 \\ \psi(\mathbf{x}(t_f), t_f) &= \mathbf{0} \end{aligned} \tag{4.123}$$

where $\mathbf{x} \in \Re^n$ are the state space variables of the dynamical system, $\mathbf{u} \in \Re^m$ the control, $t \in \Re$ is the time, t_0 and t_f are the initial and final times. The general procedure of solving the optimal control problem is done by defining an augmented cost function of the Hamiltonian which is given as

$$\mathcal{H}(\mathbf{x}, \mathbf{u}, \boldsymbol{\lambda}, t) = \mathcal{L}(\mathbf{x}(t), \mathbf{u}(t), t) + \boldsymbol{\lambda}^T \mathbf{f}(\mathbf{x}(t), \mathbf{u}(t), t) \tag{4.124}$$

By obtaining the variations of this cost function, one can obtain the necessary conditions for opti-

mality as:

$$\dot{\mathbf{x}} = \frac{\partial \mathcal{H}}{\partial \boldsymbol{\lambda}} \tag{4.125}$$

$$\dot{\boldsymbol{\lambda}} = -\frac{\partial \mathcal{H}}{\partial \mathbf{x}} \tag{4.126}$$

$$0 = \frac{\partial \mathcal{H}}{\partial \mathbf{u}} \tag{4.127}$$

Evaluating the optimal trajectory requires solving the system of ODEs to satisfy the given boundary conditions. Now, given a TPBVP, there are many methods to find the solution through standard numerical techniques. However, it generally requires an iterative procedure with an initial guess for the costates ($\boldsymbol{\lambda}$), which do not have any physical meaning in general [186]. To alleviate this problem, a solution methodology is developed that uses the semi-analytic solution of the HJ equation applied to the Hamiltonian of the optimal control problem. We seek to find a transformation from the state space variables to that of its initial condition space, while maintaining the canonicity of the equations. Thus, we seek to find a transformation between:

$$(\mathbf{q}(t), \boldsymbol{\lambda}(t)) \rightarrow (\mathbf{q}(t_0), \boldsymbol{\lambda}(t_0)) \tag{4.128}$$

for a given time span $t \in [t_0, t_f]$. Assuming we have obtained a generating function (say of type 2), the solution to find the costates for a TPBVP is simply given by

$$\boldsymbol{\lambda} = \frac{\partial \mathcal{S}_2}{\partial \mathbf{q}} \tag{4.129}$$

$$\boldsymbol{q}_0 = \frac{\partial \mathcal{S}_2}{\partial \boldsymbol{\lambda}_0} \tag{4.130}$$

$$0 = \frac{\mathcal{S}_2}{t} + \mathcal{H}\left(\mathbf{q}, \frac{\partial \mathcal{S}_2}{\partial \mathbf{q}}, t\right) \tag{4.131}$$

If such a generating function is found, one can directly evaluate the initial and final costate form

the associated relations of the generating functions by simple partial differentials

$$\boldsymbol{\lambda}_f = \frac{\partial \mathcal{S}_2}{\partial \mathbf{q}}|_{t=t_f, \mathbf{q}=\mathbf{q}_f} \tag{4.132}$$

$$\boldsymbol{\lambda}_0 = \frac{\partial \mathcal{S}_2}{\partial \mathbf{q}_0}|_{t=t_f, \mathbf{q}=\mathbf{q}_f} \tag{4.133}$$

To demonstrate the utility of such a solution methodology, let us look at a simple example of the control of a simple harmonic oscillator.

4.7.2 Simple harmonic oscillator control

The optimal control problem for the simple harmonic oscillator is considered through the minimization of the total control energy through the performance index

$$\mathcal{J} = \frac{1}{2}\int_{t_0}^{t_f} u^2 dt \tag{4.134}$$

subject to the dynamical equations of motion for the simple harmonic oscillator

$$\dot{x}_1 = x_2 \tag{4.135}$$

$$\dot{x}_2 = -x_1 + u \tag{4.136}$$

where u is the control, $[x_1, x_2]$ are the state space variables corresponding to the position and velocity of the harmonic oscillator. We consider a fixed final time problem: let $t_f = 5$ sec and $t_0 = 0$ sec. The augmented cost function (or the Hamiltonian) is then written as

$$\mathcal{H} = \lambda_1 x_2 + \lambda_2(-x_1 + u) + \frac{u^2}{2} \tag{4.137}$$

with λ as the adjoint variables which are the conjugate momenta corresponding to the states (or costates). From Hamilton's equations of motion, the evolution of the costates is governed through

the differential equations:

$$\dot{\lambda}_1 = \lambda_2 \tag{4.138}$$

$$\dot{\lambda_2} = -\lambda_1 \tag{4.139}$$

The stationary condition gives the control that results in the minimization of the Hamiltonian as:

$$0 = \frac{\partial \mathcal{H}}{\partial u} = u + \lambda_2 \qquad \Rightarrow u(t) = -\lambda_2(t) \tag{4.140}$$

The Hamiltonian can then be rewritten as:

$$\mathcal{H} = \lambda_1 x_2 - \lambda_2(x_1 + \lambda_2) + \frac{\lambda_2^2}{2} \tag{4.141}$$

Now, using our methodology from the semi-analytic solution of the Hamilton-Jacobi equation, we seek to find a canonical transformation from the old variable space, i.e. $(x_1, x_2, \lambda_1, \lambda_2)$ to a new set of variables that are the initial conditions of the trajectory, i.e. $(x_{10}, x_{20}, \lambda_{10}, \lambda_{20})$. It is important to note here that any generating function can be used at all times, and the generating function of any type can be transformed to another type through a Legendre transformation. Such a transformation is possible, because all of the generating functions are the solution of the HJ equation for the same Hamiltonian. In general, one cannot know if the generating functions will be defined for all time. It can be proven, however, that they cannot all be singular simultaneously [196, 185]. In fact, Arnold [23, 28] proves that one can define 2^n generating functions, and that at least one must be well-defined. In practice, among the four types of generating functions defined previously, one is always non-singular[197, 185, 110]. Since global singularities correspond to boundary value problems with multiple or infinite solutions, for the formulation of the TPBVP, at initial time the generating function of type 1 and type 4 is singular. This is easily recognized through their definitions, i.e. at time zero, the generating function of type 1 is a function of the variables $\mathcal{S}_1 = \mathcal{S}_1(\mathbf{x}, \mathbf{x}_0) = \mathcal{S}_1\mathbf{x}_0, \mathbf{x}_0)$ which can have infinitely many solutions. A similar situation

occurs for the generating function of type 4, but with the costates: $\mathcal{S}_4 = \mathcal{S}_4(\boldsymbol{\lambda}, \boldsymbol{\lambda}_0) = \mathcal{S}_4(\boldsymbol{\lambda}_0, \boldsymbol{\lambda}_0)$. Therefore, let us assume a generating function of type 2, i.e. of old coordinate and new momenta (costates). The HJ equation is then given by:

$$\frac{\partial \mathcal{S}_2(\mathbf{x}, \boldsymbol{\lambda}_0)}{\partial t} + \mathcal{H}(\mathbf{x}, \frac{\partial \mathcal{S}_2}{\partial \mathbf{x}}, t) = 0 \tag{4.142}$$

The methodology to solve this HJ equation is discussed in previous sections in detail, using sparse grids and the combination of basis functions to approximate the generating function. One important fact to note is that since the costates have no physical significance (for a general nonlinear dynamical system), to find the domain of discretization of the costates, an open-loop control is solved for the edge values of the domain of the states. One can note from Eq. (4.151) and Eq. (4.152) , the costates also behave like the harmonic oscillator, i.e. their phase-volume is also a torus, just like the simple harmonic oscillator. Utilizing the systematic procedure described in previous sections, the HJ equation is solved using an approximate generating function. Using monomials of total degree 2, the coefficients are obtained, as shown in the figure below.

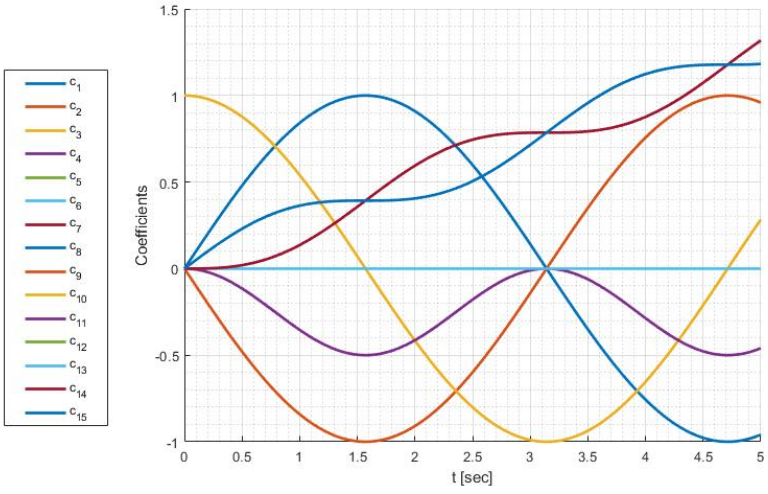

Figure 4.30: Coefficients of the basis functions for the approximate generating function of the van der Pol oscillator

Utilizing these coefficients, a functional form of the generating function can be obtained. Now, given the boundary conditions i.e. $(\mathbf{x}_{t_0}, \mathbf{x}_{t_f})$, the initial and final costates can be found directly from the generating function, as using the relations in Eq. (4.132) and Eq. (4.133) . Utilizing these relations, one can find closed form solutions for the costates given any boundary conditions. For validation purposes of the problem above with 13 basis functions, the closed form expressions for the initial and final costates are given below

$$\lambda_1(t_0) = -\frac{2\,c_4\,c_{15} - 2\,x_{1_0}\,c_{15} - c_{11}\,\left(c_5 - x_{2_0} + x_{1_f}\,c_8 + x_{2_f}\,c_{10}\right) + 2\,x_{1_f}\,c_7\,c_{15} + 2\,x_{2_f}\,c_9\,c_{15}}{4\,c_{14}\,c_{15} - {c_{11}}^2} \tag{4.143}$$

$$\lambda_2(t_0) = -\frac{2\,c_5\,c_{14} - 2\,x_{2_0}\,c_{14} - c_{11}\,\left(c_4 - x_{1_0} + x_{1_f}\,c_7 + x_{2_f}\,c_9\right) + 2\,x_{1_f}\,c_8\,c_{14} + 2\,x_{2_f}\,c_{10}\,c_{14}}{4\,c_{14}\,c_{15} - {c_{11}}^2} \tag{4.144}$$

$$\begin{aligned}\lambda_1(t_f) = {} & \frac{x_{2_0}c_8 - c_5c_8 + 2c_2c_{15} - x_{1_f}{c_8}^2 - x_{2_f}c_8c_{10} + 2x_{2_f}c_6c_{15} + 4x_{1_f}c_{12}c_{15}}{2c_{15}} \\ & - \frac{(c_8c_{11} - 2c_7c_{15})}{2c_{15}\,(4c_{14}c_{15} - {c_{11}}^2)} \\ & \frac{\left(2x_{1_0}c_{15} - x_{2_0}c_{11} + c_5c_{11} - 2c_4c_{15} + x_{1_f}c_8c_{11} - 2x_{1_f}c_7c_{15} + x_{2_f}c_{10}c_{11} - 2x_{2_f}c_9c_{15}\right)}{2c_{15}\,(4c_{14}c_{15} - {c_{11}}^2)}\end{aligned} \tag{4.145}$$

$$\begin{aligned}\lambda_2(t_f) = {} & \frac{x_{2_0}c_{10} - c_5c_{10} + 2c_3c_{15} - x_{2_f}{c_{10}}^2 - x_{1_f}c_8c_{10} + 2x_{1_f}c_6c_{15} + 4x_{2_f}c_{13}c_{15}}{2c_{15}} \\ & - \frac{(c_{10}c_{11} - 2c_9c_{15})}{2c_{15}\,(4c_{14}c_{15} - {c_{11}}^2)} \\ & \frac{\left(2x_{1_0}c_{15} - x_{2_0}c_{11} + c_5c_{11} - 2c_4c_{15} + x_{1_f}c_8c_{11} - 2x_{1_f}c_7c_{15} + x_{2_f}c_{10}c_{11} - 2x_{2_f}c_9c_{15}\right)}{2c_{15}\,(4c_{14}c_{15} - {c_{11}}^2)}\end{aligned} \tag{4.146}$$

The expressions for $\boldsymbol{\lambda}$ are in terms of the boundary conditions. Thus, the methodology provides a way to solve the TPBVP for arbitrary boundary conditions within a domain of discretization. If the final state required is the origin, one can represent the initial costates using the figure below.

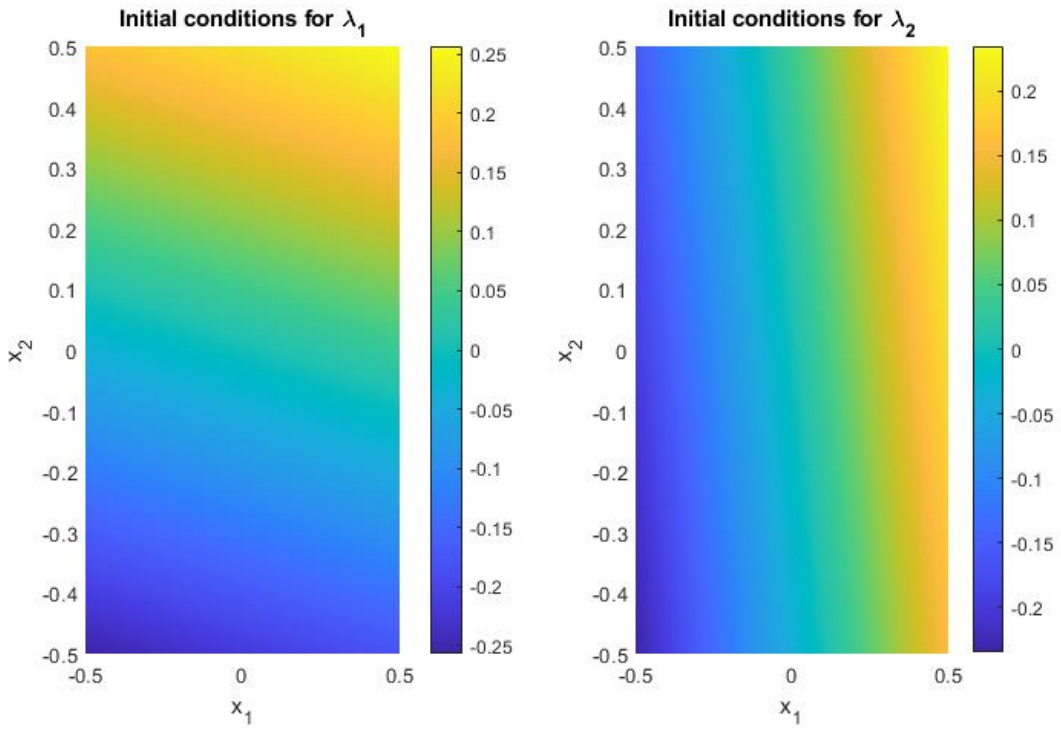

Figure 4.31: The initial condition for the costates for all solutions in the discretized domain of the phase-space for [0,0] final state

The simple harmonic oscillator is a linear dynamical system. In the next section, the control of the nonlinear dynamical system of the van der Pol equation is discussed.

4.7.3 Optimal control of the van der Pol equation

The optimal control problem for the va der Pol oscillator is considered through the minimization of the total control energy through the performance index

$$\mathcal{J} = \frac{1}{2}\int_{t_0}^{t_f} u^2 dt \tag{4.147}$$

subject to the dynamical equations of motion for the van der Pol equation

$$\dot{x}_1 = x_2 \tag{4.148}$$

$$\dot{x}_2 = -x_1 + \epsilon(1 - x_1^2)x_2 + u \tag{4.149}$$

where u is the control, $[x_1, x_2]$ are the state space variables corresponding to the position and velocity of the oscillator. We consider a fixed final time problem: let $t_f = 7$ sec and $t_0 = 0$ sec. The augmented cost function (or the Hamiltonian) is then written after eliminating the control in terms of the costates to minimize the resulting Hamiltonian as

$$\mathcal{H} = \lambda_1 x_2 + \lambda_2(-x_1 + \epsilon(1 - x_1^2)x_2 - \lambda_2) + \frac{\lambda_2^2}{2} \tag{4.150}$$

with $\boldsymbol{\lambda}$ as the adjoint variables which are the conjugate momenta corresponding to the states (or costates). From Hamilton's equations of motion, the evolution of the costates is governed through the differential equations:

$$\dot{\lambda}_1 = \lambda_2(1 + 2\epsilon x_1 x_2) \tag{4.151}$$

$$\dot{\lambda_2} = -\lambda_1 - \epsilon(1 - x_1^2)\lambda_2 \tag{4.152}$$

Now, using our methodology from the semi-analytic solution of the Hamilton-Jacobi equation, we seek to find a canonical transformation from the old variable space, i.e. $(x_1, x_2, \lambda_1, \lambda_2)$ to a new set of variables that are the initial conditions of the trajectory, i.e. $(x_{10}, x_{20}, \lambda_{10}, \lambda_{20})$. We assume a generating function of type 2, i.e. of old coordinate and new momenta (costates). The HJ equation is then given by:

$$\frac{\partial \mathcal{S}_2(\mathbf{x}, \boldsymbol{\lambda}_0)}{\partial t} + \mathcal{H}(\mathbf{x}, \frac{\partial \mathcal{S}_2}{\partial \mathbf{x}}, t) = 0 \tag{4.153}$$

The methodology to solve this HJ equation is discussed in previous sections in detail, using sparse grids and the combination of basis functions to approximate the generating function. Also, note that, just like in the procedure of Hamiltonianizing the non-Hamiltonian system, a perturbation approach is used. Therefore, the value of ϵ must be at least one order of magnitude smaller than the unperturbed problem. Utilizing the systematic procedure described in previous sections, the HJ equation is solved using an approximate generating function. Using monomials of total degree 2, the coefficients are obtained, as shown in the figure below.

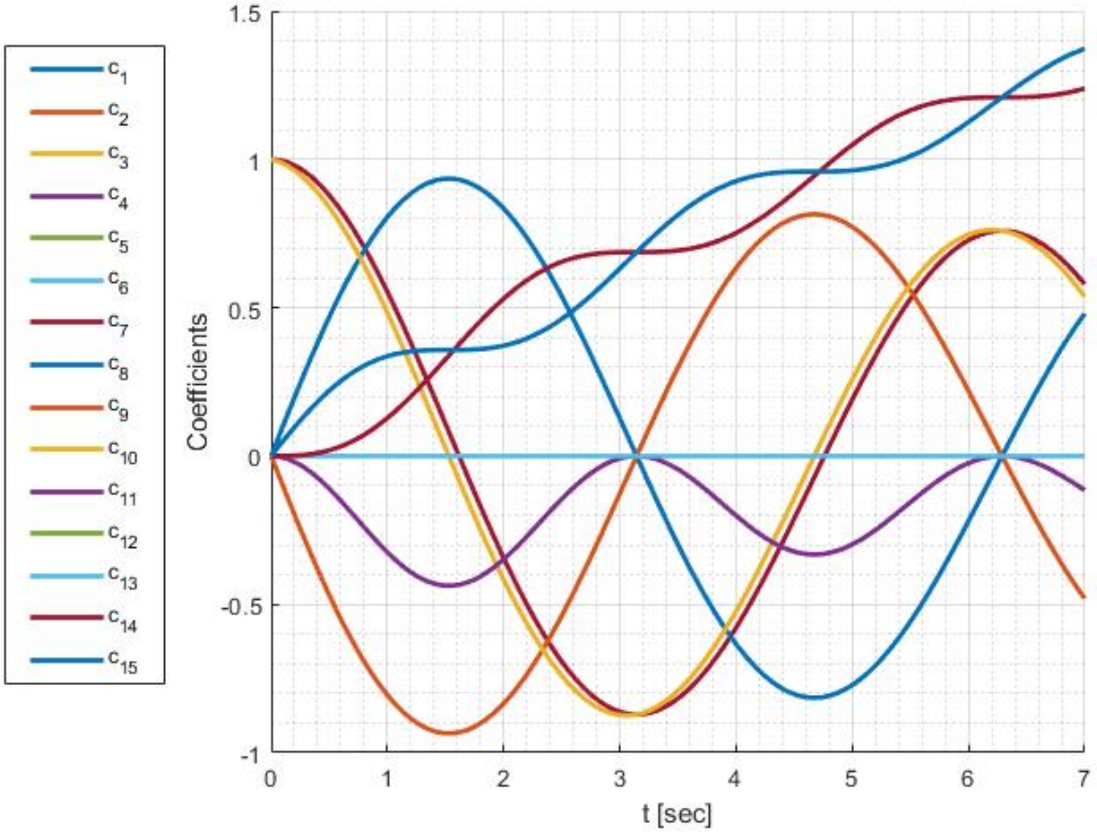

Figure 4.32: Coefficients of the basis functions for the approximate generating function of the van der Pol equation with $\epsilon = 0.1$

Utilizing these coefficients, a functional form of the generating function can be obtained. Now, given the boundary conditions i.e. $(\mathbf{x}_{t_0}, \mathbf{x}_{t_f})$, the initial and final costates can be found directly from the generating function, as using the relations in Eq. (4.132) and Eq. (4.133) . Utilizing these relations, one can find closed form solutions for the costates given any boundary conditions. Since we use the same functional form of the approximate generating function that we used to solve the optimal control problem of the simple Harmonic oscillator, the expressions for the initial and final costates are exactly the same (i.e. Eq. (4.143) - Eq. (4.146)). Thus, all that is required is to vary the coefficients. Of course, just as in the van der Pol equation case, the accuracy in the control is of the order of $\mathcal{O}(\epsilon^2)$. To demonstrate its utility, 300 random initial conditions are chosen to target a specific state within the domain of discretization. It can be seen that each of the TPBVP is solved

to an accuracy of ϵ^2.

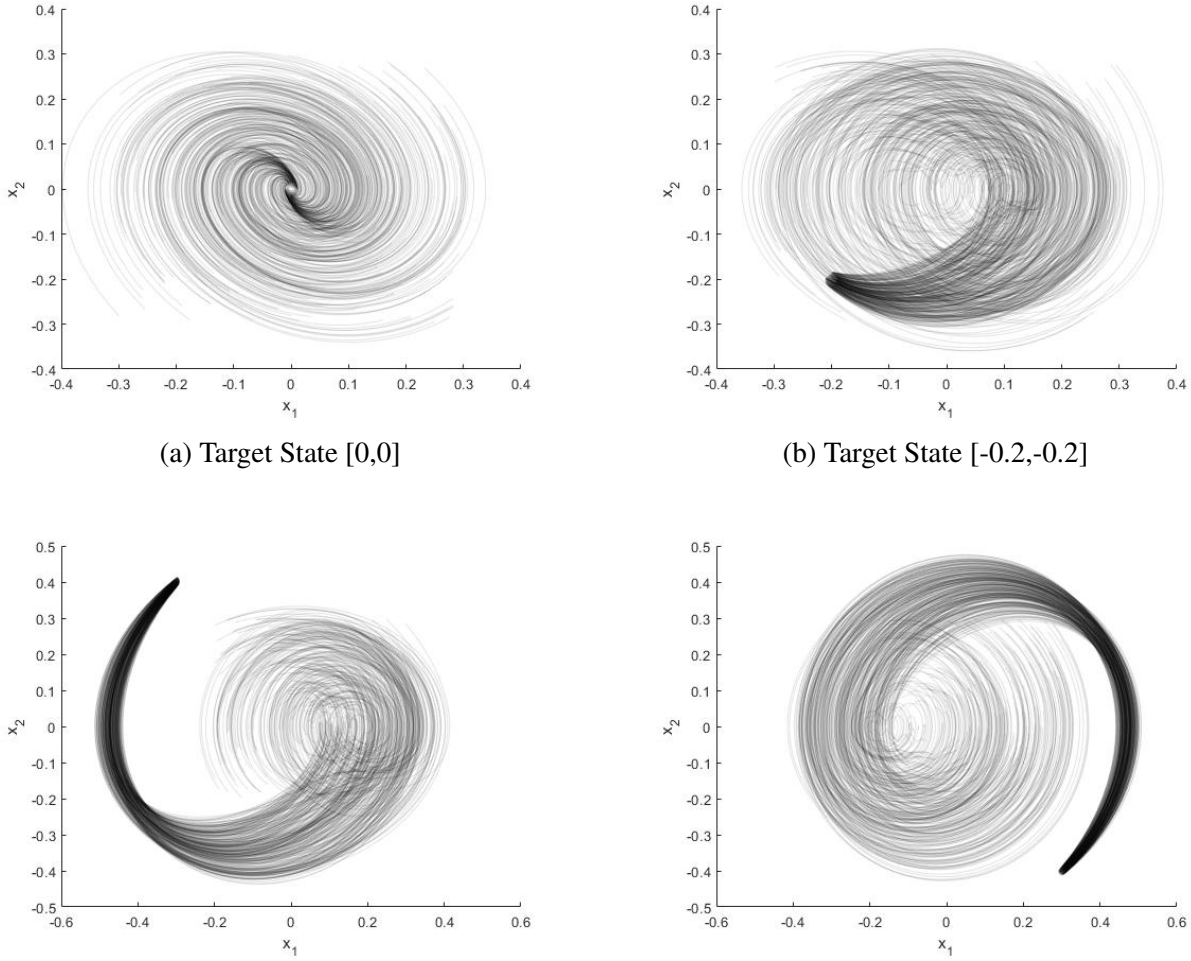

(a) Target State [0,0]

(b) Target State [-0.2,-0.2]

(c) Target State [-0.4,0.4]

(d) Target State [0.3,-0.4]

Figure 4.33: Demonstration of optimal control of the van der Pol equation for random initial conditions and a target final condition with parameters: $t_0 = 0, t_f = 7$ sec, $\epsilon = 0.1$.

Note that each of the TPBVPs was solved directly, and the coefficients of the generating function approximation have to be computed only once. Therefore, we see that the semi-analytical methodology developed can be applied directly to solving optimal control problems. In the next section, the methodology is demonstrated for a higher-dimensional TPBVP of rigid body attitude stabilization.

4.7.4 Semi-analytical solutions to the rigid body attitude stabilization problem

The spin stabilization of a rigid body in a torque free environment is considered, wherein an appropriate feedback control is obtained to suppress the rotational motion of a tumbling rigid body. The optimal control problem is defined through the performance index that minimizes the control energy

$$\mathcal{J} = \frac{1}{2}\int_{t_0}^{t_f} \mathbf{u}^T\mathbf{u}dt \tag{4.154}$$

subject to Euler's dynamical equations of motion:

$$\dot{\omega}_1 = u_1 + K_1\omega_2\omega_3 \tag{4.155}$$

$$\dot{\omega}_2 = u_2 + K_2\omega_1\omega_3 \tag{4.156}$$

$$\dot{\omega}_3 = u_3 + K_3\omega_1\omega_2 \tag{4.157}$$

where $K_1 = \frac{I_2 - I_3}{I_1}$ $K_2 = \frac{I_3 - I_1}{I_2}$ $K_1 = \frac{I_1 - I_2}{I_3}$ are the inertia parameters, I_1, I_2, I_3 are the principal moments of inertia, $\mathbf{u} = [u_1, u_2, u_3]$ is the control, and $\boldsymbol{\omega} = [\omega_1, \omega_2, \omega_3]$ is the angular velocity of the rigid body. The augmented cost function (or the Hamiltonian) can be written as:

$$\mathcal{H} = \frac{1}{2}\mathbf{u}^T\mathbf{u} + \lambda_1(u_1 + K_1\omega_2\omega_3) + \lambda_2(u_2 + K_2\omega_1\omega_3) + \lambda_3(u_3 + K_3\omega_1\omega_2) \tag{4.158}$$

The stationary condition given the relation between the control $\mathbf{u}$ and the costates $\boldsymbol{\lambda}$ through the relation: $\mathbf{0} = \frac{\partial\mathcal{H}}{\partial\mathbf{u}}$. This gives: $u_1 = -\lambda_1$, $u_2 = -\lambda_2$, and $u_3 = -\lambda_3$. Hamilton's equations of

motion can then be written as:

$$\dot{\omega}_1 = K_1\omega_2\omega_3 - \lambda_1 \tag{4.159}$$

$$\dot{\omega}_2 = K_2\omega_1\omega_3 - \lambda_2 \tag{4.160}$$

$$\dot{\omega}_3 = K_3\omega_1\omega_2 - \lambda_3 \tag{4.161}$$

$$\dot{\lambda}_1 = -K_2\lambda_2\omega_3 - K_3\lambda_3\omega_2 \tag{4.162}$$

$$\dot{\lambda}_2 = -K_1\lambda_1\omega_3 - K_3\lambda_3\omega_1 \tag{4.163}$$

$$\dot{\lambda}_3 = -K_1\lambda_1\omega_2 - K_2\lambda_2\omega_1 \tag{4.164}$$

We consider a domain of interest as a unit radius sphere of initial angular velocities. The generating function is approximated using monomials of total degree three, and a sparse grid collocation scheme is used. In six dimensions, the number of basis functions is 84, and the total grid points are 85. To demonstrate the effectiveness of the method, three cases are checked. They are as described in the table below.

Table 4.5: Test cases for attitude stabilization of rigid body

Case	I_1	I_2	I_3	t_0	
1	14 kg.m^2	10 kg.m^2	8 kg.m^2	5 sec	$I_1 > I_2 > I_3$
2	7 kg.m^2	10 kg.m^2	12 kg.m^2	7 sec	$I_1 < I_2 < I_3$
3	14 kg.m^2	10 kg.m^2	12 kg.m^2	7 sec	$I_1 > I_3 > I_2$
4	10 kg.m^2	11 kg.m^2	6 kg.m^2	5 sec	$I_2 > I_1 > I_3$

For each of the cases, 300 random initial conditions are chosen that lie in the domain of interest. The initial costates are obtained from the approximated generating function, exactly as a function of the time varying coefficients. The figures below show the time evolution of the angular velocity under the action of the optimal control. It is seen that all of the initial conditions are brought to zero (accurate to the order of the error in the approximated generating function) in the TPBVP, thereby achieving a detumbling or stabilization of the attitude motion of the rigid body.

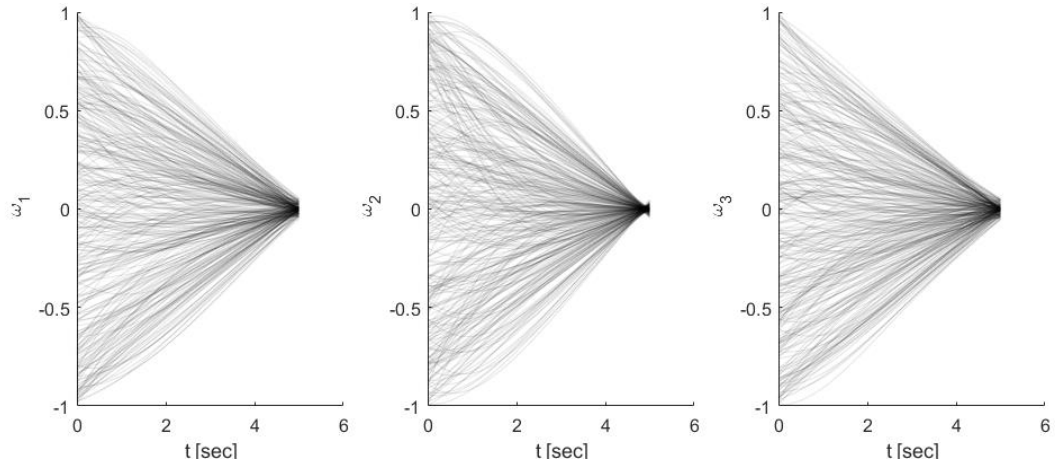

Figure 4.34: Attitude stabilization for Case 1

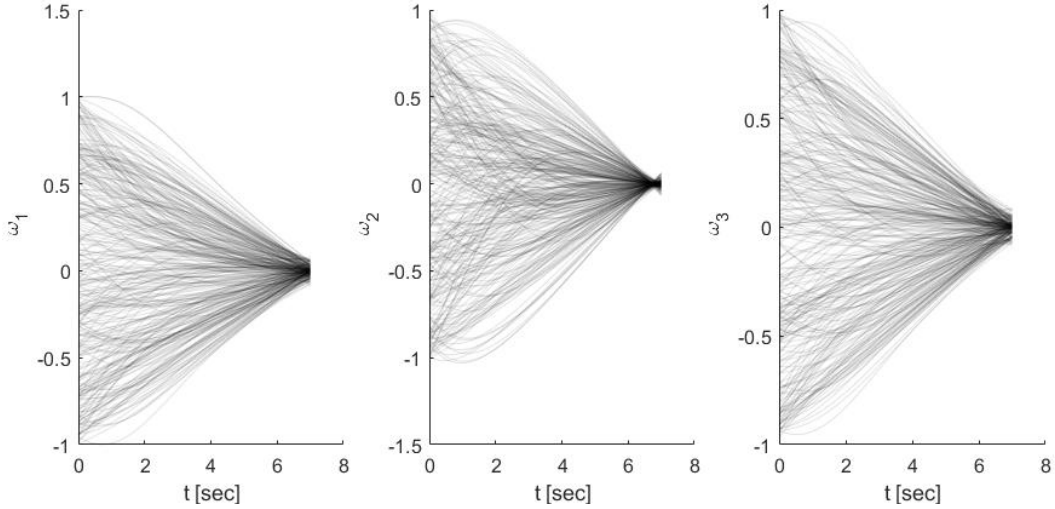

Figure 4.35: Attitude stabilization for Case 2

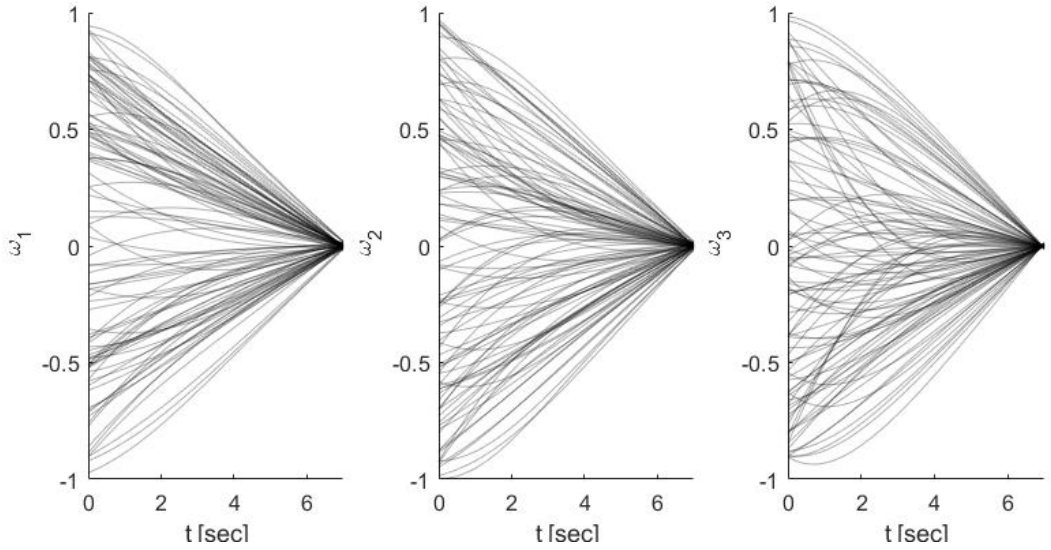

Figure 4.36: Attitude stabilization for Case 3

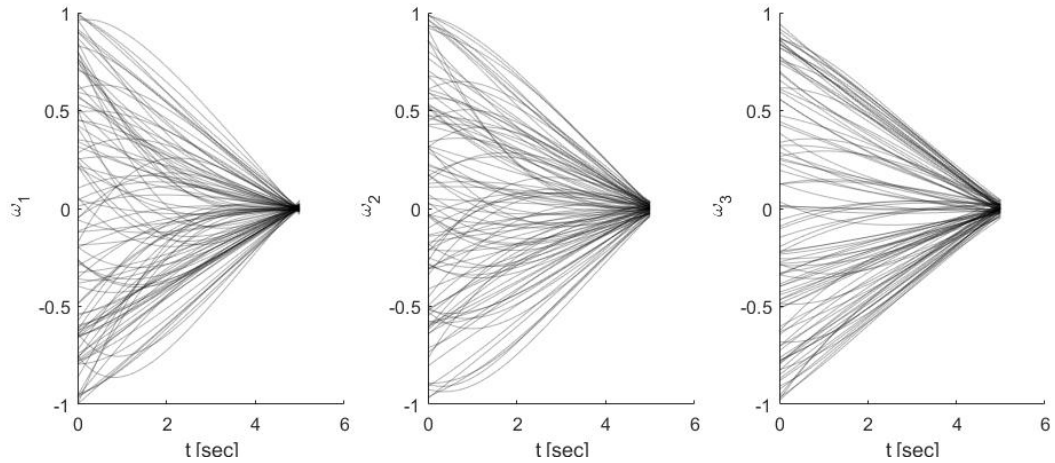

Figure 4.37: Attitude stabilization for Case 4

The figures: 4.34, 4.35, 4.36, and 4.37 show the state flow of the closed loop dynamical system with a stabilizing feedback control. Again, note that for each of the cases, the coefficients are found only once, by solving the HJ equation on the grid, to enable the transformation from the

state-space variables to those of its initial conditions, i.e.

$$(\boldsymbol{\omega}, \boldsymbol{\lambda}) \rightarrow (\boldsymbol{\omega}_0, \boldsymbol{\lambda}_0)$$

Therefore, equating partials of the generating function at final time allows us to apply the boundary conditions that give the initial and final costates. Note that one only needs to algebraically solve for the initial costates from the associated relations of the generating function (Eq. (4.132) and Eq. (4.133)). Some further deliberations on the coefficients are done in the next section.

4.7.4.1 A note on the sparsity of the coefficients

We note here that certain insight can be obtained from the structure of the equations and the Hamiltonian. These observations are summarized below:

1. The costates are linear in the Hamiltonian.
2. Each control input u_i depends only on its corresponding costate λ_i.
3. The Hamiltonian is autonomous, thus the coefficients contributing to the HJ solution have structure.
4. The control-free Hamiltonian is completely integrable

Because of the observations above, one can assume with a reasonable amount of certainty that the generating function is separable. This allows us to seek a higher degree polynomial approximation of the generating function, while keeping the number of the basis functions the same as before or even less. For reference, one can note that the number of basis functions for a separable approximation of the generating function of degree four is 43, degree five is 61, degree six is 82, and so on.

Furthermore, if we were to note the evolution of the coefficients for the higher order approximation, we observe that only six basis functions contribute to the true solution for the control. They are the quadratic terms: $\omega_1\lambda_{10}, \quad \omega_2\lambda_{20}, \quad \omega_3\lambda_{30}, \quad \lambda_{10}^2, \quad \lambda_{20}^2, \quad \lambda_{30}^2$. The remaining coefficients are

zero and do not contribute to the solution. It is indeed remarkable that the proposed methodology identifies the purely quadratic form without the cross terms from the oversized set of basis functions. Therefore, one can then identify a linear feedback control law for the spin-stabilization problem. This result agrees with the seminal solution established by Debs and Athans [198]. This unique closure with an established analytical solution provides strong evidence in support of the utility of the proposed approach.

4.8 Summary

In this chapter, a general method to obtain canonical transformations that rectifies the flow of a dynamical system is proposed. By utilizing a family of trajectories in the domain of the relevant phase volume, the sparse approximation problem for the coefficients of the generating function is formulated and solved efficiently, for arbitrary choice of basis function sets. The uniqueness of the solution is shown to be the realization of an analytical expression for the generating function from the use of numerical approximation problem. Two numerical examples of a simple harmonic oscillator and a Duffing oscillator are presented. Critical factors affecting the solution, such as the choice of the basis functions, coverage of the phase-space of old and new variables, and switch in the generating function to obtain a solution to the dynamical system, are presented. The sparsity of the coefficients in approximating the solution of the dynamical system proves valuable in discerning the final functional form for the evolution of the states. The method is refined to overcome the deficiencies by utilizing the information from the dominant physics. A semi-analytical solution to the time-dependent HJ equation is obtained by leveraging developments in sparse-approximation techniques through a collocation based scheme. This solution rectifies the flow of the perturbative part of the Hamiltonian. The utility of this method is demonstrated by solving the dynamical system of the Duffing oscillator. It is shown that the HJ solution obtained accurately captures the secular and periodic variations. Another advantage of the proposed method is that additional perturbations can be added and their corresponding generating functions can be solved for independently thus equipping us with the freedom to parallelize the process for computational efficiency. The functional form of the generating function also admits the formulation of a semi-analytical

state transition matrix.

The main problem in artificial satellite theory is considered as an example to demonstrate the utility of the proposed method. It is shown through three different cases: geosynchronous orbit, low Earth orbit and Medium Earth orbit at critical inclination that the Hamiltonian perturbations' method performs well up to a certain tolerance. Because the error in the approximated generating function is available, these errors are reduced by appropriately resizing the domain and through the addition of basis functions. A semi-analytical formulation for the state transition matrix is also given for the J_2 perturbed two-body problem in terms of the coefficients of the basis functions.

Furthermore, this chapter also treats the case of a general dynamical system admitting a non-conservative Hamiltonian. Utilizing the extended phase-space mechanics from previous chapters, we propose a methodology to Hamiltonianize non-Hamiltonian dynamical systems. The methodology developed thus serves a variety of purposes, from obtaining semi-analytical solutions to a dynamical system (Hamiltonian and non-Hamiltonian), and solving Two Point Boundary Value Problems (TPBVP). Furthermore, the HJ theory serves as a single overarching principle to a multitude of sub-disciplines, such as in optimal control and differential games through the Hamilton-Jacobi-Bellman and Hamilton-Jacobi-Isaac equations, or in general relativity through Hamilton-Jacobi-Einstein equations, or in light propagation and optics through the Eikonal equations, and many more. Therefore, the systematic procedure developed in this dissertation proves to be an encouraging step towards solving the HJ equation for applications to different arrays of problems in mechanics and engineering, specifically to treat a large class of dynamical systems. Our approach throughout this chapter has been to solve the HJ equation locally so as to ensure that the resulting form of the Hamiltonian in the transformed coordinates is zero, i.e.$\frac{\partial \mathcal{S}}{\partial t} + \mathcal{H} = \mathcal{K} = 0$. This process then renders the new variables constant for all time, thereby allowing us to obtain simple solutions to the dynamical system under consideration. Such transformations are termed rectification. The procedure of rectification is valuable in treating all kinds of dynamical systems and offers simple algebraic (depending on the approximation of the HJ solution) transformations to the original coordinates of interest. Advantages of such a rectification process are evident in obtaining the

solution to the TPBVP. We admit that the solution procedure to solve the HJ equation through the use of Galerkin type approximation may not be the best method, and other intensive methods can be used to solve the PDE within our domain of interest to obtain a more accurate solution. However, we have shown that adding basis functions and adjusting the decomposition of the domain allows us to reduce the error in the approximation, thereby empirically proving a convergence of our methodology. This indicates that with sufficient computational power and efficient methods, the HJ PDE can be solved to better accuracy. While this is a numerical issue, the fundamentals of the HJ theory outlined in this dissertation can be utilized to its full potential to obtain approximate semi-analytical solutions to a broad class of dynamical systems.

5. CONCLUDING REMARKS

This dissertation represents a first step to understanding the geometry and dynamics of complex motions. It encompasses a wide array of dynamical systems and their treatment through a broad spectrum of qualitative, analytic and semi-analytic methods. This work investigates a modern approach to mechanics, to address questions concerning approximation, symmetry and reduction, symplectic structure, relative equilibria, canonical transformations and rectification, bifurcations and chaos, and associated nonlinear stability problems. The methodologies developed naturally relate to problems of current and future interests, such as rigid body attitude motions, and multi-body dynamical environments. The geometric, analytic, and semi-analytic framework adopted here should help understand and explore some of the deep and exciting questions in astrodynamics. A number of analysis tools are presented in this investigation, including the development of qualitative tools, including the Binet-Poincaré surface of sections, stroboscopic maps, energy-based approaches to quantify internal resonances, momentum maps, velocity surfaces, etc., analytical treatment of dynamical systems for slow and fast-rotating rigid bodies through averaging techniques, semi-analytic tools for rectification of dynamical systems and their extensions to optimal control problems. While this investigation represents only part of a larger, ongoing research effort, it is intended to offer practical approaches and insightful results for an expansive treatment of general dynamical systems. The results of this work are summarized and recommendations for future work are suggested.

5.1 Investigation Summary

Qualitative treatment of dynamical systems: The qualitative treatment of dynamical systems utilizes tools of dynamical systems theory to obtain geometric insights into the nature of motions of a dynamical system. Particularly, two complex dynamical systems are considered: the attitude motion of a rigid body and the planar circular restricted three-body problem. These dynamical systems exhibit an extensive range of dynamical behavior, such as periodic solutions, quasi-periodic

solutions, parametric bifurcations, and chaotic motions.

A comprehensive exploration of the motions of particles under the framework of the planar circular restricted three-body problem led to the identification and characterization of complex dynamical structures in the Earth-Moon-Satellite multi-body system. The concept of momentum maps is introduced to interpret global dynamics of flow in dynamical systems, particularly in the vicinity of the invariant manifolds. Through the use of the inside-out topology introduced in this work, the structure of the invariant manifolds is examined in the Earth and Moon neighborhood in an effort to search for efficient direct transfers from the Earth to the Moon. The efficacy of the momentum maps is demonstrated by developing a catalog of direct transfers in the Cislunar region. A geometric analysis tool based on the velocity surfaces at different isoenergetic levels of the three-body dynamical system is developed that enables the identification of transport opportunities to Lyapunov orbits with little computational effort.

The attitude motion of a rigid body is considered under the framework of four variations of the dynamical model: the planar pitch dynamics of a rigid body in circular orbit, the planar pitch dynamics in a Keplerian orbit, the full (roll-pitch-yaw) motion of a rigid body in circular orbit, and the full dynamics of a rigid body in an eccentric orbit. Parametric dependencies influence the dynamical behavior, such as the moment of inertia and the eccentricity of the orbital motion. The dynamical system is described using classical Rodrigues parameters to exploit the pure algebraic form of the resulting equations of motion. The governing equations of roll and yaw vanish with zero initial conditions. This is identified in this work as a one-way decoupling between the pitch and roll-yaw motions. Such a decoupling allows for the study of pitch motions exclusively. The planar pitch motion of a rigid body in a circular orbit is completely reduced by obtaining an integral of motion. The existence of an integral of motion results in a co-dimension one sub-manifold of the phase space, using which an Eigenvalue analysis gives the analytical limit for motion along the separatrix, thus furnishing the boundary between oscillatory and tumbling motions. The inclusion of eccentricity introduces an external forcing term, which is studied through the use of bifurcation diagrams and stroboscopic maps depending on the eccentricity parameter. For the full dynamical

system, the stability of oscillations about an equilibrium point is investigated. Leveraging the conservation principles of gravity-gradient torques, a method of energy balance is used to determine the regions of high energy exchange in the inertia parameter space for a rigid body in a circular orbit. The apparent instability observed in the Lagrange region of the inertia parameter space is shown to be an exchange of energy between the pitch and roll-yaw motions. A method of visualizing the rigid body motion in torqued environments is also developed through the construction of an osculating polhode. A new metric to quantify the coupling between the state variables of pitch and roll-yaw motions by utilizing the information in the state transition matrix is also developed. While this metric can be applied to any dynamical system, for the case of a rigid body, this coupling is directly linked to the energy exchange between the pitch and roll-yaw motions. Noting that the gravity-gradient torque developed for the analysis of rigid body motion is an approximation to second order in the moment of inertia, a higher order gravity-gradient potential is developed and investigated for relative equilibria for a cuboidal configuration of the rigid body. The roll-pitch-yaw rigid body motion in an eccentric orbit is investigated from the point of view of the Serret-Andoyer variables. Certain simplifications are introduced that aid in the reduction of the problem and the identification of equilibrium configurations for a triaxial rigid body.

Analytic treatment of dynamical systems: The attitude motion of a rigid body is exclusively studied from an analytic perspective. Two broad cases for the rigid body motion are considered: the case of a fast-rotating rigid body, and that of a slow-rotating rigid body. The former case follows the development of a dynamical system targeted at studying the long-term dynamics of a rigid body, and is comparable to that of the motion of artificial satellites. The latter case is studied specifically to treat the attitude motion of large celestial bodies that rotate slowly as compared to artificial satellites. Such rigid bodies exhibit an external resonant commensurability between the spin and orbital motion. In this work, the Hamiltonian formulation of the attitude motion of a rigid body in a Keplerian orbit has been developed. This formulation has been done in the Serret-Andoyer variables. A Lie-series perturbation approach is used to average out the short period terms, and the averaged Hamiltonian up to fourth-order is obtained. The short period terms for the fast-rotating

rigid body dynamical system are associated with the coordinate corresponding with the angular momentum conjugate momenta, and that for the slow-rotating rigid body dynamical system is associated with the orbital mean anomaly. The extended phase-space mechanics is introduced to preserve the constant nature of the Hamiltonian and treat the external periodic forcing introduced due to the eccentricity.

Certain simplifying assumptions (like axisymmetric oblate rigid body assumption) enable us to reduce the dynamical system so that it can be treated from an analytic viewpoint and obtain physical insights into the long-term motions of the rigid body, such as relative equilibria, and critical inclinations. It is noticed that the averaged motions of a rigid body in a circular orbit may behave as if they were in a torque-free motion at the critical inclinations. These effects of critical inclinations however, disappear at fourth-order. A systematic procedure to treat slow-rotating rigid bodies in eccentric orbits has also been presented. Several interesting insights have been discussed, including the development of the resonant Hamiltonian, the existence of resonant commensurabilities and relative equilibria for commensurable frequencies of spin-orbit coupling. The effects of the nodal and apsidal precession are introduced in the Hamiltonian to facilitate a one-way coupling between the orbital and attitude variables. The evolution of the relative equilibria under the influence of these precession terms is studied. A major contribution of this work is the development of a theory for lunar librations under the framework of the simplified Hamiltonian developed in this dissertation. The three primary modes of free lunar librations of the moon: the longitudinal mode (with frequency of 2.9 years), the longitudinal mode (with frequency of 81 years), and the wobble mode (with frequency of 75 years) are studied. Their frequencies are obtained with conscientious agreements with experimental data, thereby bridging the gap between analytic and experimental results.

Semi-analytic treatment of dynamical systems: In this investigation, both numerical and analytic methods are shown to rely heavily on the manner in which they are described: i.e., the coordinate system used. Consequently, a judicious choice of the coordinate system dramatically simplifies the problem at hand. Through the use of Hamilton-Jacobi theory and recent advances

in approximation theory, this work presents a systematic procedure to mathematically obtain the best choice of coordinates that simplify the evolution of a dynamical system through rectification. The uniqueness of the solution is shown to be the realization of an analytical expression for the generating function from the use of numerical approximation problem. Another advantage of the proposed method is that additional perturbations can be added and their corresponding generating functions can be solved for independently thus equipping us with the freedom to parallelize the process for computational efficiency. The functional form of the generating function also admits the formulation of a semi-analytical state transition matrix.

This work can be broadly divided into three objectives: the treatment of Hamiltonian dynamical systems, treatment of non-conservative Hamiltonian systems, and applications to optimal control and two-point boundary value solutions. The main problem in artificial satellite theory is considered as an example to demonstrate the utility of the proposed method for Hamiltonian systems. It is shown through multiple cases that the canonical perturbations' method developed in this work performs well up to a certain tolerance. Because the error in the approximated generating function is known exactly, these errors are reduced by appropriately resizing the domain and by expanding the basis-function dictionary. Utilizing the extended phase-space mechanics from previous chapters, a methodology to Hamiltonianize non-Hamiltonian dynamical systems is presented. It is legitimized through the treatment of many dynamical systems, like the Duffing equation, the van der Pol equation, the simple harmonic oscillator with cubic damping, and others. The rectification methodology is then applied to solve the two-point boundary value problem for the van der Pol equation and the attitude stabilization problem in finite time. The fundamentals of the Hamilton-Jacobi theory outlined in this dissertation can be utilized to its full potential to obtain approximate semi-analytical solutions to a broad class of dynamical systems.

5.2 Recommendations for future work

As is the case with many research endeavors, options for future work are numerous. A few areas of interest that could serve to enhance and continue the investigation are as follows. The development of dynamical models for the attitude motion of slow and fast rotating rigid bodies,

as well as multi-body dynamics, has applications in investigating the long-term evolution of space debris in the earth and the cislunar environment. Of particular interest is to potentially use information from Cassini's states for synchronous motions, and to develop disposal strategies for spent space objects.

Another interesting application of our work is towards the investigation of resonant motions of celestial bodies exhibiting chaotic motions, such as the motion of Hyperion. Furthermore, the parametric study into the nature of oscillations for pre and post impact effects and momentum transfer dynamics can be examined. This can be extensively used to study feasibility of the upcoming Double Asteroid Redirection Test (DART) mission by NASA.

Finally, one could utilize the semi-analytic methodology developed in this work towards a multitude of applications. Since the Hamilton-Jacobi theory serves as a single overarching principle to many sub-disciplines, such as in optimal control and differential games through the Hamilton-Jacobi-Bellman and Hamilton-Jacobi-Isaac equations, or in general relativity through Hamilton-Jacobi-Einstein equations, or in light propagation and optics through the Eikonal equations, and many more. Extension of the canonical perturbation methods developed in this work can be used to treat large scale optimal control problems, evaluate optimality of neighboring solutions, applications to land, air, and space vehicles, self-driving mechanics, motion planning, fleet dynamics, network delays, etc. Game theoretic applications can be investigated through the use of the Hamilton-Jacobi Isaacs equation, with a particular focus on human-machine interactions, prediction and mitigation strategies, etc. The semi-analytic methods for rectification and averaging developed in this paper are envisioned to enforce Arnold's observation: *The technique of generating functions for canonical transformations, developed by Hamilton and Jacobi, is the most powerful method available for integrating the differential equations of dynamics.*

REFERENCES

[1] R. T. Eapen, M. Majji, and K. T. Alfriend, "Attitude dynamics of a rigid body in keplerian motion," *Celestial Mechanics and Dynamical Astronomy*, vol. 133, no. 1, pp. 1–25, 2021.

[2] T. Kane, "Attitude stability of earth-pointing satellites," *AIAA Journal*, vol. 3, no. 4, pp. 726–731, 1965.

[3] A. Deprit, "Free rotation of a rigid body studied in the phase plane," *American Journal of Physics*, vol. 35, no. 5, pp. 424–428, 1967.

[4] P. Gurfil, A. Elipe, W. Tangren, and M. Efroimsky, "The serret-andoyer formalism in rigid-body dynamics: I. symmetries and perturbations," *Regular and Chaotic Dynamics*, vol. 12, no. 4, pp. 389–425, 2007.

[5] D. Pflüger, B. Peherstorfer, and H.-J. Bungartz, "Spatially adaptive sparse grids for high-dimensional data-driven problems," *Journal of Complexity*, vol. 26, no. 5, pp. 508–522, 2010.

[6] D. E. Smith, M. T. Zuber, R. J. Phillips, S. C. Solomon, S. A. Hauck, F. G. Lemoine, E. Mazarico, G. A. Neumann, S. J. Peale, J.-L. Margot, *et al.*, "Gravity field and internal structure of mercury from messenger," *science*, vol. 336, no. 6078, pp. 214–217, 2012.

[7] B. A. Archinal, M. F. A'Hearn, E. Bowell, A. Conrad, G. J. Consolmagno, R. Courtin, T. Fukushima, D. Hestroffer, J. L. Hilton, G. A. Krasinsky, *et al.*, "Report of the iau working group on cartographic coordinates and rotational elements: 2009," *Celestial Mechanics and Dynamical Astronomy*, vol. 109, no. 2, pp. 101–135, 2011.

[8] P. Bretagnon, "Theory for the motion of all the planets-the vsop82 solution," *Astronomy and Astrophysics*, vol. 114, pp. 278–288, 1982.

[9] D. H. Eckhardt, "Theory of the libration of the moon," *The Moon and the planets*, vol. 25, no. 1, pp. 3–49, 1981.

[10] N. Rambaux and E. Bois, "Theory of the mercury's spin-orbit motion and analysis of its main librations," *Astronomy & Astrophysics*, vol. 413, no. 1, pp. 381–393, 2004.

[11] S. Chapra and R. Canale, "Numerical methods for engineers 7th edn (columbus," 2015.

[12] J. G. Williams, A. S. Konopliv, D. H. Boggs, R. S. Park, D.-N. Yuan, F. G. Lemoine, S. Goossens, E. Mazarico, F. Nimmo, R. C. Weber, *et al.*, "Lunar interior properties from the grail mission," *Journal of Geophysical Research: Planets*, vol. 119, no. 7, pp. 1546–1578, 2014.

[13] F. Varadi, S. Musotto, W. Moore, and G. Schubert, "Normal modes of synchronous rotation," *Icarus*, vol. 176, no. 1, pp. 235–249, 2005.

[14] E. Bois and D. Vokrouhlicky, "Relativistic spin effects in the earth-moon system.," *Astronomy and Astrophysics*, vol. 300, p. 559, 1995.

[15] R. B. Roncoli, "Lunar constants and models document," *JPL D-32296, Sept*, 2005.

[16] J. Guckenheimer and P. Holmes, *Nonlinear oscillations, dynamical systems, and bifurcations of vector fields*, vol. 42. Springer Science & Business Media, 2013.

[17] T. Paul, "On the status of perturbation theory," *Mathematical Structures in Computer Science*, vol. 17, no. 2, pp. 277–288, 2007.

[18] H. Poincaré, "Sur les équations aux dérivées partielles de la physique mathématique," *American Journal of Mathematics*, pp. 211–294, 1890.

[19] H. Poincaré, *Les méthodes nouvelles de la mécanique céleste*, vol. 3. Gauthier-Villars, 1899.

[20] H. Poincaré *et al.*, "Sur une forme nouvelle des équations du problème des trois corps," *Acta Mathematica*, vol. 21, pp. 83–97, 1897.

[21] G. D. Birkhoff, *Dynamical systems*, vol. 9. American Mathematical Soc., 1927.

[22] V. I. Arnold, V. V. Kozlov, and A. I. Neishtadt, *Mathematical aspects of classical and celestial mechanics*, vol. 3. Springer Science & Business Media, 2007.

[23] V. I. Arnold, "The topology of real algebraic curves," in *Vladimir I. Arnold-Collected Works*, pp. 251–253, Springer, 1973.

[24] S. Smale *et al.*, "Differentiable dynamical systems," *Bulletin of the American mathematical Society*, vol. 73, no. 6, pp. 747–817, 1967.

[25] S. Smale, "Problems on the nature of relative equilibria in celestial mechanics," in *Manifolds—Amsterdam 1970*, pp. 194–198, Springer, 1971.

[26] S. H. Strogatz, *Nonlinear dynamics and chaos: With applications to physics, biology, chemistry, and engineering*. CRC press, 2018.

[27] D. T. Greenwood, *Classical dynamics*. Courier Corporation, 1997.

[28] V. I. Arnol'd, *Mathematical methods of classical mechanics*, vol. 60. Springer Science & Business Media, 2013.

[29] J. L. Junkins and H. Schaub, *Analytical mechanics of space systems*. American Institute of Aeronautics and Astronautics, 2009.

[30] J. L. Junkins and J. D. Turner, *Optimal spacecraft rotational maneuvers*. Elsevier, 2012.

[31] E. T. Whittaker, *A treatise on the analytical dynamics of particles and rigid bodies*. CUP Archive, 1937.

[32] P. C. Hughes, *Spacecraft attitude dynamics*. Courier Corporation, 2012.

[33] H. Schaub, J. L. Junkins, *et al.*, "Stereographic orientation parameters for attitude dynamics: A generalization of the rodrigues parameters," *Journal of the Astronautical Sciences*, vol. 44, no. 1, pp. 1–19, 1996.

[34] C. Truesdell, "The rational mechanics of flexible or elastic bodies: 1638-1788," *Leonhardi Euleri Opera Omnia, Ser. 2*, 1960.

[35] M. Abramowitz, I. A. Stegun, and R. H. Romer, "Handbook of mathematical functions with formulas, graphs, and mathematical tables," 1988.

[36] D. DeBra, R. Delp, *et al.*, "Rigid body attitude stability and natural frequencies in a circular orbit," *J. Astronaut. Sci*, vol. 8, no. 1, pp. 14–17, 1961.

[37] L. Meirovitch and F. B. Wallace, *Attitude stability of a spinning passive orbiting satellite*, vol. 665. National Aeronautics and Space Administration, 1967.

[38] H. A. Karasopoulos, *Nonlinear dynamics of the planar pitch attitude motion for a gravity-gradient satellite*. University of Cincinnati, 1994.

[39] T. R. Smith and N. Bosanac, "Motion primitives summarizing periodic orbits and natural transport mechanisms in the earth-moon system,"

[40] J. Breakwell and R. Pringle Jr, "Nonlinear resonance affecting gravity-gradient stability.," 1966.

[41] D. Hitzl, "Nonlinear attitude motion near resonance.," *AIAA Journal*, vol. 7, no. 6, pp. 1039–1047, 1969.

[42] V. Modi and R. Brereton, "Periodic solutions associated with the gravity-gradient-oriented system. i-analytical and numerical determination.," *AIAA Journal*, vol. 7, no. 7, pp. 1217–1225, 1969.

[43] X. Tong and F. P. Rimrott, "Numerical studies on chaotic planar motion of satellites in an elliptic orbit," *Chaos, Solitons & Fractals*, vol. 1, no. 2, pp. 179–186, 1991.

[44] V. Beletski, "Motion of an artificial satellite about its center of mass', translated from russian," *NASA TT F-429, TT67-51366*, 1966.

[45] H. A. Karasopoulos and D. L. Richardson, "Investigation of chaotic motions for a gravity-gradient satellite in orbit about an oblate central body," in *Graz International Astronautical Federation Congress*, 1993.

[46] V. Beletsky, "The libration of a satellite on an elliptic orbit," in *Dynamics of Satellites/Dynamique des Satellites*, pp. 219–230, Springer, 1963.

[47] V. Zlatoustov, D. Okhotsimsky, V. Sarychev, and A. Torzhevsky, "Investigation of a satellite oscillations in the plane of an elliptic orbit," in *Applied mechanics*, pp. 436–439, Springer, 1966.

[48] B. Koch and B. Bruhn, "Chaotic and periodic motions of satellites in elliptic orbits," *Zeitschrift für Naturforschung A*, vol. 44, no. 12, pp. 1155–1162, 1989.

[49] V. Zlatoustov and A. Markeev, "Stability of planar oscillations of a satellite in an elliptic orbit," *Celestial mechanics*, vol. 7, no. 1, pp. 31–45, 1973.

[50] R. H. Battin, *An Introduction to the Mathematics and Methods of Astrodynamics, revised edition*. American Institute of Aeronautics and Astronautics, 1999.

[51] L. Meirovitch, *Methods of analytical dynamics*. Courier Corporation, 2010.

[52] M. R. C. da Silva, "Attitude stability of a gravity-stabilized gyrostat satellite," *Celestial mechanics*, vol. 2, no. 2, pp. 147–165, 1970.

[53] R. Pringle Jr, "Effect of perturbed orbital motion on a spinning symmetrical satellite," *Journal of Spacecraft and Rockets*, vol. 11, no. 7, pp. 451–455, 1974.

[54] R. T. Eapen and C. Frueh, "Averaged solar radiation pressure modeling for high area-to-mass ratio objects in geosynchronous orbits," *Advances in Space Research*, vol. 62, no. 1, pp. 127–141, 2018.

[55] R. T. Eapen, *Averaged Solar Radiation Pressure Modeling for High Area-to-Mass Ratio Objects in Geostationary Space*. PhD thesis, Purdue University, 2017.

[56] C. Früh and T. Schildknecht, "Attitude motion of space debris objects under influence of solar radiation pressure and gravitiy," in *63rd international Astronautical congress*, 2012.

[57] R. Eapen, M. Majji, and K. T. Alfriend, "Equilibria associated with the attitude dynamics of a rigid body in keplerian motion," in *AAS/AIAA Astrodynamics Specialist Conference*, 2018.

[58] J. L. Junkins and P. Singla, "How nonlinear is it? a tutorial on nonlinearity of orbit and attitude dynamics," *Advances in the Astronautical Sciences*, vol. 115, no. SUPPL., pp. 1–45, 2003.

[59] M. Cullagh, "On the rotation of a solid body," *Proceedings of the Royal Irish Academy (1836-1869)*, vol. 2, pp. 520–526, 1840.

[60] O. Gerlach, "Attitude stabilization and control of earth satellites," *Space Science Reviews*, vol. 4, no. 4, pp. 541–582, 1965.

[61] M. Vitins, "Keplerian motion and gyration," *Celestial mechanics*, vol. 17, no. 2, pp. 173–192, 1978.

[62] L. Landau and E. Lifshitz, "Mechanics, course of theoretical physics, volume 1. butterworth-heinemann," 1976.

[63] O. Winter and C. Murray, "Resonance and chaos: I. first-order interior resonances," *Astronomy and Astrophysics*, pp. 290–304, 1997.

[64] R. De la Llave *et al.*, "A tutorial on kam theory," in *Proceedings of Symposia in Pure Mathematics*, vol. 69, pp. 175–296, Citeseer, 2001.

[65] V. F. Lazutkin, *KAM theory and semiclassical approximations to eigenfunctions*, vol. 24. Springer Science & Business Media, 2012.

[66] G. Floquet, "Sur les équations différentielles linéaires à coefficients périodiques," in *Annales scientifiques de l'École normale supérieure*, vol. 12, pp. 47–88, 1883.

[67] I. G. Malkin, *Theory of stability of motion*, vol. 3352. US Atomic Energy Commission, Office of Technical Information, 1959.

[68] C. Früh, T. M. Kelecy, and M. K. Jah, "Coupled orbit-attitude dynamics of high area-to-mass ratio (hamr) objects: influence of solar radiation pressure, earth's shadow and the visibility in light curves," *Celestial Mechanics and Dynamical Astronomy*, vol. 117, no. 4, pp. 385–404, 2013.

[69] V. Kuryakov, "A method of constructing polhodes of an intermediate motion in the dynamics of a rigid body," *Journal of Applied Mathematics and Mechanics*, vol. 50, no. 5, pp. 666–669, 1986.

[70] H. Goldstein, "Classical mechanics, volume i," 1953.

[71] A. Deprit and A. Elipe, "Complete reduction of the euler–poinsot problem," *Journal of the Astronautical Sciences*, vol. 41, no. 4, pp. 603–628, 1993.

[72] J. A. Serret, *Mémoire sur l'emploi de la méthode de la variation des arbitraires dans la théorie des mouvements de rotation*. Firmin Didot, 1866.

[73] H. Andoyer, "Cours de mécanique céleste (paris: Gauthier-villars et cie)," 1923.

[74] A. Deprit, "Canonical transformations depending on a small parameter," *Celestial mechanics*, vol. 1, no. 1, pp. 12–30, 1969.

[75] M. Lara and S. Ferrer, "Complete closed form solution of a tumbling triaxial satellite under gravity-gradient torque," in *22nd AAS/AIAA Space Flight Mechanics Meeting, Charleston, SC*, 2012.

[76] K. C. Laurini and W. H. Gerstenmaier, "The global exploration roadmap and its significance for nasa," *Space Policy*, vol. 30, no. 3, pp. 149–155, 2014.

[77] K. Boudad, K. Howell, and D. Davis, "Near rectilinear halo orbits in cislunar space within the context of the bicircular four-body problem," in *2nd IAA/AAS SciTech Forum, Moscow, Russia*, 2019.

[78] B. Hufenbach, K. Laurini, N. Satoh, C. Lange, R. Martinez, J. Hill, M. Landgraf, and A. Bergamasco, "International missions to lunar vicinity and surface-near-term mission scenario of the global space exploration roadmap," in *IAF 66th International Astronautical Congress*, 2015.

[79] R. Whitley, M. Landgraf, N. Sato, M. Picard, K. Goodliff, K. Stephenson, S. Narita, Y. Gonthier, A. Cowley, S. Hosseini, *et al.*, "Global exploration roadmap derived concept for human exploration of the moon," 2017.

[80] C. Conley, "Low energy transit orbits in the restricted three-body problems," *SIAM Journal on Applied Mathematics*, vol. 16, no. 4, pp. 732–746, 1968.

[81] J. S. Parker, "Families of low-energy lunar halo transfers," in *AAS/AIAA SpaceFlight Mechanics Conference, AAS06-132, Tampa, Florida*, pp. 22–26, Citeseer, 2006.

[82] J. S. Parker and G. H. Born, "Direct lunar halo orbit transfers," *The Journal of the Astronautical Sciences*, vol. 56, no. 4, pp. 441–476, 2008.

[83] B. F. Villac and D. J. Scheeres, "Escaping trajectories in the hill three-body problem and applications," *Journal of guidance, control, and dynamics*, vol. 26, no. 2, pp. 224–232, 2003.

[84] G. Gómez and J. M. Mondelo, "The dynamics around the collinear equilibrium points of the rtbp," *Physica D: Nonlinear Phenomena*, vol. 157, no. 4, pp. 283–321, 2001.

[85] G. Gómez, W. S. Koon, M. Lo, J. E. Marsden, J. Masdemont, and S. D. Ross, "Connecting orbits and invariant manifolds in the spatial restricted three-body problem," *Nonlinearity*, vol. 17, no. 5, p. 1571, 2004.

[86] A. Jorba and J. Masdemont, "Dynamics in the center manifold of the collinear points of the restricted three body problem," *Physica D: Nonlinear Phenomena*, vol. 132, no. 1-2, pp. 189–213, 1999.

[87] R. T. Eapen and R. K. Sharma, "Mars interplanetary trajectory design via lagrangian points," *Astrophysics and Space science*, vol. 353, no. 1, pp. 65–71, 2014.

[88] N. L. Parrish, E. Kayser, S. Udupa, J. S. Parker, B. W. Cheetham, and D. C. Davis, "Ballistic lunar transfers to near rectilinear halo orbit: Operational considerations," in *AIAA Scitech 2020 Forum*, p. 1466, 2020.

[89] A. F. Haapala and K. C. Howell, "Representations of higher-dimensional poincaré maps with applications to spacecraft trajectory design," *Acta Astronautica*, vol. 96, pp. 23–41, 2014.

[90] K. C. Howell, D. C. Davis, and A. F. Haapala, "Application of periapse maps for the design of trajectories near the smaller primary in multi-body regimes," *Mathematical Problems in Engineering*, vol. 2012, 2012.

[91] A. D. Cox, K. C. Howell, and D. C. Folta, "Transit and capture in the planar three-body problem leveraging low-thrust invariant manifolds," *Celestial Mechanics and Dynamical Astronomy*, vol. 133, no. 5, pp. 1–21, 2021.

[92] M. E. Paskowitz and D. J. Scheeres, "Robust capture and transfer trajectories for planetary satellite orbiters," *Journal of guidance, control, and dynamics*, vol. 29, no. 2, pp. 342–353, 2006.

[93] D. E. C. Davis, *Multi-body trajectory design strategies based on periapsis Poincaré maps*. PhD thesis, Purdue University, 2011.

[94] R. T. Eapen and R. K. Sharma, "A study of halo orbits at the sun–mars l 1 lagrangian point in the photogravitational restricted three-body problem," *Astrophysics and Space Science*, vol. 352, no. 2, pp. 437–441, 2014.

[95] V. Szebehely, "Theory of orbits. yale university," 1967.

[96] M. Hénon, "Numerical exploration of the restricted problem, v," *Astronomy and Astrophysics*, vol. 1, pp. 223–238, 1969.

[97] J.-M. Petit and M. Hénon, "Satellite encounters," *Icarus*, vol. 66, no. 3, pp. 536–555, 1986.

[98] D. J. Grebow, *Trajectory design in the Earth-Moon system and lunar South Pole coverage*. PhD thesis, Purdue University, 2010.

[99] S. Wiggins, S. Wiggins, and M. Golubitsky, *Introduction to applied nonlinear dynamical systems and chaos*, vol. 2. Springer, 1990.

[100] R. T. Eapen, K. C. Howell, and K. T. Alfriend, "On the use of zero-momentum surfaces to identify transport opportunities to planar lyapunov orbits," in *AAS/AIAA Spaceflight Mechanics Conference*, 2020.

[101] T. Swenson, M. Lo, B. D. Anderson, and T. Gorordo, "The topology of transport through planar lyapunov orbits," in *2018 Space Flight Mechanics Meeting*, p. 1692, 2018.

[102] T. A. Pavlak, *Trajectory design and orbit maintenance strategies in multi-body dynamical regimes*. PhD thesis, Purdue University, 2013.

[103] E. T. Campbell, *Bifurcations from families of periodic solutions in the circular restricted problem with application to trajectory design*. PhD thesis, Purdue University, 1999.

[104] A. H. Nayfeh and B. Balachandran, *Applied nonlinear dynamics: analytical, computational, and experimental methods*. John Wiley & Sons, 2008.

[105] A. H. Nayfeh, *Introduction to perturbation techniques*. John Wiley & Sons, 2011.

[106] J. E. Marsden and T. S. Ratiu, "Introduction to mechanics and symmetry, vol. 17 of texts in applied mathematics," *Springer-Verlag,*, vol. 1, no. 2, pp. 2–1, 1999.

[107] H. Goldstein, C. Poole, and J. Safko, "Classical mechanics addison-wesley," *Reading, MA*, p. 426, 1980.

[108] D. L. Blanchard and F. Chan, "Separation of variables in the special diagonal hamilton-jacobi equation: Application to the dynamical problem of a particle constrained on a moving surface," 1973.

[109] V. I. Arnold, S. P. Novikov, *et al.*, "Symplectic geometry," in *Dynamical systems IV*, pp. 1–138, Springer, 2001.

[110] V. I. Arnol'd, *Catastrophe theory*. Springer Science & Business Media, 2003.

[111] T. Fukushima and H. Ishizaki, "Elements of spin motion," *Celestial Mechanics and Dynamical Astronomy*, vol. 59, no. 2, pp. 149–159, 1994.

[112] F. Klein, "über das brunssche eikonal," *Zeitschrift für Mathematik und Physik*, vol. 46, pp. 372–375, 1901.

[113] G.-i. Hori, "Theory of general perturbation with unspecified canonical variable," *Publications of the Astronomical Society of Japan*, vol. 18, p. 287, 1966.

[114] A. A. Kamel, "Perturbation theory based on lie transforms and its application to the stability of motion near sun-perturbed earth-moon triangular libration points," 1970.

[115] A. A. Kamel, "Lie transforms and the hamiltonization of non-hamiltonian systems," *Celestial mechanics*, vol. 4, no. 3, pp. 397–405, 1971.

[116] I. A. Sadov, "The action-angle variables in the euler-poinsot problem," *Journal of applied mathematics and mechanics*, vol. 34, no. 5, pp. 922–925, 1970.

[117] H. Kinoshita, "Theory of the rotation of the rigid earth," *Celestial mechanics*, vol. 15, no. 3, pp. 277–326, 1977.

[118] S. Ferrer and M. Lara, "On roto-translatory motion: Reductions and radial intermediaries," *The Journal of the Astronautical Sciences*, vol. 59, no. 1-2, pp. 22–40, 2012.

[119] H. Kinoshita, H. Yoshida, and H. Nakai, "Symplectic integrators and their application to dynamical astronomy," *Celestial Mechanics and Dynamical Astronomy*, vol. 50, pp. 59–71, 1991.

[120] H. Kinoshita, "First-order perturbations of the two finite body problem," *Publications of the Astronomical Society of Japan*, vol. 24, p. 423, 1972.

[121] M. Lara, T. Fukushima, and S. Ferrer, "First-order rotation solution of an oblate rigid body under the torque of a perturber in circular orbit," *Astronomy & Astrophysics*, vol. 519, p. A1, 2010.

[122] P. F. Byrd and M. D. Friedman, "Elliptic integrals of the third kind," in *Handbook of Elliptic Integrals for Engineers and Physicists*, pp. 223–239, Springer, 1954.

[123] D. Brouwer and G. M. Clemence, *Methods of celestial mechanics*. Elsevier, 2013.

[124] S. Ferrer and M. Lara, "Families of canonical transformations by hamilton-jacobi-poincar\'e equation. application to rotational and orbital motion," *arXiv preprint arXiv:0906.5312*, 2009.

[125] N. Hatten and R. P. Russell, "The eccentric case of a fast-rotating, gravity-gradient-perturbed satellite attitude solution," *Celestial Mechanics and Dynamical Astronomy*, vol. 130, no. 11, pp. 1–26, 2018.

[126] V. V. Beletski, *Motion of an artificial satellite about its center of mass*, vol. NASA TT F-429. Israel program for scientific translations, 1966.

[127] M. D. Shuster *et al.*, "A survey of attitude representations," *Navigation*, vol. 8, no. 9, pp. 439–517, 1993.

[128] J. F. San-Juan, L. M. Lopez, and R. Lopez, "Higher-order analytical attitude propagation of an oblate rigid body under gravity-gradient torque," *Mathematical Problems in Engineering*, vol. 2012, 2012.

[129] J. E. Cochran, "Effects of gravity-gradient torque on the rotational motion of a triaxial satellite in a precessing elliptic orbit," *Celestial mechanics*, vol. 6, no. 2, pp. 127–150, 1972.

[130] M. Zanardi and L. S. Moreira, "Analytical attitude propagation with non-singular variables and gravity gradient torque for spin stabilized satellite," *Advances in Space Research*, vol. 40, no. 1, pp. 11–17, 2007.

[131] K. T. Alfriend, R. Dasenbrock, H. Pickard, and A. Deprit, "The extended phase space formulation of the vinti problem," *Celestial mechanics*, vol. 16, no. 4, pp. 441–458, 1977.

[132] R. T. Eapen, M. Majji, and K. T. Alfriend, "Extended phase-space realization for attitude dynamics of an axisymmetric body in eccentric orbit,"

[133] C. A. WAGNER, "Gravitational experiments for a proposed venus orbiter," 1969.

[134] A. Lemaitre, S. D'Hoedt, and N. Rambaux, "The 3: 2 spin-orbit resonant motion of mercury," *Celestial Mechanics and Dynamical Astronomy*, vol. 95, no. 1, pp. 213–224, 2006.

[135] R. Eapen, M. Majji, and K. T. Alfriend, "Extended phase-space realization for attitude dynamics of an axisymmetric body in eccentric orbit," in *AAS/AIAA Astrodynamics Specialist Conference*, 2019.

[136] S. D'Hoedt and A. Lemaitre, "The spin-orbit rotation of mercury," in *Dynamics of Extended Celestial Bodies and Rings*, pp. 169–181, Springer, 2006.

[137] S. D'Hoedt, A. Lemaitre, and N. Rambaux, "Note on mercury's rotation: the four equilibria of the hamiltonian model," *Celestial Mechanics and Dynamical Astronomy*, vol. 96, no. 3, pp. 253–258, 2006.

[138] M. Moons, "Physical libration of the moon," *Celestial Mechanics*, vol. 26, pp. 131–142, 1982.

[139] M. Moons, "Analytical theory of the libration of the moon," *The Moon and the planets*, vol. 27, no. 3, pp. 257–284, 1982.

[140] B. Noyelles, J. Frouard, V. V. Makarov, and M. Efroimsky, "Spin–orbit evolution of mercury revisited," *Icarus*, vol. 241, pp. 26–44, 2014.

[141] S. D'Hoedt and A. Lemaitre, "The spin-orbit resonance of mercury: a hamiltonian approach," *Proceedings of the International Astronomical Union*, vol. 2004, no. IAUC196, pp. 263–270, 2004.

[142] N. Rambaux, T. Van Hoolst, V. Dehant, and E. Bois, "Inertial core-mantle coupling and libration of mercury," *Astronomy & Astrophysics*, vol. 468, no. 2, pp. 711–719, 2007.

[143] G. Colombo, "Cassini's second and third laws," 1966.

[144] S. J. Peale, "Generalized cassini's laws," *The Astronomical Journal*, vol. 74, p. 483, 1969.

[145] R. Cappallo, R. King, C. Counselman, and I. Shapiro, "Numerical model of the moon's rotation," *The moon and the planets*, vol. 24, no. 3, pp. 281–289, 1981.

[146] N. Rambaux and J. Williams, "The moon's physical librations and determination of their free modes," *Celestial Mechanics and Dynamical Astronomy*, vol. 109, no. 1, pp. 85–100, 2011.

[147] S. T. Habibullin, "On the systems of selenographic coordinates, their determination and terminology," *The moon*, vol. 3, no. 2, pp. 231–238, 1971.

[148] T. J. Moore and V. S. Ertürk, "Comparison of the method of variation of parameters to semi-analytical methods for solving nonlinear boundary value problems in engineering," *Nonlinear Engineering*, vol. 9, no. 1, pp. 1–13, 2019.

[149] T. J. Moore and M. R. Jones, "Solving nonlinear heat transfer problems using variation of parameters," *International Journal of Thermal Sciences*, vol. 93, pp. 29–35, 2015.

[150] A. Barari, M. Omidvar, A. R. Ghotbi, and D. D. Ganji, "Application of homotopy perturbation method and variational iteration method to nonlinear oscillator differential equations," *Acta Applicandae Mathematicae*, vol. 104, no. 2, pp. 161–171, 2008.

[151] S. Liao, "Comparison between the homotopy analysis method and homotopy perturbation method," *Applied Mathematics and Computation*, vol. 169, no. 2, pp. 1186–1194, 2005.

[152] J. Biazar, E. Babolian, and R. Islam, "Solution of the system of ordinary differential equations by adomian decomposition method," *Applied Mathematics and Computation*, vol. 147, no. 3, pp. 713–719, 2004.

[153] F. Ayaz, "Solutions of the system of differential equations by differential transform method," *Applied Mathematics and Computation*, vol. 147, no. 2, pp. 547–567, 2004.

[154] S. S. Ardahaie, A. J. Amiri, A. Amouei, K. Hosseinzadeh, and D. Ganji, "Investigating the effect of adding nanoparticles to the blood flow in presence of magnetic field in a porous blood arterial," *Informatics in Medicine Unlocked*, vol. 10, pp. 71–81, 2018.

[155] D. D. Ganji and R. A. Talarposhti, *Numerical and Analytical Solutions for Solving Nonlinear Equations in Heat Transfer*. IGI Global, 2017.

[156] M. Hatami, D. D. Ganji, and M. Sheikholeslami, *Differential transformation method for mechanical engineering problems*. Academic Press, 2016.

[157] A. Moradi and H. Ahmadikia, "Analytical solution for different profiles of fin with temperature-dependent thermal conductivity," *Mathematical Problems in Engineering*, vol. 2010, 2010.

[158] F. R. Moulton, *An introduction to celestial mechanics*. Macmillan, 1914.

[159] M. Bogdanova, "On a generalization of the method of variation of parameters," in *Doklady Akademii nauk BSSR*, vol. 6, pp. 285–287, 1962.

[160] S. T. Mohyud-Din, M. A. Noor, and A. Waheed, "Variation of parameters method for initial and boundary value problems 1," 2010.

[161] J. D. Kečkić, "Additions to kamke's treatise, vii: Variation of parameters for nonlinear second order differential equations," *Publikacije Elektrotehničkog fakulteta. Serija Matematika i fizika*, pp. 31–36, 1976.

[162] R. T. Eapen, M. Majji, K. T. Alfriend, and P. Singla, "Semi-analytic solutions to the hamilton-jacobi equation with applications to orbit propagation in perturbed two-body regimes,"

[163] N. A. Lemos, "Incompleteness of the hamilton-jacobi theory," *American Journal of Physics*, vol. 82, no. 9, pp. 848–852, 2014.

[164] C. G. Jacobi, "Ueber die reduction der integration der partiellen differentialgleichungen erster ordnung zwischen irgend einer zahl variablen auf die integration eines einzigen systemes gewöhnlicher differentialgleichungen.," 1837.

[165] J. F. Carinena, X. Gracia, G. Marmo, E. Martinez, M. C. Munoz-Lecanda, and N. Roman-Roy, "Geometric hamilton–jacobi theory," *International Journal of Geometric Methods in Modern Physics*, vol. 3, no. 07, pp. 1417–1458, 2006.

[166] D. Salopek and J. Stewart, "Hamilton-jacobi theory for general relativity with matter fields," *Classical and Quantum Gravity*, vol. 9, no. 8, p. 1943, 1992.

[167] M. G. Crandall, L. C. Evans, and P.-L. Lions, "Some properties of viscosity solutions of hamilton-jacobi equations," *Transactions of the American Mathematical Society*, vol. 282, no. 2, pp. 487–502, 1984.

[168] M. G. Crandall and P.-L. Lions, "Viscosity solutions of hamilton-jacobi equations," *Transactions of the American mathematical society*, vol. 277, no. 1, pp. 1–42, 1983.

[169] E. Trélat, "Global subanalytic solutions of hamilton–jacobi type equations," *Annales de l'Institut Henri Poincaré (C) Non Linear Analysis*, vol. 23, no. 3, pp. 363–387, 2006.

[170] R. W. Beard, G. N. Saridis, and J. T. Wen, "Galerkin approximations of the generalized hamilton-jacobi-bellman equation," *Automatica*, vol. 33, no. 12, pp. 2159–2177, 1997.

[171] N. Sakamoto and A. J. van der Schaft, "Analytical approximation methods for the stabilizing solution of the hamilton–jacobi equation," *IEEE Transactions on Automatic Control*, vol. 53, no. 10, pp. 2335–2350, 2008.

[172] M. Boulbrachene and M. Haiour, "The finite element approximation of hamilton-jacobi-bellman equations," *Computers & Mathematics with Applications*, vol. 41, no. 7-8, pp. 993–1007, 2001.

[173] Z. Hao, K. Fujimoto, and Y. Hayakawa, "Approximate solutions to the hamilton-jacobi equations for generating functions: The general cost function case," in *2013 9th Asian Control Conference (ASCC)*, pp. 1–6, IEEE, 2013.

[174] L. Grüne, "An adaptive grid scheme for the discrete hamilton-jacobi-bellman equation," *Numerische Mathematik*, vol. 75, no. 3, pp. 319–337, 1997.

[175] N. Adurthi, P. Singla, and M. Majji, "Sparse approximation–based collocation scheme for nonlinear optimal feedback control design," *Journal of Guidance, Control, and Dynamics*, vol. 40, no. 2, pp. 248–264, 2017.

[176] J. Liouville, "Note sur l'intégration des équations différentielles de la dynamique, présentée au bureau des longitudes le 29 juin 1853.," *Journal de Mathématiques pures et appliquées*, pp. 137–138, 1855.

[177] V. I. Arnol'd, "Critical points of smooth functions and their normal forms," *Russian Mathematical Surveys*, vol. 30, no. 5, p. 1, 1975.

[178] A. A. Kamel, "Expansion formulae in canonical transformations depending on a small parameter," *Celestial Mechanics*, vol. 1, no. 2, pp. 190–199, 1969.

[179] H.-J. Bungartz and M. Griebel, "Sparse grids," *Acta numerica*, vol. 13, no. 1, pp. 147–269, 2004.

[180] K. L. Judd, L. Maliar, S. Maliar, and R. Valero, "Smolyak method for solving dynamic economic models: Lagrange interpolation, anisotropic grid and adaptive domain," *Journal of Economic Dynamics and Control*, vol. 44, pp. 92–123, 2014.

[181] V. Barthelmann, E. Novak, and K. Ritter, "High dimensional polynomial interpolation on sparse grids," *Advances in Computational Mathematics*, vol. 12, no. 4, pp. 273–288, 2000.

[182] G. Arfken, "Orthogonal polynomials," *Mathematical Methods for Physicists,*, pp. 520–521, 1985.

[183] R. Broucke, "The lagrangian theory of stäckel systems," *Celestial mechanics*, vol. 25, no. 2, pp. 185–193, 1981.

[184] V. I. Arnol'd, B. Dubrovin, A. Kirillov, I. Krichever, *et al.*, *Dynamical Systems IV: Symplectic geometry and its applications*, vol. 4. Springer Science & Business Media, 2001.

[185] V. M. Guibout and D. J. Scheeres, "Solving relative two-point boundary value problems: Spacecraft formulation flight transfers application," *Journal of guidance, control, and dynamics*, vol. 27, no. 4, pp. 693–704, 2004.

[186] C. Park and D. J. Scheeres, "Solutions of optimal feedback control problems with general boundary conditions using hamiltonian dynamics and generating functions," in *Proceedings of the 2004 American Control Conference*, vol. 1, pp. 679–684, IEEE, 2004.

[187] R. Eapen, M. Majji, K. T. Alfriend, and P. Singla, "Canonical transformations via a sparse approximation-based collocation method for dynamical systems," in *AAS/AIAA Astrodynamics Specialist Conference*, 2019.

[188] D. Brouwer, "Solution of the problem of artificial satellite theory without drag," tech. rep., YALE UNIV NEW HAVEN CT NEW HAVEN United States, 1959.

[189] Y. Kozai, "The motion of a close earth satellite," *The Astronomical Journal*, vol. 64, p. 367, 1959.

[190] J. P. Vinti, "Theory of the orbit of an artificial satellite with use of spheroidal coordinates.," *The Astronomical Journal*, vol. 65, p. 353, 1960.

[191] B. Mahajan, S. R. Vadali, and K. T. Alfriend, "Exact delaunay normalization of the perturbed keplerian hamiltonian with tesseral harmonics," *Celestial Mechanics and Dynamical Astronomy*, vol. 130, no. 3, pp. 1–25, 2018.

[192] J. Choi and B. D. Tapley, "An extended canonical perturbation method," *Celestial mechanics*, vol. 7, no. 1, pp. 77–90, 1973.

[193] W. F. POWERS and B. D. TAPLEY, "Canonical transformation applications to optimal trajectory analysis.," *AIAA Journal*, vol. 7, no. 3, pp. 394–399, 1969.

[194] W. Powers and J. McDanell, "Switching conditions and a synthesis technique for the singular saturn guidance problem," *Journal of Spacecraft and Rockets*, vol. 8, no. 10, pp. 1027–1032, 1971.

[195] C. Park, V. Guibout, and D. J. Scheeres, "Solving optimal continuous thrust rendezvous problems with generating functions," *Journal of Guidance, Control, and Dynamics*, vol. 29, no. 2, pp. 321–331, 2006.

[196] V. I. Arnol'd, V. Goryunov, O. Lyashko, and V. Vasil'ev, "Singularity theory ii classification and applications," in *Dynamical systems VIII*, pp. 1–235, Springer, 1993.

[197] L. Hörmander *et al.*, "On the theory of general partial differential operators," *Acta mathematica*, vol. 94, pp. 161–248, 1955.

[198] A. Debs and M. Athans, "On the optimal angular velocity control of asymmetrical space vehicles," *IEEE Transactions on Automatic Control*, vol. 14, no. 1, pp. 80–83, 1969.